Energy saving technologies and optimisation of energy use for decarbonised iron and steel industry

WANG, RUIQI

Energy saving technologies and optimisation of energy use for decarbonised iron and steel industry

Ruiqi Wang

Thesis submitted towards the degree of
Doctor of Philosophy

Department of Engineering
Durham University
United Kingdom
January 2022

Dedicated to

my parents

Energy saving technologies and optimisation of energy use for decarbonised iron and steel industry

Abstract

The iron and steel industry relies significantly on fossil energy use and is one of the largest energy consumers and carbon emitters in the manufacturing sector. Simultaneously, a huge amount of waste heat is directly discharged into the environment during steel production processes. Conservation of energy and energy-efficient improvement should be a holistic target for iron and steel industry. There is a need to investigate and analyse potential effects of application i.e., a number of primary and secondary energy saving and decarbonisation technologies to the basic energy performance and CO_2 emissions profile of iron and steel industry. A 4.7Mt annual steel capacity iron and steel plant in the UK is selected as a case study.

By carrying out a comprehensive literature review of current primary and secondary energy saving and decarbonisation technologies, suitable technologies are categorised based on their purpose of utilisation and installation positions. It is found that fuel substitution technologies and waste heat recovery technologies have wide application prospects in iron and steel industry. To further investigate effects of these technologies on the UK integrated steelwork, a comprehensive model of iron and steel production processes is built by using the software Aspen Plus. The model is fully validated and is used to examine the specific energy consumption and direct CO_2 emissions. Energy consumption and CO_2 emissions of whole production chain to produce a ton of crude steel are 17.5 GJ and 1.06 t. Waste heat from hot coke and gas cooling could cover 40% of electricity consumed in the plant if coking process has the maximum coke capacity.

To implement primary energy saving and decarbonisation technologies, the performance of blast furnace is optimised first by substituting coke with bio-reducers based on the proposed model. Three biomass substitutions are considered to reduce coke rate and CO_2 emissions of ironmaking process. Results show that coke demand of per ton of hot metal and CO_2 emissions of the ironmaking process are improved by replacing partial coke with biomass. An optimal coke replacement is operated with 200 kg bio-oil and 222 kg coke when producing one ton of product. The reaction involving bio-syngas has the most potential to reduce CO_2 emissions.

To find a sustainable way to capture CO_2 and recover waste heat onsite, a model of adopting

organic Rankine cycle with amine-based CO_2 capture in ironmaking process is introduced. In comparison with different reducing agents injected into BF, bio-oil has the most advantage to improve energy consumption of CO_2 capture system. CO_2 emissions from total sites can be maximumly reduced by 69% through the method of CO_2 capture with waste heat recovery technologies. The combination of various decarbonised technologies creates great opportunity to reduce CO_2 emissions.

A mass-thermal network of iron and steel industry is finally built up, where primary and secondary energy saving technologies are implemented to optimise energy use and reduce CO_2 emissions. The general guideline i.e., 5-step method is summarised to optimise the mass-thermal network. Exergy analysis is used to evaluate overall network after applications of energy saving and decarbonisation technologies. Injection of biomass-based syngas can maximumly increase the exergy efficiency of ironmaking process. Sinter and BOF steelmaking processes are related with mass ratio of hot metal. Optimisation insights of energy use and decarbonisation for steelwork are revealed based on exergy efficiency and destruction results.

Declaration

The work in this thesis is based on research carried out by the author, at the Department of Engineering, Durham University. No part of this thesis has been submitted elsewhere for any other degree or qualification and it is all my own work unless referenced to the contrary in the text.

Parts of the work in the thesis has been published in the following paper:

- **R. Wang**, L. Jiang, Y. Wang, A.P. Roskilly Energy saving technologies and mass-thermal network optimization for decarbonized iron and steel industry: A review. Journal of Cleaner Production. 2020, 274:122997.

Acknowledgements

Foremost, I would like to express my deep gratitude to my supervisors, Prof. Tony Roskilly, Dr Yaodong Wang, and Dr Long Jiang, for their patience, for providing me constant support, for their guidance and sharing their knowledge and experience with me. They are always responsible and positive throughout my PhD study, and their help and instruction are vital to my thesis completion.

I would also like to thank many nice colleagues and staffs from previous Sir Joseph Swan Centre at Newcastle University and current group at Durham University. They provide me very comfortable and friendly working environment. It has been a unique trip studying at two top universities.

I would like to express my special thanks to my therapist Dr Syrita Khalef. I went through a very tough period since lockdown. She insistently soothes my anxiety, and helps me to get rid of depression. I could not achieve my research without her support and help.

Lastly, I express my endless gratitude to my friends, my partner, and my parents, who never give up supporting me whenever I am successful or not, and unconditionally encourage me to chase my dream so far.

Publications

- **R. Wang**, L. Jiang, Y. Wang, A.P. Roskilly. Energy saving technologies and mass-thermal network optimization for decarbonized iron and steel industry: A review. Journal of Cleaner Production. 2020, 274:122997.
- **R. Wang**, L. Jiang, Z. Ma, A. Gonzalez-Diaz, Y. Wang, A.P. Roskilly Comparative Analysis of Small-Scale Organic Rankine Cycle Systems for Solar Energy Utilisation. Energies. 2019, 12(5), 829.
- L. Jiang, **R. Wang**, A. Gonzalez-Diaz, A. Smallbone, R.O. Lamidi, A.P. Roskilly. Comparative analysis on temperature swing adsorption cycle for carbon capture by using internal heat/mass recovery. Applied Thermal Engineering. 2020, 169:114973.
- L. Jiang, **R. Wang**, A.P. Roskilly. Techno-economic analysis on a small-scale organic Rankine cycle with improved thermal driven pump. Energy Conversion and Management. 2020, 217:112979.
- L. Jiang, **R. Wang**, X Tao, A.P. Roskilly. A hybrid resorption-compression heat transformer for energy storage and upgrade with a large temperature lift. Applied Energy, 2020, 280: 115910.

Conferences

- **R. Wang**, A. Gonzalez-Diaz, L. Jiang, Y. Wang, A.J. Smallbone, A.P. Roskilly. CCS on iron and steel industry: Mass-Thermal network to reduce CO_2 emissions in UK, UKCCS Research Conference, Edinburg, 2019.
- **R. Wang**, L. Jiang, Y. Wang, A.P. Roskilly. Process simulation of blast furnace operation with biomass syngas injection for clean production, International Conference of Applied Energy, Sweden, 2019.

Contents

List of Figures

List of Tables

Nomenclature

$\alpha, \beta, \gamma, \delta$	The number of atoms
ρ	Density, $kg \cdot kmol^{-1}$
η	Energy efficiency
φ	Mole fraction
κ	Replacement ratio
a, b, c, k	Coefficients of the yield model
a_e	Effective interfacial area per unit of volume of stage
C_p	Specific heat, $kJ \cdot kg^{-1} \cdot K^{-1}$
CP	Column capacity parameter
CR	Capture rate
D	Diameter, m
DE	Direct CO_2 emission
e	Specific energy consumption, $GJ \cdot t^{-1}$
E	Energy consumption, kJ
ex	Specific exergy, $W \cdot t^{-1}$
Ex	Exergy flow rate, W
f	Conversion factor
F_p	Packing factor
G	Gibbs free energy, $kJ \cdot kg^{-1}$
Gas	Gas volume flow rate, $m^3 \cdot s^{-1}$
h	Specific enthalpy, $kJ \cdot kg^{-1}$
H	Height of packed column, m
$HETP$	Height equivalent to a theoretical plate, m
I	Irreversibility rate, W
$k_{g,n}$	Gas film mass transfer coefficient, $kmol \cdot s^{-1} \cdot m^{-2} \cdot kPa^{-1}$
$k_{l,n}$	Liquid film mass transfer coefficient, $m \cdot s^{-1}$
$Lean$	Lean loading

Liq	Liquid volume flow rate, $m^3 \cdot s^{-1}$
m	Mass flow rate, $t \cdot s^{-1}$
M	Mass, ton
n	Mole number
N	The number of stages in a column
p	Energy calorific value, $kJ \cdot t^{-1}$
P	Pressure, bar
Q	Heat flow rate, W
r	CO_2 reduction rate
R	Ideal gas constant, $J \cdot K^{-1} \cdot mol^{-1}$
R_p	Expansion ratio
s	Specific entropy, $kJ \cdot kg^{-1} \cdot K^{-1}$
S	Entropy, $kJ \cdot kg^{-1} \cdot K^{-1}$
T	Temperature, K
u	Gas velocity, $m \cdot s^{-1}$
Vo, O, N, S	Content of volatile matter, oxygen, nitrogen, sulphur, %
W	Work, W
y	Yield of product, %

Abbreviations

AC	Activated carbon
BF	Blast furnace
BFG	Blast furnace gas
BOF	Basic oxygen furnace
COG	Coke oven gas
CC	Continuous casting
CCS	CO_2 capture and storage
CDQ	Coke dry quenching
CHP	Combined heat and power
CMC	Coal moisture control
DC	Direct current

DCC	Direct contact cooler
DRI	Direct reduced iron
EAF	Electric arc furnace
ECOARC™	Ecological and economical high-efficient arc furnace
EIP	Eco-industrial park
FB	Fluidised bed
HBS	Hot blast stove
KC	Kalina cycle
LDG	Linz-Donawitz gas
LHV	Low heating value
MDEA	Methyldiethanolamine
MEA	Mono-ethanolamine
MSP	Membrane separation process
ORC	Organic Rankine cycle
PCI	Pulverised coal injection
PCM	Phase change material
PRA	Pre-reduced agglomerates
PSA	Pressure swing adsorption
SCOPE21	Super coke oven for productivity and environmental enhancement toward the 21st century
SEC	Specific energy consumption
SSW	Segregation slit wire
TEG	Thermoelectric generator
TRT	Top pressure recovery turbine
VSD	Variable speed drive

Subscripts

0	Dead state
abs	Absorber
bio	Biomass-based reducing agent

c	Cold side
C	Carbon
com	Compressor
cond	Condenser
crude	Crude steel
daf	Dry and ash free
des	Desorption
DRI	Direct reduced iron
eva	Evaporator
ex	Exergy
exp	Expander
f	Formation
flue	Flue gas
g	Gas
h	Hot side
HM	Hot metal
hx	Heat exchanger
i	The *i*th process
j	The *j*th inlet energy
in	Inlet
l	Liquid
lat	Latent heat
m	Mass
mit	Mitigated
n	The *n*th stage in a column
out	Output
preheat	Preheater
pro	Product
pu	Pump
re	Reaction

ref	Reference
regen	Regeneration
s	Superficial
S	Sulphur
sen	Sensible heat
sol	Solvent
str	stripper
superheat	Superheater
tot	Total
wf	Working fluid

Chapter 1

Introduction

1.1 Research background

The industrial sector encompasses activities that largely depend on energy, which leads to being a major factor for the competitiveness of industrial sector. The industrial sector uses more delivered energy than any other end-use sector, consuming about 55% of the world's total delivered energy, which continues to account for the largest share of delivered energy consumption [1]. According to distinct industry types, energy-intensive industries are responsible for 69% of all world industrial energy consumption. Additionally, the increasing demand for energy leads to the increase of greenhouse gases (GHG) emissions [2]. As a representative indicator of global warming, industrial CO_2 emissions from fuel combustion are over 19% of global GHG emissions [3].

Iron and steel production is a fundamental index of national prosperity and plays a leading role in the world economy. The sector employs high temperature furnaces for iron and steel production, which has become the second largest energy consumer in the industry [4]. Driven by increases in crude steel production, the sector's energy consumption grew by 6.2% annually from 2000 to 2011 [5]. Besides, carbon dioxide (CO_2) emissions from iron and steel plants account for the highest proportion of about 27% in manufacturing sector [6]. Iron and steel industry has achieved considerable improvements in recent decades, however, it still reveals great potentials to further reduce energy use and CO_2 emissions by about 20%, i.e., saving 4.7 EJ of energy and 350 Mt of CO_2 [7, 8]. These improvements could be achieved by saving energy during or after the manufacturing processes.

One of the major energy saving technologies considers primary energy. Most of primary energy are consumed in the iron and steel production processes where three quarters of energy use comes from coal [9]. Coal is the fuel sources to generate heat for melting the burden, and it is also used for producing coke which is the main reducing agent for removing oxygen in the iron ores. Furthermore, the actual resource efficiency of global steel production is only 32.9% due to a large number of energy losses [10]. With rapidly rising price of primary energy, it is quite significant to further improve energy efficiency, which could reduce fossil fuel consumption and CO_2 emissions in iron and steel

industry [11, 12]. Various energy saving technologies/measures have been adopted to reduce the usage of primary energy in iron and steel plants. These improvements include composition regulation of incoming energy flows, adjustment of energy-related processes, and utilisation of outgoing flows in the iron and steel industry [13]. These technologies ultimately aim to reduce the energy demands in iron and steel industry, and they should be optimised based on a mass network.

Recovery of secondary energy is the other considerable energy saving option. The secondary energy in iron and steel enterprises is mainly composed of by-products [14] and waste heat [15]. A large number of outgoing excess gases such as coke oven gas (COG), blast furnace gas (BFG), and Linz-Donawitz gas (LDG) are generated from steelworks [16], which account for approximately 30% of total energy consumption in steel enterprises [14]. It is evident that by-product gas or slag is the medium that could either be directed used or transferred into thermal energy and power [17]. With regard to waste heat in the steel mills, currently only about 25% of residual heat is recovered by a few commercial technologies [18]. Thus further improving the energy efficiency of waste heat utilisation is still of great value. Various thermal conversion technologies could be good candidates in terms of heat supply/storage, power generation, and refrigeration. Heat supply and storage could be achieved by heat exchanger and storage reactor. Heat exchangers are most commonly used to transfer heat from combustion exhaust gases to the other place where the heat is needed [19]. The typical thermal driven power generation cycles are Rankine cycle, organic Rankine cycle (ORC) [20], Kalina cycle (KC) [21], thermoelectric cycle [22], etc. Thermal driven refrigeration could be generally classified into absorption [23], adsorption [24], and thermoelectric refrigeration [25], which could meet cooling demands for the office buildings in steel mill. It is extensively acknowledged that the demands for waste heat recovery technologies should not only supply the heat but also work as power, refrigeration and energy storage in a district.

The integration of various energy types should be taken into account when each kind of technology is ensured. The utilisation and selection of technologies are quite complicated if various heat sources and different demands are required to be satisfied [26]. It is demonstrated that high-quality integration of different technologies should be accomplished to realise high efficient use of industrial waste heat through thermal network utilisation, including heating, power generation, cooling, energy storage and transportation [27]. From previous work, the energy saving in iron and steel industry mainly concentrates on the primary energy in terms of different operation processes. It

could provide more insights if the primary and secondary energy saving technologies could be effectively related and optimised as a network.

1.2 Research aims and objectives

This research focuses on primary and secondary energy savings in iron and steel production, and aims to analyse the energy performance and CO_2 emissions profile of optimised iron and steel plant. The concept of mass-thermal network optimisation in iron and steel industry is presented and summarised. Mass network optimisation lies in reducing primary energy demands whereas thermal network optimisation relies on the supply sides for energy savings which are dependent and independent. The main objectives of the study are as follows:

a) To review overall primary and secondary energy saving technologies applied in iron and steel industry, and investigate the suitable primary and secondary technology for further optimisation;

b) To collect plant data from industrial reports and references, simulate and validate the basic model of iron and steel integrated production process;

c) To evaluate the energy performance and CO_2 emissions of incorporating biomass into iron and steel production based on the basic case simulation;

d) To calculate potentials of CO_2 emissions reduction and energy savings when iron and steel production applies amine-based CO_2 capture and waste heat recovery technologies;

e) To develop a primary and secondary energy optimisation model for the iron and steel industry and achieve an energy saving target from an overall perspective.

1.3 Structure of the thesis

The main body of this thesis is organised as:

a) Chapter 2 presents an overall literature review of efficient use of primary and secondary energy in iron and steel industry, meanwhile the research gap could be found for improvement of energy use and CO_2 emissions reduction in the iron and steel industry;

b) Chapter 3 gives a complete simulation of an iron and steel plant in UK including raw material preparation, iron making, and steel producing processes; a validation of model will be given between comparison of results and reference data;

c) Chapter 4 derives an evaluation of injecting biomass into ironmaking process from full iron and steel production chain; three substitution scenarios of introducing biomass as reductant, namely charcoal, bio-oil and bio-syngas are considered and analysed with process simulation in Aspen Plus software to obtain process energy and material balances;

d) Chapter 5 presents a model of adopting ORC with amine-based CO_2 capture in ironmaking process; the benefits for CO_2 capture when applying waste heat recovery technologies are investigated.

e) Chapter 6 puts forward a concept of mass-thermal iron and steel network and basic guideline of optimising network; the method of exergy analysis will be used for evaluating optimisation potential of network.

f) Chapter 7 gives conclusions of whole dissertation.

Chapter 2

Literature review

This chapter presents a literature review of energy saving technologies in iron and steel industry. The overarching metallurgical routes and energy consumption of iron and steel industry is first summarised. The overview of primary energy and secondary energy saving technologies includes recently established and introduced technologies, and also describes those which could be available in the future. The technologies are categorised based on their purpose of utilisation and installation positions. To clarify the framework of this literature review, the concerning roadmap of is indicated in Figure 2.1, in which Figure 2.1a represents main concepts of energy, improvements and mass/thermal optimisation while Figure 2.1b generally summarises and clarifies their classifications.

2.1 Iron and steel metallurgical routes

Figure 2.1 shows an overview of iron and steel metallurgical routes which are composed of two basic routes: (1) primary route where iron ores and scrap are used as the raw materials, (2) secondary route from recycled steel scrap [28, 29].

2.1.1 Primary steel production route

Primary steel production route includes raw material preparation, iron making, and steel producing processes. Blast furnace (BF) and basic oxygen furnace (BOF) integrated process accounts for the most primary crude steel making, which is approximately 64% of global steel production [30]. BF-BOF route consists of sintering, pelletising, coking, iron making and steel making processes.

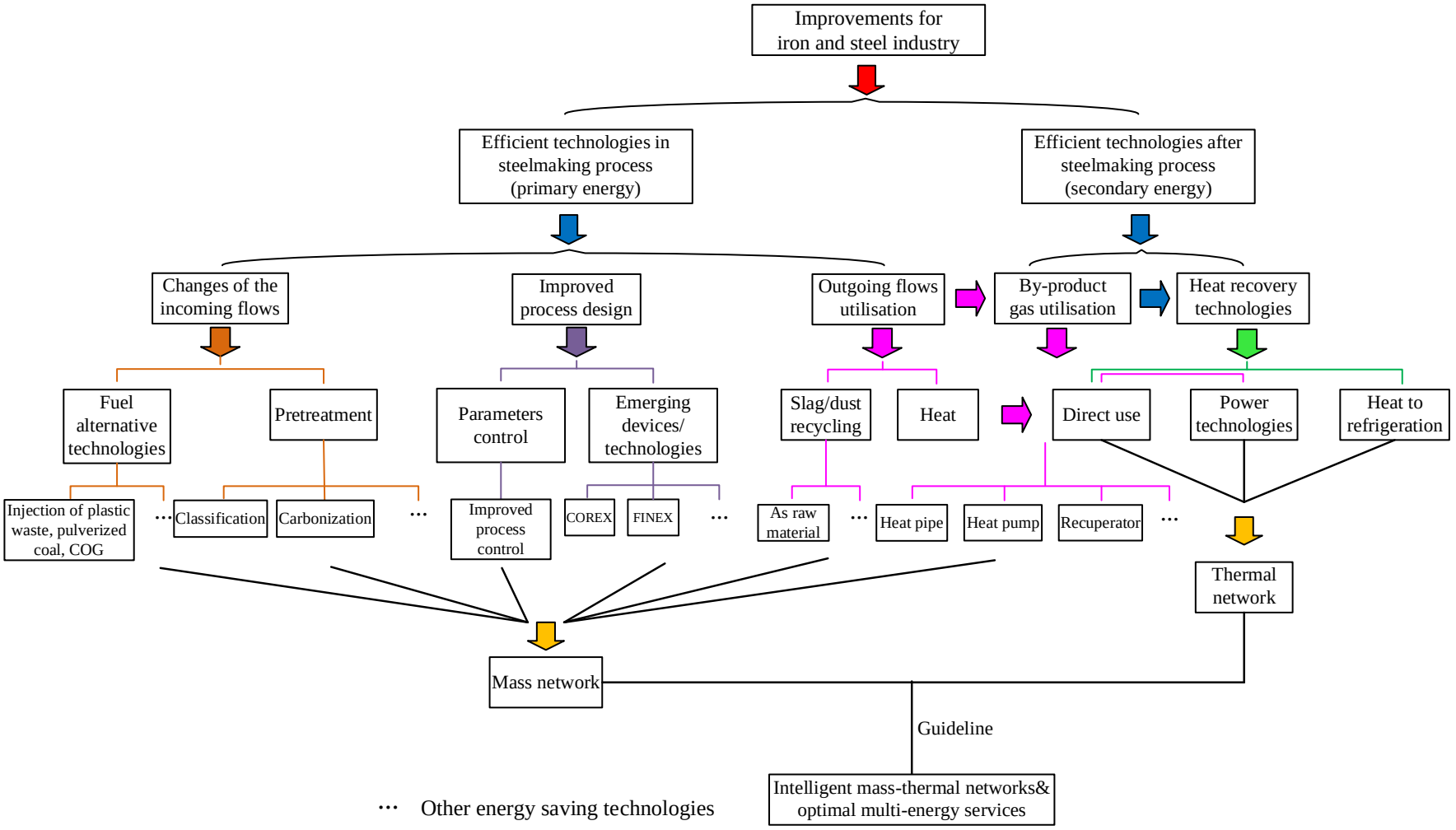
Improvements for iron and steel industry
Efficient technologies in steelmaking process (primary energy)
Efficient technologies after steelmaking process (secondary energy)
Changes of the incoming flows
Improved process design
Outgoing flows utilisation
By-product gas utilisation
Heat recovery technologies
Fuel alternative technologies
Pretreatment
Parameters control
Emerging devices/ technologies
Slag/dust recycling
Heat
Direct use
Power technologies
Heat to refrigeration
Injection of plastic waste, pulverized coal, COG
Classification
Carbonization
Improved process control
COREX
FINEX
As raw material
Heat pipe
Heat pump
Recuperator
Thermal network
Mass network
Guideline
Intelligent mass-thermal networks& optimal multi-energy services
… Other energy saving technologies

(a)

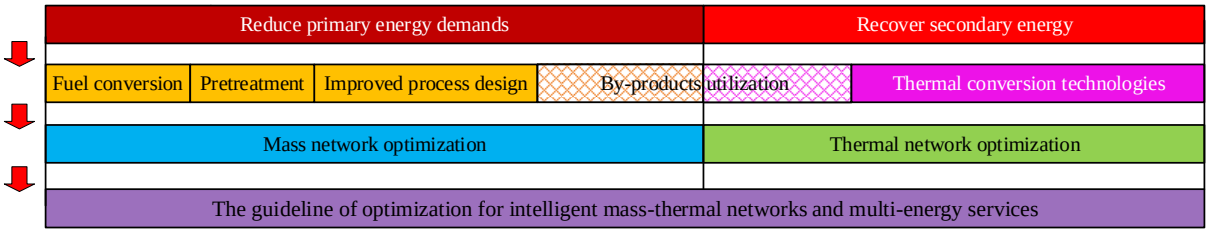

(b)

Figure 2.1: Roadmap of efficient use of energy in iron and steel industry (a) main concepts; (b) general summarisation.

Sintering and pelletising are two main processes related with ore agglomeration. They are used to enhance physical properties and reducibility of iron ores and minerals that will be used for subsequent iron making in BF [31]. Sintering process blends ores, additives, coke breeze and recycled iron together, and converts ore fines ($<$5mm) into larger porous lump sinter ($>$5mm) [32]. Pelletising process crushes and grinds the iron ores to produce round and crystallised iron ore pellet with a size of 9-16mm. Coking process pyrolyses coal in a high temperature and oxygen-free atmosphere to produce coke. Coke is a necessary raw material used in the BF, which is a chemical reductant and a permeable support to allow gases through the furnace [33]. The combustion of coke in the furnace could release heat to raise the temperature.

For all primary steel production processes, they proceed from the same chemical reactions. In the BF iron making process, coke is reacted with the sinter or pellet ore, which results in molten iron product i.e., pig iron [31]. Carbon impurities and concentration of alloying elements of iron product are removed (from 4-5% to 0.01-4%) in the BOF process. Open hearth furnace is an energy-intensive steel making technology and has nearly been phased out [28]. Direct reduction and smelting reduction are two technologies that offer alternatives to BF-BOF for iron making. Two processes could not consider the demand for the energy-intensive processes, i.e., iron ore agglomeration and coke making [33]. The iron from the direct reduction route referred to as sponge iron is fed into the electric arc furnace (EAF) steel making process.

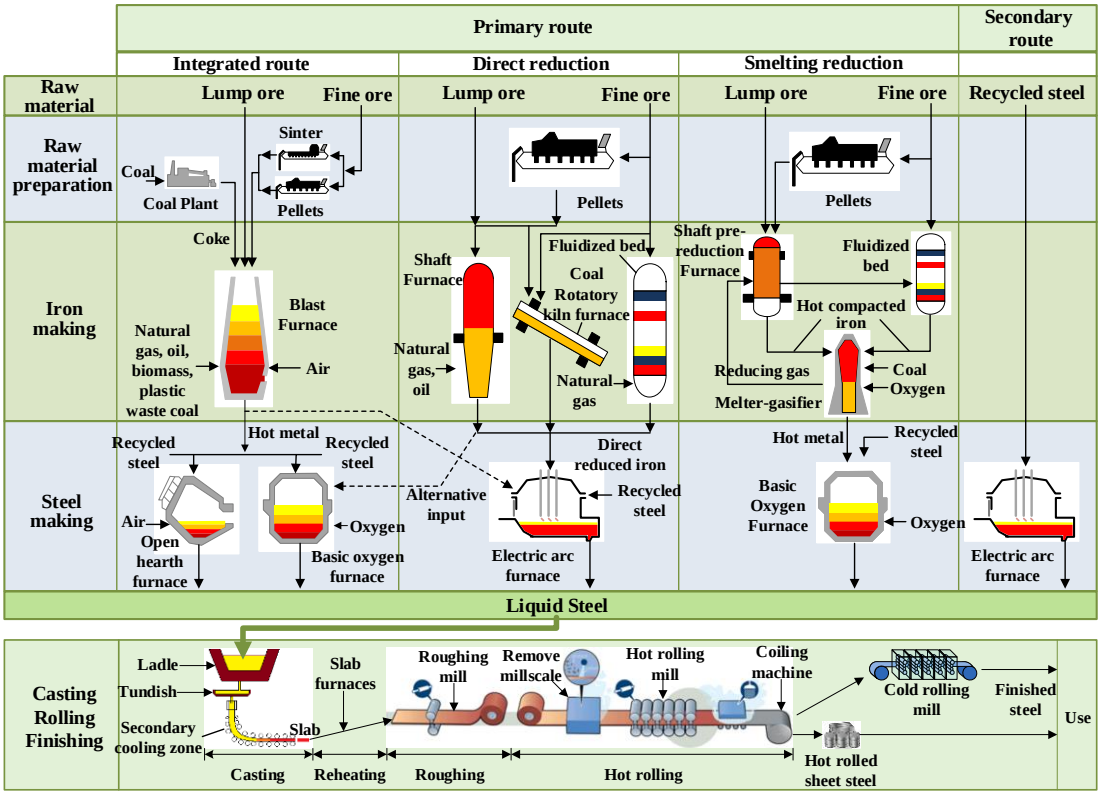

Figure 2.2: Iron and steel production routes, adapted from references [34, 35].

2.1.2 Secondary steel production route

In the secondary route i.e., EAF, the recycled steel scrap is melted by using high power electric arcs generated between graphite and feedstock. Since there is no raw material preparation and iron making steps, EAF has much lower energy consumption [36]. For the long-term perspective, substituting BOF steel making with EAF is a reasonable solution to energy conservation and cost control, as the energy of melting the scrap is electrical and less depend on high carbon contents of fossil fuel. Although plenty of the electricity used for EAF may be supported by coal-fired power plants, iron and steel industry will be less dependent on coal due to the reduction in BF-BOF production, which contributes to lower energy intensity and greenhouse gas emissions [37].

2.1.3 Steel casting, rolling, and finishing route

After steel production, the process is followed by continuous casting (CC) production and rolling. The molten steel will be transferred to continuous caster where semi-finished steel products are formed into various solid forms. Before entering the market, most steel products are further processed to form final shapes in the rolling mills. Steel rolling is conducted in both hot and cold rolling mills.

Hot rolling process consumes electricity and fossil fuels in furnaces which are used to reheat the steel slabs or billets formed during casting [38]. Steel coils from hot rolling continue to be sent to cold mill where the thickness is further reduced. Finishing is the final production step that includes different processes which are annealing, pickling, and surface treatment [39].

2.2 Energy consumption of iron and steel industry

In 2017, total energy demand of iron and steel sector grew to 33.44 EJ, which accounted for 21.4% of final energy consumption of the world industry [40]. The proportions by using fuels in the world iron and steel sectors are presented in Figure 2.3. It is indicated that coal serves as the primary fuel to generate coke and power, which accounts for the largest part (around 75%) [17, 40]; 9% of the final energy is consumed by natural gas which can effectively power the process especially in the direct reduced iron (DRI) production; the rest of energy consumption comes from secondary energy i.e., electricity (12%), heat (3%), and other fuel gas and oil products.

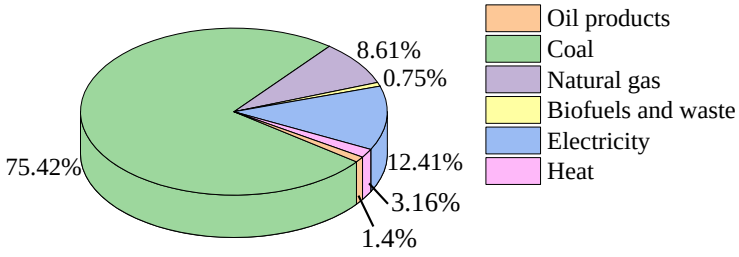

Figure 2.3: Energy distribution in world iron and steel sectors [9].

Figure 2.4 indicates the energy input of main steel producing countries. It is noted that different countries have different energy distributions in steel production routes. The iron and steel industry in China consumes the most fossil fuel i.e., coal and produces 94.1% of crude steel through BOF route. Comparably, crude steel production in United States mostly adopts EAF steel making route (62.7%) and natural gas (53.98%). This is mainly because mature and industrialised economy supplies a large scrap steel for EAF steel making in United States. Since India is rich in coal resource and has limited source of natural gas, coal-based DRI is a leading way to supply the feedstock for EAF [41]. In other countries, their use of electricity or natural gas is nearly related to the share of EAF steel production.

In 2015, the aggregated global energy intensity dropped slightly to 20.9 $GJ \cdot t^{-1}$ crude steel from

21.1 GJ·t^{-1} in 2010 [9]. Considering main production processes, energy use by BF-BOF route is estimated as 18.7 GJ·t^{-1} crude steel. The typical energy consumption of DRI-EAF pathway is about 22.4 GJ·t^{-1} crude steel. The energy intensity of smelting reduction to BOF processes is about 21.4 GJ·t^{-1} crude steel. The scrap-based EAF has the lowest energy footprint of 6.7 GJ·t^{-1} crude steel. By adopting best available technology, energy performance levels worldwide in all steel production routes would save 9 EJ per year [40].

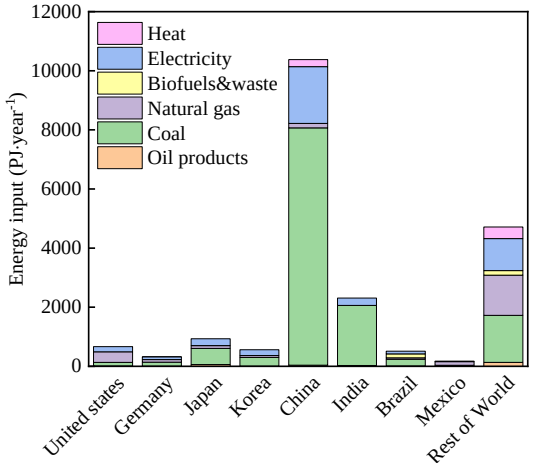

Figure 2.4: Energy input of main steel producing countries in 2015 [42].

Energy efficiency policies of iron and steel industry have led to partial retrofit of existing furnaces with energy-efficient equipment. The iron and steel sector still has vast technical potentials to further reduce energy consumption by around 20% [43]. Figure 2.5 presents the estimated energy saving potentials based on current production capacities and technologies. Annual energy savings potential is indicated by the bars and the values are shown on the left y-axis. Energy savings potential of per ton of steel is shown as a point in the figure, and read by the right y-axis. Average global specific energy saving potential is 4.3 GJ·t^{-1} crude steel and China accounts for 70% of potential energy savings. Most of this potential could be realised by improving BF and steel finishing processes as well as recycling steelworks by-product gases. Electricity production from BFG offers an important opportunity for steel plant to maximise the usage of input fuels [5].

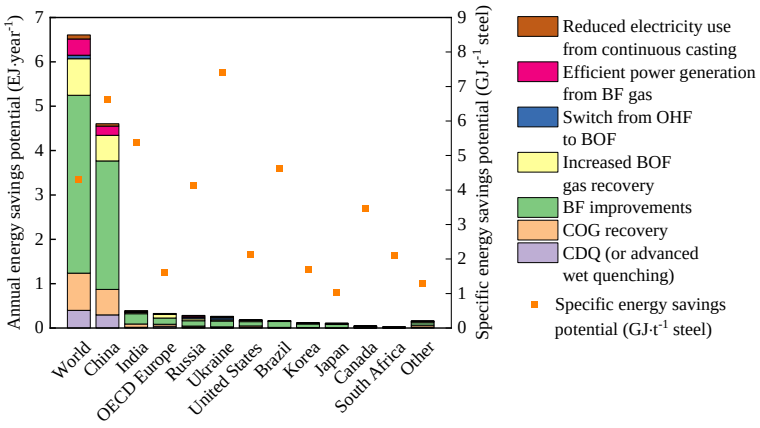

Figure 2.5: Energy saving potentials for iron and steel industry based on best available technologies (published in 2014) [5].

2.3 Primary energy saving technologies

The primary energy is the largest component of operating cost for many steel producers [44], thus the primary energy saving opportunities should be assessed based on actual energy demands. It is of great importance to consider the efficient technologies in aspect of mass balance i.e., mass optimisation. The technologies can be manifested in the incoming and outgoing flows of a plant, as well as the specifications of the installed facilities. The detailed analysis of efficient technologies for primary energy is conducted in terms of specific energy savings and investment cost which are demonstrated as follows.

2.3.1 Changes of the incoming flows

The direct input of raw materials and energy for each process and facility are included in the incoming flows of iron and steel industry. Energy saving technologies for incoming processes mainly refer to energy substitution and pretreatment of feedstock, which generally tend to reduce consumption of fossil fuels and raw materials. Energy substitution aims to replace fossil fuels with cleaner energy and to increase the share of renewable resources [45]. Pretreatment of feedstock is considered as a good way to enhance productivity of each plant.

a) Fuel substitution technologies

The consumption of coal-dominated energy in the iron and steel industry has undermined sustainable development [45]. The energy sources of steel production processes needs to shift from

coal to natural gas, hydrogen, electricity, biomass, etc. [46]. Various approaches are summarised and presented in Figure 2.6 It is demonstrated that iron and steel production has been gradually decarbonised by reducing the use of coal, which would be partially replaced by natural gas, oil, plastic waste, hydrogen, electricity, integration with CO_2 capture and storage (CCS), utilisation and storage technology and sustainable biomass technology [47, 48].

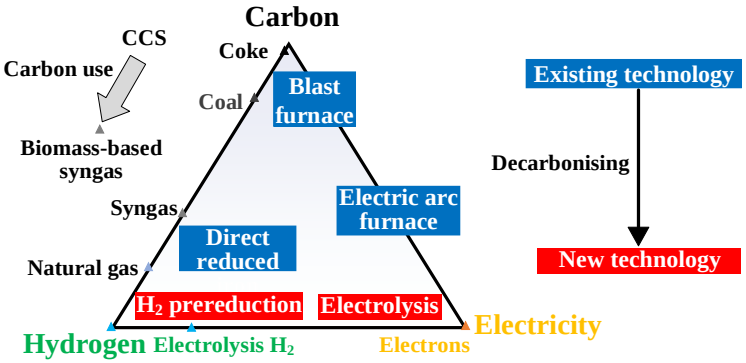

Figure 2.6: Framework of steel triangle processing route [47].

To reduce expensive coke consumption and CO_2 emissions in coke making process, pulverised coal injection (PCI) has been widely used as the auxiliary fuel in the BF process. Finely ground dried coal is injected with gas into BF through the tuyère as a partial replacement for the coke [49], which will decrease the coke ratio of the BF and improve the net energy efficiency [50]. Similar to PCI, natural gas injection could substitute part of coke, but it is typically applicable to medium-sized furnaces which usually have an annual production rate of 1.4-2.5 million tons of iron [51]. Besides, natural gas and pulverised coal can be simultaneously injected into BF tuyères by using a combined fuel lance [52]. The injection of oils and waste oil is beneficial, which is similar with the natural gas injection. The amount of injected oil is within the range of 65-130 $kg \cdot t_{HM}^{-1}$ (t_{HM} means ton of produced hot metal)[53]. It is desirable to reuse waste plastics for the better utilisation of energy resources due to their higher heating values and higher H_2 contents when comparing those with coal [54]. The maximum level for plastic injection at the tuyères level could reach 70 $kg \cdot t_{HM}^{-1}$ [53]. H_2 can react with iron ore to achieve reducing coke and above alternative reducing agents in BF. The indirect reduction process by H_2 has the advantage of zero CO_2 emission in the produce gas [55]. COG and BFG are recovered as supplementary fuel in most of steel plants. Various combustion processes could reuse these gases such as blast generation in hot stoves or coke oven firing [53].

Burgeoning attentions have been paid to the biomass as a renewable substitute in the iron and steel industry. For the integrated steel plant, biomass has been inserted into coal compound during coke making process to produce bio-coke which is effective in reducing the gasification temperature in BF [56]. In sintering process, the substitution of 25% coke breeze with biochar is an suitable method to optimise productivity and quality of sinter [57]. The biomass-based reducing agents, e.g. charcoal, bio-oil, and syngas could be injected into the BF from the top or through tuyères to minimise the coke consumption [58]. Novel carbon composite agglomerates have been investigated to renovate outdated coke ovens and low reduction rate operation of BF [59]. The pretreatment and upgrading processes of raw biomass are required in these applications.

Table 2.1 reviews representative fuel substitution technologies and their potentials to reduce coke used in the BF. These results are based on the actual performance of operating BF or mathematical modelling. Depending on the amount of auxiliary injectants, mean coke rate of the furnace is 334 $kg \cdot t_{HM}^{-1}$, and a theoretical minimum of 200 $kg \cdot t_{HM}^{-1}$ is necessary to enable stable furnace operation [60]. In comparison with all the reductants, 200-250 $kg \cdot t_{HM}^{-1}$ coke can be replaced, which may result in lower emissions [61]. Due to the advantages of high reliability and easy operation, PCI has better performance to reduce coke consumption in BF operation. Although the usage of biomass in steel industry shows great potentials, there are still lots of challenges in terms of technical and economic aspects.

Table 2.1: List of representative fuel substitution technologies in the BF.

Fuel alternative technologies	Injection rate of auxiliary injectants	Coke rate $kg \cdot t_{HM}^{-1}$	Ref.
PCI	190-210 $kg \cdot t_{HM}^{-1}$	280-300	[62]
Natural gas injection	96-158 $m^3 \cdot t_{HM}^{-1}$	341-410	[63]
Heavy oil injection	140 $kg \cdot t_{HM}^{-1}$	300	[64]
Plastic waste injection	35 $kg \cdot t_{HM}^{-1}$ + 71 $kg \cdot t_{HM}^{-1}$ heavy oil	372	[65]
COG injection	50 $kg \cdot t_{HM}^{-1}$	322	[66]
H_2 injection	27.5 $kg \cdot t_{HM}^{-1}$	389.8	[60]
Charging lump charcoal	200 $kg \cdot t_{HM}^{-1}$	260	[67]
Biomass-oil injection	140 $kg \cdot t_{HM}^{-1}$	455	[68]
Biomass-syngas injection	10.5 $GJ \cdot t_{DRI}^{-1}$ for DRI production	-	[69]

b) Pretreatment of feedstock

Before charging raw materials into iron and steel works, pretreatment is always essential for the quality and purity of feedstock. The pretreatment methods mainly involves granulation and torrefaction, which can be classified as physical and chemical process. Physical pretreatment is used to control particle size and moisture content of raw materials. In sinter plant, new coating and granulation technologies have developed to improve sintering productivity and reducibility [70]. The segregation slit wire (SSW) system is an advanced charging system which is developed in Japan as shown in Figure 2.7. It is a device to reduce coarse granule and maintain a constant particle size of limonite, which could increase permeability of the sintering mixture and reduce the return fine. Some steel works in China and Japan segregate the raw materials on pellets, and produce quasi-particles within a mean size of 3–5 mm [71]. It is an effective way to improve the permeability and then form the thick sinter layer to reduce reaction temperature and energy consumption. In coke oven, it is proved that the densification of coals to a relative material density of 80%, i.e., a compact density around 1100 $kg \cdot m^{-3}$ is advantageous [72]. The stamp charging technology is usually used to compact the coal, where the coal blends are previously compressed into a "coal cake" and then charged vertically into the oven. With stamp charging, the coke oven productivity is increased by 10-12% [73]. For the modern BF process, controlling particle segregation to obtain a desired gas flow and smooth operation is very significant [74]. Bell-less top systems are adopted for proper burden distribution and segregation of input materials into the furnace, which can enhance the furnace operational stability and increase the productivity [75].

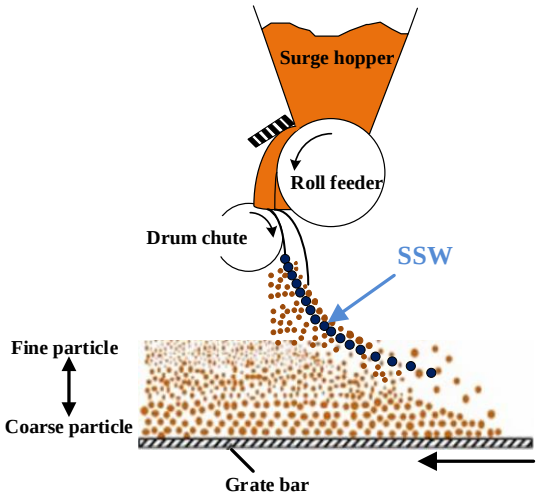

Figure 2.7: Schematic diagram of SSWs [70].

The general methods to remove the moisture of feedstock include preheating and drying. Coal moisture control (CMC) was introduced to Japan in the 1980s [76], because coke making process requires the application of coal blends with a correctly matched level of moisture. This industrial application controls the moisture of feedstock for coke producing from a normal 8-10% to around 6% without hindering the charging operation [49]. The process is different from coal preheating and drying because it leads to the strict stabilisation of moisture content in the coal blend. Low pressure steam and waste heat from COG are generally used as the heat source of humidity control. For instance, Nippon steel succeeded in developing the fluidised bed (FB) type CMC which exhibited high heat exchange efficiency and solved the problem of indirect heat exchange between the coking coal and steam as shown in Figure 2.8 [77].

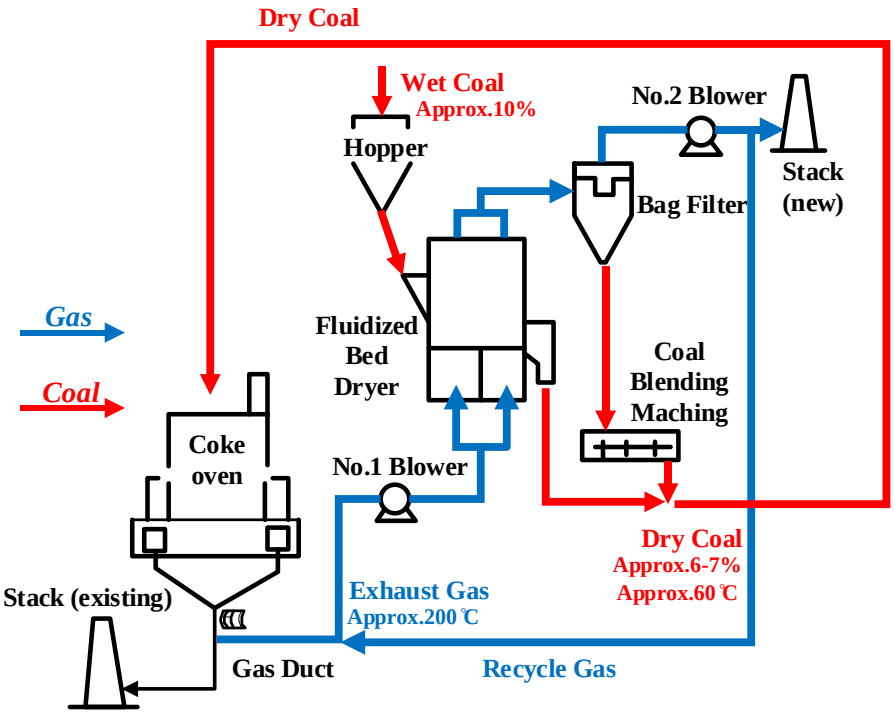

Figure 2.8: Nippon Steel & Sumikin Engineering's FB type CMC process flow [78].

Compared with physical process, chemical pretreatment always aims to improve the quality of raw materials that are prior to iron and steel making processes. In general, high iron content and low gangue content of sinter or pellet, and moderate ash content of coke are all good factors for BF injection [53]. Apart from the usual feedstock of BF, a newly developed pre-reduced agglomerates

(PRA) were proposed in Japan. The PRA was reduced simultaneously with agglomeration on existing sintering machine [79]. It has excellent high temperature properties to reduce pressure drop and thickness of the BF cohesive zone, which is quite conducive to BF productivity. Hot metal chemical pretreatment is a process that performs on hot metal after the tapping of BF and before decarbonisation in a BOF [80]. In most cases, this process is composed of desulphurisation, dephosphorisation and desiliconisation. The general desulphurisation process can be divided into flux injecting and mechanical stirring which are shown in Figure 2.9. The dephosphorisation and desiliconisation are not as common as the desulphurisation due to their costly and sophisticated process. The common way usually injects agents and oxidizing compounds into the torpedo car or hot metal transfer ladles as shown in Figure 2.10 [81].

In the secondary steel making route, steel scrap can be integrated into production processes as alternative raw material. Due to global demand for steel scrap, exportation of recycled scrap steel becomes an attractive option [82]. Scrap pretreatment is often required to obtain high-quality scrap metal which includes routine sorting, flame cutting, and packing. In developed countries, the scrap recycling industry has been established with centralised import, processing and distribution [83]. It reveals vast potentials to reduce resource, energy consumption and waste emissions through steel scrap pretreatment.

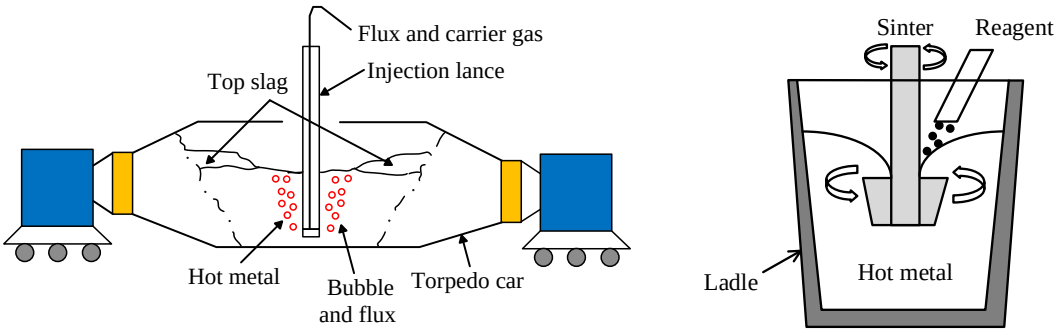

Figure 2.9: The hot metal desulphurisation process (a) Injection process of hot metal desulphurisation using a torpedo car; (b) Mechanical stirring process for hot metal desulphurisation using a charging ladle [80].

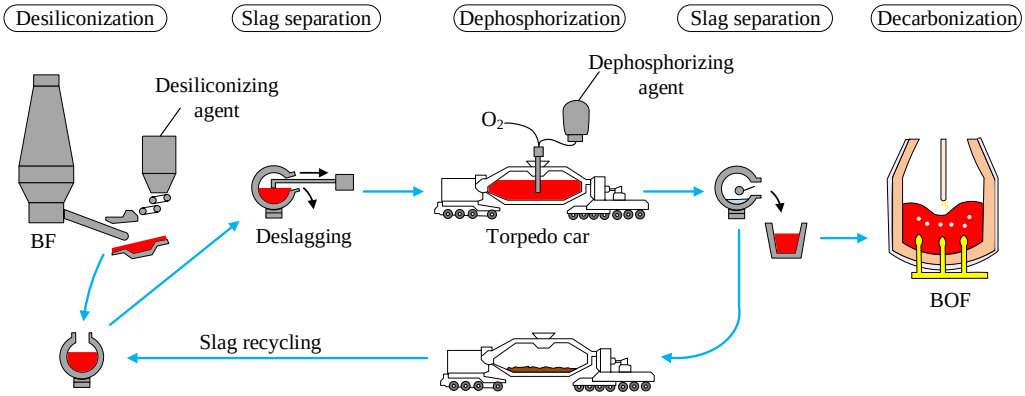

Figure 2.10: Exemplified steps for desiliconisation and dephosphorisation of hot metal [81].

Table 2.2 lists general pretreatment technologies and their improvement effect. The ratio of energy savings is used to reveal the fuel saving potentials of various pretreatments. The indicator is calculated based on the energy consumption before and after installation, which can be expressed as:

$$\text{Ratio of energy savings} = \frac{E_0 - E_1}{E_0} \times 100\% \quad (2.1)$$

where E_0 is energy consumption before measures installation, E_1 is energy consumption after installation. The input and output of each process in iron and steel industry refers to [84].

According to improvement effects and energy savings of selective pretreatment technologies, it is found that the chemical pretreatment technologies, such as charging PRA into BF, have more significant energy savings than that of physical pretreatment technologies. Moreover, the suitable particle size of charging materials has a vital role for productivity improvement of manufacturing facilities.

Table 2.2: List of selective pretreatment technologies for steel and iron industry.

Pretreatment technologies		Improvement effect	Ratio of energy savings [a]	Ref.
Burden distribution	Sinter SSW charging	Increase 5% productivity	5.6%	[49]
	Coke stamp charging	Increase 10%-12% productivity	9.1%-16.7%	[85]
	Bell-less top BF	Increase 2.5% productivity	2.4%	[76]
Coke moisture control		Increase 2% coke strength	0.72%	[51, 86]
PRA in BF		45% pre-reduction	23%	[79]
EAF charge scrap preheating		Increase 33% productivity	3.2% [a]	[81]

[a] The energy use of scrap-based EAF refers to [40].

2.3.2 Improved process design

With increment of crude steel production, further reduction of energy use and CO_2 emissions

require more innovation beyond existing technologies [38]. Novel process design is developed and valued in terms of various parameters improvement and emerging energy-efficient devices.

a) Parameter control technologies

Temperature, pressure, gas flow rate and oxidising atmosphere of combustion are all taken as the parameters that need to be controlled in iron and steel making processes. Through optimised design of multiple parameters, it can further improve total working performance of iron and steel industry [87].

Temperature is always required to be high to decompose the structure of iron ore and coal in current steel making, which aims to overcome kinetic and thermodynamic limits of chemical reactions in the reduction of iron oxide, and to provide steel in a liquid form [88]. Considering low-carbon and energy-efficient development, various unit operations can be performed at a lower temperature than that in present processes. Low-temperature sinter process controls oxygen concentration to facilitate the solid phase reaction, which could significantly save energy and improve performance of sinter ore [89]. Coking process can happen at a lower temperature (800 ℃) instead of 1000 ℃ by heating the coke while it descends into the BF. Direct reduction process uses a synthesis gas or solid fuel directly to achieve reduction of iron oxide below melting point [90]. Low-temperature rolling i.e., warm-rolling or ferritic rolling is attempted to produce steels between 440°C and 850 ℃ to replace the conventional grades of hot rolling and cold rolling [91, 92]. These new steel products are conducive to energy savings, cost effectiveness and productivity.

Pressure is controlled to reduce energy consumption in iron and steel industry. The high pressure application in coke oven is effective to control gases emissions, thus creating large saving in process steam requirement and increased by-products yield [81]. During iron smelting process, the increased top pressure of BF is feasible to lower gas velocity and increase retention time for gas-solid reactions, which could enable a good furnace operation and energy recovery of BF [81]. A large roots-style mechanical vacuum booster pump is installed in steel vacuum degassing and vacuum oxygen decarburising processes for better dust handling. Advances of this facility offer significant savings in energy consumption, costs reduction, speed increment, improvements in flexibility and overall productivity for steel degassing operations [93]. Table 2.3 lists working conditions of temperature and pressure control technologies. Common conditions of various processes are also presented.

Table 2.3: Working conditions of temperature and pressure control technologies.

Improvement technologies	Working conditions	Common conditions	Ref.
Low-temperature sintering	1200°C	1300°C -1480°C	[53, 89]
Low-temperature coking	800°C	1100°C	[88, 94]
Low-temperature iron making	900°C-1000°C	1200°C -2000°C	[53, 88]
Low-temperature rolling	440°C -850°C	500°C -1300°C (hot rolling)	[91, 95]
High pressure ammonia liquor aspiration system in coke oven	35-40 bar	Ammonia stripper at 1.37 bar	[81, 94]
High BF top pressure	> 0.5 bar	0.2-0.5 bar	[81, 96]
Large roots-style mechanical vacuum booster pump for degassing	0.001 bar	0.00067 bar	[93]

Variable speed drive (VSD) technologies have drawn bourgeoning attention in the last decade [97]. The steel making pumps and fans for dust and gas extraction are important loads in terms of electricity saving potential, which are excellent candidates for VSDs. By applying VSD in iron and steel sectors, the energy saving could reach 6.3 TWh [98]. VSD can be installed on compressors of coke oven to reduce energy consumption of COG pressurisation process [33]. Also it can be equipped in the BOF and EAF processes for a better match of the fan speed with the requirements of steel making due to the frequent variation of flue gases volumes [33]. To avoid excessing air that may decrease combustion efficiency and lead to excessive waste gases, the installation of VSD on combustion air ventilators on reheating furnace in hot rolling can help to control oxygen level [51].

Ventilation control technologies e.g., air leakage reduction, oxygen enrichment and blast dewetting are indispensable for energy saving in the steel production. It is indicated that improper sealing system and damaged components in a compressed air device can cause the air leakage, which is a mainly source of waste energy in the steelworks. Improvement could be obtained by attaching a new seal between air seal bar and slide bed on the equipment side [99]. Air tight EAF technology through sealing slag door can significantly reduce all other air entries and thermal losses in the fumes [100]. In BF process, the methods of oxygen enrichment, over-pressure, dehumidification of the blast air in the hot stoves are implemented for a higher flame temperature to achieve more effective combustion of fuels and reduce coke demands [50, 101].

Energy savings of above-mentioned technologies are not obvious when the separated parameter control technology is applied. Thus it is necessary to develop a control system that combines all parameters together which could meet handling conditions to optimise energy consumption and cost.

b) Energy-efficient devices

Energy-efficient equipment is regarded as the opportunity to reduce energy intensity and CO_2 emissions in iron and steel industry. These technologies, e.g. novel adopted processes and advanced process controls, have reduced energy intensity by 30% since 1990 [51]. This section will summarise emerging energy-efficient devices and technologies in terms of production routes from raw material preparation to finishing process.

Considering low emissions and sintering process optimisation, waste gas recovery device and energy-efficient ignition oven are developed. The sinter strand is housed to recirculate waste gases from different parts of strand and back to the sintering process [53]. The process could use CO content of waste gas as an energy source. Meanwhile, the recycled gas can provide most of oxygen that is required to burn the fuel. In order to save the fuel for ignition ovens, high-efficient multi-slit burner [81] and line burner [102] in ignition furnace are used, which can control the duration of the flame to minimise ignition energy.

For a coke plant, there are considerable heat loss and CO_2 emissions in the conventional process of wet quenching. The coke stabilisation quenching is considered to reduce coke consumption by keeping hot coke in contact with water from both top and bottom of quenching tower. However, taking the risks of water consumption and contamination, this technology may have a limited potential advantage. One alternative solution is coke dry quenching (CDQ) procedure i.e., the coke is cooled by an inert gas [13]. In this way, CDQ system could collect and reuse thermal energy of the red-hot coke as steam. Other types of advanced coke oven, i.e., single chamber coking reactor and non-recovery coke oven, have been successfully installed in the coke plant [103]. A systematic coke oven technology i.e., super coke oven for productivity and environmental enhancement toward the 21st century (SCOPE21) has been demonstrated in Japan [104]. The technology includes three sub-processes, i.e., rapid preheating of coal feeding, rapid carbonisation and further heating of carbonised coke. The schematic is shown in Figure 2.11.

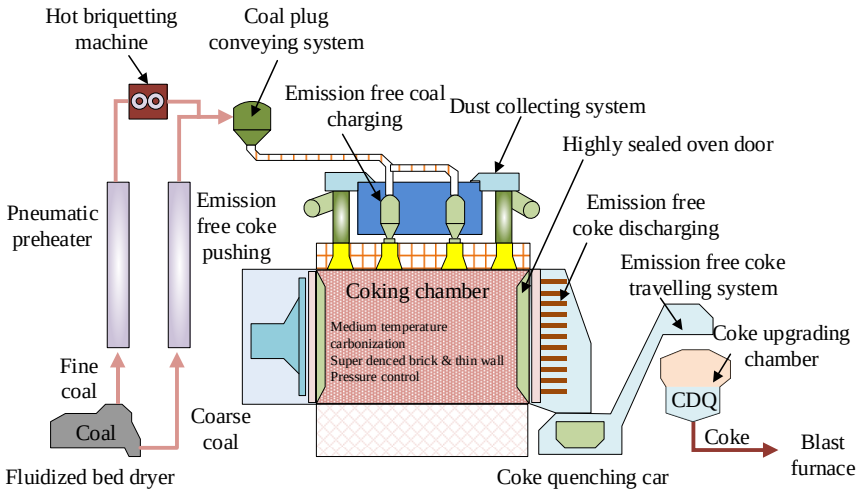

Figure 2.11: Schematic diagram of SCOPE21 process flow [81].

Hot blast stove (HBS) is one of the most important units in the BF iron making route [105]. Conventional HBSs with internal and external chambers have a number of drawbacks which can be resolved if the combustion chamber is eliminated, i.e., to develop a top combustion HBS known as "shaftless hot stove". The top combustion hot stove can provide complete gas combustion without pulsation, which could achieve the high efficient combustion even in the operation only with flue gas [106]. A novel Kalugin shaftless stove with a smaller diameter pre-chamber at the top of the dome has become a future top combustion hot stove. With regard to further reduce CO_2 emissions of iron making, many options are proposed, e.g. Corex, Finex, Tecnored, Itnk3 process, Paired straight hearth furnace, Coal-based HYL process, Coal-based MIDREX® process. [50]. These technologies have been reviewed and compared by Hasanbeigi et al. [103], which are considered as the promising alternatives of traditional iron making process. Corex, Finex, and Coal-Based HYL process are already commercialised, but with very low adoption rate in the steel industry worldwide.

One of the major innovations in BOF steel making lies in injection system of converter furnace. Top blown BOFs have been converted to combined blowing process with an additional bottom agitation [107]. A small amount of inert gas will be injected to BOF from the bottom of the convertor, which is mixed with oxygen injected from top of furnace. Inert gas injection is beneficial to reduce the flux and oxygen consumption. Energy savings in EAF depend largely on the highly efficient arc furnace. The furnaces such as direct current (DC) arc furnace and Comelt furnace both operate on a DC basis. DC can generate the heat which is used to melt and stir the steel after charging scrap into arc furnace [49]. Various arc furnaces for preheating the scrap, i.e., Contiarc furnace, post combustion

shaft furnace, ecological and economical high-efficient arc furnaces (ECOARC™) have been developed and put into practice. It is demonstrated that using waste heat to preheat the scrap can reduce power consumption of EAFs. Furthermore, new transformers and electric systems have been installed on EAF operators to enhance the power of the furnaces [51].

Technologies in casting, rolling, and finishing processes may dramatically reduce energy consumption. These efficient opportunities refer to innovation heating furnaces, e.g. Rapidfire™ edge heater [108], flameless oxyfuel combustion furnace [109], walking beam furnace, and regenerative burner, which can provide more furnace heating capacity and lower fuel consumption. Casting, rolling and finish processes need to meet various demands, thus it is necessary to provide solutions by supplying linking lines e.g. a CC machine that produces slabs, blooms and billets by pouring molten steel into a mould [49]. Other integrated technologies are adopted in iron and steel industry e.g. endless strip production that combines casting and rolling into a continuous process [110], and continuous annealing lines that integrate cleaning, heating, cooling, temper rolling and refining in a single line [102, 111].

Digital control system is an integrated monitoring and control system which is mainly composed of direct digital control computers, sensors and devices. It provides loop control and advanced control of process with a standard of set value of process computer [112]. Based on real-time monitoring each iron and steel production step, the processing data will be collected and sent by digital control system, which will increase the operation efficiency of equipment and savings of energy and cost. Many mathematical models and control systems, as well as advanced testing equipment like material level instrument, device for continuous measurement of permeability, multi-gas analyser, laser contouring system, neural networks, etc. have been developed successively by large-scale iron and steel enterprises. Other measures concern general crosscutting utilities that apply to the industry, e.g. energy monitoring and management systems, preventive maintenance practices [81].

Table 2.4 summarises general energy-efficient devices, technologies and their characteristics according to iron and steel production routes. The emerging technologies generally have the higher investment cost and difficulties to replace existing construction. But they are still attractive opportunities to reduce emissions and energy consumption for iron and steel industry in the future.

Table 2.4: List of energy-efficient devices for iron and steel industry.

Process	Technologies	Improvement effect	Investment cost	Limitation	Ref.
Sinter	Partial recycling of waste gas from the whole strand	Reduce coke breeze consumption by 10–15%	$ 18.6 million [a]	Operational flexibility of the strand	[53]
	Multi-slit burner in ignition furnace	Reduce ignition energy by 30%	-	-	[81]
Coking	CDQ	Generate 0.5-0.7 t steam·t^{-1} coke and 0.504-0.67 electricity·t^{-1} coke	$ 99.3·t^{-1} coke	Coke blowing up and carrying-over phenomenon	[51, 113]
	Single chamber system coking reactor	Improve thermal efficiency from 38% to 70%	-	Mostly considering for new plants	[51]
	Non-recovery coke ovens	Produce 2.3-2.5 GJ electrical power·t^{-1}coke	$ 365 million [b]	Emission requirements and demand of steam quality	[53, 81]
	SCOPE21	Reduce 21% energy consumption	Reduce 18% and 16% production and construction cost	-	[81]
BF	Top combustion HBS	Save energy in the hot stove by 1-2% (5000 m^3 BF)	-	Impossible to replace the existing stove/difficult to control gas-air ratio	[106]
	Kalugin shaftless hot stove	Increase thermal efficiency by 8-12%	$ 9.58 million (2500 m^3 BF)	-	[17]
BOF	BOF bottom stirring	Reduce flux quantities by more than 10%	-	Difficult to maintain the continuation of effective stirring	[107]
EAF	DC arc furnace	Save 0.036-0.32 GJ·t^{-1} steel	$ 22.13 million [c]	-	[49]
	Comelt furnace	Save 0.36 GJ·t^{-1} steel	Reduce maintenance costs	-	[33]
	Contiarc furnace	Reduce energy losses by 0.792 GJ·t^{-1} steel	-	-	[51]
	Post-combustion shaft furnace	Reduce 0.28-0.4 GJ electric power·t^{-1} liquid steel	Customised operating cost	-	[51, 114]
	ECOARC™	Save 0.36 GJ·t^{-1} steel	More initial costs in a short term	-	[102]
	ECOARC light™	Save 0.252-0.288 GJ·t^{-1} steel	Lower initial cost	-	[102]
	Ultra-high power transformers	Save 0.061 GJ·t^{-1} steel	$ 3.9·t^{-1} steel	Installation sites	[51]
	Eccentric bottom tapping	Save 0.054 GJ·t^{-1} steel	$ 4.5·t^{-1} steel [d]	Limited by the size, type and life of the existing one	[51]
Casting/ Rolling/ Finishing	Rapidfire™ edge heater	Save energy by 28%	Lower installation cost	-	[108]
	Flameless oxyfuel combustion	Increase 50% heating capacity and decrease 40% fuel consumption	Depend on the cost of oxygen	High CO_2 concentrations during oxy-fuel coal combustion	[109]
	Walking beam furnace	Reduce 25% electricity and 37.5 fuel consumption	Lower operation cost	Mostly by means of natural gas	[51]

Process	Technologies	Improvement effect	Investment cost	Limitation	Ref.
	Regenerative burner	Save 800-1000 crude oil equivalent·year^{-1}	Lower maintenance cost for ladle refractory	-	[49]
	CC machine	Reduce 0.072-0.108 GJ power·t^{-1} steel	\$ 99.29·t^{-1} steel	Solidification control	[49, 115]
	Castrip® process	Save energy by 80-90% over conventional methods	Lower capital cost	High heat flux	[116]
	Endless strip production	Reduce energy by 45%	Lower investment and processing cost	-	[110]
	Continuous annealing line	Reduce fuel consumption by 33%	\$ 225 million [e]	High installation costs	[33, 102]
Integrated improvement	Strengthen heating furnace radiation	Save 0.191 GJ·t^{-1}	\$ 0.56 million (1.5 million t heating furnace)	-	[117]
	Improved process control	Save 0.05–0.4 GJ·t^{-1} product	\$ 0.19–1.56 ·t^{-1} steel	-	[51]

[a] The investment of a total waste gas flow of 1.2 million Nm^3·h^{-1} from three sinter strands was EUR 17 million in Netherlands. The cost was converted to USD according to current exchange rate in April 2020.

[b] The investment includes the coke oven facilities, coal handing and the power plant for a 1.2 million t coke·year^{-1} greenfield heat recovery plant in 1998, US.

[c] The investment includes equipment cost JPY 2000 million and construction cost JPY 400 million. The cost was converted to USD according to current exchange rate in April 2020.

[d] The investment only includes modification cost which is for a Canadian plant with an annual production capacity of 760000 t.

[e] The investment is for a continuous annealing facility with a capacity of about 5000000 t·year^{-1} in US.

2.3.3 Outgoing flow utilisation

The useful outputs from global steel production can be recycled during the making process or sold for use by other industries. The main by-products generated from iron and steel production are slags (90% by mass), dusts, sludge and by-product gas [118]. Molten slag and process gas are all exhausted at different temperatures which carry a great deal of waste heat. Considering local and global steel production, by-products as value-added products or extra energy output, become environmental concerns and cost-saving opportunities in industrial applications [119]. This section mainly focuses on the direct utilisation of by-products and wastes. Waste heat utilisation from slag and by-product gas will be separately illustrated in Section 2.3.

a) Utilisation of slag and dust

Slag in steel industry can be classified into BF slag and steel making slag [120]. BF slag has been categorised into three main types by the cooling ways, i.e., air-cooled, granulated, and pelletised (or expanded). BF slag can be safely used as the raw material in the cement industry due to the low iron content. Steel making slag uses similar cooling method as air-cooled BF slag which could be reused in soil conditioners and fertilisers.

For iron and steel metallurgical processes, dust and sludge are collected in the aspirating equipment. Before BFG is recovered by a top pressure recovery turbine (TRT) generator, a dry-process dust collector will be used for cleansing BFG. Two typical dry-process dust collectors have been used to avoid large temperature and pressure loss of the gas that passes through the dust collector, bag-filter collectors and electrostatic precipitators [121]. Since BF dust generally contains high level of carbon and iron, it can be recycled through sinter making process. The effectiveness of BF sludge has been investigated as an adsorbent to purify contaminated solutions. Steel making sludge needs to be optimally dried and become operable before recycling. The agglomeration of steel making sludge could be the ideal approach to maximise its use in sinter feed [122].

Table 2.5 lists specific characteristics and general recycling technologies of slag, dust and sludge in iron and steel industry. Utilisation of solid by-products can prevent them from being transported to landfill, which can save natural resources as well as significantly reduce CO_2 emissions [118].

Table 2.5: List of slag and dust recycling technologies for iron and steel industry.

Source	Characteristics	Recycling technologies	Ref.
BF air-cooled slag	Hard and dense	Make construction aggregate; Used in concrete-based products, road, clinker raw material, railroad ballast, roofing, mineral wool and soil conditioner	[118]
BF granulated slag	Sand-sized particles of glass	Make cementitious material	[123]
	Crystalline and amorphous BF slag	Used as an adsorbent of phosphate from water solutions	[124]
BF pelletised slag	Vesicular texture	Make lightweight aggregate	[118]
BF flue dust and sludge	High level of iron oxides and coke fines	Produce sinter	[125]
	High carbon content of the sludge	As an adsorbent for Cu^{2+} from aqueous solutions; As a reducing agent to remove zinc from the steel making dusts.	[122, 126]
BOF slag	High density and a high crushing strength	Produce concrete	[127]
	The content of calcium and magnesium silicates	CO_2 sequestration	[127]
	The phosphorus content of slag	As fertilisers for crops	[128]
	Hard characteristics	Used as the base and sub-base layer of road	[122]
	High porosity and large surface area	Marine applications	[127, 129]
BOF dust and sludge	Very high iron and appreciable amount of CaO content	Recycled to iron and steel industry; Land filled, road bed and cement production.	[122]

b) By-product gas recovery and conversion

Three main by-product gases i.e., COG, BFG and LDG are generated in the processes from coal to steel as shown in Figure 2.12. The concerning component, heat value and quantity of by-product gas are indicated in Table 2.6. In general, these streams contain similar compound with different proportions [34]. By-product gases utilisation from integrated iron and steel works can be divided into three main categories:

- To serve as a fuel for power generation in a nearby power plant or reuse as fuel for steel plant.
- To recover the valuable compound, e.g., H_2 and CH_4.
- To obtain a high value-added product, such as methanol, dimethyl carbonate, etc.

As the first generated gas, COG is produced from dry distillation of coking coals in the absence of oxygen. It could be not only used as a heating source but also mixed with BFG for power generation. Besides, COG can potentially generate a high value added products by reacting with CO_2 and CO [130]. BFG serves as a by-product of BF in the furnace process. It is used to blend with other gases e.g. natural gas for combustion to generate the power, which could be combined with steam cycles for a higher efficiency of 42% in steel mill applications. Besides, it could increase furnace temperature through combustion [131]. LDG is created from pig iron during the steel making process.

LDG recovery is the most energy-saving technology in the BOF process [33]. By-product gases have a close relationship with reduction of primary energy while it is quite significant for thermal utilisation. The above two applications will be discussed in different following subsections. This part mainly focuses on recovering by-product gases for valuable compound and producing a high value-added product.

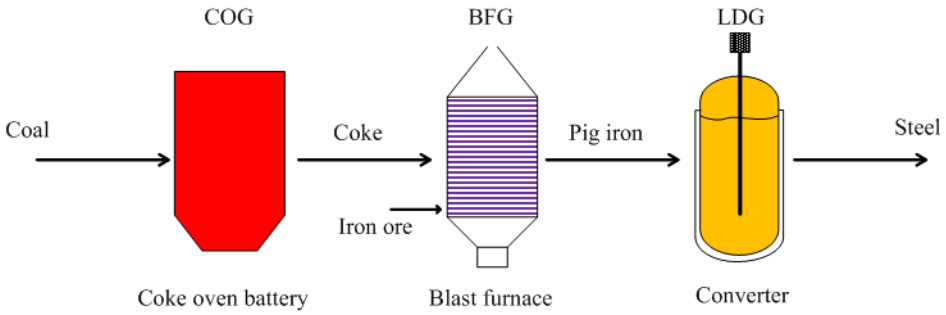

Figure 2.12: The main operating processes of by-product gas.

Table 2.6: The properties of by-product gas in iron and steel industry [34, 132].

Type	Source	Chemical composition	Heat value ($kJ \cdot m^{-3}$)	Production/t product
COG	Coke oven battery	H_2: 45–64%; CH_4: 20–30%; CO: 5–10%; CO_2: 2–5%; O_2: 0.1–4%.	16000–19300	400-450 $m^3 \cdot t^{-1}$ coke
BFG	BF	H_2: 4%; CO: 25%; CO_2: 20%; N_2:41%.	3000–3800	1400-1800 $m^3 \cdot t^{-1}$ iron
LDG	Converter	CO_2: 15–20%; O_2: ≤2.0%; CO: 60–70%; N_2: 10–20%; H_2≤1.5%.	7500–8000	80-100 $m^3 \cdot t^{-1}$ liquid steel

Considering valuable compound recovery, H_2, CH_4 and CO are the primary candidates. Due to their different proportions in off-gas, it may cause different recovery levels. H_2 and CH_4 are easier to be recovered from COG, and CO is usually recovered from BFG. The main recovery technologies could be pressure swing adsorption (PSA) and membrane separation process (MSP). Cryogenic separation is also suitable to be applied if gas proportion and external conditions are satisfied. It is demonstrated that 90% of H_2 could be recovered by using PSA with a purity up to 99.99%. Comparably, 80–98% of H_2 could be recovered with a purity of 90–99%. By using PSA or MSP, the

quality of CH_4 concentrated stream may be improved. Only PSA and chemical absorption systems are suitable to separate CO from BFG due to high proportion of N_2 [34]. These two systems are also applicable for separating CO_2 from BFG and LDG. Activated methyldiethanolamine (MDEA) is a common solvent for CO_2 absorption [133]. Another possibility for CO_2 capture is to convert CO contained in BFG and LDG into CO_2 for concentrating the stream [134]. This process can be accomplished by using water gas shift reaction under high temperature and pressure. The absorption solvent will be used to separate CO_2 generated from shift reaction [133].

Coke oven gas is highly rated as a feedstock to obtain the value-added products due to its high content of organic compound. Syngas production from COG is mainly composed of steam reforming, dry reforming and partial oxidation processes [135]. The steam reforming of CH_4 is currently the main technology for syngas production. The CO_2 (dry) reforming is regarded as the alternative processes to steam reforming, which has been widely proposed. The partial oxidation of CH_4 is a mildly exothermic reaction, which is more cost-efficient. H_2/CO ratio of syngas from the partial oxidation is between that of syngas obtained from steam and dry reforming. It is possible to synthesise methanol with the use of COG-derived syngas when it is produced from dry reforming at a H_2/CO ratio close to 2 [136]. COG with rich H_2 contents is considered to be ideal for a sustainable methanol production as it can meet the criteria of resource utilisation and environmental protection [135, 137]. Half of CO_2 produced upon methanol consumption will be recycled in the dry reforming process [138]. Synthetic natural gas could be produced through a co-methanation reaction of CO and CO_2 (CO_x) in COG for CH_4 enrichment by using appropriate catalysts [135]. Ni-based catalysts have been widely employed for methanation reaction because of their high selectivity for CH_4 and low cost [139]. Ni/MgO/Al_2O_3 catalysts exhibit excellent activity, stability and resistance to carbon deposition for the catalytic conversion of tar in H_2-rich hot COG [140].

Table 2.7 summarises the selected research studies for off-gas recovery and thermochemical by-product gases in terms of simulation, experiment and techno-economic analysis.

Table 2.7: Selected research works for off-gas recovery and thermochemical by-product gases.

Gas	Use	Experiment/Simulation	Remarks	Ref.
COG	H_2 recovery	Thermal analysis& experiment	Layered beds are filled with zeolite 5A for a seven-step two-bed PSA process for producing H_2	[141]
COG	H_2 recovery	Thermal analysis& experiment	H_2 separation process is segmented into four sections in terms of the saturated temperature and content of the components in COG	[142]
COG	H_2 and CH_4 recovery	Experiment	A prism membrane is used to purify COG; H_2 and CH_4 have the purity higher than 90% and 60%	[143]
BFG	CO_2 and CO recovery	Experiment	A bench scale PSA plant is constructed; 6.3 t CO_2 is recovered with a 225 seconds cycle time and 33% CO_2 concentration of raw gas	[144]
LDG	CO recovery	Experiment	A first CO-PSA commercial plant was constructed in 1989; The product CO capacity of plant is 150 $N \cdot m^3 \cdot h^{-1}$	[145]
BFG	CO_2 separation	Economic analysis	The polymeric gas separation membrane is used to separate CO_2; Cost is from \$ 25-36$\cdot t^{-1}$ CO_2 [a]	[146]
BFG&LDG	CO_2 separation	Experiment	CO_2 is recovered by absorption in a Selexol® process	[133]
COG	H_2 production by reforming	Simulation	The sorption-enhance steam reforming can obtain higher amount and purity of H_2 than those in the common steam reforming	[147]
COG	Syngas production	Experiment	The H_2-rich COG is converted to syngas via the partial oxidation and CO_2 reforming at a high space velocity and lower temperature	[148]
COG	Methanol production	Experiment	The production capability of COG has reached 2.06 million tons	[137]
COG&LDG	Methanol production	Thermal analysis& experiment	The stored heat from the intermittently emitted LDG is supplied to COG; Methanol is finally produced from the obtained gas	[149]
COG&LDG	Methanol production	Techno-economic analysis	Using excess COG and 40% of the available LDG to produce methanol shows efficient gas utilisation	[150]
BFG&COG	Higher alcohol production	Environmental and economic evaluation	Using BFG&COG, higher alcohols are produced and annual CO_2 emissions reduction is 14820 t	[151]
COG	COG methanation	Experiment	Toluene could be completely converted into CH_4, CO and CO_2 over bimetallic catalysts	[152]

[a] The cost for a two stage membrane process which recoveries CO_2 up to 99% and keeps inert N_2 below 5% is EUR 23-33$\cdot t^{-1}$ CO_2. It was converted to USD according to current exchange rate in April 2020..

2.4 Efficient technologies for secondary energy

It is obvious that the secondary energy is considered to be utilised after primary energy is explored as much as possible. This is mainly because the mass network optimisation in primary energy is mainly based on the single process and flow improvements. Secondary energy resources are considerable which are produced during the steel making processes. These resources could be converted into steam or other forms such as power, heating and cooling output to meet the concerning requirements in the iron and steel works.

Secondary energy resources can be categorised into by-products and waste heat. Compared with the utilisation and conversion of by-product in Section 2.3.3, utilisation of by-products for secondary energy recovery are possible in three different forms: recovery as hot air or from steam, conversion of waste heat through chemical reaction, and the use of thermoelectric power generation [15]. The rest of waste heat from iron and steel production processes could be categorised by dividing temperature range into low, medium, and high-quality sources, and the range could be different when considering different classification criteria. Temperature of high-quality heat source is generally higher than 500°C, which includes high temperature heating furnace flue gas, high temperature liquid, and high temperature solid e.g., sintering materials, coke and steel. Temperature of medium quality heat source usually ranges from 150°C to 500°C, including sintering flue gas and hot stove flue gas. Low quality of heat source is commonly lower than 150°C, including waste steam, hot water, all kinds of low temperature flue gas and low temperature materials [8].

2.4.1 Utilisation of by-product for secondary energy recovery

This section mainly focuses on recovering secondary energy from by-products, i.e., high temperature slag and furnace gases in terms of heating and power generation.

a) Slag thermal utilisation

Blast furnace slag in iron-making process is discarded at the high temperature of 1450-1650°C [120]. Steel making slag is formed in a molten or red-hot state at a temperature of 1300-1700°C [153]. Therefore, a great deal of high-grade heat is carried with the slag which accounts for 10% of waste energy and 35% of high-temperature waste heat in steel industry. Compared with utilisation of slag in Section 2.2.3, high-temperature waste heat recovery technologies of slag are vital to achieve energy

saving and emission reduction in the iron and steel industry. Current heat recovery technologies can be generally classified into physical and chemical methods. Physical methods have been widely investigated, for example mechanical crushing, air blast and centrifugal granulating process. With respect to chemical methods, CH_4 reforming reaction and coal gasification process take the leading roles. These waste heat recovery and utilisation technologies have been partially reviewed [154]. Table 2.8 lists selected researches for molten slag sensible heat recovery under different methods.

Table 2.8: Selected researches for molten slag sensible heat recovery technologies.

Slag	Heat recovery technologies	Research/ Demonstration	Remarks	Ref.
Physical method				
BF slag	Mechanical impingement	Not for a long-term commercial use	Generate 250°C saturated steam and 65% heat recovery rate	[155]
BF slag	Stirring crushing	Experiment	Recover 59% of slag energy	[156]
BF slag	Rotating drum process	Experiment	Heat recovery rate of 40-60%	[154]
BOF slag	Air blast method	Demonstration	Recover 41% and 39% of heat by the steam and hot air	[157]
BF slag	Air blast by rotating cup atomiser	Demonstration	Recover 59% of the slag heat	[157]
BF & BOF slag	Spinning granulating	Demonstration	Obtain hot air at a temperature of above 600°C	[157]
Chemical method				
BF slag	Drive thermoelectric power generation device	Simulation	Produce 0.93 kW power per square meter heat transfer area and achieve 2% conversion efficiency	[158]
BF slag	Produce H_2-rich gas by wet sludge gasification	Experiment	Heat recovery rate of 64.35%	[159]
BF slag	Produce H_2-rich gas by catalytic pyrolysis of biomass	Experiment	Achieve complete pyrolysis of biomass	[160]
BF slag	Produce syngas by bio-oil dry reforming	Experiment	The conversion of optimal bio-oil can reach 90.15%	[161]
BF & BOF slag	Biomass gasification	Experiment	Recover 1.1 MJ heat from the slags·kg^{-1} biomass	[162]
BF slag	Steam gasification of coal	Kinetic analysis	BF slag accelerates the gasification rate	[163]
BF slag	Pyrolysis of printed circuit boards	Experiment	The boards are effectively pyrolysed with a slag/board ratio of 5:1	[164]
BF & BOF slag	Convert hot slag into qualified raw materials in cement, concrete and road pavement	Demonstration	The upper limit proportion for the amount of modifiers is about 19–25 wt.%	[165]
BF & BOF slag	Convert hot slag into glass ceramics, mineral wool and potassium silicate fertiliser	Demonstration	The energy save rate is up to 80%	[165]

b) By-product gas for thermal utilisation

As mentioned above, by-product gas is a main part of secondary energy resources, which accounts for 30–40% of total energy consumption of iron and steel industry. In addition to direct utilisation of by-product gases illustrated in Section 2.2.3, the gases can be served as a fuel by means of their thermal and chemical energy. For thermal use, the gases are burned for heating different furnaces, steel before rolling, slabs or fed to a thermal power plant. It is indicated that most steel mills in Europe have developed thermal integration projects and Chinese steel mills start to convert COG into liquefied gas.

Coke dry quenching recovers the sensible heat of red-hot coke by using inactive gas in a dry process. After coke is cooled to approximately 200°C, the circulating gas has been heated up to 800°C or higher which could generate high temperature and pressure steam in the boiler. The steam is used as process medium or driving force for power generation [166]. During iron smelting process, BFG has a pressure of 2-2.36 bar and temperature of approximately 200°C at the top of furnace. Equipping TRT unit is the best way to recover the thermal energy contained in the BFG [167]. Energy is recovered by means of an expansion turbine which is installed after the top gas cleaning device [53]. TRT systems are categorised as wet and dry systems, depending on the method that they use to remove the dust particles. A typical modern TRT of the dry type generates 0.055 $MWh \cdot t^{-1}$ of pig iron under the condition of high-pressure operation of the BF, whereas a wet-type TRT generates 0.03 $MWh \cdot t^{-1}$ of pig iron [50]. The schematic flow diagram of wet and dry TRT processes is shown in Figure 2.13. Other case studies using by-product gases for thermal use in iron and steel industry are summarised in Table 2.9.

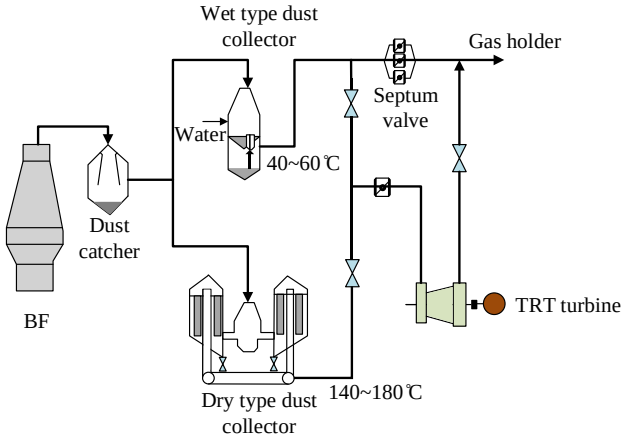

Figure 2.13: The schematic flow diagram of wet and dry TRT systems [49].

Table 2.9: Selected cases for thermal utilisation of by-product gases.

Gas type	Use	Steel company/Location	Remarks	Ref.
BFG&COG	Power generation	ArcelorMittal Tubarão/ Brazil	Three power plants are based on Rankine regenerative cycle; Plant 1 and 2 generate 132 MW whereas Plant 3 produces 69 MW	[168]
BFG&COG	Power generation	-/China	On-site test of using the recovered waste fuel gas to power the boiler; A high stability could be achieved	[169]
BFG&COG	Power generation	Alchevsk Coke Plant/Ukraine	Use 9 MW turbine generator to generate a net annual power of 54×10^3 MWh	[170]
BFG&COG	Heating and power generation	Sandvik AB (scrap-based steel plant/Sweden	Gases are to drive combined heat and power (CHP) plant for power generation and district heating; TRT technology is used to generate electricity with 0.04-0.06 MWh electricity$\cdot t^{-1}$ of iron	[13]
COG	Power generation	Profusa/Spain	Plant power output could reach 8.95 MW	[171]
COG	Heating and power generation	Shandong Jinneng Coal Gasification Co., Ltd./China	Power output is around 0.0016 MWh$\cdot m^{-3}$ with 3.09 kg simultaneous steam production	[135]
LDG	Power generation	Aceralia/Spain	Plant power output could reach 0.0121 MW	[171]
LDG&COG	Heating and power generation	-/Spain	When the energy is produced only with LDG&COG, 169.42 $Nm^3\cdot$MWh of natural gas are saved	[172]

2.4.2 Waste heat usages

a) Heating

Heat exchanger is the most investigated methods to recover waste heat in the iron and steel industry. Recuperators, regenerators, and heat pipe are used for preheating and reheating [19]. Recuperator has a variety of types, which are determined by heat transfer methods in terms of simple radiation, convective, tube type, combined radiation and convection type. It usually exchanges high temperature heat which comes from either metallic or ceramic materials. Regenerators are more frequently used for coke ovens, which are adopted to preheat the hot blast and blast stoves used in iron making. Regenerative furnaces are composed of two grid chambers and each contains refractory material i.e., the checker. In one chamber the combustion gases pass through the checker and enters the furnace in the other chamber, and the checker is heated, or regenerated with the outgoing hot exhaust gas. The furnace operates alternatively, and the flow is reversed so that the new combustion air can be heated by the checker. A typical diagram of regenerative furnaces is shown in Figure 2.14.

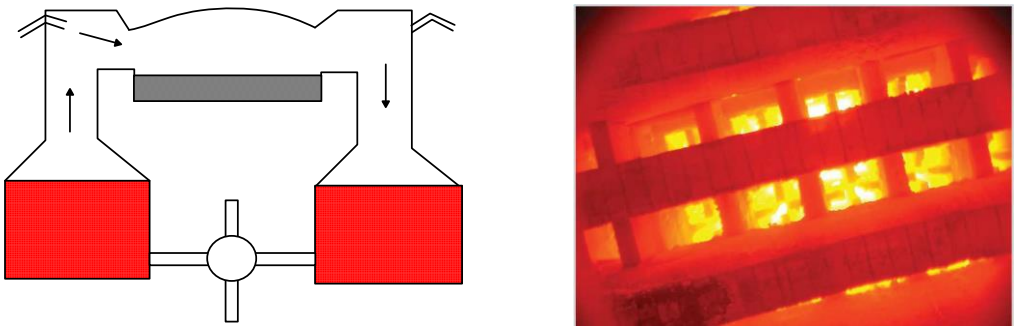

(a) (b)

Figure 2.14: A typical diagram of regenerative furnace (a) schematic, (b) photo [4].

As a common heat exchanger in steel mill, waste heat boiler is suitable to recover heat from medium to high temperature exhaust gases and is used to generate steam as an output which can be used for power generation or back to the system for energy recovery. It mainly consists of water tubes that are placed in parallel to each other and in the direction of the heat leaving the system [15]. An auxiliary burner is usually needed if the waste heat is not sufficient to produce the required amount of steam [173]. Sensible heat of coke can be captured by CDQ in which hot coke is quenched by inert gases and the recovered thermal energy is used to generate steam in a downstream boiler [174]. When the BOF uses the open combustion system, a waste heat boiler is always required to recover waste

heat which results from the reaction of oxygen in the furnace gas duct [15].

Another heat recovery device is the gas to gas passive air preheater for low to medium temperature, which could be generally divided into plate type and heat pipe. Plate type is quite common which has different parallel plates for hot and cold gas flow [175]. Considering heat pipe type, working fluids are operated between hot and cold ends of each pipe which has a capillary wick structure [176]. Ma et al. [19] designed and established a waste heat recovery experimental system by using a heat pipe heat exchanger for recovering the heat in a slag cooling process. It is indicated that heat transfer performance is improved by using online cleaning device. Thermal resistance of outer surface is reduced by removing the dirt.

Heat pump is thermodynamically originated from an inversed Carnot cycle, which happens in the opposite direction of spontaneous heat transfer. Based on this thermal cycle, it is defined as a device that could absorb heat from a relatively cold source and release it to a hot source by consuming a small amount of external power [177]. Heat pump systems show great potentials to extract heat from various heat sources. For instance, cooling water in the iron and steel industry which could be used for the antifreeze of coke, crush and sieving system, and district heating of office and operating rooms. It is worth noting that the upgraded heat should be reused in industrial processes of steel work. It is meaningless to upgrade the heat source for power generation or other energy conversion systems by using heat pump systems though energy efficiency will be improved slightly. Table 2.10 summarises selective case studies of heat to heat technologies in steel and iron industry.

Table 2.10: Selected studies of heat to heat technologies for iron and steel industry.

Process	Waste heat recover method	Technologies	Remarks	Ref.
Sintering	Recover the sinter cooler's exhaust gas as steam, and reuse of exhaust heat as thermal source of sinter production	Recirculation	The system allows up to about 60% of exhaust heat from the sinter cooler to be reused as steam or electricity	[178]
Coking	Preheat the coke oven using the remaining recycled gas	Regenerator	Regenerators are suitable for high temperature applications with dirty exhausts	[15]
	Extract hot gas from the oven flue gas to provide a heat source	Radial heat pipe	The system can produce saturated steam $0.19 \cdot t^{-1}$ coke	[179]
	CDQ to generate steam	Waste heat boiler	For a plant with 450000 $t \cdot y^{-1}$ coke capacity, 450×10^3 $MWh \cdot y^{-1}$ steam can be produced	[49, 51]
Iron making	Recover waste heat from the combustion exhausts for reheating the BF and preheating the combustion air	Regenerator	The typical operating temperature of reheating furnaces (1350°C) is achieved without natural gas enrichment	[15, 180]
	Hot stove waste heat recovery device	Rotary, plate and heat pipe	The recovery rate of hot stove flue gas sensible heat ranges from 40-50%	[49]
	Recover waste heat from cooling water	Heat pump	Waste heat can cover 50% of the total heat need from Nyköping city	[181]
Steel making	Recover waste heat from the furnace gas duct	Waste heat boiler	0.19 $GJ \cdot t^{-1}$ energy can be saved when implementing heat recovery method	[84]
	Recover waste heat in a slag cooling process	Heat pipe	As waste water mass flow rate varies between 0.8-1.9 $m^3 \cdot h^{-1}$, effectiveness of the exchanger ranges from 0.085-0.192	[19]
Rolling	Recover waste heat in a steel wires cooling process	Flat heat pipe	Heat recovery rate during laboratory test is 0.005MW and in the industrial test is 0.01 MW	[18]

b) Power generation

For low grade heat recovery, power generation technologies are still considered to be the major energy conversion methods if no heating, cooling or other demands are required to be satisfied. Thermal driven power technologies have various thermal cycles in terms of different heat source temperatures. Rankine cycle is a typical thermodynamic cycle which converts waste heat to mechanical power. The suitable temperature for steam Rankine cycle is better to be higher than 340°C. Otherwise, the cycle becomes less efficient due to low pressure steam [182]. Performance of ORC and KC are better than that of Rankine cycle when using low temperature heat source. Similar with Rankine cycle, organic working fluids with low boiling point temperatures are adopted to utilise the lower temperature heat source such as industrial waste heat and solar heat. Low temperature heat is transferred into useful work output [183]. The most appropriate temperature range for ORC depends on the selected refrigerant, which will have an influence on thermal efficiency. Nonetheless, the main disadvantage of Rankine type cycle is that the endothermic evaporation process keeps constantly boiling which could not well match the trend of heat source. Due to the large temperature difference, energy efficiency cannot be further improved. Comparably, KC was invented in the 1980s. It has a variable temperature gradient in the evaporating process by using binary mixture of ammonia and water, which could bring about a relatively high energy efficiency [184]. Besides, thermoelectric power generation and thermophotovoltaic systems are being developed that can generate electricity directly from heat [185, 186]. Table 2.11 indicates heat to power cycles for waste heat recovery in terms of heat source type, temperature range, thermal efficiency and capital cost. Rankine cycle and KC have the relatively high suitable temperature range of heat source whereas ORC has a lower temperature range. Thermoelectric generator (TEG) may have a wider temperature range by using various TEG materials. However, this technology has a lower thermal efficiency which hasn't been large-scale demonstrated in the iron and steel industrial section and its capital cost is higher than other power generation technologies [187].

Table 2.11: Heat to power cycles for waste heat recovery [4].

Cycle	Heat source	Temperature	Thermal efficiency	Capital cost
Rankine cycle	Exhaust from furnaces.	340-550°C	28%-42%	\$ 1.1-1.4·MW^{-1}
KC	Exhaust from furnaces or boiler.	100-400°C	19%-38%	\$ 1.1-1.5·MW^{-1}
ORC	Gas and boiler exhaust, heated water	70-300°C	4%-10%	\$ 1.5-3.5·MW^{-1}

Thermoelectric Generation	Not yet demonstrated in industries	150-1000°C	2-10%	$ 20-300·MW^{-1}
Thermophotovoltaic systems	Exhausts from CC	1000-1500°C	2-7%	$ 0.4-3.4·MW^{-1}

One representative case of KC in steelwork is shown in Figure 2.15 which is in Kashima Steel Works of Japan. The demonstration operated by Sumitomo Metals has successfully recovered waste process heat and generating 3.45 MW sustainable power since the September of 1999. More than a decade after installation, KC power plant continues to operate efficiently and reliably [188]. For demonstration of ORC systems, Ramirez et al.[20] presented a project i.e., a large-scale ORC plant in a steel mill which has been installed at ORI MARTIN in Brescia (Italy). Waste heat was recovered from the fumes of the EAF to produce saturated steam which was then delivered to the ORC for power generation. The ORC system has a power output of 1.8 MW and a net efficiency of 21.7%. Table 2.12 indicates selected case studies of KC and ORC systems in steel and iron industry.

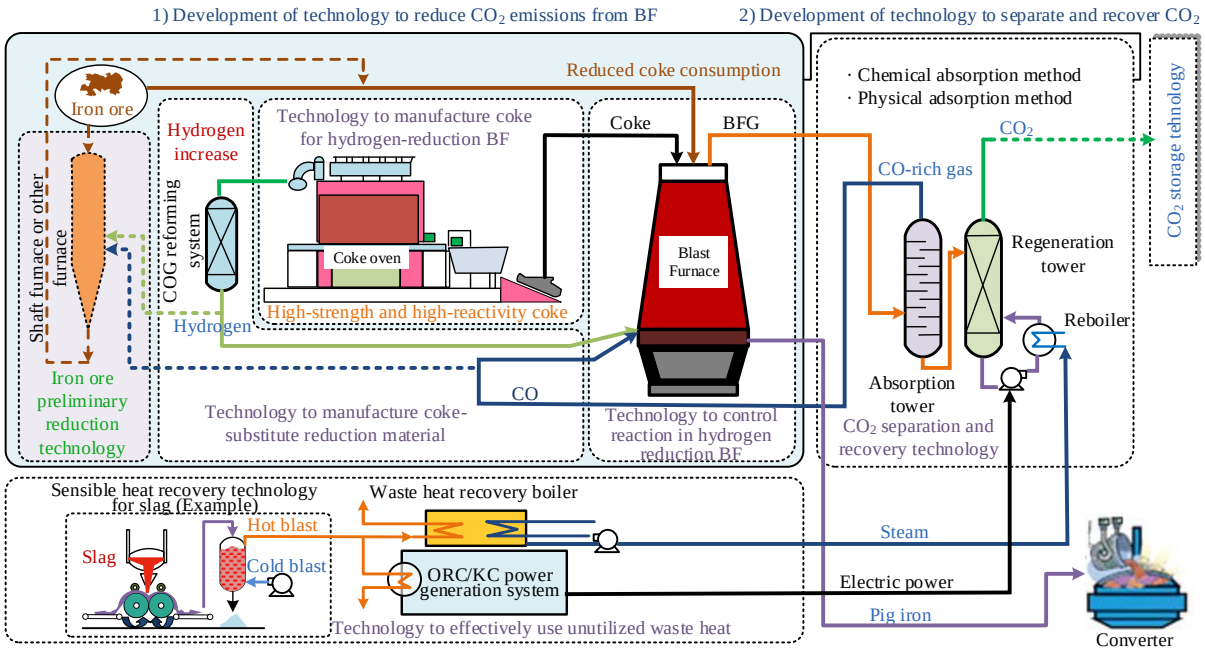

(a)

(b)

Figure 2.15: Case of KC demonstration with steel industry (a) schematic, (b) photo [189].

Table 2.12: The demonstration studies of KC and ORC systems for steel and iron industry.

Waste heat	Cycle	Working fluid	Remarks	Ref.
Waste industrial heat source/98°C	KC	Ammonia water	4.5 MW power output is achieved with a water flow rate of 1300 t·hour^{-1}; The total investment cost is about $ 4 million or about $1.1·MW^{-1}	[188]
Exhaust gas from coke production/ 221°C	ORC	Benzene	The net electric efficiency of 11% provides an electricity generation estimate of 80 MW·t^{-1} coke	[190]
Flue gases/529.6°C	ORC	Siloxane	ORC has a power output of 1.8 MW and a net efficiency of 21.7%	[20]
Residual heat from off-gas of reheating furnace	ORC	Siloxane	The 0.7 MW nominal capacity unit is installed operated by NatSteel in Singapore	[191]
Waste heat of off-gas from EAF/245°C	ORC	Siloxane	It is the world first ORC based energy recovery system at an Electric Steel melting plant in Riesa Germany, which could produce 2.7 MW nominal capacity	[192]
Waste heat from EAF /245°C	ORC	Siloxanes	An electricity output could reach 0.521 MW and 4.52 MW heat can be supplied for a CHP heat network	[193]
Waste heat from walking beam slab reheat furnace/122°C	ORC	R245fa	The ORC has a power output of 0.2518 MW and an energy efficiency of 10.2%	[194]

c) Refrigeration

Thermal driven refrigeration technology is another research hot spot for low grade heat recovery [195]. Compared with power generation cycle, the relatively low heat source temperature is further utilised due to their operational principle. Various thermal cycles could be adopted to realise cooling effect, e.g. absorption cycle and adsorption cycle.

Absorption refrigeration is basically composed of four components i.e., generator, evaporator, condenser and absorber. Through high pressure and low pressure level, heat could be converted to the cooling effect through generating process of generator and evaporation process of evaporator. The

common working pairs are ammonia-water and lithium bromide (LiBr)-water. Ammonia-water working pair could achieve freezing condition and air conditioning condition, which is mainly applied in freezer due to the fact its evaporation temperature can reach as low as -60°C. Lithium bromide-water working pair could only operate for air conditioning condition. The lowest thermal driven temperature lithium bromide-water absorption chiller is about 90°C which is much lower than ammonia-water system i.e., about 120°C [196]. For commercial use, lithium bromide-water absorption chiller has been the most commonly used unit. Similar to absorption refrigeration, adsorption refrigeration is composed of adsorber, desorber, condenser and evaporator. Heat could be converted to the cooling effect through desorption process of desorber in high pressure side and evaporation process of evaporator. It is based on solid-gas reaction using various working pairs in terms of water-based, e.g., zeolite as well as ammonia-based, e.g. $CaCl_2$, which could be generally classified into physical sorption and chemical sorption. Physical adsorption is driven by Van der Waals force whereas chemical reaction happens between the adsorbent and the adsorbate, and new types of molecules will be formed in the adsorption process [197, 198]. Currently, silica-gel water adsorption chiller is the only commercial product, which has a desorption temperature as low as 55°C [199, 200]. Table 2.13 generally summarises thermal driven refrigeration cycles for waste heat recovery in terms of working pair, driven temperature, thermal efficiency and their characteristics. Driving temperature and thermal efficiency are all related with constraint temperature. 5°C evaporation temperature is used for water chiller whereas -15°C evaporation temperature is mainly adopted for ammonia systems. LiBr-water absorption refrigeration could be applied to the iron and steel industry whereas silica-gel water adsorption system is relative mature technology in real application. Other types are required for further improvement though they have the potential advantages of achieving the freezing condition.

Table 2.13: Heat to refrigeration cycles for waste heat recovery [200, 201].

Cycle	Working pair	Status	Driving temperature/Thermal efficiency	Remarks
Absorption refrigeration	Ammonia-water	Demonstration	Double stage, 75°C/0.25; Basic, 120°C/0.55; Generator-absorber heat exchange, 120-160°C/0.8-1.4.	High pressure, achieve freezing condition
	LiBr-water	Commercial use	Double lift, 60°C/0.35; Single effect, 90°C/0.7; Variable effect, 90-135°C/0.8-1.1;	Suitable for solar energy air conditioning

			Double effect, 150°C/1.3.	
Adsorption refrigeration	Water-based, e.g. silica-gel water, zeolite water, etc.	Demonstration	Silica-gel water, 55-120°C/0.6; Zeolite water, 150°C/0.3 etc.	Simple structure and easy to control
	Ammonia-based, e.g. metal halide ammonia, etc.	Lab-scale	$CaCl_2$ ammonia, 120°C/0.3-0.4; $SrCl_2$ ammonia, 120°C/0.3-0.4 etc.	Achieve freezing condition
	Other-based, e.g. Activated carbon (AC) methanol	Lab-scale	AC methanol, 70-120°C/0.2.	Achieve freezing condition

For thermal driven refrigeration, it could be adopted as a separated technology, which is able to be integrated with power generation technology for extra cooling effect. It is generally acknowledged that power and refrigeration cogeneration is a desirable way for waste heat recovery in most applications of steel industry. The cogeneration could be generally classified into two types, i.e., combined cycle and cascading cycle. The combined cycle commonly achieves the cooling and power output in one working cycle [202] whereas cascading cycle is to produce the respect effect in a half cycle [203]. The combined cycle could reach a high thermal efficiency, and cascading cycle can gain a high exergy efficiency of heat source [204]. Although various cogeneration research studies have been investigated, less demonstration has been reported in iron and steel industry due to demands, cost, and space. Presenting these studies is to reveal the potentials and advantages of cooling technologies in real application which keeps the consistency and completeness of the heat driven options for thermal network in this paper.

Table 2.14 shows selected studies and demonstrations of thermal driven refrigeration which tend to be applied in steel and iron industry. Due to unique characteristic of ammonia-working pair, studies of combined cycle based on KC are comprehensively investigated. The cascading system by using the commercial technology is more suitable for real application. Thermal driven refrigeration e.g., LiBr-water absorption chiller and silica gel-water chiller could be good candidates as the second stage of cascading system for power and refrigeration cogeneration.

Table 2.14: Selected studies of thermal driven refrigeration in steel and iron industry.

Waste heat	Cycle	Working pair	Another cycle	Research	Remarks	Ref.
Exhaust gas /350°C	Absorption	Ammonia-water	KC	Thermal analysis	Thermal and exergy efficiency are 24.2% and 37.3%	[205]
Exhaust gas /450°C	Absorption	Ammonia-water	KC	Thermal analysis	18.2% reduction is realised in energy consumption	[206]
Hot water/ 140°C	Absorption	LiBr-water	ORC	Simulation	The system reaches thermal efficiency and exergetic efficiency of 38% and 26 %	[207]
Hot water/above 75°C	Absorption	LiBr-water	ORC	Simulation	The simulated thermal efficiency of the combined cycles is improved by 1.5%	[208]
Hot water/95°C	Adsorption	$CaCl_2$-$BaCl_2$-NH_3	ORC	Thermal analysis	Energy and exergy efficiencies are 10.1-13.1% and 18.5-20.3%	[203]
Hot oil/140°C	Adsorption	Silica-gel/ AQSOA-ZO2/MOF water	ORC	Thermal analysis	Maximum adsorption power efficiency is 4.3% using silica-gel, while maximum ORC power efficiency is 18.3% using R141b	[209]
Flue gases/250°C	Adsorption	Silica-gel water	ORC	Experiment (Demonstration)	Two systems are cascaded to produce 3 MW electricity and 0.05 MW cooling power	[210]

2.5 Summary

Iron and steel industry consumes considerable primary and secondary energy. Improving energy efficiency are developed in terms of steel products, technologies and operating practices which could more or less reduce energy consumption, respectively. To further explore the potentials of energy saving, the demands and supplies should be considered from an overall perspective.

In this chapter, a comprehensive literature review of primary and secondary energy saving and decarbonised technologies of iron and steel industry are developed. Detailed metallurgical routes of iron and steel production are described. The contributions have been classified into three levels. First, the overarching energy consumption in iron and steel industry is presented. Second, independent and interdependent primary and secondary energy technologies are clearly reviewed and compared. Primary energy technologies aim to reduce the energy demands while the secondary energy technologies consider the conversion of thermal energy. Finally, the review found that fuel substitution technologies and waste heat recovery technologies have wide application prospects in iron and steel industry. Although these technologies have been practiced in many iron and steel cases, the combination of two kinds of measures and an overall optimisation of integrated system have rarely been studied. The following chapters will mainly revolve around this research gap.

Chapter 3

Process simulation of iron and steel plant

Global crude steel production climbs with the increase of the demands, which has grown by seven times since 1950 and it is expected to increase by 1.5 times before 2050 [211]. Inevitably, the continuous increase in steel production and consumption will bring about an increase in industry's energy use. In this chapter, a process simulation based on a real iron and steel plant with a 4.7 Mt annual steel capacity in the UK is developed for further investigation of energy saving technologies and mass-thermal network optimisation. Current development of iron and steel industry in the UK are summarised. Details of mass and energy balances of each process are described here.

3.1 Current status of iron and steel industry in the UK

Iron and steel industry is the largest industrial sector in the UK in terms of energy demand and greenhouse gas (GHG) emissions which account for 25% of GHG from UK manufacturing (as seen in Figure 3.1) [212]. Large amounts of GHG emissions result from major consumption of coal in iron and steel industry. As shown in Figure 3.2, coal consumption peaked at 264PJ in 1973, and declined dramatically to 25PJ in 2017, but it is still a crucial energy source of the UK iron and steel sector. The rest of the final energy consumption come from natural gas, electricity and petroleum. The use of natural gas grew to the peak at 73PJ in 2000 but it began to fall after that. Primary electricity shows the highest consumption at 53 PJ in 1979 and is followed by a gradual decrement. Petroleum has gradually been eliminated and no longer been an energy source in the sector. The overall energy intensity of UK steel manufacturing experiences a significant drop over the last fifty years and is mainly accompanied by a drop in crude steel production capacity.

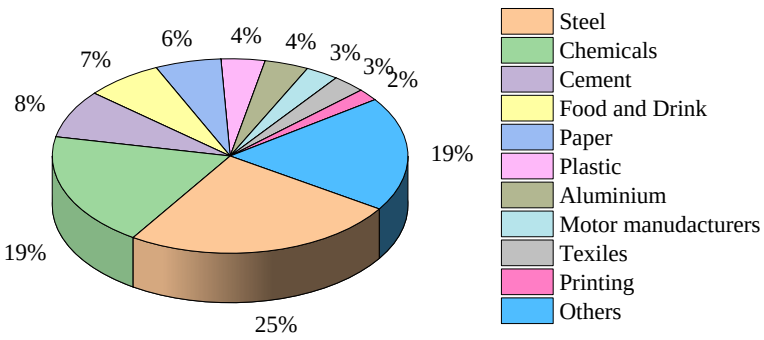

Figure 3.1: Greenhouse gas emissions from UK manufacturing, 2007 [213].

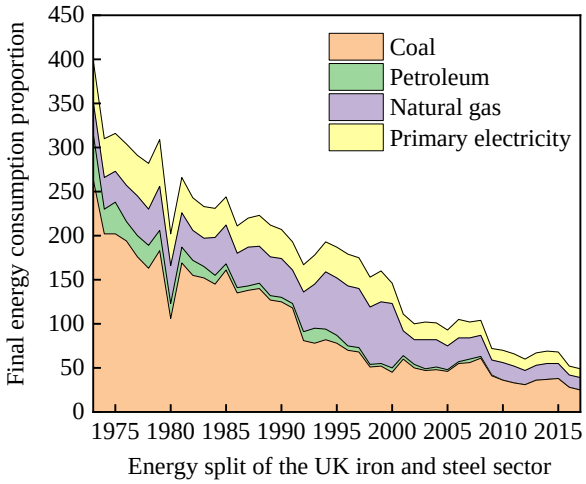

Figure 3.2: Energy split of UK iron and steel from 1973 to 2017, [214].

Since 1970, iron and steel industry in UK has been substantially declined and experienced reconstruction. Figure 3.3 presents current iron and steel sector distribution in UK based on different production routes. Steel production in UK is concentrated in the BF/BOF route (ore-based steelmaking/primary steelmaking) and the EAF (scrap-based steelmaking/secondary steelmaking). Primary steelmaking is spread over three UK integrated steelworks (Teesside works, Scunthorpe, and Port Talbot), and secondary steelmaking is distributed in four steel plants (Rotherham, Tremorfa, and two in Sheffield) [212]. In recent years, steel producers adopt actions of reduction in steel capacity to achieve target of energy conservation and emission reduction. Nearly half the decrease in industrial GHG emissions results from these measures [215]. Energy saving technologies from primary and secondary energy sources also play a critical role in energy and CO_2 emissions savings for UK iron and steel processing. In this study, the base case of iron and steel plant is based on one of the biggest private steel sectors at Port Talbot in South Wales.

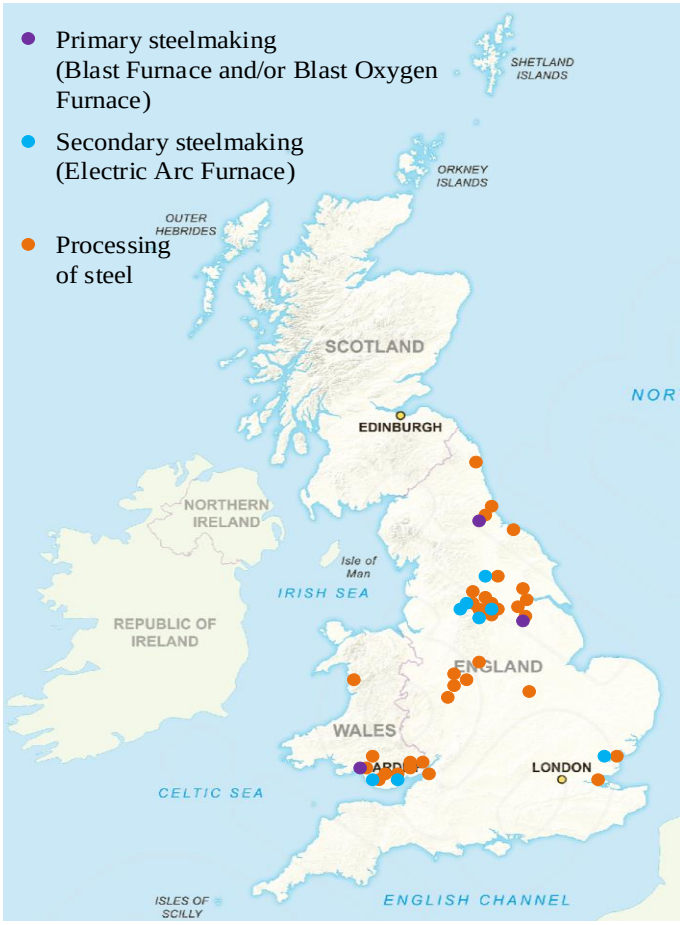

Figure 3.3: Iron and steel distribution in UK [216].

3.2 The studied system

A nearly 4.7 million tons of annul steel slab capacity iron and steel plant is considered as the studied base case throughout the thesis. The plant is an integrated iron and steel production lines based on primary steel production route with a power plant. The whole steelworks are characterised as networks of interdependent flows through primary products and by-products from each process. These processes are composed of raw material preparation, iron making, steel making, and steel casting and rolling. In this system, BF process is the main operational unit where the reduction of oxide ores occurs. The ore input of BF is from pure sinters. Therefore, the system is not covered with pelletising plant. Main reducing agents of ironmaking process are coke and PC. Waste heat recovered in the process and from by-product gases are used as heating sources for each unit and the main fuel for a nearby power plant. It is assumed that the kinetic energy of heat transfer and working fluid in the

cycles are negligible. Also heat losses and pressure drop of components in the system are negligible. The reference environmental temperature and pressure are 25 ℃ and 1 bar.

3.2.1 Input and output streams

An overview of production streams of each process is presented as Figure 3.4 to Figure 3.12. Data in the figures have been provided by Tata Steel Europe LTD, [217]. Data is averaged over the years and the error margin of data is reported to be ±10%. Information on gases came from the environmental department of the participating site and information on cooling water was obtained from cooling tower manufacturers. Steam waste heat has not been quantified by thermal energy audit used for this study. It is estimated that the steam energy waste from the system of 11 bar pressure is at 0.83 PJ·yr^{-1}, which is equivalent to approximately £5 million of natural gas utilisation. The demands of resources are different for various production routes.

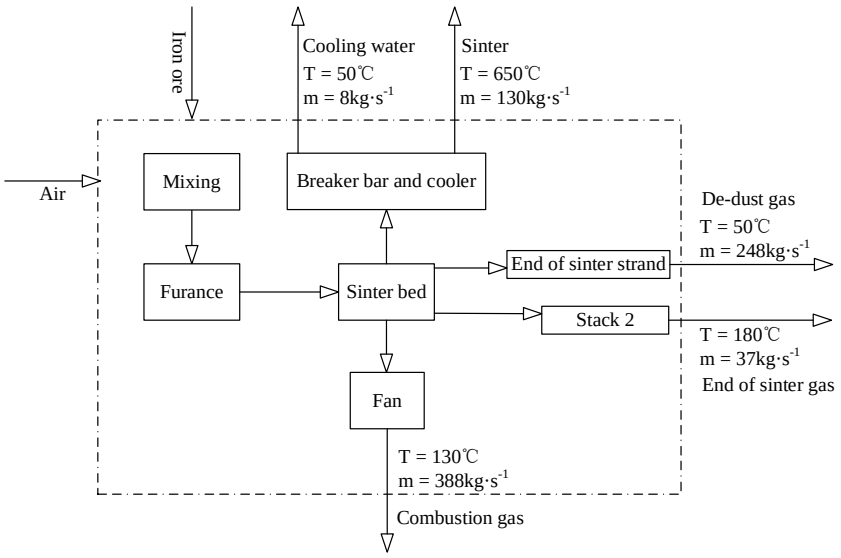

Figure 3.4: Sinter production process diagram.

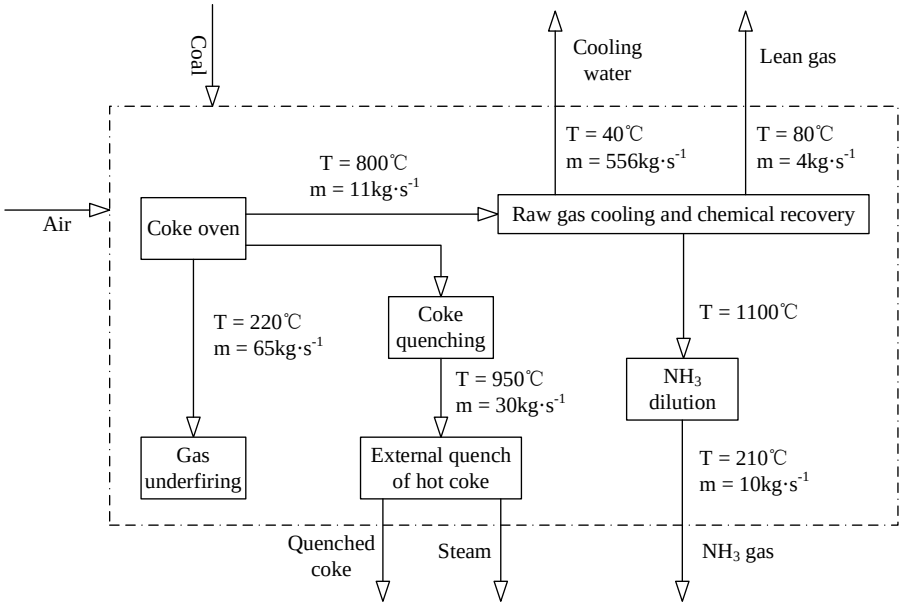

Figure 3.5: Coke production process diagram.

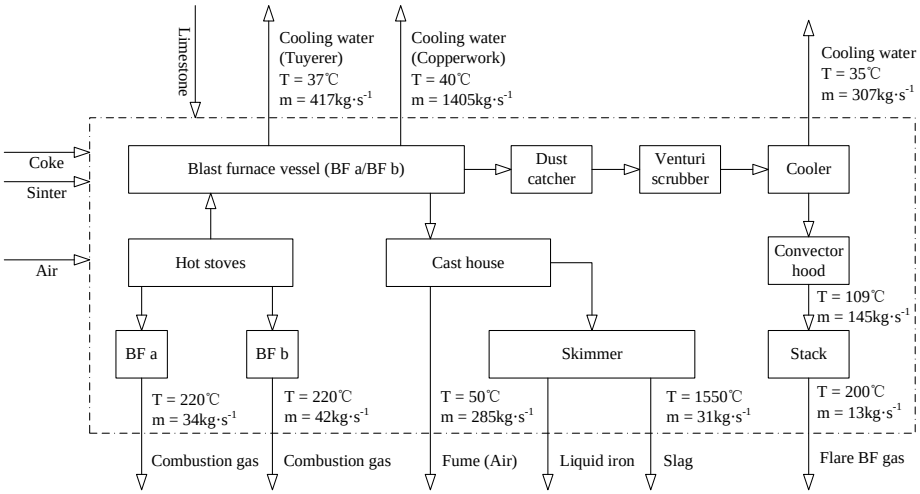

Figure 3.6: BF ironmaking process diagram.

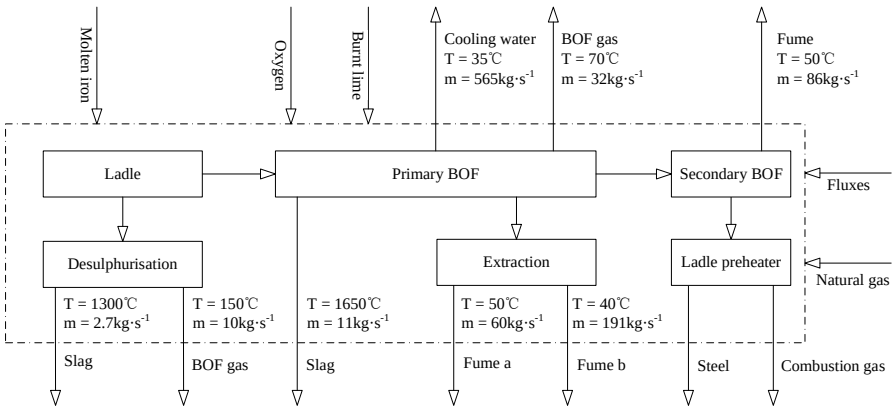

Figure 3.7: BOF steelmaking process diagram

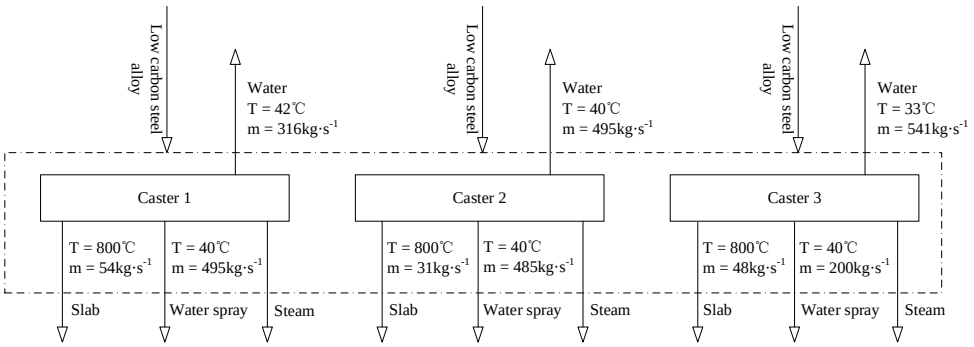

Figure 3.8: CC process diagram

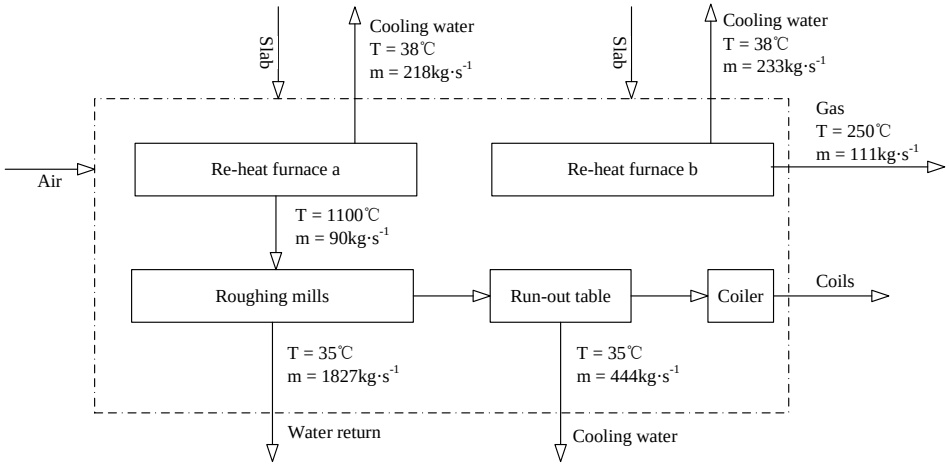

Figure 3.9: Hot rolling process diagram

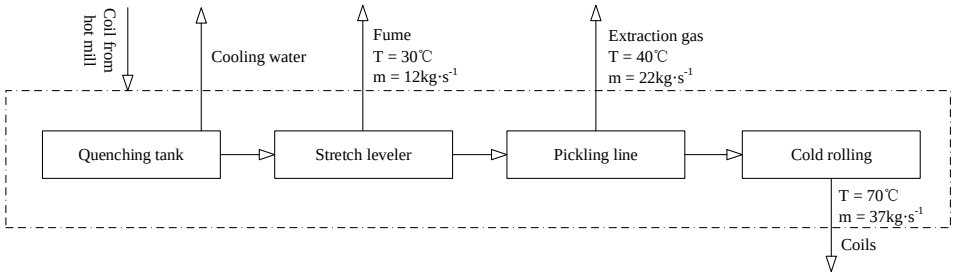

Figure 3.10: Cold rolling process diagram

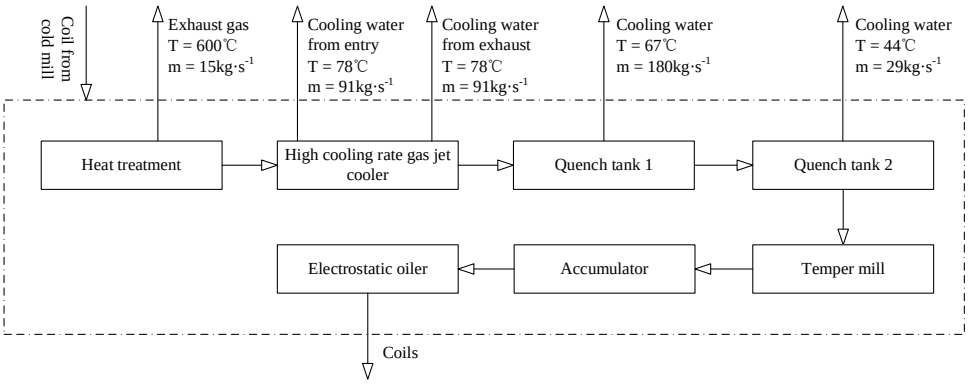

Figure 3.11: Annealing process diagram

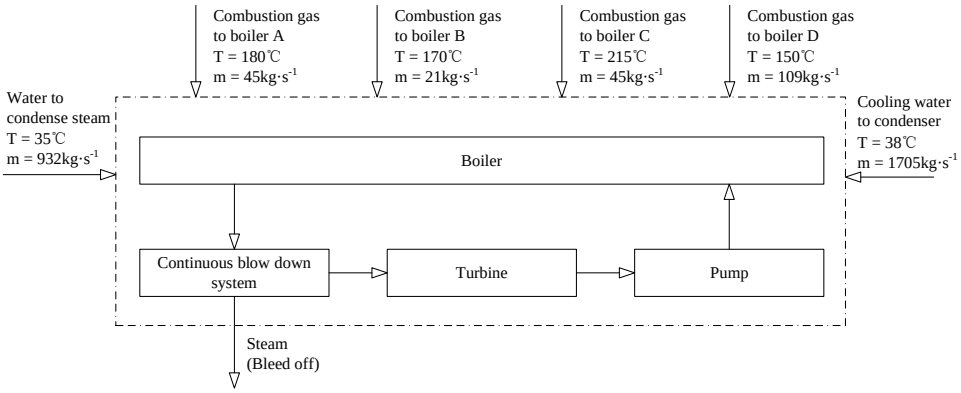

Figure 3.12: Power plant process diagram

The capacity of each production process is given in Table 3.1. Nearly 4.7 million tons sinter of annul capacity is produced in the sinter plant. The yield of coking plant in this study is 0.9 million tons of coke per year which significantly depends on the properties of coal and coking process itself. A high productivity BF with annual production of 4.3 million tons pig iron is used here. Total 4.9 million tons liquid steel is achieved in the primary BOF steelmaking procedure. After CC process, total yield of cast steel is recorded as 4.7 million tons.

Table 3.1: Capacity of each production process.

Product	Total sinter	Total coke	Total pig iron	Total liquid steel	Total cast
Capacity ($Mt \cdot yr^{-1}$)	4.7	0.9	4.3	4.9	4.7

As specific data with regard to the input is not mentioned in above figures, mass flow and energy flow of each plant i.e., resources consumption of per ton of product are taken from McBrien et al. [84].

The injection and output rate of each process are shown in Table 3.2. The second column lists mass flow factor of each flow, which can calculate results of input and output when the quantity of product is known. In order to use a unified unit to describe input and output, one ton of pig iron capacity is set as the baseline, thus the results in the third column reflect the demand and production when producing one ton of pig iron or using one ton of pig iron as feedstock. The unit is expressed as kilogram of per ton of hot metal ($kg \cdot t_{HM}^{-1}$). Followed by the sinter production and coking process, the applied sinter rate and coke rate of BF amount to 1394 $kg \cdot t_{HM}^{-1}$ and 410 $kg \cdot t_{HM}^{-1}$, respectively. Meanwhile, 102 $kg \cdot t_{HM}^{-1}$ PC is consumed as BF auxiliary reducing agent.

Table 3.2: Mass and energy flows within iron and steel industry processes

Stream	Mass flow ($t_{stream} \cdot t_{product}^{-1}$) [84]	Mass flow ($kg \cdot t_{HM}^{-1}$)
Sinter inputs		
Ore	1	1394
Coke breeze	0.05	69
Combustion air	0.6	836.4
Sinter outputs		
Sinter	1	1394
Exhaust	0.65	906.1
Coking inputs		
Coal	1.3	533
COG	0.1	41
Air	1.1	451
Coking outputs		
Coke	1	410
COG	0.2	82
Tar	0.1	41
Flue gas	1.1	451
BF inputs		
Coke	0.41	410
Coal	0.102	102
Sinter	1.394	1394
Air	1.22	1220
Natural gas	0.058	58
BF output		
Pig iron	1	1000
BFG	1.6	1600
Slag	0.3	300
Blast stove exhaust	0.21	210
BOF inputs		
Pig iron	0.98	1000
Scrap	0.09	91.837
Oxygen	0.07	71.429
BOF outputs		
BOF exhaust	0.1	102.041
Slag	0.03	30.612
Steel	1	1020.408
Casting inputs		
Steel	1	1020.408
Casting outputs		
Steel	1	1020.408

Rolling inputs		
Steel	1	1020.408
Natural gas	0.03	30.612
Air	0.72	734.694
Rolling outputs		
Reheat exhaust	0.76	775.510
Steel out	1	1020.408

Figure 3.13 shows mass flow of the studied case in the form of a Sankey diagram. The width of each link represents the quantity of mass flow. The figure shows the iron and steel production chain from inputs on the left side to the outputs on the right side. A small amount of natural gas is required for BF ironmaking and hot rolling processes. Generally, it is used to complement the combustible gases at processes or input as the fuel gas. Air is drawn through the feedstock layer by fans for combustion and it is the largest input part of the entire supply chain. Hot blast stoves in ironmaking process will heat compressed air for feeding hot blast to the BF. In this case, coke yield of coking plant presents deficit to requirements of ironmaking, thus 49% of coke input comes from purchase. BF ironmaking process is the largest mass and energy consuming unit. For steel making, a 14% scrap is recycled for utilisation as input of ferrous burden. A small yield loss of iron and steel in the BF and BOF are presented as formation of slag. Apart from the main steel product, flue gases and BFG show the significant proportion of output and about half of these gases could be recovered to supply process heat or to raise temperature of furnaces.

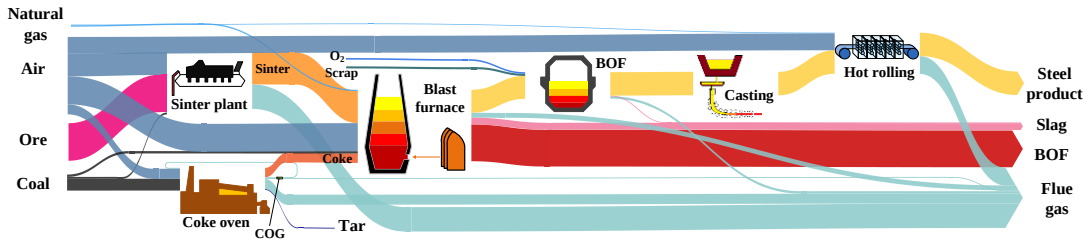

Figure 3.13: Mass Sankey diagram for primary steel making supply chain.

3.2.2 Waste heat sources

To evaluate waste heat stream exist in the whole processes, calculation of the quantity of energy is used as equation 3.1 [218]:

$$\dot{Q}_{waste} = \dot{m} C_p \Delta T \tag{3.1}$$

where $\dot{Q}_{waste}$ is the heat quantity of waste heat stream, which represents thermal energy carried by

waste heat streams, $\dot{m}$ is mass flow rate of the substance, C_p is the average specific heat of waste heat flow within the temperature difference, and ΔT is temperature difference.

The main sources available for thermal energy recovery are illustrated in Table 3.3. Thermal energy from granulation products, i.e., sinter, coke and slag are usually recovered for preheating air and input, whereas those from steel products such as steel, cast steel and rolled steel are rarely reused. These high temperature steel outputs always carry the heat to the following process, thus there is no heat exchange existing. Sinter flue gas at temperature of 300-350°C is the main stream available for recovery. Most of the exhaust gas at 250°C from coke oven is reused in the plant. Hot stove exhaust at 250°C from BF and rolling exhaust at maximum temperature of 700°C are commonly recovered and wildly employed through all processes. The large quantities of waste heat within low temperature range are also available in the cooling water at temperature around 50°C, which can be upgraded with a heat pump. The by-product gases from coking, BF, and BOF involve the chemical energy that could be applied for combustion. It should be noted that waste streams due to inefficiencies in the process could not be captured.

Table 3.3: Heat outputs and chemical energy produced from per ton of steel [4, 84, 219].

Process	Output	T (°C)	Target temperature (°C)	Heat capacity ($GJ \cdot t^{-1} \cdot °C^{-1}$)	Thermal energy ($GJ \cdot t^{-1}$)
Thermal energy from solid product	Sinter	700-800	25	$1.21 \cdot 10^{-3}$-	0.88-0.94
	Coke	1000-1100	25	$0.5 \cdot 10^{-3}$	0.55-0.59
	Steel	1200-1600	1200	$3.5 \cdot 10^{-3}$	0.7-1.39
	Cast steel	800	700	$5.7 \cdot 10^{-3}$	0.3-0.57
	Hot rolled steel	900	25	$0.6 \cdot 10^{-3}$	0.53
Thermal energy from slag	BF slag	1450-1500	25	$0.3 \cdot 10^{-3}$	0.49
	BOF slag	1500-1700	25	$0.03 \cdot 10^{-3}$	0.02-0.05
Thermal energy from gas	Sinter flue gas	300-350	25	$2.1 \cdot 10^{-3}$	0.34-0.69
	COG	649-982	25	$0.2 \cdot 10^{-3}$	0.17-0.18
	Coking flue gas	250	25	$0.4 \cdot 10^{-3}$	0.10
	BFG	180-500	25	$1.7 \cdot 10^{-3}$	0.32-0.82
	Blast stove exhaust	250	25	$0.3 \cdot 10^{-3}$	0.06
	LDG	1600-1800	25	$0.1 \cdot 10^{-3}$	0.18-0.21
	Rolling exhaust	700	25	$0.3 \cdot 10^{-3}$	0.20
Thermal energy from cooling water	Sinter cooling water	50	25	$5.8 \cdot 10^{-3}$	0.146
	Coking cooling water	40	25	$6.9 \cdot 10^{-3}$	0.104
	BF cooling water	40	25	0.063	0.95

	BOF cooling water	35	25	$7.9 \cdot 10^{-3}$	0.079
	CC cooling water	30-45	25	0.028	0.3-0.55
Chemical energy	COG	649-982	25	$0.2 \cdot 10^{-3}$	0.69
	BFG	180-500	25	$1.7 \cdot 10^{-3}$	4.12
	LDG	1600-1800	25	$0.1 \cdot 10^{-3}$	0.13

3.3 Process modelling

Since the integrated iron and steel production processes are complex multi-component systems, to fully analyse and examine the properties of each flow and build a basic model which could be applied when data of case study is limited, Aspen Plus simulation software is used here and it is a very powerful process simulator and a mathematical tool for many types of thermodynamic calculations and the steady-state simulation of complex chemical processes [220]. The software offers operations like separators, reactors or columns, databases for the physical properties of the chemical components and mathematical algorithms for the iterative convergence of recycling loops [221].

There are several ways to build up process models, ranging from simple time and event driven approach to highly sophisticated models which are between system simulation iterations. The inputs and outputs of each subsystem are communicated between each applicable subsystem [222]. During the simulation, each parameter and controlling will be adjusted repeatedly to simulate the best operation conditions. The proposed improvements need to be added to mitigate energy consumption and increase overall efficiency. The simulated results must be compared with the real-time data to validate the accuracy of the simulation. Furthermore, process evaluations like sensitivity analyses and process optimisation also can become possible through Aspen Plus.

Based on the process evaluations of case studies, a model that combines calculated production flow and equations of the whole iron and steel production processes will be set up including all required parameters such as temperature, pressure and flow rate. The Solids method is used to calculate the properties of all the components, which is a common property and calculation method for solids and pyrometallurgy applications. In case study, all the working cycles and components operate under steady-state conditions and thermodynamic equilibrium. These process models can be built for each production plant to provide proper data and solve the specific problem.

3.3.1 Modelling of the sinter plant

The sinter process is applied to combust the mixture of raw material ores and coke breeze into the agglomerate. Ores contain a large number of hematite (Fe_2O_3) and its composition is shown in Table 3.4. Coke breeze obtained from the on-site coke plant is directly used as fuel for sintering. The sinter strand is divided into four temperature zones which are four equilibrium reactors with temperature of 150 ℃, 1200 ℃, 900 ℃, and 700 ℃, respectively. These zones are driven by Gibbs free energy minimisation operation model RGibbs in the Aspen Plus. The reactor can efficiently calculate chemical equilibrium in multiphase and systems. The calculation is to find a solution that minimises total Gibbs energy of the system. The sintering is progressed along the sequence of reactors. The first equilibrium reactor with temperature of 150 ℃ is the preheating zone. Output sinter stream is then divided into two or more material streams through the component splitter. Stream order and split fraction which is defined for fraction of inlet stream going to different outlet are two factors needed to be specified for splitter. Air flow is spread to three main reactors to create sufficient sintering heat. A number of metallurgical reactions overlap and influence each other between the solid, liquid, and gaseous phases during the sintering process. After sintering, the produced materials leaving from reactors are combined in a mixer to the cooling, crushing and screen columns.

Figure 3.14 indicates the total flow-sheet of iron and steel plant simulated in Aspen Plus.

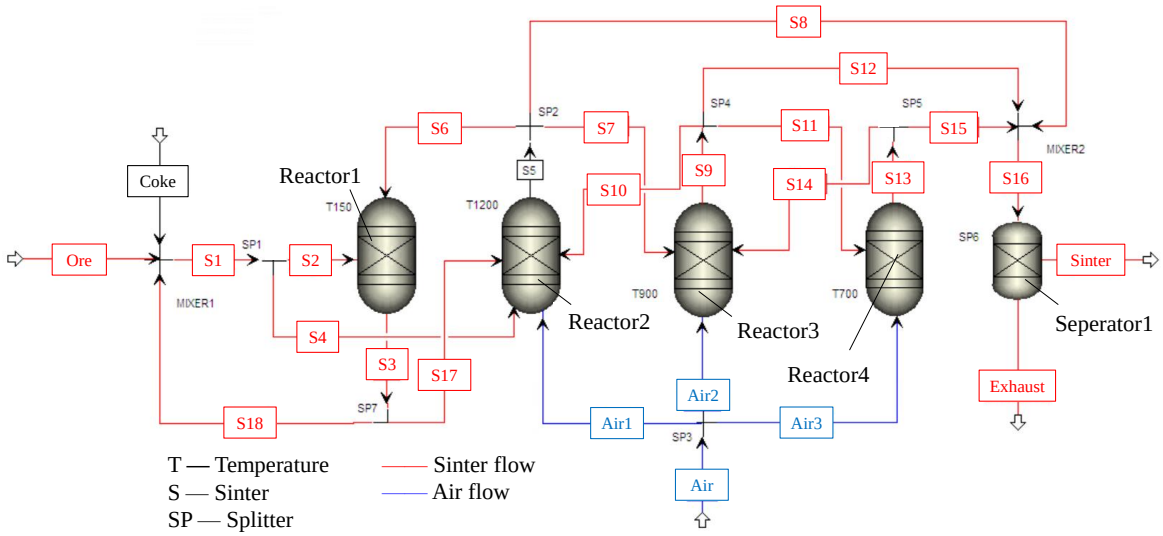

Figure 3.14: Schematic diagram of the sinter strand process in Aspen Plus.

Table 3.4: The composition of raw material ore.

Component	Value %
Fe_2O_3	82.45
CaO	7.27
SiO_2	6.44
Al_2O_3	2.38
MgO	1.18
MnO	0.29

3.3.2 Modelling of the coke oven

Coke is a necessary material used in BF, which is produced from coking plant. As shown in Figure 3.15, the whole coking plant constitutes four operation units, i.e., coking, flue gas cooling, coke quenching, and COG quenching. The main coking process takes place in the coke oven where coal is slowly burnt at 1100 ℃ to become coke product. Modelling approach for coke oven section adopts the reactor RYield which aims to make mass balance calculations and specify the component yields. The proximate and ultimate analysis of primary coking coal is shown in Table 3.5.

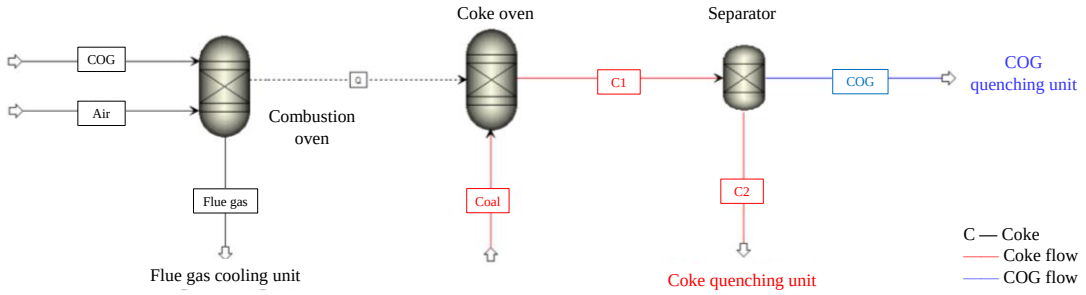

Figure 3.15: Schematic diagram of the coke plant in Aspen Plus.

Table 3.5: Proximate and ultimate analyses for the coal.

	Coal
Proximate analysis (wt%, dry)	
Moisture	0
Fixed carbon	68.78
Volatile material	16.48
Ash	14.74
Ultimate analysis (wt%, dry)	
Ash	14.74
Carbon	79.02
Hydrogen	0.6
Nitrogen	1.28
Chlorine	0
Sulphur	1.14
Oxygen	3.22

The yield model of the coking process refers to [94], which are shown as equations 3.2 to 3.8:

$$y_{coke} = 103.19 - 0.75Vo_{coal} - 0.0067T_{coking} \quad (3.2)$$

$$y_{COG} = k\sqrt{Vo_{coal} - y_{coke}Vo_{coke}} \quad (3.3)$$

$$y_{tar} = -18.36 + 1.53Vo_{daf,coal} - 0.026(Vo_{daf,coal})^2 \quad (3.4)$$

$$y_{benzen} = -1.61 + 0.144Vo_{daf,coal} - 0.0016(Vo_{daf,coal})^2 \quad (3.5)$$

$$y_{H_2O} = \frac{18}{16}aO_{daf} \quad (3.6)$$

$$y_{ammonia} = \frac{17}{14}bN \quad (3.7)$$

$$y_S = cS_{daf} \quad (3.8)$$

where y_{coke}, y_{COG}, y_{tar}, y_{benzen}, y_{H_2O}, $y_{ammonia}$, y_S represent the yield of coke, COG, tar, benzene, H_2O, ammonia, and sulphur, respectively; Vo_{coal} and Vo_{coke} are the content of volatile matter of coal and coke (wt%, dry); $Vo_{daf,coal}$, O_{daf} and S_{daf} are the content of volatile matter, oxygen, and sulphur of the ash free coal (wt%, dry), respectively; N is the content of nitrogen of coal (wt%, dry), respectively; T_{coking} is coking temperature; k, a, b, c are coefficients of yield model, as listed in Table 3.6. The calculated yields of coking process are shown in Table 3.7.

Table 3.6: Coefficients of yield model [94].

Coefficient	*k*	*a*	*b*	*c*
Value	3.3	0.42	0.15	0.17

Table 3.7: Composition of products from coking process.

Composition	Coke	COG	Crude benzenes	Coal tar	Sulfur	NH_3	H_2O
Proportion (wt%)	83.41	12.27	1.50	0.58	0.23	0.23	1.78

Energy for heating the coking stream is provided by burning a mixture of air and recycled COG in combustion chambers. All of the combustion chambers are lined with heating walls that supply flues and air through inlet nozzles. Generally the average heating brick temperature is set at 1150 ℃ to 1350 ℃ [53]. The RGibbs reactor is used to simulate the combustion process. The composition of cleaned COG is listed at Table 3.8. The largest proportion of H_2 and methane makes COG a higher calorific value about 17540 kJ·m^{-3}. The heat of flue gas emitted from combustion oven is recycled in the flue gas cooling unit which is combined with COG quenching unit.

Table 3.8: The composition of COG [94].

Composition	H_2	CH_4	CO	N_2	CO_2	C_2H_4	O_2
Volume fraction (%)	58	26	6.2	4.5	2.2	2.5	0.6

During the process of coal dry-distillation, the volatile matter in the coal is released to form raw COG. The gas is further processed in the COG quenching unit where COG is cooled and cleaned. In this thesis, the modelling of COG cleaning, i.e., recovering tar, benzene, and sulphur is not included since it is out of the targets for this study. Figure 3.16 shows the schematic diagram of COG cooling combined with flue gas cooling section. The flue gas from combustion chamber is used as economiser to pre-heat the feed water. Then the excess heat of flue gas is recovered by generating low pressure steam. To recycle waste heat in the high temperature raw COG, pre-heated feed water is input to the COG cooling unit. Superheated intermediate pressure (IP) steam is produced through evaporator and superheater. The IP steam further enters IP turbine to generate electricity. Input parameters in the model are given in Table 3.9.

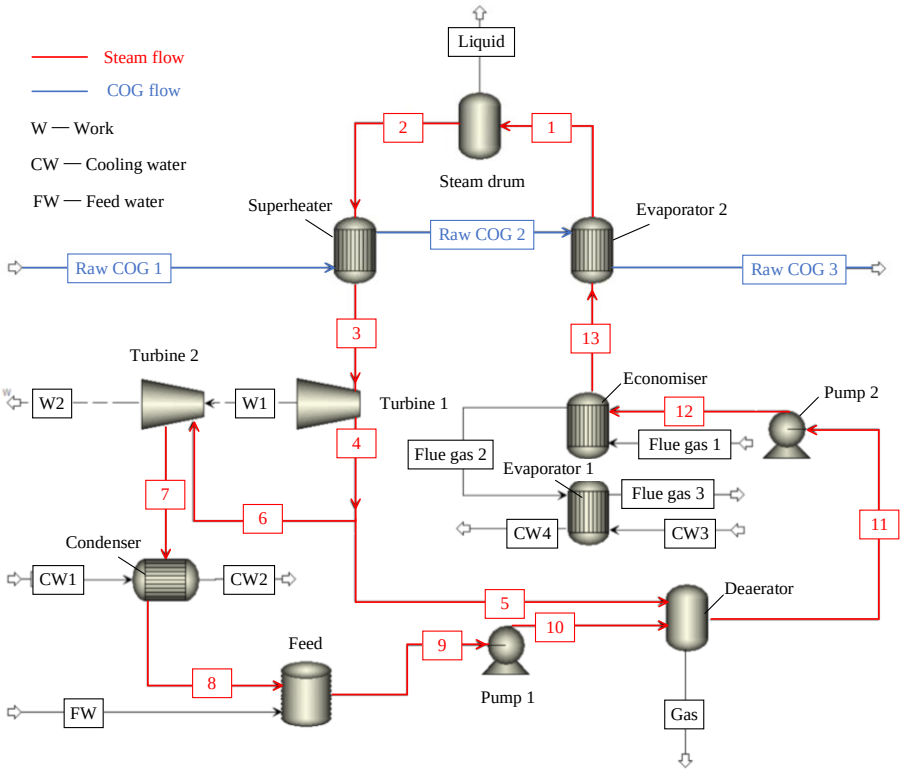

Figure 3.16: Schematic diagram of COG cooling combined with flue gas cooling in Aspen plus.

Table 3.9: Input parameters of COG and flus gas cooing model in Aspen plus.

Component	Parameter	Value
Economiser	Cold stream outlet temperature [a]	230 ℃
Evaporator 1	Cold stream outlet vapour fraction	1
	Cold side outlet pressure [a]	3 bar
Evaporator 2	Hot stream outlet temperature [a]	450 ℃
Steam drum	Vapour fraction	1
Superheater	Cold stream outlet temperature [a]	450 ℃
Turbine 1	Discharge pressure	1.1678 bar
	Isentropic efficiency	0.75
Turbine 2	Discharge pressure [a]	0.03 bar
	Isentropic efficiency	0.75
Condenser	Hot stream outlet vapour fraction	0
Pump 1	Discharge pressure	1.1678 bar
	Efficiency	0.65
Deaerator	Outlet temperature [a]	104 ℃
Pump 2	Discharge pressure [a]	48 bar
	Efficiency	0.65
Raw COG flow	Mass flow rate	107.5 $kg \cdot t_{HM}^{-1}$
	Inlet temperature	1053.56 ℃
Feed water flow	Mass flow rate	470 $kg \cdot t_{HM}^{-1}$
CW1, CW2	Mass flow rate	4600 $kg \cdot t_{HM}^{-1}$
CW3, CW4	Mass flow rate	408 $kg \cdot t_{HM}^{-1}$

[a] Values are taken from reference [94].

Coke product from coke oven is sent to a dry quenching tower where inert gas is used to cool down the red hot coke. Therefore, a large number of thermal energy is recovered during the CDQ process. The flow diagram of CDQ process model is shown in Figure 3.17. As shown in diagram, the inert gas is recirculated by passing through a series of heat exchangers which are used to heat feed water. The feed water is then sent to the IP steam cycle to generate electricity. Specific parameters in the model are given in Table 3.10. Operating conditions of IP steam cycle and IP turbine are same as those in the COG and flue gas cooling section.

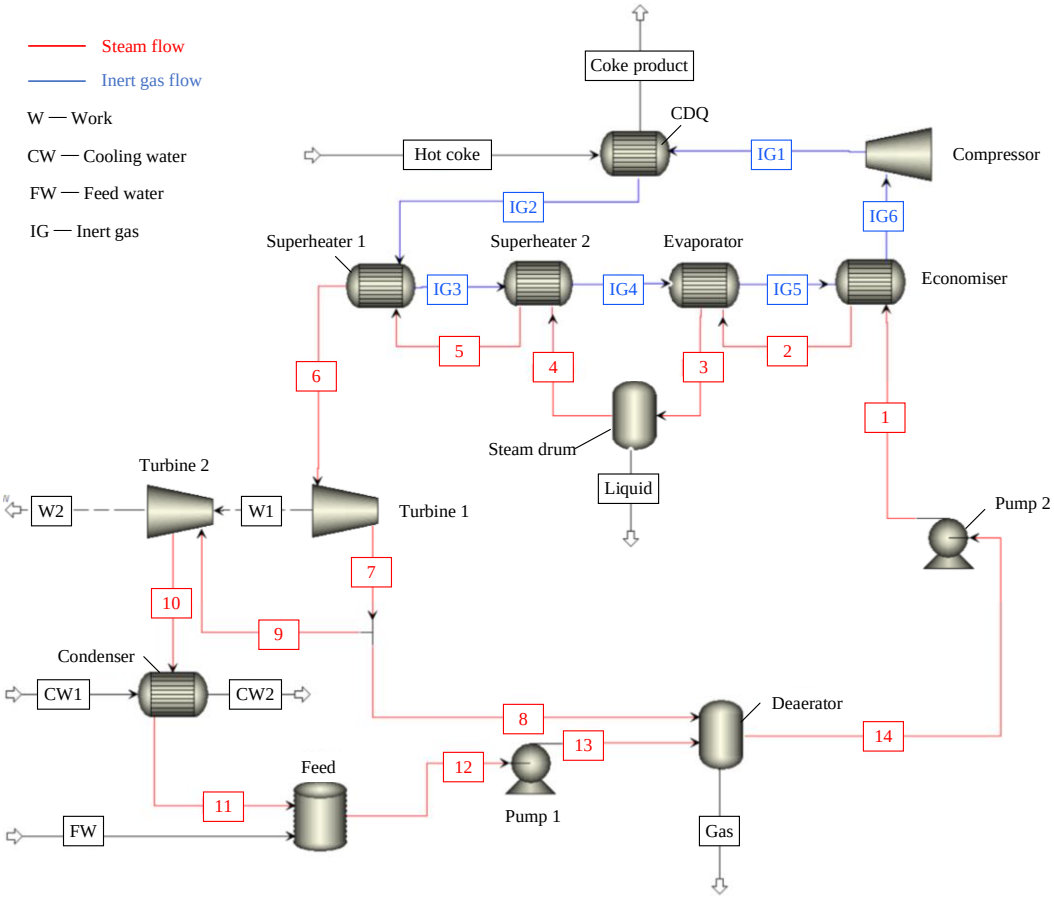

Figure 3.17 Schematic diagram of coke quenching unit in Aspen plus.

Table 3.10: Input parameters of CDQ model in Aspen plus.

Component	Parameter	Value
CDQ	Hot stream outlet temperature [a]	200 °C
Compressor	Hot side outlet pressure	1.0019 bar
Economiser	Cold stream outlet temperature [a]	230 °C
Evaporator 1	Cold stream outlet vapour fraction	1
Superheater 1	Cold stream outlet temperature [a]	450 °C
Superheater 2	Cold stream outlet temperature	350 °C
Steam drum	Vapour fraction	1
Coke flow	Mass flow rate	542.1 $kg \cdot t_{HM}^{-1}$
	Inlet temperature	1053.56 °C
Inert gas flow	Mass flow rate	825.5 $kg \cdot t_{HM}^{-1}$
Feed water flow	Mass flow rate	272.3 $kg \cdot t_{HM}^{-1}$

[a] Values are taken from reference [94].

3.3.3 Modelling of the iron making process

In this study, reduction of iron oxide to hot metal is accomplished with solid coke and pulverised coal. A high productivity furnace with a daily production of nearly 11781 $t \cdot t_{HM}^{-1}$ at an ore burden of 1394 $kg \cdot t_{HM}^{-1}$, coke rate of 410 $kg \cdot t_{HM}^{-1}$, and PC rate of 102 $kg \cdot t_{HM}^{-1}$ is used here. The specific weight of

ore burden and coke are 1800 kg·m^{-3} and 470 kg·m^{-3}, respectively [223]. Thus to produce one ton of hot metal, 1.65 m^3 (1394/1800+410/470) volume is needed in the BF for loading required feedstock. It is known that a standard 3800 m^3 BF has 3260 m^3 useful burden volume with 10 m throat and 14 m hearth, which needs 1.53 m^3 volume burden per day for producing one ton of hot metal [223]. In proportion, the design parameters of BF in this study are calculated and shown in Table 3.11.

Table 3.11: Technical parameters for BF in basic case.

Parameter	Reference [223]	This study
Furnace volume	3800 m^3	4818 m^3
Useful burden volume	3260 m^3	4134 m^3
Throat diameter	10 m	12.7 m
Hearth diameter	14 m	27.8 m

The model flowsheet is presented in Figure 3.18. The starting point for ironmaking process is feeding coke and agglomerated iron ore into the BF from the top. The PC as the addition of energy input is introduced into BF through tuyéres which are equally placed around the circumference of the furnace. Coke and PC are both modelled as nonconventional solids in the simulation. Before feeding solids to the reactor and combustion oven, coke and PC need to be decomposed into their constituent elements, which are completed in the RYield block. The proximate and ultimate analyses of coke and PC are considered for decomposition and the data are shown in Table 3.12. The high temperature air enriched in oxygen produced in the HBSs is also blown from the tuyéres. Hot blast and auxiliary reducing agent PC are reacted in the combustion oven to provide counter reducing gas flow with a high flame temperature. This combustion oven is simulated by using RGibbs block.

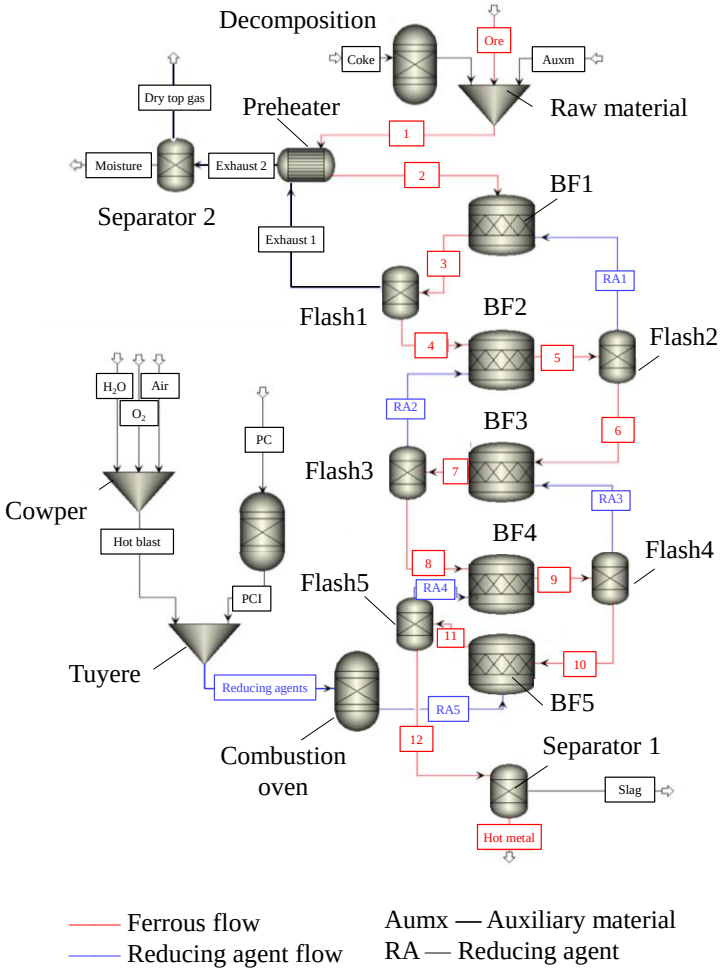

Figure 3.18: Schematic diagram of the iron making process in Aspen Plus.

Table 3.12: Proximate and ultimate analyses for the pulverised coal and coke.

	Coke	PC
Proximate analysis (wt%, dry)		
Moisture	0	0
Fixed carbon	89.7	68.78
Volatile matter	3.17	16.48
Ash	7.13	14.74
Ultimate analysis (wt%, dry)		
Ash	7.13	14.74
Carbon	89.7	79.02
Hydrogen	1.62	0.6
Nitrogen	0.62	1.28
Chlorine	0	0
Sulphur	0.31	1.14
Oxygen	0.62	3.22

Following a series of counter-current reactions in the BF where solids descend and reducing gases ascend, iron oxide is reduced and the liquid iron is produced, correspondingly. The main chemical reactions that derive the reduction of iron oxides are simulated in the stoichiometric reactor,

i.e., RStoic model. The continuous melting process are divided in sequential five temperature zones where the peak temperature could be higher than 1500 ℃. The reaction equations and temperatures of five zones are listed in Table 3.13. Following iron burden and coke moving down the furnace, removal of oxygen starts at around 500 ℃. The main step is the reduction of Fe_2O_3 to magnetite (Fe_3O_4), meanwhile a small portion of Fe_2O_3 is reduced to wustite (FeO) by carbon monoxide. The additive, i.e., calcite ($CaCO_3$), is initially decomposed to calcium oxide around the temperature of 800 ℃, and the process is simulated in the reactor BF2. At this stage, all of the Fe_3O_4 is reduced to FeO. The temperature of metal gradually increases to approximately 1000 ℃ as the burden further descends the furnace. In this zone, considerable amounts of CO gas are generated from carbon gasification and then gradually diffuse and rise through pores of ore particles, resulting in the direct reduction of FeO to iron. Hot blast injected from tuyéres gasifies coke to generate hot gas of which the temperature is generally in the range of 1900-2300 ℃ [223]. Side reactions, such as SiO reduction into Si, and MnO conversion to Mn are all considered in this area.

Table 3.13: Temperature parameter and chemical reactions of RStoic model.

Blocks	T(℃)	Reactions
BF1	500	$3Fe_2O_3+CO=2Fe_3O_4+CO_2$ $Fe_2O_3+CO=2FeO+CO_2$
BF2	850	$Fe_3O_4+CO=3FeO+CO_2$ $CaCO_3=CaO+CO_2$
BF3	1000	$FeO+CO=Fe+CO_2$ $CO_2+C=2CO$
BF4	1300	$CO_2+C=2CO$ $CO+MnO=Mn+CO_2$
BF5	1900	$C+O_2=CO_2$ $FeO+C=Fe+CO$ $2C+SiO_2=Si+2CO$

After these reactions, hot metal and slag are removed from the furnace hearth and tapped into cast house where liquid iron and slag are separated. Since the slag has a lower density than that of hot metal, slag would float on the hot metal. Hot metal is then transported to steel plant and slag is processed to produce materials for various purposes. The subsequent dispose of slag is not included in this research. BFG coming to the top of furnace and is sent to a purificatory unit consisting a bag house and filter. The method to recover waste heat from BFG will be analysed in detail in Chapter 5.

3.3.4 Modelling of the steel making process

The molten pig iron is subsequently poured into the ladle of steelmaking process. This model flowsheet is shown in Figure 3.19. In the steel plant, hot metal is refined in two main steps. The first step is to remove sulphur in the hot metal, which is usually called desulphurisation. In this case, fluxes such as limestone and CaC_2 are used to remove the sulphur according to equation 3.9, and this process is simulated by using RGibbs block. The process of preheating desulphurisation ladle by burning fuel gas is also modelled in RGibbs block.

$$2CaO+3S+CaC_2=3CaS+2CO \quad (3.9)$$

Followed by desulphurisation, the rest of unwanted chemical elements, i.e., C, Si, P, and Mn in the pig iron are oxidised by adding oxygen into the converter. Oxygen reacts with Si, Mn, C, P in sequence to produce SiO_2, MnO, CO, and P_2O_5. The whole oxidisation reaction in BOF is opposite to that in the BF. A tiny fraction of Fe can be re-oxidised, and the formed FeO is discharged with slag. The energy required to raise temperature in BOF is generated from molten pig iron and reaction of carbon and oxygen. A large number of heat is released from oxidisation of carbon and other elements, causing surplus heat and high temperature that the heat is consumed by melting additional steel scrap. Generally, the scrap accounts for 10-30% of the total steelmaking charge. Injection rate of scrap is 89.45 $t \cdot t_{HM}^{-1}$ in this case. The whole converter unit is simulated by using RGibbs block**.** Table 3.14 shows chemical compositions of metallic charges in the basic oxygen steelmaking process.

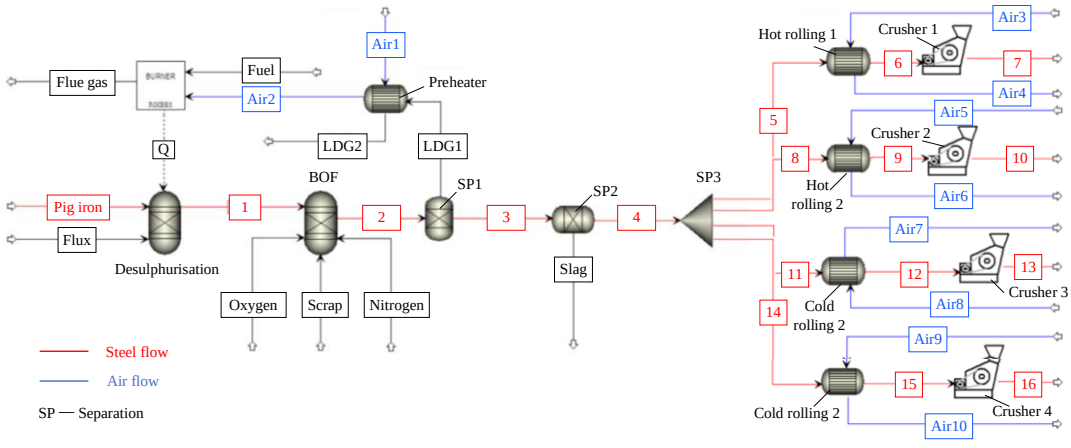

Figure 3.19: Schematic diagram of the steel making process in Aspen Plus.

Table 3.14: Chemical compositions of the metallic charges.

Input material	Chemical composition, %					
	Fe	C	Si	S	P	Mn
Steel scrap [224]	97.69	0.66	0.95	0.014	0.055	0.633
Pig iron	94.52	3.99	0.65	0.13	0.1	0.61

The steel finishing process varies with different specifications of products. It is worth noting that hot rolling presses steel at very high temperature, while cold rolling takes place at room temperature. Hot rolling heats up steel billets to 926 °C and then the steel is rolled into the aimed shape. Cold finishing includes turning, grinding, and polishing, which are used to further refine hot rolled steel. To simplify processes of steel finishing in the simulation, the model that in the right portion of Figure 3.19 consists of heat exchangers to control cooling temperature and crushers to define certain thickness and width of steel products. Specific properties of steel products refer to the product list from World Steel Association [225].

3.4 Modelling validation

To validate the present iron and steel production model, data from literatures are set as inlet flow rates of each model, and results calculated from models are compared with original output from these publications. The validation results are shown in Table 3.15. The sinter plant and steel making plant are validated by data sets from McBrien et al [84]. Results show that sinter plant has larger error because the presented model combines iron ores and coke breeze into agglomerate product, while coke in the reference is used as fuel to completely provide heat for combustion and ends to exhaust gas. It is necessary to define the final destination of coke breeze to eliminate the error of sinter plant. Result of slag from model of steel making plant shows the largest error, because computer modelling can utilise specific percentage to calculate outputs, which is more accurate than data from pilot plant. Coking plant is validated by real information published by Qin et al [94], which shows a good agreement between the reference and present work. Iron making process is validated with information published by Suzuki et al [226]. Errors of all the outputs are smaller than 3%, resulting from difference between defined yields and practical operation. It is worth noting that the model of iron and steel production in the present study is reliable to be used in further calculations and it reproduces the behaviour of the iron and steel production system.

Table 3.15: Comparison of model with present work and references

Process	Inputs ($kg \cdot t_{HM}^{-1}$)		Outputs ($kg \cdot t_{HM}^{-1}$)			Error (%)
			Comparison	Present study	McBrien et al [84]	
Sinter plant	Ore	1593	Sinter	1672.99	1593	5.02
	Coke	79.65				
	Combustion air	955.8	Exhaust	955.33	1035.45	7.74
Coke oven	Inputs ($kg \cdot t_{HM}^{-1}$)		Comparison	Present study	Qin et al [94]	Error (%)
	Coal	543.04	Coke	417.417	417.720	0.07
			COG	61.41	61.43	0.03
			Crude benzenes	7.56	7.51	0.67
	COG	41.77	Tar	2.9	2.88	0.69
			Ammonia	1.15	1.17	1.71
	Air	459.49	Sulphur	1.15	1.14	0.88
			Water	8.91	8.93	0.22
Iron making	Inputs ($kg \cdot t_{HM}^{-1}$)		Comparison	Present study	Suzuki et al [226]	Error (%)
	Coke	410.87	Hot metal	972.77	1002.13	2.93
	Coal	102.22				
	Sinter	1396.97	Slag	273.39	277.99	1.65
	Air	1222.60				
	Natural gas	58.12	BFG	2248.11	2215.14	1.49
Steel making	Inputs ($kg \cdot t_{HM}^{-1}$)		Comparison	Present study	McBrien et al [84]	Error (%)
	Pig iron	974.04	Steel	1008.04	993.92	1.42
	Scrap	89.45	Slag	27.75	29.82	6.94
	Oxygen	69.57	BOF exhaust	100.29	99.39	0.9

3.5 Performance of system

3.5.1 Evaluation method

The performance evaluation of the system focuses on the energy consumption and CO_2 emissions. Considering the whole iron and steel production chain, specific energy consumption (SEC) is often used to define the ratio between the energy input and the useful output in a component [227]. In order to reflect a compatible indicator for all processes, the crude steel production is used as the useful products. The SEC in per ton of crude steel for each process is described as equation 3.10:

$$e = \frac{\sum E_{j,in}}{M_{crude,out}} = \frac{\sum M_{j,in} \cdot p_{j,in}}{M_{crude,out}} \tag{3.10}$$

where $E_{j,in}$ is the *j*th energy input in the process, $M_{j,in}$ is mass of the *j*th inlet energy, $p_{j,in}$ is energy calorific value of the *j*th energy, $M_{crude,out}$ is produced amounts of crude steel.

Large amount of CO_2 would exist in the by-product gases of each component. The on-site direct CO_2 emissions in per ton of crude steel product is defined as equation 3.11:

$$DE_{i,CO_2} = \frac{M_{tot,CO_2}}{M_{crude,out}} \tag{3.11}$$

where M_{tot,CO_2} is total CO_2 emissions of specific process.

Generally, the process efficiency of the BF is represented as the percentage of reductant utilised for reduction of the ferrous content. When the efficiency equals to one, the reducing agent is completely consumed in the whole chemical reactions. As CO is the only reducing agent in the base case, the process efficiency can be calculated by measuring the change of CO and CO_2 composition of top gas exiting the furnace, which could be expressed as equation 3.12 [223]:

$$\eta_{BF} = \frac{\varphi_{CO_2}}{\varphi_{CO} + \varphi_{CO_2}} \times 100\% \tag{3.12}$$

where η_{BF} is the process efficiency of the BF and is also called as the utilisation rate of CO gas, φ_{CO} and φ_{CO_2} denote the mole fraction of CO and CO_2 in the top gas, respectively.

The mass end energy balances of each process are described as equation 3.13 and 3.14:

$$\sum_1^i \dot{m}_{in} - \sum_1^i \dot{m}_{out} = 0 \tag{3.13}$$

$$\sum \dot{Q} - \sum \dot{W} = \sum_1^i \dot{m}_{in}\,\dot{h}_{in} - \sum_1^i \dot{m}_{out}\dot{h}_{out} \tag{3.14}$$

where $\dot{Q}$ and $\dot{W}$ are heat transfer rate and work inputs, $\dot{h}_{in}$ and $\dot{h}_{out}$ are specific enthalpies of inlet and outlet stream, respectively.

Energy efficiency is defined as the ratio of outlet enthalpy to inlet enthalpy, which could be calculated as equation 3.15:

$$\eta = \frac{E_{out}}{E_{in}} = \frac{1 - E_{loss}}{E_{in}} \tag{3.15}$$

3.5.2 Results and discussions

a) SEC and direct CO_2 emissions

Figure 3.20 shows the base case results of SEC and direct CO_2 emissions of each process. Total energy consumption and CO_2 emissions of whole iron and steel production chain are 17.5 $GJ{\cdot}t^{-1}_{\text{crude steel}}$ and 1.06 $t{\cdot}t^{-1}_{\text{crude steel}}$, respectively. The largest energy consumption occurs in iron making process, which could achieve 13.04 $GJ{\cdot}t^{-1}_{\text{crude steel}}$. That is because the major energy sources are coke and PC and lots of sensible heat is needed for hot blast. Energy consumed in ironmaking is used to drive the chemical reactions of iron oxides to iron. To produce one ton of crude steel, energy of 1.98 GJ, 1.46 GJ, and 1.02 GJ are required in sintering, coking, and steel making processes, respectively. Steel making process consumes the most electricity since the CC and rolling processes

are power driven devices. The results show that total direct CO_2 emissions in the base case are 1.06 $t{\cdot}t_{\text{crude steel}}^{-1}$. BF iron making process accounts for the largest CO_2 emissions which is up to 0.5 $t{\cdot}t_{\text{crude steel}}^{-1}$ due to the injection of carbon-based reducing agents. The minimum CO_2 emissions are estimated to be 0.17 $t{\cdot}\,t_{\text{crude steel}}^{-1}$ for steel making process because of the lowest fossil fuel consumption. Sintering and coking sections have specific CO_2 emissions level of 0.21 $t{\cdot}t_{\text{crude steel}}^{-1}$ and 0.19 $t{\cdot}t_{\text{crude steel}}^{-1}$, respectively.

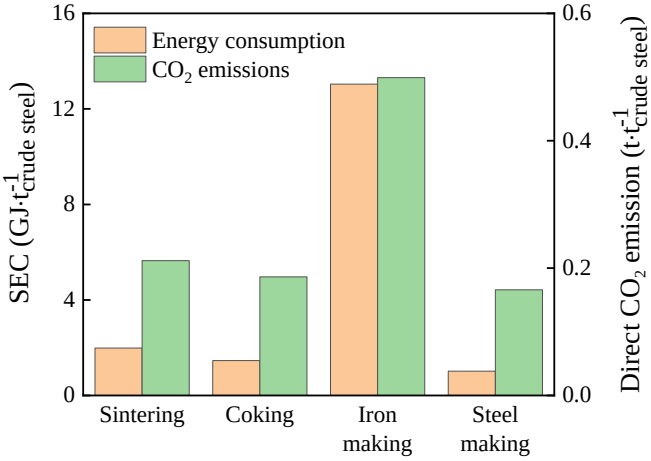

Figure 3.20: Energy consumption and direct CO_2 emissions of each process.

b) Effect of PC/coke ratio in iron and steel production

In our system, PC is the auxiliary reducing agent to replace a certain amount of coke, which is injected at the lower part of furnace through tuyere and gasified in the raceway. It is important to control the injection rate of PC, since the maximum amount of injected PC is reported about 250 $kg{\cdot}t_{HM}^{-1}$ while coke has similar amount [61]. Higher injection rate of PC would result in limitations of BF operation such as more demand of oxygen, irregular flame temperature, and lower top gas temperature, etc. Thus in this section, PC/coke ratio in the BF is set as variable to investigate its effect in SEC and CO_2 emissions, as well as performance of total production chain. Injection rates of PC and coke are with the range of 0-256 $kg{\cdot}t_{HM}^{-1}$, and 256-512 $kg{\cdot}t_{HM}^{-1}$, respectively.

Figure 3.21 shows the results of SEC and direct CO_2 emissions when PC/coke ratio varies from 0 to 1. It is indicated that both energy consumption and CO_2 emissions decrease with the increase of PC/coke ratio. When PC/coke ratio is 0.25, i.e., the value of base case, the SEC and CO_2 emissions could reach to 17.5 $GJ{\cdot}t_{\text{crude steel}}^{-1}$ and 1.063 $t{\cdot}t_{\text{crude steel}}^{-1}$. When PC/coke ratio is 0, it means zero PC

is used as reducing agent and all the reductants are from coke. This situation causes the whole production system with the largest SEC and CO_2 emissions, which are 18.3 GJ·$t^{-1}_{\text{crude steel}}$ and 1.071 t·$t^{-1}_{\text{crude steel}}$, respectively. The main reason is that higher carbon content in coke than that in coal generates more heat and CO_2 emissions when using coke. Meanwhile the higher consumption of coke affects upstream coking production that utilises more energy and emits larger CO_2. When ratio is 1, it represents that PC has the same mass flow rate as the coke, i.e., 256 kg·t^{-1}_{HM}. Then the SEC and CO_2 emissions decrease by 10.3% and 2% to 16.4 GJ·$t^{-1}_{\text{crude steel}}$ and 1.05 t·$t^{-1}_{\text{crude steel}}$, respectively. It is worth nothing that direct CO_2 emissions doesn't drop greatly with the increase of the PC/coke ratio, which demonstrates that PC has less effect on reducing CO_2 emissions.

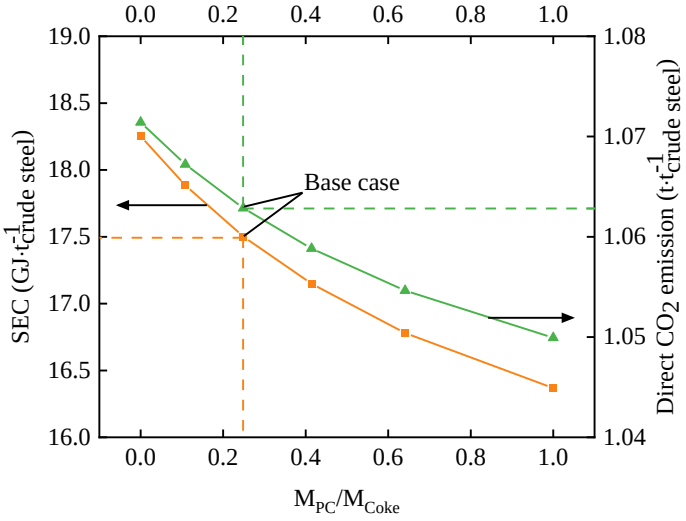

Figure 3.21: SEC and direct CO_2 emissions of whole site vs. various PC/Coke ratio in ironmaking.

Figure 3.22 indicates process and energy efficiencies of BF iron making with various PC/coke ratios. Both process and energy efficiencies increase with the higher input of PC, which are in the range from 0.33 to 0.42, and 0.31 to 0.48, respectively. In the base case, the process efficiency is 0.37. When the highest PC is input, the largest increment of process efficiency could reach 13.5%. It is demonstrated that the injectants PC are all converted to CO which is completely reacted with iron oxides. The higher process efficiency reflects the less percentage of CO in the top gas. With the same amount of PC and coke, PC could reduce more iron oxides into iron, achieving the goal to decrease the coke consumption. Similarly, energy efficiency of base case is 0.36 and is improved by up to 32.9% when PC/coke ratio rises from 0.25 to 1. Burning coal with pure oxygen generates a flame

temperature around 2000 ℃ due to increased heat input by PC injection, resulting in higher energy efficiency. It is indicated that PC with coke as reducing agents is beneficial to improve process and energy efficiency of BF system.

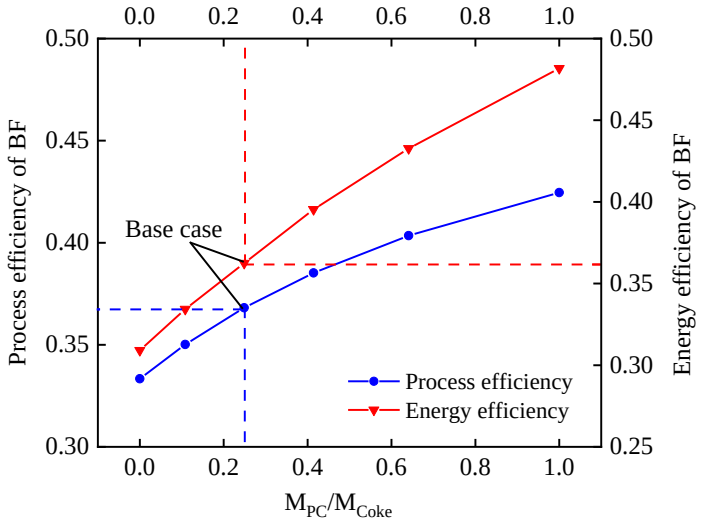

Figure 3.22: BF process efficiency and energy efficiency vs. various PC/Coke ratio in ironmaking.

c) Effect of CDQ and COG cooling on CO_2 reduction

1063 GWh electricity is totally consumed in the basic iron and steel plant, which is entirely contributed by fossil-based power plant. Table 3.16 lists electricity consumption allocation of five units in iron and steel plant. Note that CC and rolling process has the largest utilisation of power, since the steel rolling machines are driven by electricity.

Table 3.16: Electricity consumption of each production process in iron and steel plant.

Process	Sintering	Coking	Iron making	Steel making	CC and rolling
Electricity consumption ($kWh \cdot t_{HM}^{-1}$)	27.8	55.6	27.8	27.8	111.1

In the coking plant, waste heat from hot red coke and COG cooling are recovered to generate electricity by steam turbine. The power outputs are related to the coal consumed in the coking process. According to the PC/coke ratios discussed above, corresponding quantity of coal feedstock ranges from 332.8 $kg \cdot t_{HM}^{-1}$ to 665.6 $kg \cdot t_{HM}^{-1}$. Figure 3.23 reveals power generation and heat input by recovering waste heat from CDQ and COG cooling. The horizontal axis shows the change of coal

injection. Black and red lines show the trends of power output with the increase of coal, while blue and green lines depict effects of increased coal on heat input. It is indicated that power output and heat input of both CDQ and COG cooling electricity generation increase when more coal is used. Heat provided by hot coke and COG range from 55.8 MW to 111.6 MW and 37.1 MW to 74.1 MW, respectively. The power output by CDQ and COG power generation increase from 14.9 MW to 29.8 MW and 12.2 MW to 24.3 MW, respectively. Both power output and heat input of CDQ technology are higher than that of COG cooling. The main reason is that temperature and mass flow rate of coke is much higher than that of COG. Their energy efficiencies are calculated through power output divided by thermal energy input, which are 26.7% and 32.8% for CDQ and COG cooling, respectively. Under the basic scenario that coal injection rate is 533 $kg \cdot t_{HM}^{-1}$, electricity of 23.9 MW and 19.5 MW are severally generated from CDQ and COG cooling.

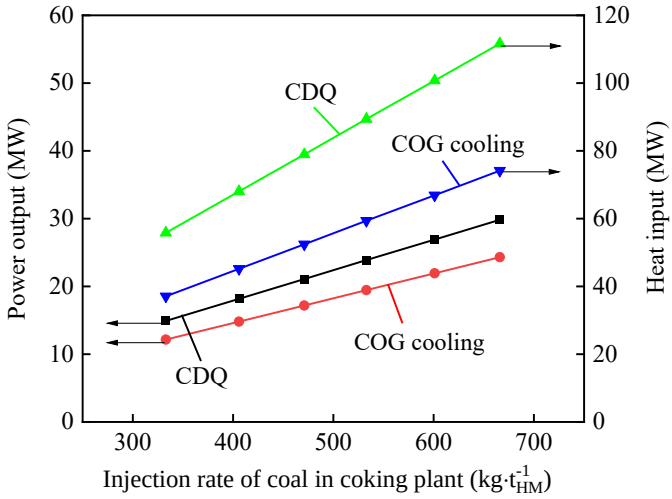

Figure 3.23: Power outputs and heat input when recovering waste heat from CDQ and COG vs. various injection rate of coal in coking plant.

The generated electricity from CDQ and COG cooling could be transported to the on-site plant, which means it will cover a proportion of electricity purchased from fossil-based power plant. Based on actual electricity consumption in iron and steel plant, the percentage of regenerative power accounted for total electricity consumed is shown in Figure 3.24. The results are also investigated with the change of coal injection. When consumed coal ranges from 332.8 $kg \cdot t_{HM}^{-1}$ to 665.6 $kg \cdot t_{HM}^{-1}$, electricity generation varies from 130.6 GWh to 261.2 GWh (CDQ) and 106.5 GWh to 212.9 GWh

(COG cooling). Thus CDQ and COG cooling could provide 11% to 22% and 9% to 18% percentages of total electricity. The waste heat utilisation by CDQ replaces higher electricity. It is worth noting that 40% of electricity could be substituted if coking process has the maximum coke capacity. The base case scenario could achieve 29% reduction of electricity consumption. Under this scenario, waste heat technologies are beneficial to energy saving in the iron and steel plant.

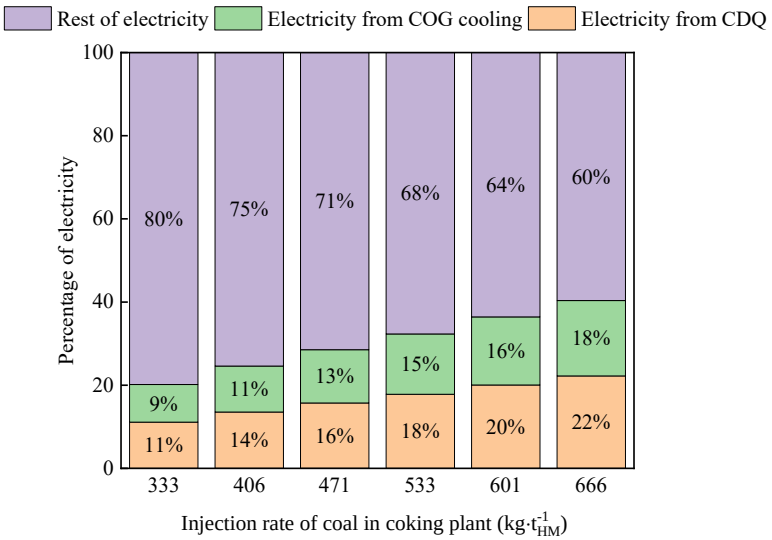

Figure 3.24: Share of different electricity sources in the iron and steel plant vs. various injection rate of coal in coking plant.

To calculate the amount of CO_2 emissions reduction due to a certain quantity of fossil-based electricity be replaced by electricity generated from waste heat recoveries, CO_2 emissions factors of different power sources are used. Table 3.17 shows the summary of CO_2 emissions factors from natural gas, coal, oil based power generation sectors, which are taken from reference [228]. All the oil and coal power plants have gradually shut down in the country and natural gas power plant plans to reduce its capacity. CO_2 emissions factors of three fossil-based plants are chosen to evaluate mitigation of CO_2.

Table 3.17: CO_2 emissions factors from different power generation sectors [228].

Sector	Natural gas	Coal	Oil
Emission factor (Mt CO_2 eq·TWh^{-1})	0.4116	1.1172	1.3409

The results are shown in Figure 3.25, of which Figure 3.25(a) indicates CO_2 reduction due to CDQ. Comparably, Figure 3.25(b) shows the effects on CO_2 emissions by COG cooling. Since

electricity capacity is the dominant parameter for CO_2 emissions, the specific electricity generation from CDQ and COG cooling are set as variable which are reflected at the x-axis. Blue, black, and red lines represent CO_2 emissions from natural gas, coal, and oil under the condition of same amounts of renewable electricity, respectively. If electricity from oil, coal, and natural gas power plants is covered by electricity from CDQ, CO_2 emissions of oil, coal, natural gas power plants can be reduced up to 350 kt, 291.9 kt, 107.5kt, respectively. For electricity generated from COG cooling, the technology can reduce CO_2 emissions of oil, coal, and natural gas plants up to 285.5kt, 237.9 kt, 87.6 kt, respectively. Although the largest electricity capacity could achieve the maximum CO_2 emissions reduction, it also causes higher CO_2 emissions from coking process due to increased coal injection. Under current condition of coking, electricity from CDQ could only reduce CO_2 emissions to 280.5 kt, 233.7 kt, 86.1 kt for oil, coal, natural gas power plant, respectively. Similarly, electricity from COG cooling in the base case reduces CO_2 emissions to 228.6 kt for oil plant, 190.5 kt for coal plant, 70.2 kt for natural gas plant. To avoid increment of on-site CO_2 emissions, further reduction is achieved by implementing advanced energy saving and CO_2 reduction technologies, such as fuel substitution, and CO_2 capture.

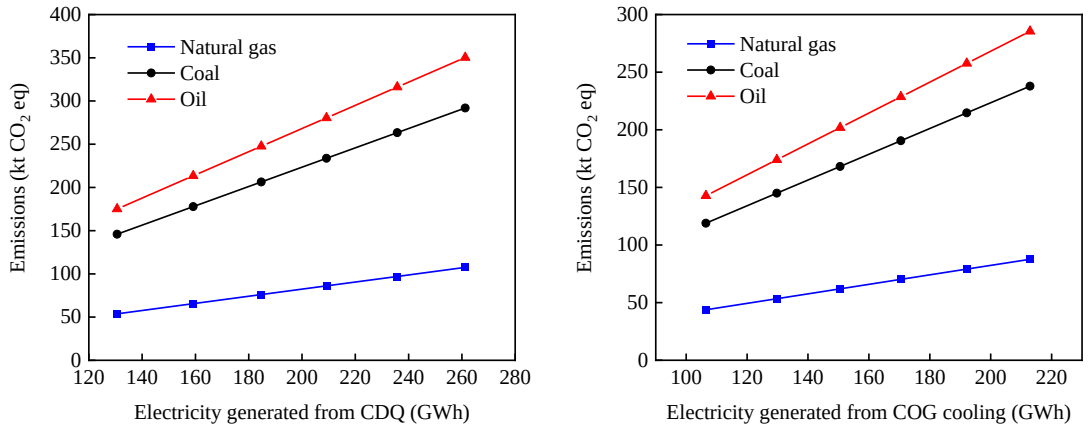

(a) (b)

Figure 3.25: CO_2 emissions vs. electricity generated from (a) COG cooling; (b) CDQ [228].

3.6 Summary

A 4.7 Mt steel capacity iron and steel plant in UK is presented in this chapter. Current iron and steel industry in UK mainly faces two challenges which are decarbonation and energy reconstruction. The iron and steel plant is used to carry out energy saving and decarbonation technologies based on

its fundamental conditions. Information given by the plant includes production streams and capacity. In order to supplement mass and energy flows that are not included in the information, mass flow factors from reference are used. Available sources for waste heat recovery of the plant include energy from products and exhaust gases. These waste streams can be further recycled on-site and reduce energy consumption.

A comprehensive model of iron and steel production flows is built through Aspen Plus. Sinter and coking process are used to prepare raw materials for ironmaking. Ironmaking BF process is the dominated unit in the whole production chain. Crude steel is formed in the steelmaking BOF and the final steel products export from CC and rolling.

Energy consumption and CO_2 emissions are evaluated for basic iron and steel plant. Total energy consumption and CO_2 emissions of whole production chain are 17.5 GJ and 1.06 $t \cdot t_{crude\ steel}^{-1}$, respectively. The largest energy consumption is 13.04 $GJ \cdot t_{crude\ steel}^{-1}$ at iron making process, meanwhile BF process emits the largest quantity of CO_2 of 0.5 $t \cdot t_{crude\ steel}^{-1}$. PC/coke ratio in the BF has vital influence on energy saving but less effect on reducing CO_2 emissions. Both process and energy efficiencies increase with the higher input of PC. When the highest PC is input, the largest increment of BF process efficiency and energy efficiency could reach 15% and 32.9%, respectively.

Heat provided by hot coke and COG is transferred to form electricity. The power output has maximumly achieved to 29.8 MW and 24.3 MW for CDQ and COG power generation. The renewable electricity could cover 40% of electricity consumed in the plant if coking process has the maximum coke capacity, and it also can reduce CO_2 emissions from oil, coal, natural gas power plants. However, direct CO_2 emissions still need to be reduced by introducing highly efficient energy saving and CO_2 reduction technologies.

Chapter 4

Blast furnace with biomass injection for cleaner production

As one of the most energy-intensive industries, iron and steel plants account for the highest share of CO_2 emissions from the manufacturing sector, at about 27% [229]. Currently BF facility is still the most important unit for pig iron production. The BF-BOF route accounts for almost 70% CO_2 emissions of iron and steel industry [230]. This is due to the use of carbon related fuels that dominate the main heat source and reducing agents in the iron making processes. The carbon in these fossil-based energies is finally released in form of CO_2 to the environment. Lots of process modifications have been developed to improve BF efficiency and reduce CO_2 emissions. Among all of these choices, renewable reducing agents are gathering the momentum to reduce the use of fossil-dominated energy and CO_2 emissions for BF. In this chapter, a simulation of introducing three kinds of biomass namely charcoal, bio-oil, and bio-syngas as reductants into BF process was developed to investigate coke replacement potential and CO_2 reduction potentials. The analyses explicitly studied and compared reduction efficiency and CO_2 profiles of base case after adding bio-reducers into BF process.

4.1 Biomass-based reducing agents in BF iron making

Numerous types of biomass have been investigated as possible substitutes for fossil-based reducing agents in the ironmaking process. Since the carbon content of biomass feedstock is lower compared to usual reducing agents in iron and steel making, biomass raw material needs to be converted into bio-reducers through various technologies [231]. Thermochemical conversion technologies make it possible to produce solid, liquid and gaseous bio-reducers. Figure 4.1 presents the main thermochemical conversion pathways of biomass. After the step of pre-treatment, raw materials are pyrolysed or gasifised with the high temperature to form valuable products. The most typical products from biomass feedstock are charcoal, bio-oil, and syngas. Generally, these products need a further conversion in order to upgrade their properties, which could be better utilised in

different applications such as metallurgical and chemical industries. For BF iron making, the main factors for biomass being the reducing agents are sufficient reducing ability and heat value. All of these biomass-based reducing agents used for pig iron production cannot fully replace top charged coke due to their low crushing strength when compared with that of coke. Thus for most of cases, biomass is used as an auxiliary reducing agent during the ironmaking process.

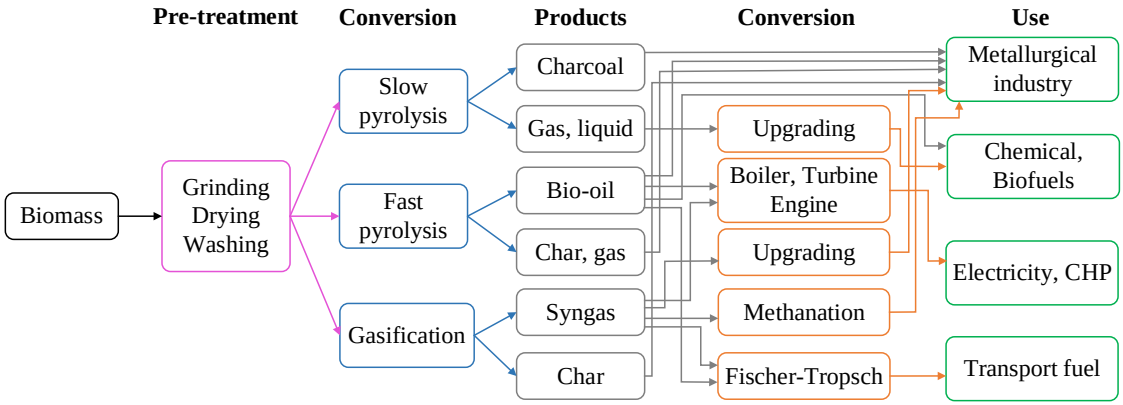

Figure 4.1: Pathways to producing biomass-based reducing agents [231].

4.1.1 Charcoal

The major solid bio-reducer i.e., charcoal is derived from wood-based feedstock through slow pyrolysis which heats the biomass to 300-600 ℃ for half an hour to several hours in the absence of air. The charcoal is highly carbonised and its properties are well comparable to coke injectant in BF. Table 4.1 lists four types of charcoal samples produced from different raw materials. It can be found that the composition of charcoal is similar to that of coke and PC. Compared to chemical properties of coke and PC shown in Table 3.12, the carbon content of the charcoal can be generally higher than that of PC. The sulphur content of the charcoal is low around 0.01-0.03% compared to fossil-based reducing agents (PC: 1.14%; coke: 0.31%). Low sulphur content of charcoal is advantageous for BF operation. The share of ash in the charcoal differs among different wood types. The maximum ash content is up to 7.76%, whereas the lowest percentage is only 0.6%. The oxygen and volatile matter content in the charcoal are high compared to coke and PC. The high existence of two compositions would decrease energy content of charcoal.

Table 4.1: Chemical composition of charcoal.

	Charcoal 1 [67]	Charcoal 2 [67]	Charcoal 3 [67]	Charcoal 4 [232]
Wood species	Eucalyptus	Oak	Olive	Red gum
Proximate analysis, wt%				
Ash	0.6	7.76	3.28	2.7
Volatile matter	18.82	20.7	22.63	18.8
Fixed carbon	80.69	70.85	74.06	78.5
Ultimate analysis, wt%				
Carbon	88.26	87.86	88.48	84.84
Oxygen	8.42	9.03	7.78	12.3
Hydrogen	2.71	2.51	3.37	2.53
Nitrogen	0.21	0.58	0.37	0.3
Sulphur	0.03	0.03	0	0.01

4.1.2 Bio-oil

Contrary to slow pyrolysis, fast pyrolysis heats the biomass to 400-600 ℃ for a few seconds in the absence of air [233]. Bio-oil as one of the major products from fast pyrolysis of biomass is a complex mixture of oxygenated and phenolic compounds. The properties of bio-oil depend greatly on the biomass feedstock and pyrolysis technologies. Table 4.2 compares properties of bio-oil with fossil oil. It is worth noting that bio-oil produced from wood-based feedstock has a few disadvantages that are actually not ideal conditions of being the reducing agent for BF. These undesired properties are reflected in high moisture, high ash content, and high oxygen. Compared with bio-oil from wood, bio-oil from microalgae has similar elemental composition and nearly comparable heating value to those of fossil-based oil. It seems that bio-oil from microalgae has higher quality for use in metallurgical processes than that from wood-based materials. Bio-oil injection rate of 140 $kg \cdot t_{HM}^{-1}$ has been reported using mathematical modeling, which results in coke consumption of 455 $kg \cdot t_{HM}^{-1}$ [234].

Table 4.2: Comparison of bio-oil derived from wood and heavy oil [235].

Product (wt%)	Bio-oil from wood	Bio-oil from microalgae	Fuel oil
Moisture	15-30	\	0.1
Ash	0-0.2	\	0.1
Carbon	54-58	76.22	85
Hydrogen	5.5-7	11.61	11
Oxygen	35-40	11.24	1
Nitrogen	0-0.2	0.93	0.3

4.1.3 Biomass-based syngas

The bio-syngas through biomass gasification has been one of the most widespread and attractive auxiliary reducing agents, which has the advantage of rich H_2 and CO [236]. Gasification technologies operate at temperature around 600-1400 ℃ with the presence of 30-50% of oxygen or

air atmosphere. The bio-syngas used for reducing agent purposes has low heating value (LHV) and the properties resemble hot reducing gas. The key factor to the syngas as a reducer for ironmaking is sufficient reducibility, which requires proportion of CO and H_2 in the mixture of CO, CO_2, H_2 and H_2O above 90% of total volume [237]. To increase the content of H_2 and CO, the decrease of biomass particle size and drying of biomass feedstock will be required prior to biomass gasification [238, 239]. The purification of bio-syngas is inevitable after biomass gasification. Then the decrement of CO_2 content in the bio-syngas is necessary before it can be used as a reducing agent.

The composition of syngas also highly depends on the applied gasification technologies and processing conditions [240]. A number of gasifiers has been developed to produce a syngas suitable for different applications, e.g. allo-thermal, auto-thermal and entrained flow gasifiers. Table 4.3 lists properties of syngas from different gasifiers in comparison to syngas from coal gasification. Allo-thermal gasification uses separated FBs to gasify biomass and produce heat, while auto-thermal gasification normally employed a single FB. Entrained flow gasification operates at very high temperature and convert the mixture of powered biomass and oxygen to a dust flame. Syngas from allo-thermal technology has the highest proportion of H_2 and the largest LHV, which is more suitable to utilise in ironmaking applications.

Table 4.3: Properties of biomass-based syngas from different gasification technologies [16].

Properties (vol%, dry)	Allo-thermal	Auto-thermal	Entrained flow	Coal-based
H_2	40	26	39	32
CO	25	20	38	55
CO_2	21	35	20	8
CH_4	10	13	0.1	0
C_2H_4	2.5	3	0	0
N_2	1.5	3	3	3
H_2/CO	1.6	1.3	1.0	0.6
LHV ($MJ \cdot m^{-3}$)	14	12	10	11

4.2 Reaction of biomass-based reducing agents in iron making

Three basic reaction systems are involved when using biomass-based reducing agents in the ironmaking process. Their reaction equations are applied in Aspen Plus simulation. The following subsections will separately describe three systems. These reactions are: Iron oxide reduction, boudouard equilibrium, homogeneous water gas shift reaction.

4.2.1 Iron oxide reduction

The iron ore reduction reactions by charcoal, bio-oil, and bio-syngas have different behaviours. The high content of fixed carbon in the charcoal and bio-oil makes whole reactions occurring between C and Fe_2O_3 or CO and Fe_2O_3. For iron oxides reduction by biomass-based syngas, reactions of hematite occur in H_2 and CO atmospheres. The sequential reactions of iron oxides take place as following equations 4.1 to 4.8:

$$CO + 3Fe_2O_3 \rightarrow 2Fe_3O_4 + CO_2 \quad (4.1)$$

$$H_2 + 3Fe_2O_3 \rightarrow 2Fe_3O_4 + H_2O \quad (4.2)$$

$$4CO + Fe_3O_4 \rightarrow 3Fe + 4CO_2 \quad (4.3)$$

$$4H_2 + Fe_3O_4 \rightarrow 3Fe + 4H_2O \quad (4.4)$$

$$CO + Fe_3O_4 \rightleftharpoons 3FeO + CO_2 \quad (4.5)$$

$$H_2 + Fe_3O_4 \rightleftharpoons 3FeO + H_2O \quad (4.6)$$

$$CO + FeO \rightleftharpoons Fe + CO_2 \quad (4.7)$$

$$H_2 + FeO \rightleftharpoons Fe + H_2O \quad (4.8)$$

To identify iron oxides reduction degree under given temperature and composition of reducing gases, the Baur-Glaessner diagram is used here to illustrate reaction equilibrium. Figure 4.2 shows the diagram where the dotted line presents gas equilibrium with H_2, and the solid lines are reaction with CO. The x-axis reflects volume fraction of CO or H_2 in the reduction gas, while the y-axis gives the reaction temperature. Both iron oxide reactions with CO or H_2 could distributed into three zones in the diagram, i.e., the Fe_3O_4, the FeO, and the Fe zone. Fe_2O_3 is stable only when the CO or H_2 gas composition is zero. Thus the region of Fe_2O_3 is presented at the rightmost side.

It can be seen from the figure, at the temperature of 570 °C, the transformations of Fe_3O_4 to FeO and Fe_3O_4 to Fe begin. When temperature is below 570 °C, Fe_2O_3 rapidly transit into Fe_3O_4 at the atmosphere that has high concentration of reducing gases. Additionally, Fe_3O_4 is reduced to metallic iron when H_2 percentage is higher than 80%, and share of CO is higher than 50%. The rest two stages of indirect reduction of Fe_2O_3 will start when temperature is higher than 570 °C. With the temperature increases, more pig iron is produced. Fe_3O_4 is firstly reacted with reducing gases at the second stage, meanwhile the produced FeO is further reduced to iron. The third stage, i.e., FeO to Fe always requires the most reductant.

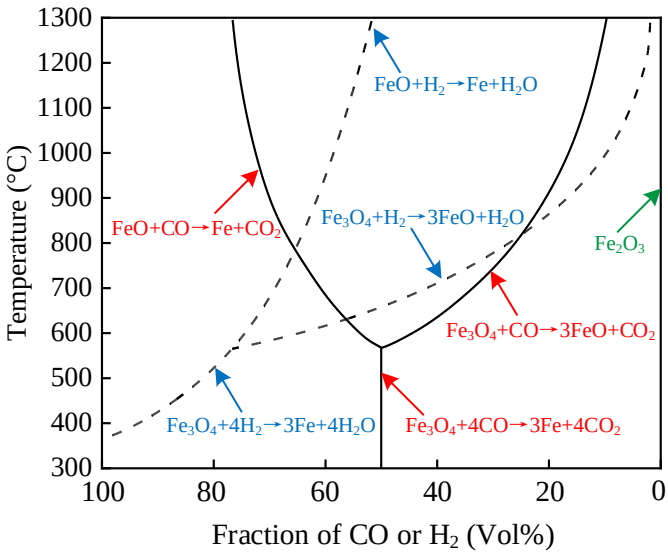

Figure 4.2: The Baur-Glaessner equilibrium diagram for H_2 and CO reduction of iron oxides [241].

4.2.2 Boudouard equilibrium

For the iron oxides reduction by charcoal and bio-oil, the Boudouard equilibrium exists between solid carbon, CO_2 and CO. The equilibrium is described by the equations 4.9 and 4.10. The reactions start with carbon gasification with oxygen below 700 ℃ to form CO_2. Then the considerable amount of CO gas is generated from reaction of CO_2 and carbon, meanwhile CO gas gradually diffuses and rises through pores of ore particles, resulting in the indirect reduction of Fe_2O_3 [242].

$$C + O_2 \rightarrow CO_2 \tag{4.9}$$

$$CO_2 + C \rightarrow 2CO \tag{4.10}$$

Temperature and pressure are two main factors of Boudouard reaction. Figure 4.3 shows gas composition under 3 different pressures and temperature in the range of 100-1300 ℃. Ratio of CO to the mixture of CO and CO_2 is used to reflect the change of gas composition. It is indicated that gas ratios at three different pressures have same trends with the increase of temperature. When temperature is in the range of 200 ℃ to 400 ℃, ratio is around zero, thus the reaction barely occurs and no CO is generated. A significant increase of ratio appears when temperature is over 400 ℃, as a result, CO is rapidly formed from carbon. The Boudouard reaction continues to carry out until the temperature is higher than 1200 ℃, meanwhile gas ratio reaches 100% and carbon is completely transformed into CO. There are slight differences among gas composition as a function of temperature at three pressures. Gaseous mixture at higher pressure needs higher temperature to achieve complete

oxidisation of carbon. The terminal temperatures are 1000 ℃, 1100 ℃, and 1200 ℃ when reactions happen at pressures of 1 atm, 5 atm, and 10 atm, respectively.

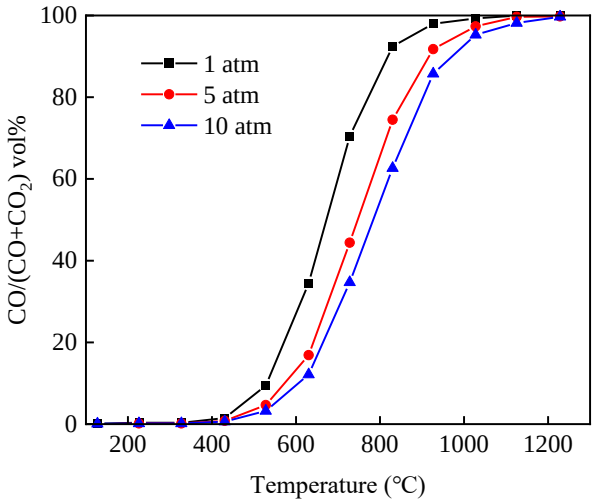

Figure 4.3: $CO/(CO+CO_2)$ ratio under defined pressure vs. various reaction temperatures [241].

4.2.3 Water gas shift equilibrium

When iron oxides are reduced by the mixture of H_2 and CO, CO can react with water vapour to form CO_2 and H_2. The reaction is called water gas shift conversion which is necessary since a large amount of CO and H_2 contained in the furnace. The reaction equilibrium is expressed as equation 4.11:

$$CO_2 + H_2 \leftrightarrow CO + H_2O \tag{4.11}$$

Figure 4.4 shows variation of gaseous volume fraction with the increase of temperature. Despite the reaction equilibrium shows sensitivity to temperature variation, the water gas shift equilibrium is reversible at any temperature. H_2 decreases firstly for the indirect reduction in the lower zone of BF where temperature is over 1400 ℃ and CO concentration is rich. The reaction of CO_2 and H_2 is mildly endothermic from forward direction of equilibrium. It could be found that CO fraction and H_2O fraction increase gradually, and CO_2 and H_2 are consumed with the increase of temperature ranging from 400 ℃-1500 ℃. During the upward process, content of H_2 starts to increase by re-producing from water gas shift reaction. In the upper zone of BF, CO is the dominate reducing agent, therefore, CO has lower concentration in this area. At the beginning of reaction, CO and H_2O have fraction of 42% and 1%, respectively they are increased by 29% and 114% to 54% and 14%. Comparably, fractions of CO_2 and H_2 decrease from 33% and 24% to 21 % and 11 %, which are

reduced by 36% and 54%, respectively.

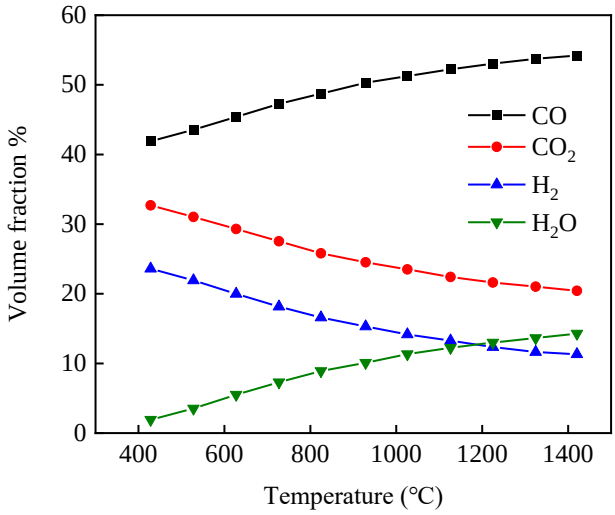

Figure 4.4: Volume fraction of gases in the water gas shift reaction vs. various temperature [241].

4.3 System description of BF operation with biomass

4.3.1 Basic structure

A schematic diagram of conventional BF with auxiliary reducers is shown in Figure 4.5. The dotted boxes represent each block boundary. The whole scheme links five blocks together, i.e., BF unit, the fossil-based reducers unit, the burden unit, biomass-generated reducers unit and the atmosphere. CO_2 releases from top gas of BF and is absorbed by the natural biomass, which results in a circle among the BF, atmosphere and biomass. BF with auxiliary reducing agents generally consumes mean coke rate of 334 $kg \cdot t_{HM}^{-1}$, and a theoretical minimum coke rate of 200 $kg \cdot t_{HM}^{-1}$ is necessary to enable stable furnace operation [50, 250]. In this case, auxiliary biomass-based reducing agents are used to decrease the coke consumption. Fossil-based coke and raw materials are fed into the BF from top. In contrast with that, powered charcoal, bio-oil, and bio-syngas are injected into BF via tuyeres which require less mechanical strength than that of top charging.

Modelling of three substitution scenarios is similar to the BF operation with coke and PC. Tuyeres injections also use decomposition model, i.e., RYield reactor. The processes of biomass pyrolysis and biomass gasification are not included in the modelling since they are not the main targets for this study. Amounts of charcoal and bio-oil use in the BF are estimated in the range of 0-200 $kg \cdot t_{HM}^{-1}$ because of the theoretical minimum coke rate. According to the calculated amounts of CO

and H_2 needed for reducing all Fe_2O_3, the injection rate of biomass-based syngas is estimated from 0-3000 $kg \cdot t_{HM}^{-1}$ based on different gas composition. By changing the biomass injection rate through BF tuyere, the maximum coke replacement ratio could be calculated. CO_2 emissions profile of selected biomass-based scenarios is estimated and compared to check their CO_2 reduction potentials. To investigate impact of biomass injection on the performance of the whole production chain, SCE and direct CO_2 emissions are calculated from total sites. The operating parameters of each unit used in Aspen Plus simulation are taken from Chapter 3. The scenario which only uses coke as reducing agent in the BF is considered as the reference model and compared with cases that input auxiliary reducers, of which the coke rate is set as 500 $kg \cdot t_{HM}^{-1}$. Input mass flows of the cases are listed in Table 4.4.

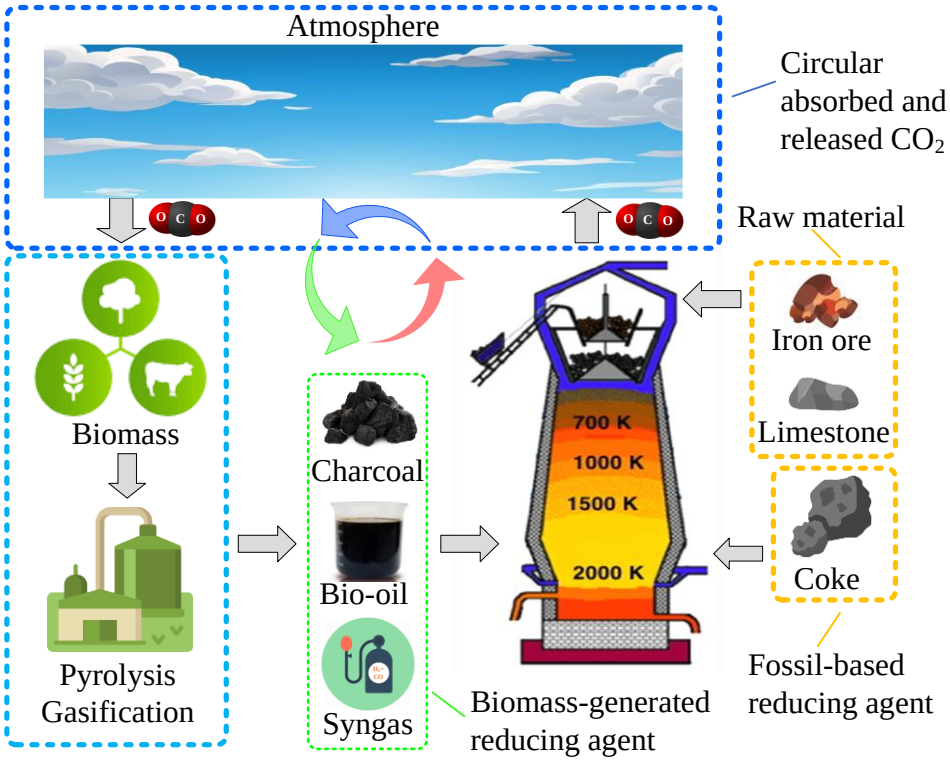

Figure 4.5: Schematic diagram of BF operation with injection of biomass-based reducing agents.

Table 4.4: Input mass flows in the BF processes

Mass flow ($kg \cdot t_{HM}^{-1}$)	Only coke injection	PC injection	Charcoal injection	Bio-oil injection	Bio-syngas injection
Coke	500	410	Calculated	Calculated	Calculated
PC	\	102	\	\	\
Charcoal	\	\	0-200	\	\
Bio-oil	\	\	\	0-200	\
Bio-syngas	\	\	\	\	0-3000

Iron burden	1593	1593	1593	1593	1593
Auxiliary material	15	15	15	15	15
Hot blast	1532.44	1532.44	1532.44	1532.44	1532.44
Oxygen	473.5	473.5	473.5	473.5	473.5

4.3.2 Biomass feedstock

Since the target of this study is to evaluate the effect of biomass-based reducing agents' injection on the overall iron and steel production chain, especially for its energy consumption and CO_2 emissions, the preparation and properties of biomass are adopted from existing researches. Chemical properties of charcoal are chosen from the reference [67]. Charcoal was produced in a vertical tubular muffle furnace and derived from eucalyptus feedstock with carbonisation temperature of 360 ℃. The bio-oil is produced from microalgae heterotrophic cells that was subjected to have pyrolysis in the FB reactor at a temperature of 500 ℃. The details of chemical properties of the chosen charcoal and bio-oil are shown in table 4.5.

Table 4.5: Chemical properties of charcoal and bio-oil.

	Charcoal [67]	Bio-oil [243]
Ultimate analysis (wt%)		
Carbon	88.26	76.22
Hydrogen	2.71	11.61
Oxygen	8.42	11.24
Nitrogen	0.21	0.93
Sulphur	0.03	\
Proximate analysis (wt%)		
Moisture	0	\
Ash	0.6	\
Volatile matter	18.82	
Fixed carbon	80.69	
LHV ($MJ \cdot kg^{-1}$)	32.4 [244]	41

Considering the availability of biomass in European regions, the biomass from wood and agricultural residues are the best candidates for syngas production and utilisation in iron and steel industry. According to the gasification technologies of biomass mentioned in Section 4.1.3, it is assumed that the biomass-based syngas used in our system is produced from listed gasification technologies. To evaluate the effects of H_2/CO ratio on coke rate and CO_2 emissions, H_2/CO volume ratios range from 0.6-1.6 are considered, which corresponds to four compositions of syngas and four gasification technologies as shown in Table 4.3. Table 4.6 shows amounts of H_2 and CO in the syngas under different H_2/CO ratios.

Table 4.6: H_2 and CO composition of biomass-based syngas.

H_2 and CO ($kg \cdot t_{HM}^{-1}$)	H_2/CO ratio							
	1.6		1.3		1.0		0.6	
	H_2	CO	H_2	CO	H_2	CO	H_2	CO
100	10.3	89.7	8.5	91.5	6.8	93.2	4.0	96.0
200	20.5	179.5	17.0	183.0	13.7	186.3	8.0	192.0
300	30.8	269.2	25.5	274.5	20.5	279.5	12.0	288.0
400	41.0	359.0	34.0	366.0	27.3	372.7	16.0	384.0
500	51.3	448.7	42.5	457.5	34.2	465.8	20.0	480.0
600	61.5	538.5	51.0	549.0	41.0	559.0	23.9	576.1
700	71.8	628.2	59.5	640.5	47.8	652.2	27.9	672.1

4.4 Evaluation method

4.4.1 Evaluation of biomass effects on energy consumption and CO_2 emissions

The reduction in energy consumption and CO_2 emissions of iron and steel plant by injecting biomass-based reducing agents are evaluated by indexes i.e., SEC and direct on-site CO_2 emissions which are calculated by equations 3.10 and 3.11. The coke replacement rate is used to define the amount of coke replaced by the injected reducing agent during BF process. Typically each reducing agent has different coke replacement ratios. With the increase of injected auxiliary reducing agents, the replacement ratio will tend to a constant value. To elaborate the biomass injection impacts on the coke consumption, coke replacement ratio κ is used to describe the change of the coke, which can be expressed as equation 4.11:

$$\kappa = \frac{\Delta M_{\text{coke}}}{M_{bio}} = \frac{M_{\text{ref,coke}} - M_{\text{bio,coke}}}{M_{bio}} \tag{4.11}$$

where ΔM_{coke} is the difference between coke rate in reference case $M_{\text{ref,coke}}$ and coke rate resulting from using a certain number of bio-reducers $M_{\text{bio,coke}}$; M_{bio} is the injection rate of biomass in BF.

To estimate the mitigation of CO_2 emissions when injecting biomass-based reducing agents, CO_2 reduction rate r is defined. The reduction rate means mitigated CO_2 emissions in per ton of specific biomass demand, which can be evaluated as equation 4.12:

$$r = \frac{\Delta M_{CO_2}}{M_{bio}} = \frac{M_{\text{ref},CO_2} - M_{bio,CO_2}}{M_{bio}} \tag{4.12}$$

where ΔM_{CO_2} is the difference between CO_2 emissions in reference case M_{ref,CO_2} and emissions in the case which injects a certain number of biomass M_{bio,CO_2}.

As shown in Figure 4.5, carbon and CO_2 in the biomass enters BF and are released in the form of CO_2. Further, biomass absorbs gaseous CO_2 from the atmosphere by photosynthesis during its growth. From a full system perspective that combines biomass, BF process, and atmosphere together, there is

zero CO_2 emission from biomass, which means the biomass is carbon neutral. The evaluation of net CO_2 emissions is necessary to clarify the emissions that cannot be avoided. The net CO_2 emissions from the BF process operation with charcoal and bio-oil can be expressed as equation 4.13:

$$M_{net,CO_2} = M_{bio,CO_2} - M_{bio,C} \times f \tag{4.13}$$

where M_{net,CO_2} is net CO_2 emissions resulting from BF process with injection of biomass-based reducing agent; $M_{bio,C}$ is carbon content in the biomass, for bio-syngas, $M_{bio,C}$ means CO content in the syngas; f is conversion factor for carbon or CO to CO_2, which are $\frac{44}{12}$ and $\frac{44}{28}$, respectively.

4.4.2 Performance analysis of system

Performance analysis of injecting biomass-based reducing agents to iron and steel system is based on the first and second thermodynamic laws. It is assumed that the kinetic energy of heat transfer and working fluid in the cycles are negligible. Also heat losses and pressure drop of components in the system are negligible. The reference environmental temperature and pressure are 25 ℃ and 101.3kPa. The energy analysis is formulated in a similar way as energy balances in section 3.6.1 (equations 3.13-3.15). The second thermodynamic analysis will be elaborated in Chapter 6 through exergy analysis.

The process efficiency is also used here to identify the utilisation rate of biomass-based reducing agents in the BF. As the CO is the primary reducer when injecting charcoal and bio-oil, the process efficiency is expressed as same as equation 3.12. For the Fe_2O_3 simultaneously reduced by H_2 and CO, the process efficiency of BF is defined as the equation 4.13:

$$\eta_{BF} = \frac{\varphi_{CO_2} + \varphi_{H_2O}}{\varphi_{CO} + \varphi_{CO_2} + \varphi_{H_2} + \varphi_{H_2O}} \times 100\% \tag{4.13}$$

where φ_{H_2} and φ_{H_2O} represent the mole fraction of H_2 and H_2O in the top gas, respectively.

Pure H_2 situation can be regarded as the theoretical maximum percentage of H_2 in syngas. The utilisation rate of H_2 in BF could also be assessed based on the mole fraction of H_2 and H_2O in the top gas, which can be calculated as equation 4.14:

$$\eta_{BF} = \frac{\varphi_{H_2O}}{\varphi_{H_2} + \varphi_{H_2O}} \times 100\% \tag{4.14}$$

It is assumed that H_2 produced from water electrolysis, and the power to produce 1mol H_2 is 285.9kJ. The reduced CO_2 emissions in per ton of H_2 demand are evaluated as equation 4.15:

$$r = \frac{\Delta M_{CO_2}}{M_{H_2}} = \frac{M_{\mathrm{ref},CO_2} - M_{H_2,CO_2}}{M_{H_2}} \tag{4.15}$$

where M_{H_2} is the injection rate of H_2 in BF, and M_{H_2,CO_2} is CO_2 emissions in the case which injects H_2.

4.5 Performance analysis of introducing biomass into BF

4.5.1 Effect of biomass injection on coke consumption and CO_2 emissions

In this section, coke consumption and CO_2 emissions of BF process after injecting three substituted reductants, namely charcoal, bio-oil, and bio-syngas are observed. According to the composition of each kind of biomass, the injection rates of charcoal, bio-syngas, and bio-syngas vary from 0-200 kg·t_{HM}^{-1}, 0-200 kg·t_{HM}^{-1}, 0-3000 kg·t_{HM}^{-1}, respectively. Figure 4.6 indicates effects of charcoal and bio-oil injections on the coke rate and on-site CO_2 emissions of BF. Red and black lines symbolise results of coke rate with the increase of reducing agent, whereas CO_2 emissions are reflected on the green and blue lines. With the increase of charcoal and bio-oil injection rate, coke rate and CO_2 emissions decrease gradually resulting from biomass injection and reduction of coke consumption. The descending of coke rate shows more significant trend than that of CO_2 emissions. Injection of 500 kg·t_{HM}^{-1} coke represents that all the reductants consumed in BF is coke, resulting in the highest CO_2 emissions of 631 kg·t_{HM}^{-1}. When injection of charcoal attains the up-limit, i.e., 200 kg·t_{HM}^{-1}, the amount of coke reduces to 286.2 kg·t_{HM}^{-1} and CO_2 emissions is equivalent to 602 kg·t_{HM}^{-1}. Thus coke consumption has reduced by 42.8%, whereas only 5% of preliminary CO_2 emissions is reduced and CO_2 reduction is 29 kg·t_{HM}^{-1}. Coke rate of BF using bio-oil as auxiliary reducing agent decreases from 500 kg·t_{HM}^{-1} to 222.6 kg·t_{HM}^{-1}, which causes 55.5% of coke reduced. CO_2 emissions of bio-oil case can be reduced by 28.2% to 453 kg·t_{HM}^{-1} compared to that of operation from the reference case and the CO_2 reduction is 178 kg·t_{HM}^{-1}. Clearly, bio-oil as a reducing agent has a better ability to replace coke and reduce CO_2 emissions than charcoal. Both charcoal and bio-oil have higher gasification reactivity than coke, which is the main reason that results in lower coke consumption. Due to 11.6% content of bio-oil is H_2, partially H_2 also act as a reducing agent, thus bio-oil can substitute more coke than charcoal.

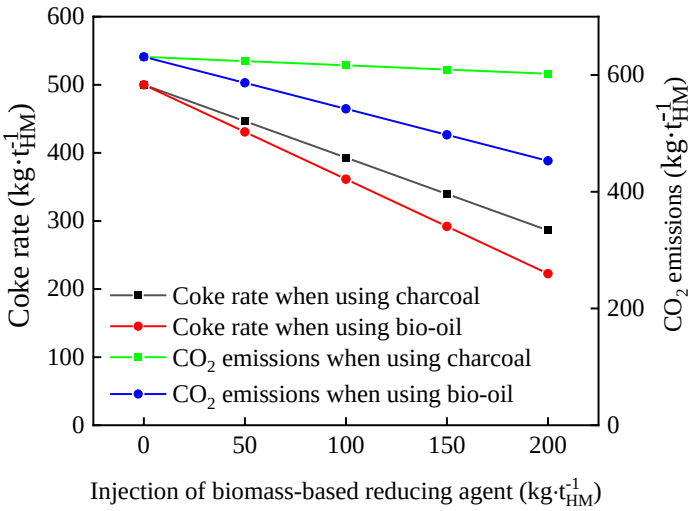

Figure 4.6: Coke rate and CO_2 emissions of BF when injecting charcoal and bio-oil.

Ratio of H_2/CO is the dominant parameter for biomass-based syngas as a reductant, which is considered in the range of 0.6 to 1.6 in this study. It is assumed that all the Fe_2O_3 are reduced by CO, as a result, 674 kg CO is needed for producing one ton of hot metal. The injection rate for H_2 to reduce entire Fe_2O_3 to Fe is 51 kg·t_{HM}^{-1}. Thus the scenario maintains the maximum quantity of total H_2 and CO in the syngas to 700 kg·t_{HM}^{-1}. Based on this amount, bio-syngas that needed for BF operation are 890 kg·t_{HM}^{-1}, 1300 kg·t_{HM}^{-1}, 2892 kg·t_{HM}^{-1}, 1734 kg·t_{HM}^{-1}, respectively for H_2/CO ratios of 0.6, 1.0, 1.3, and 1.6. Figure 4.7 shows coke rate of BF with the change of H_2 and CO in the syngas. As can be observed, coke consumption decreases with the increase of H_2 and CO_2. When the H_2/CO ratio of bio-syngas is 1.6, coke rate of BF drops swiftly first and then keeps constant at 224 kg·t_{HM}^{-1} after total H_2 and CO reaching 500 kg·t_{HM}^{-1}. A similar trend of decline appears when H_2/CO ratio is 1.3, of which coke rate plummets to 222 kg·t_{HM}^{-1} and then reaches a plateau when 600 kg·t_{HM}^{-1} H_2 and CO are input. Achieving same level of coke rate needs more injection of bio-syngas if H_2/CO ratio is 1.0. For the lowest ratio, i.e., 0.6, coke consumption can only decrease to 277 kg·t_{HM}^{-1}. It could be found that the increase of H_2 content in the syngas leads to higher amount of coke being substituted. Moreover, the descend rate of burden is accelerated in the atmosphere of high H_2 concentration. Thus the ratio of 1.6 is a superior choice for both saving bio-syngas and reducing coke rate. As coke rate has bottomed out, the rest of coke burnt in the BF is mainly as a contributor for heat. It also indicates that coke consumption in the BF cannot be fully substituted.

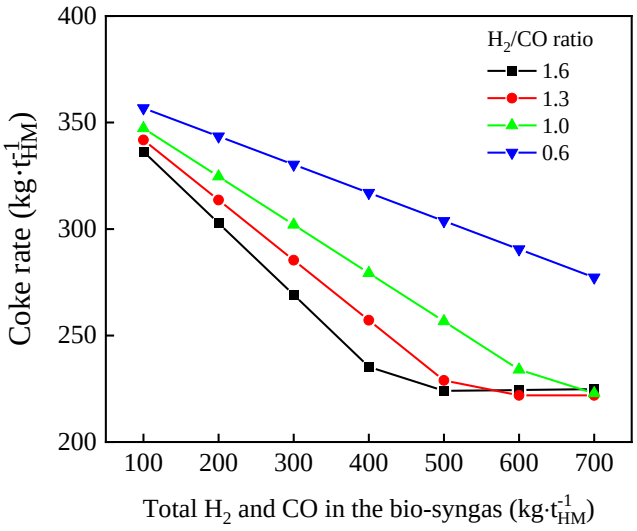

Figure 4.7: Coke rate of BF when injecting biomass-based syngas.

CO_2 emissions when bio-syngas is input to BF are given in Figure 4.8. CO_2 emissions with the increase of bio-syngas appear slightly different trends compared to the change of coke rate. When H_2/CO ratio of syngas is 1.3, CO_2 emissions of BF increase from 631 kg·t_{HM}^{-1} to 1299 kg·t_{HM}^{-1} by increasing the injection rate of bio-syngas, which are considerably larger than emissions of case that only utilises coke as reducing agent. The higher CO_2 emissions is mainly because CO_2 in the syngas is simultaneously discharged from BF with top gas. CO_2 accounts for 35 vol% of bio-syngas with 1.3 H_2/CO ratio, and CO_2 contents reach up to 1762 kg·t_{HM}^{-1} when total H_2 and CO in the syngas are 700 kg·t_{HM}^{-1}. This portion of CO_2 barely has reaction in BF, resulting in the highest CO_2 emissions in the top gas larger than reduction of CO_2 emissions. Other three kinds of bio-syngas can achieve reducing CO_2 emissions of BF. Especially for the syngas that H_2/CO ratio is 1.6, CO_2 emissions plummet to 54.4 kg·t_{HM}^{-1} and start to be constant when total contents of H_2 and CO are 600 kg·t_{HM}^{-1}. This demonstrates that contents of H_2 in the syngas are enough to reduce all Fe_2O_3 to iron, and CO_2 contained in the syngas is converted to CO due to Bondouard reaction. The minimum CO_2 emissions of injecting bio-syngas with H_2/CO ratios of 1 and 0.6 into BF could be decreased to 154 kg·t_{HM}^{-1} and 206 kg·t_{HM}^{-1}, respectively. Depending on various H_2/CO ratios of bio-syngas, CO_2 contained in the syngas would have different reactions occurred in BF. High CO_2 concentration inside furnace causes fractional CO_2 directly emitting from top, whereas low CO_2 concentration environment would preferentially induce transformation of CO_2 into CO.

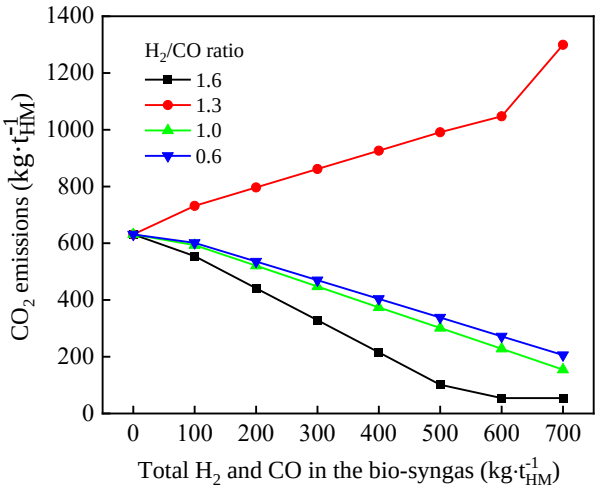

Figure 4.8: CO_2 emissions of BF when injecting biomass-based syngas.

Based on above results of CO_2 emissions under the conditions of different biomass-based reducing agents, the reduction of CO_2 emissions could maximumly reach 29 kg·t_{HM}^{-1}, 178 kg·t_{HM}^{-1}, and 576 kg·t_{HM}^{-1} for charcoal, bio-oil, and bio-syngas, respectively. As biomass is a carbon neutral material, the index of net CO_2 emissions is calculated to distinguish the quantality of CO_2 that only derives from fossil-based reducing agent. Figure 4.9 indicates net CO_2 emissions of BF process when injecting biomass as auxiliary reducing agent, in which Figure 4.9(a) shows the results of injecting charcoal and bio-oil, and Figure 4.9(b) reflects the case of bio-syngas. It is indicated that the net CO_2 emissions have significant decrements, which demonstrates that CO_2 generated from coke can be effectively mitigated by injecting biomass into BF. As shown in Figure 4.9(a), net CO_2 emissions decrease from 631 kg·t_{HM}^{-1} to 56.8 kg·t_{HM}^{-1} with the increase of charcoal. Similarly, net CO_2 emissions of case that injects bio-oil could reduce to 56.9 kg·t_{HM}^{-1}. Both final net CO_2 emissions are much lower than the emissions taking into account the carbon contents in the biomass. This is mainly because only a small proportion of coke acts as reducing agent in the BF.

After eliminating a large number of CO_2 in the bio-syngas with H_2/CO ratio of 1.3, net CO_2 emissions drop rapidly to 106 kg·t_{HM}^{-1} and turn to be constant when total H_2 and CO vary from 0 to 300 kg·t_{HM}^{-1}, which presents a completely opposite trend to originally CO_2 emissions. Analogous results also appear in the situations of H_2/CO ratio 1.6 and 1.0, in which the lowest net CO_2 emissions are 54 kg·$t_{HM}^{-1}$and 66 kg·t_{HM}^{-1}, and the turning points appear when total H_2 and CO are 300 kg·t_{HM}^{-1} and 400 kg·t_{HM}^{-1}, respectively. Unchanged net CO_2 emissions with further increment of bio-syngas

indicates coke rate of BF has reached a level of theoretically minimum, thus no more CO_2 can be reduced by injecting bio-syngas. Only for H_2/CO ratio 0.6 that results in the lowest H_2 content, net CO_2 emissions witness a continuous downward trend to 52 $kg \cdot t_{HM}^{-1}$ when total H_2 and CO in the range of 0-700 $kg \cdot t_{HM}^{-1}$. It reveals that higher amounts of bio-syngas are needed to substitute coke if the syngas has lower H_2/CO ratio.

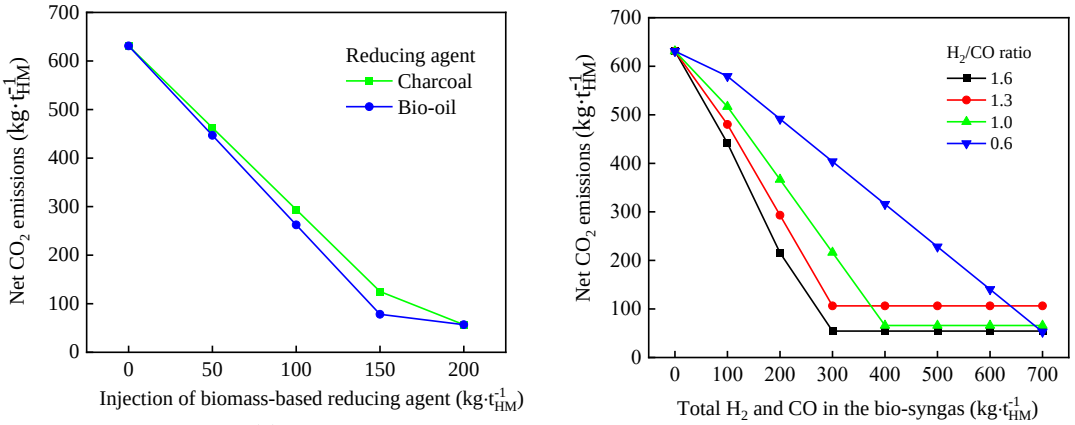

Figure 4.9: Net CO_2 emissions of BF when injecting: (a) charcoal and bio-oil, (b) bio-syngas.

The resulting coke replacement and reduction of CO_2 emissions generated by injecting charcoal and bio-oil into BF are shown in Figure 4.10. The up-limit coke replacement ratios are 1.07 and 1.39 for charcoal and bio-oil respectively. It implies that per kilogram coke can replace 1.07 kilograms coke, compared to 1.39 kilograms coke that can be replaced by per kilogram of bio-oil. The maximum level of coke replacement ratio corresponds to the theoretically lowest coke rate. Thus injecting 200 $kg \cdot t_{HM}^{-1}$ charcoal has ability to substitute 43% of coke required by BF process. Likewise, 200 $kg \cdot t_{HM}^{-1}$ bio-oil can replace 56% of coke consumed by Fe_2O_3 reduction process. Due to the less energy density of charcoal, charcoal has lower coke replacement rate than bio-oil. More energy originating from coke is needed for charcoal to satisfy molten temperature in the lower zone of furnace, which principally results in lower coke replacement rate.

CO_2 reduction rates are calculated to be 0.14 and 0.89 for charcoal and bio-oil based on on-site emissions including carbon in the biomass. Purple columns represent the net CO_2 reduction rates by injection charcoal and bio-oil, which reach 3.37 and 3.68 and the values are considerably higher than CO_2 reduction rates. Accordingly, carbon content in the biomass is an essential factor to estimate CO_2 mitigation performance of biomass. It is necessary to clearly define the sink of CO_2 emissions. If CO_2

gases are eventually released into atmosphere, the CO_2 reduction ability of biomass is determined by CO_2 reduction rate. Comparably, if CO_2 gases are further absorbed by plants, the CO_2 mitigation factor of associated biomass is equal to the net CO_2 reduction rate. It can be found that per kilogram of bio-oil reduces more CO_2 emissions from BF than charcoal, which is in accordance with the results of coke replacement ratio. Higher coke replacement ratio gives rise to the less coke consumption, hence the lower CO_2 emissions.

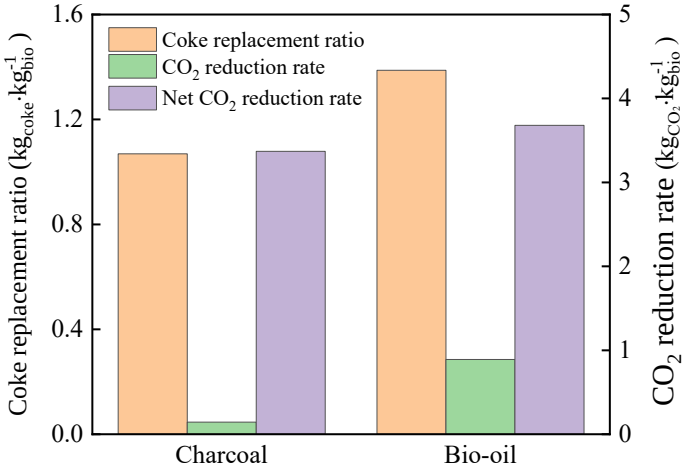

Figure 4.10: Coke replacement ratio and CO_2 reduction rate of BF when injecting charcoal and bio-oil.

Coke replacement ratios of bio-syngas with the change of injection amounts are shown in Figure 4.11. The variations of ratios are highly sensitive to injection rate and H_2/CO ratio of bio-syngas. H_2/CO ratio has effect on the injection quantities of syngas, then increasing amounts of syngas cause decreased substitution ratio of coke. The highest ratio is 1.13 when bio-syngas is injected at 127 $kg \cdot t_{HM}^{-1}$ and the H_2/CO ratio is 0.6, whereas the lowest value is 0.096 when 2892 $kg \cdot t_{HM}^{-1}$ syngas with H_2/CO ratio of 1.3 are input. It can be concluded that the lower injection rates of bio-syngas provide the desired results to save the amount of coke. Compared with coke replacement ratios of charcoal and bio-oil, bio-oil has the best performance to reduce coke consumption under the conditions of same injection rates. Besides the effects of heating value, it is also because higher contents of H_2 in the bio-syngas requires additional oxygen and heat to maintain a suitable adiabatic flame temperature. Excessive H_2 in the BF would inhibit reducing reaction, which leads to a supplementary of coke to have reducing reaction with the rest iron ores.

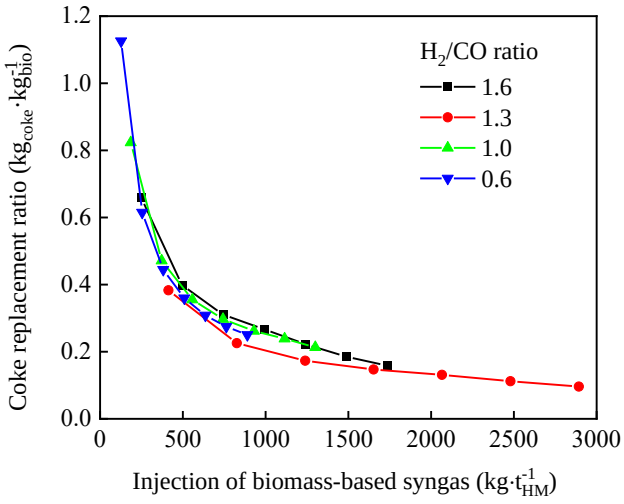

Figure 4.11: Coke replacement ratio of BF when injecting biomass-based syngas.

The potential of CO_2 reduction by injecting bio-syngas into BF is also reflected in CO_2 reduction rate and net CO_2 reduction rate, of which the results are shown in Figure 4.12. Because the assessment of CO_2 reduction rate considers release of carbon contained in the coke and biomass to the atmosphere, using bio-syngas with H_2/CO ratio of 1.3 cannot achieve mitigation of CO_2 emissions. As shown in Figure 4.12(a), CO_2 reduction rates for syngas with H_2/CO ratios of 1.0 and 0.6 both increase firstly with higher injection of syngas and then the trends become smooth, of which the ranges are 0.2 to 0.37 and 0.23 to 0.48, respectively. CO_2 reduction ability of bio-syngas with H_2/CO ratio 1.0 is lower. This is because the coke replacement ratio of syngas with H_2/CO ratio 1.0 is lower than that with ratio 0.6. It is worth noting that a significant drop of CO_2 reduction rate is found when the syngas with H_2/CO ratio 1.6 is injected from 1239 $kg \cdot t_{HM}^{-1}$ to 1734 $kg \cdot t_{HM}^{-1}$. The decrement is due to the fact that CO_2 emissions of BF have reached the lowest when injected amount of bio-syngas is higher than 1239 $kg \cdot t_{HM}^{-1}$. The further reduction of CO_2 emissions equals to zero but more bio-syngas are still injected to the BF, which restricts the enhancement of reduction rate. In summation, under the conditions of same injection rates of bio-syngas, CO_2 reduction potential is the maximum when the H_2/CO is 0.6, followed by 1.6, and 1.0.

Figure 4.12(b) illustrates net CO_2 reduction rate with the change of injection rate and H_2/CO ratio of bio-syngas. The net reduction rates have been improved without taking account of carbon credits in the biomass. It could be found that for H_2/CO ratio 1.6, 1.3, and 1.0, the rates of CO_2 reduction rise rapidly as reduction proceeds and tend to decrease after the lowest CO_2 emissions which correspond

to the highest reduction rates of 0.84, 0.42, and 0.76, respectively. Only for H_2/CO ratio 0.6, the net reduction rate increases when the injection rate varies from 127 $kg \cdot t_{HM}^{-1}$ to 890 $kg \cdot t_{HM}^{-1}$. The increase stalls at point of the lowest CO_2 emissions, after which net CO_2 reduction rate would decrease if more syngas is provided. A vertical comparison reveals that bio-syngas with ratio 1.6 has the greatest capacity to reduce net CO_2 emissions, meanwhile, syngas with ratio 1.3 has the least net reduction potential. H_2 content of the bio-syngas acts as a more important role in CO_2 reduction control. Moreover, bio-syngas with ratio 1.3 needs the most quantality to maintain particular gas composition, resulting in per unit of syngas mitigates the minimum net CO_2 emissions.

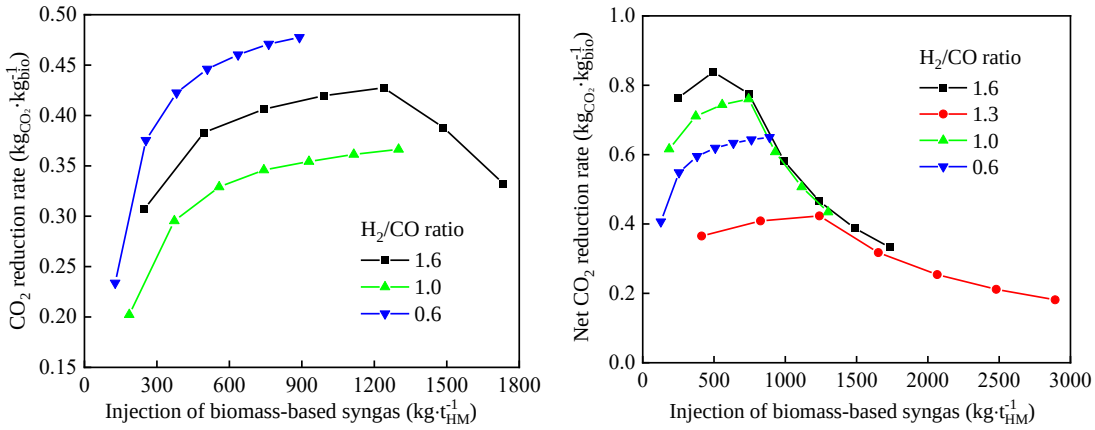

Figure 4.12.: CO_2 reduction of BF when injecting biomass-based syngas: (a) CO_2 reduction rate, (b) net CO_2 reduction rate.

Combined with the above coke replacement ratios and CO_2 reduction rates of bio-reducers, estimated amount of required auxiliary reducing agents along with coke are summarised in Table 4.7. The results enable the most efficient operation in terms of specific reducing agent injection rate. It is widely acknowledged that coke consumption in BF cannot be entirely replaced, even so, coke amount has been decreased by using auxiliary reducing agents. Minimum coke amount could reach 222 $kg \cdot t_{HM}^{-1}$ when bio-oil is at an injection rate of 200 $kg \cdot t_{HM}^{-1}$. Bio-syngas has relatively large mass rate due to the share of other gaseous components in the syngas. Comparing with results reviewed in the Table 2.1, coke rate along with additional PCI can be reduced from 280 $kg \cdot t_{HM}^{-1}$ to 256 $kg \cdot t_{HM}^{-1}$. The performance of bio-oil as auxiliary reducing agent has also been improved, of which the coke rate has

a reduction of 233 $kg \cdot t_{HM}^{-1}$ to 222 $kg \cdot t_{HM}^{-1}$. Moreover, coke consumption based on bio-syngas injection for various H_2/CO ratios built on this research, fills the vacant of these results from literatures.

Table 4.7: Estimated amounts of reducing agents used in the BF process.

Scenarios	Coke $kg \cdot t_{HM}^{-1}$	PC $kg \cdot t_{HM}^{-1}$	Charcoal $kg \cdot t_{HM}^{-1}$	Bio-oil $kg \cdot t_{HM}^{-1}$	Bio-syngas $kg \cdot t_{HM}^{-1}$	Total $kg \cdot t_{HM}^{-1}$
Only coke	500	\	\	\	\	500
PC with coke	256	256	\	\	\	512
Charcoal	286	\	200	\	\	486
Bio-oil	222	\	\	200	\	422
Bio-syngas (H_2/CO 1.6)	224	\	\	\	1238	1462
Bio-syngas (H_2/CO 1.3)	285	\	\	\	1240	1525
Bio-syngas (H_2/CO 1.0)	279	\	\	\	743	1022
Bio-syngas (H_2/CO 0.6)	277	\	\	\	890	1167

4.5.2 Effect of biomass on BF operation

In this section, effects of biomass-based reducing agent on BF operation are analysed. Firstly, process efficiencies when BF injects with different reductants are given in Figure 4.13. Due to the difference among the injection rates, Figure 4.13(a) focuses on charcoal and bio-oil, while Figure 4.13(b) shows the results of bio-syngas under the condition of different H_2/CO ratios.

As shown in Figure 4.13(a), the biomass flow rate is in the range of 0 to 200 $kg \cdot t_{HM}^{-1}$. Both process efficiencies of charcoal and bio-oil increase with more supply of biomass. A level up of the overall process efficiency indicates that the utilisation of charcoal and bio-oil could accelerate reducing reaction with Fe_2O_3. It also demonstrates that conversion rates of CO to CO_2 are improved by using charcoal and bio-oil. The process efficiency when BF operates with charcoal is increased by 1.5% from 0.41 to 0.42, which is manifestly lower than that when bio-oil is input. Bio-oil as a substitute of coke could improve process efficiency of BF by 10.3% from 0.41 to 0.46. Under the dual function of reduction of CO_2 emissions and coke rate, bio-oil highlights the advantage of replacing coke in BF.

Different from results of operating with charcoal and bio-oil, bio-syngas leads to a contrary trend of process efficiency. It is evident that process efficiencies decrease with the increase of bio-syngas injection. Although H_2 in the syngas could efficiently react with Fe_2O_3, it simultaneously restrains the reaction between Fe_2O_3 and CO, thus leaving more content of CO in the BFG. With the increment of mass rate of bio-syngas, the amount of CO input would highly exceed the quantity of CO as a reducing agent, resulting in the entire process efficiency declined. For different H_2/CO ratios, the

process efficiencies decreased with the increased ratio when BF operates with the same amount of bio-syngas. It is apparent that process efficiency reaches the highest when H_2/CO ratio is 0.6, which ranges from 0.67 to 0.35. When bio-syngas has H_2/CO ratio of 1.6, the efficiency is the lowest ranging from 0.62 to 0.27. The variation tendency of process efficiency is mainly due to H_2 content in the syngas. When H_2 concentration is higher, the reducing reaction with bio-syngas is dominated by H_2, so it could impair the ability of CO to boost the reducing reaction and less CO_2 would be generated in the BFG. According to the equation of process efficiency, the results become lower if the increased amount of CO largely outweighs the CO_2 emissions. To recommend a better H_2/CO ratio for introducing bio-syngas into BF, a further analysis of H_2/CO ratio effect on BF operation is needed.

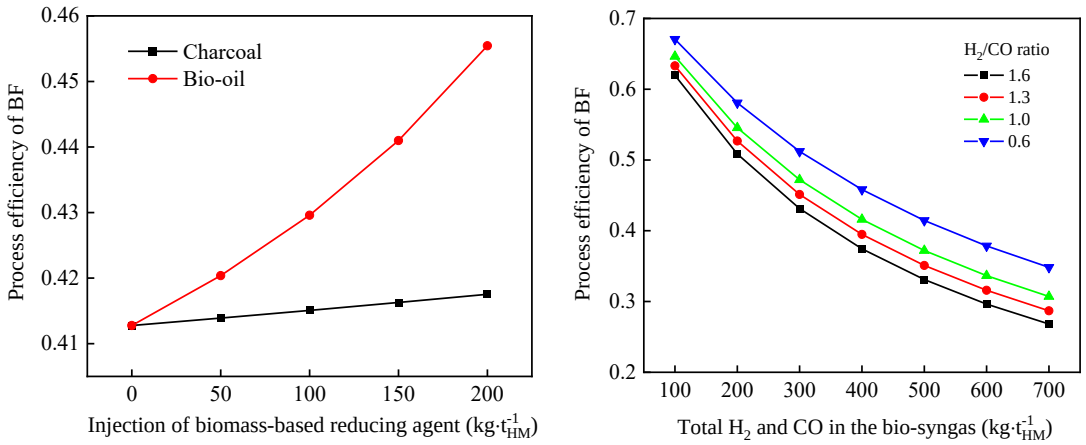

Figure 4.13: BF process efficiency vs. various biomass-based reducing agent ratio in ironmaking (a) charcoal and bio-oil; (b) bio-syngas.

Effects of H_2/CO ratio on BFG composition and temperature are shown in Figure 4.14. Normally the components of BFG without drying consist of CO_2, CO, H_2, N_2, O_2, and H_2O. Total amount of H_2 and CO in the syngas under the conditions of different ratios is 700 $kg \cdot t_{HM}^{-1}$. As H_2/CO ratio changed, gas composition presents an irregular trend which is mainly related with the initial gas proportion of bio-syngas. Total percent of hydrogen-based gases, i.e., H_2 and H_2O, increases from 16% to 33% with the increment of H_2 content in the syngas. When the H_2/CO ratio is higher, it implies higher H_2 concentration in the bio-syngas. Most of H_2 would be consumed first for removing oxygen from the iron and transformed to H_2O contained in the BFG. Especially for syngas with H_2/CO ratio 1.6 and 1.3, the injection rates of H_2 reach 71.8 and 59.5 $kg \cdot t_{HM}^{-1}$ respectively, which can guarantee reducing reaction of all the iron-based materials. Thus final share of H_2 and H_2O in the BFG is the highest

when H_2/CO ratio achieves 1.6. Total percentage of carbon bearing gases which are CO_2 and CO varies slightly at any H_2/CO ratios. And the content of N_2 in syngas is used to maintain flow rate of BFG. On the other hand, temperature of BFG is attributed to injection rate of bio-syngas, appearing as an increased trend with more bio-syngas input. When H_2/CO ratio is 1.3, there is the largest amount of bio-syngas injected, i.e., 2892 $kg \cdot t_{HM}^{-1}$, and the temperature of BFG reaches the highest at 458 ℃.

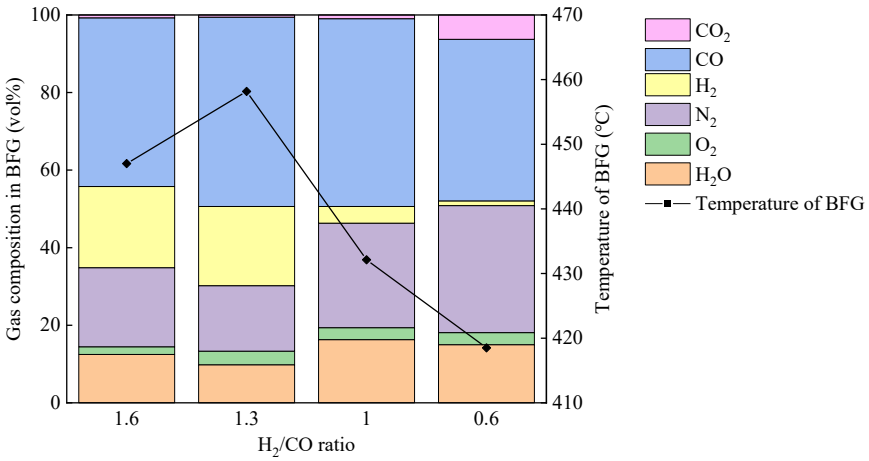

Figure 4.14: Effects of H_2/CO ratio on the BFG composition and temperature.

In order to further estimate the effect of H_2/CO ratio on Fe_2O_3 reduction, distribution of H_2 utilisation at different stages is analysed and the results are shown in Figure 4.15. There are four main approaches to the utilisation of H_2, including reduction of FeO, Fe_3O_4, Fe_2O_3, and discharged as exhaust gas. As H_2/CO ratio decreased, the H_2 content would decrease, which causes a reduction of distribution of H_2 application. Thus the percentage of H_2 indirect reduction to all the H_2 orientations would increase. The bio-syngas has H_2 content of 28 $kg \cdot t_{HM}^{-1}$ when H_2/CO ratio is 0.6, however, this amount of H_2 can only be supplied for transition of FeO to Fe, and H_2 expelled through top gas comes from coke decomposition. The amount of H_2 as reducing agent accounts for 78%, and 22% of H_2 are eventually wasted as exhaust gas. When the H_2/CO ratio is 1.6 and the H_2 injection rate is 72 $kg \cdot t_{HM}^{-1}$, the content of H_2 could satisfy all three steps of Fe_2O_3 reduction. The H_2 reduction ratios of Fe_2O_3, Fe_3O_4, and FeO are 7%, 13%, and 40%, respectively. It is demonstrated that the reduction of Fe_2O_3 consumes the lowest H_2, and most of H_2 contents in the bio-syngas are consumed for reduction of FeO to Fe. The optimal H_2/CO ratio of bio-syngas is achieved at the value of 1.6 when injection rate of bio-syngas is 1734 $kg \cdot t_{HM}^{-1}$.

Hydrogen of the bio-syngas usually reacts preferentially with iron bearing materials compared to CO of the syngas. This happens because the diffusion behaviour of H_2 is much higher than that of CO. The diffusion coefficient increases with increased temperature and H_2 content in the gas mixture. A higher temperature will lead to the faster gas molecule movement. Reduction with H_2 is endothermic, and reduction with CO is exothermic, thus the H_2 reduction is more suitable in the case of higher temperature. As bio-syngas is injected first to the lower zone of furnace where temperature is the highest, H_2 molecule moves faster to react with iron-based burdan. Therefore, it is also verfied that H_2 in the bio-syngas is beneficial to the overall reduction processes in the BF. The H_2/CO ratio of bio-syngas is better within 1.6-1.3.

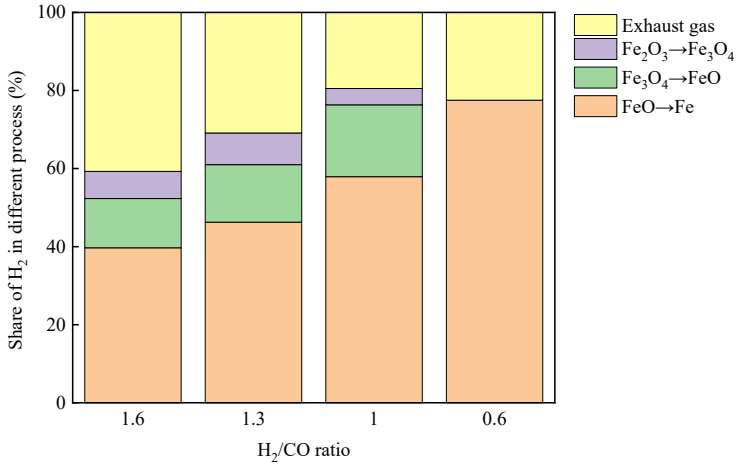

Figure 4.15: Effects of H_2 on different reduction stages of bio-syngas with various H_2/CO ratio.

4.5.3 Overall performance of biomass-based reducing agent injection

Finally, the resulting SEC and CO_2 emissions generated by BF operation with different reducing agents are shown in Figure 4.16 and 4.17. An apparent result can be seen in Figure 4.16 is that the BF process injection with auxiliary reducing agent has a lower total site SEC than the reference case, i.e., using only coke. The maximum SEC could achieve 18.4 GJ·t_{crude}^{-1} for BF with coke injection, of which BF process accounts for the largest percentage and contributes to 14.7 GJ·t_{crude}^{-1}. For scenarios that substitute coke with PC, charcoal, and bio-oil, all the values of SEC reduce from 18.4 GJ·t_{crude}^{-1} to 17.5 GJ·t_{crude}^{-1}, 17.8 GJ·t_{crude}^{-1}, and 17.7 GJ·t_{crude}^{-1}, respectively. Lower SEC for case PC is because charcoal and bio-oil injected into BF have higher heating value than that of PC. Energy consumed in the BF compose of energy supply from coke, auxiliary reducing agent, and air. Under the conditions

of constant energy densities of coke and air, the heating value of biomass could severely affect the final SEC of ironmaking process. The lowest energy consumption is found in the case of bio-syngas, which is only 15.1 GJ·t_{crude}^{-1}. When injecting bio-syngas into BF, H_2 content in the syngas reduces the heating value. And it reveals that bio-syngas is more efficient at energy saving of ironmaking process.

In terms of energy distribution, energy consumption of sintering, coking, BF, and BOF process form total site SEC. It is certain that BF process consumes the maximum energy ranging from 10.9 GJ·t_{crude}^{-1} to 13.9 GJ·t_{crude}^{-1}, followed by sintering process. The process SEC of coking also varies with the change of reducing agent applied in BF. When BF only injects coke as reducing agent, coking process needs the most coal feedstock to produce appropriate amount of coke that needed in the BF, causing SEC of coking unit to 1.9 GJ·t_{crude}^{-1}. It is demonstrated that SEC of coking process is affected by coke rate of BF. With the decrease of coke rate, process SEC of coking would reduce. In addition, SEC of sintering and steelmaking processes remain constant when BF operates with different reducing agents, which is evaluated especially in relation to productivity of ironmaking. Output of BF process maintains same even with different reducing agents. Thus auxiliary reducing agent has no effect upon the energy demand of sintering and steelmaking processes.

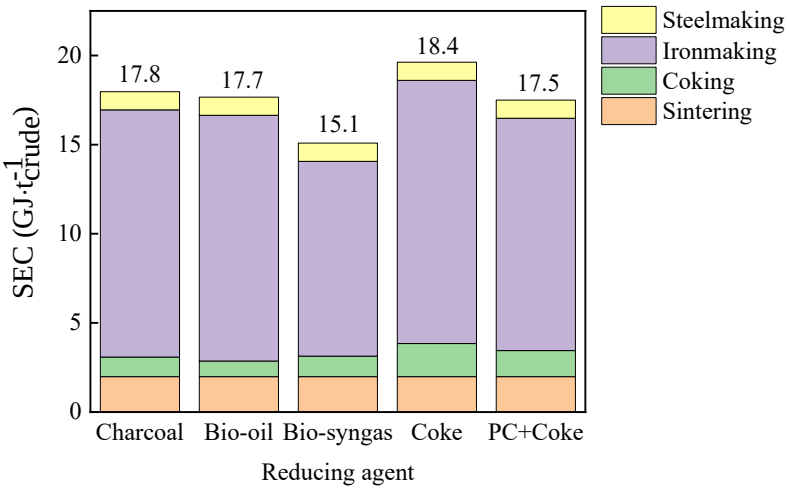

Figure 4.16: Specific energy consumption when injecting biomass-based reducing agent.

CO_2 emissions of on-site BF process in terms of injecting different reducing agents are shown in Figure 4.17. Total site CO_2 emissions is the sum of CO_2 contribution of each production unit. It can be found that the maximum CO_2 emissions occurs when BF only operates with coke, which is the

same as SEC. The largest reduction of CO_2 emissions could happen when bio-syngas is utilised in BF as auxiliary reducing agent. The reduction rate achieves 51% from 1.2 $GJ \cdot t_{crude}^{-1}$ to 0.59 $GJ \cdot t_{crude}^{-1}$. Taking cases that inject coke, charcoal, bio-oil, and PC into consideration, ironmaking process discharges more CO_2 than other three units. This is because only CO acts as a reducing agent in these cases, and CO is eventually converted into CO_2. Similar to the SEC situation, CO_2 contributions of sintering and steelmaking keep unchanged, with no regard to different reducing agents. CO_2 emissions of coking process increase with injecting higher coke into BF. It can be concluded that the replacement of coke by auxiliary reducing agent improves the total site SEC and CO_2 emissions, however, it cannot influence conditions of sintering and steelmaking processes. Meanwhile, the optimisation of system could reach the most promising SEC and CO_2 emissions level by introducing bio-syngas into BF process.

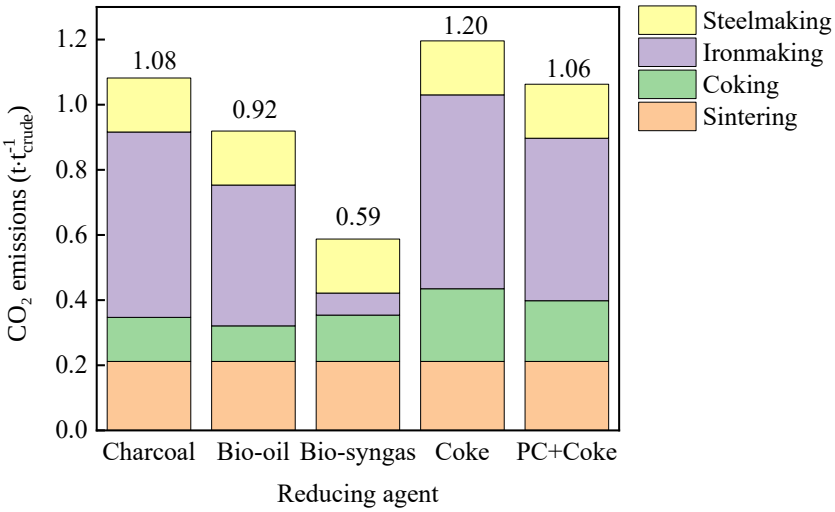

Figure 4.17: Direct CO_2 emissions when injecting biomass-based reducing agent.

4.6 Summary

In this chapter, the performance of BF is optimised first by substituting coke with biomass-based reducing agents. The possibilities of converting biomass feedstock into reducing agent have been discussed. Three cases that processes with charcoal, bio-oil, and bio-syngas are designed to explore the potential of coke replacement and CO_2 emissions reduction. The model of cases is built and simulated by Aspen Plus based on three reactions among reducing agents and iron bearing materials. Besides the effect of biomass on BF operation, total site SEC and CO_2 emissions from full-length

manufacturing process are also analysed. Injection rates of different biomass are main variables to evaluated system, while bio-syngas needs additional consideration of H_2/CO ratios.

As a results, charcoal, bio-oil, and bio-syngas can be utilised in BF as auxiliary reducers with a certain amount. The results indicate that coke demand per ton of hot metal can be decreased and CO_2 emissions are reduced when bio-reductants are injected into BF. An optimal coke replacement is operated with 200 $kg \cdot t_{HM}^{-1}$ bio-oil and 222 $kg \cdot t_{HM}^{-1}$ coke. The reaction involving bio-syngas has the most potential to reduce CO_2 emissions, and the favourable H_2/CO ratio ranges from 1.6 - 1.3. Carbon content in the biomass has relatively large effect on the final CO_2 emissions. It is necessary to clarify the sink and boundary of each CO_2 emissions evaluation. Based on systematic results of energy consumption and CO_2 emissions, it can be found that biomass barely has influence on sintering and steelmaking. Further performance study of sintering and steelmaking should focus on the productivity of ironmaking.

Table 4.8 lists the main advantages and disadvantages for three kinds of bio-reductant after overall evaluation of BF operating with biomass-based reducing agent.

Table 4.8: Advantages and disadvantages for three bio-reducers.

Biomass	Advantages	Disadvantages
Charcoal	• High yield • High heating value • Well comparable to coke	• High oxygen and volatile matter • Low replacement of coke • Low CO_2 reduction rate
Bio-oil	• High coke replacement • High BF process efficiency	• High content of oxygen, ash, and moisture • Particular raw material
Biomass-based syngas	• Great potential to reduce CO_2 emissions • H_2 in the syngas has high reducing ability	• Hard to remove other gases in the syngas • High amount of syngas needed to control the results of reduction

Chapter 5

CO_2 capture combined with waste heat recovery for iron making process

It is noted that the aforementioned ways i.e., BF operation with biomass-based syngas has the largest CO_2 reduction rate, but it is still not enough to reduce CO_2 emissions and improve energy efficiency from fossil-based sources. To further achieve the targets, both CO_2 capture and waste heat recovery technologies should be adopted. It is widely acknowledged that carbon capture is recognised as the cost-effective method to reduce energy-related emissions in various industries. In our basic system, CO_2 discharged from BF process accounts for 18% of the top gas, and it is the largest emission source in the whole iron and steel production chain. Meanwhile blast stove exhaust exits from furnace at around 250 ℃. To recycle abundant low grade heat from hot stove flue gas, ORC technology has been demonstrated as a feasible choice due to its simple configuration and high reliability. In order to reduce energy penalties caused by CO_2 capture, ORC is used for providing CO_2 compression power and solvent regeneration heat. In this chapter, ORC combined the CO_2 capture is integrated into a biomass-based BF process. The study aims to find a sustainable way to improve energy efficiency and a high CO_2 recovery. Different possibilities of implementing CO_2 capture and ORC into an iron and steel plant is analysed. From the viewpoints of CO_2 reduction and energy balances, performance analysis is conducted to compare the proposed system and the reference case.

5.1 Amine-based carbon capture in the iron and steel production

Generally, carbon capture can be classified into three types, i.e., pre-combustion capture, post-combustion capture, and oxy-fuel combustion. The technology that intends to capture CO_2 from the flue gas which usually has a low concentration of CO_2 (3-20%) is referred to as post-combustion CO_2 capture. Amine-based CO_2 capture is a well-known post-combustion capture technology for gas sweetening and is considered as one of the most attractive CO_2 capture options due to its process simplicity and maturity [245]. As one of the main solvents used for post-combustion CO_2 capture,

mono-ethanolamine (MEA) is very reactive and can effectively remove a high volume of acid gas from flue gases [246].

Figure 5.1 presents a simplified MEA-based CO_2 absorption process scheme. The capture plant using MEA usually consists of an absorber and a stripper. The most commonly accepted reaction mechanism of MEA and CO_2 is zwitterion mechanism. The zwitterion is a type of intermediate that is instantaneously neutralised by MEA and then forms carbamate [247]. Two steps of reaction between MEA and CO_2 could be expressed as equations 5.1 and 5.2. The existence of carbamate is unstable when CO_2 loading is high. ${CO_3}^{2-}/{HCO_3}^{-}$ is formed at high CO_2 concentration, which is usually described as equation 5.3. As can be seen from equations, CO_2 desorption from rich solvent is a reverse process of CO_2 absorption.

$$CO_2 + RNH_2 \leftrightarrow {RNH_2}^{+}COO^{-} \quad (5.1)$$

$${RNH_2}^{+}COO^{-} + RNH_2 \leftrightarrow RNHCOO^{-} + {RNH_3}^{+} \quad (5.2)$$

$$RNH_2 + CO_2 + H_2O \leftrightarrow {HCO_3}^{-} + {RNH_3}^{+} \quad (5.3)$$

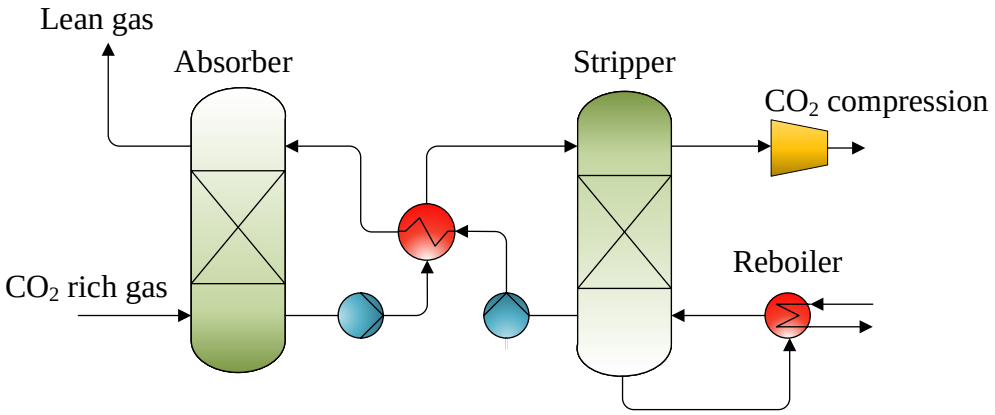

Figure 5.1: MEA-based CO_2 capture process configuration.

Several projects have attempted to implement MEA-based CO_2 capture to ironmaking BFG and other steelmaking off-gas steams, e.g. the Ultra-Low CO_2 Steelmaking program attempts to separate CO_2 from top gas and reinjects CO back in BF. [248]. It is found that these projects have rarely moved into commercial scale, which is mainly due to high separation costs. The separation costs for MEA-based CO_2 recovery from BFG with 30-40% CO_2 is estimated at \$ $71.7 \cdot t^{-1}$ CO_2 [249]. More importantly, the capture processes are energy-intensive and a large quantity of energy are required for solvent regeneration. Regeneration heat is often provided by additional fossil fuel combustion, which

incurs extra investment costs and CO_2 emissions. Through the recovery of excess heat from industrial sites to drive an amine-based absorption process, the production of process steam and CO_2 emissions at the power plant could be decreased. Under this scenario, low heat recovery technologies e.g. as ORC for power generation are integrated with CO_2 capture to further reduce energy penalty [250].

Applications of low grade heat recovery technologies in iron and steel production have been summarised in the Section 2.3.2. Table 5.1 summarises several integrated cases of CO_2 capture and ORC in power plants. ORC system could provide electricity for CO_2 compression. However, there is limited research on the CO_2 capture of iron and steel plant integrated with ORC. The integrated system in this chapter aims to partly cover the demands of electricity and regeneration heat for CO_2 capture, meanwhile achieving the goal of reduce CO_2 emissions.

Table 5.1: Several examples of integration of CO_2 capture and ORC in industries

Application	ORC power output	Net power output	Captured CO_2 ($kg \cdot s^{-1}$)	Capture method	Ref.
Natural gas combined cycle power plant	2.02 MW	381.2 MW	42.43	MEA absorption	[251]
Liquefied natural gas cycle	0.11 MW	0.39 MW	2.78	Condensation	[252]
Coal-fired power plant	12.8 MW	255.5 MW	62.8	MEA absorption	[253]
Combined system of ORC and carbon capture	0.69 MW	0.63 MW	2.8	MEA absorption	[254]
Thermal power plant	17.4 MW	300.7 MW	0.5 mol CO_2/ mol MEA	MEA absorption	[255]

5.2 System description and modelling

Figure 5.2 illustrates the general schematic diagram of decarbonised BF ironmaking process integrated with ORC. The process is composed of a BF operation with biomass-based reducing agent injection, a MEA-based CO_2 capture and compression system, and an ORC system. The whole system is modelled using Aspen Plus.

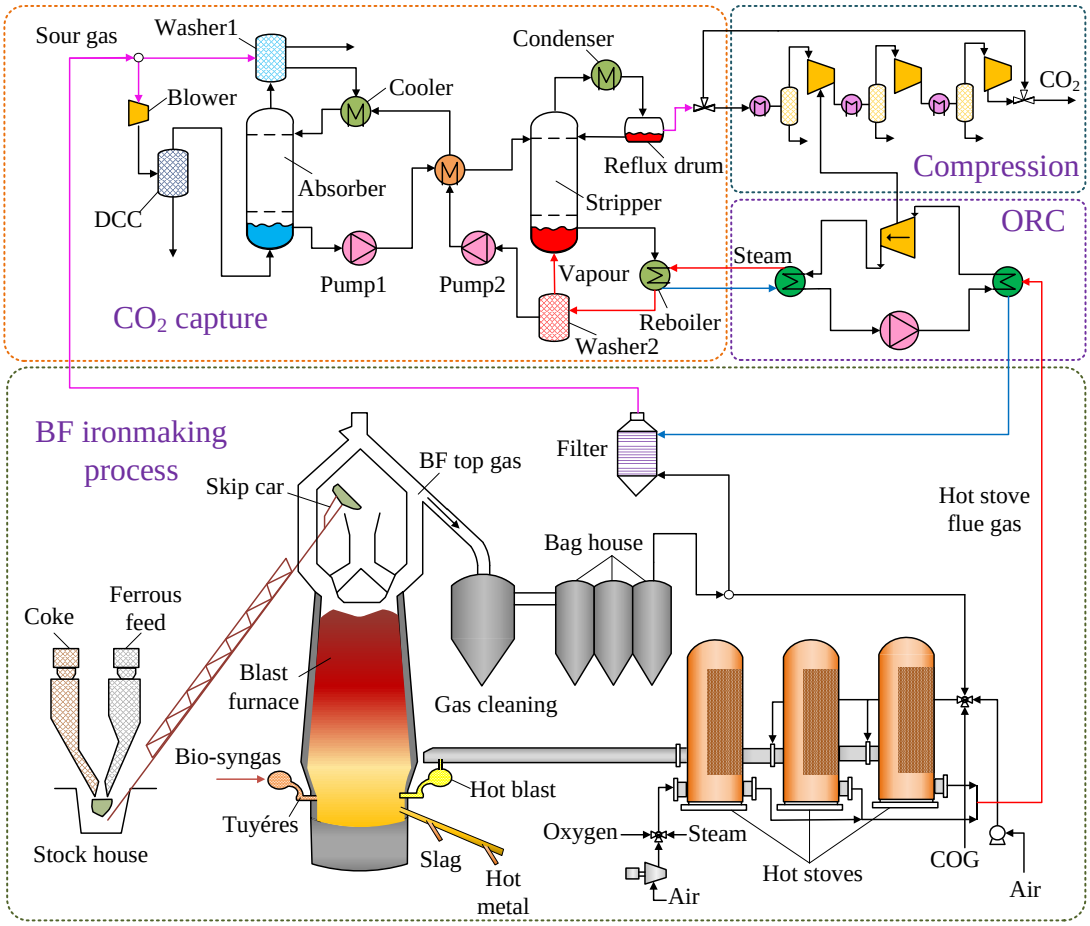

Figure 5.2: Schematic diagram of decarbonised BF ironmaking process.

5.2.1 BF ironmaking unit

The modelling of BF unit is based on the current BF simulation in Section 3.4.3. Coke is produced in coke ovens and the iron ore has been previously agglomerated in the sinter or pelletizing plants. The biomass-based syngas and hot blast are injected into the BF through tuyéres. In the BF ironmaking plant, the major sources of CO_2 emissions come from the BF top gas and hot stoves. The off-gas exits the top of the furnace and proceeds firstly to the cleaning equipment where the significant amounts of sulphur, oxygen or contaminants are removed from the BFG. Partial cleaned BFG and COG is burned as fuel gases in the HBS. The combustion of flue gases could provide preheated air at a temperature from 900℃ to 1250℃, which allows achieving the smelting temperature in the BF [256].

Table 5.2 shows simulated results of BFG composition when BF operates with different reducing agents. All the details of input streams refer to Table 4.4. In the cases of which inject biomass as auxiliary reducing agent, the demands of charcoal, bio-oil, and bio-syngas are 200 $kg \cdot t_{HM}^{-1}$, 200

$kg \cdot t_{HM}^{-1}$, and 1734 $kg \cdot t_{HM}^{-1}$, respectively. It can be seen that 1.2% CO_2 exists in the flue gas from case of bio-syngas and it nearly reduces 92% CO_2 emissions compared with that of the basic case which only injects coke as reducing agent in BF. Thus carbon capture technology is used to further reduce CO_2 from flue gases of which the CO_2 concentrations range from 14.8% to 18.2%.

Table 5.2: Key parameters of BFG simulated results.

Parameters	Only coke injection	PC injection	Charcoal injection	Bio-oil injection	Bio-syngas injection
Gas composition (vol %)					
O_2	3.9	3.9	3.7	2.9	3.0
N_2	47.0	47.4	47.8	53.1	35.0
H_2	5.1	4.3	5.2	5.8	16.7
CO	25.8	26.2	25.5	23.4	44.1
CO_2	18.2	18.3	17.7	14.8	1.2
Flow rate ($kg \cdot s^{-1}$)	319.3	319.1	312.4	275.6	345.3
Temperature (℃)	386	385	387	391	426

5.2.2 CO_2 capture unit

Any of the gas that not consumed in the stoves will enter CO_2 capture system combined with exhaust gas from HBS. The process starts with a blower to mitigate pressure drop in column of absorber. Then a direct contact cooler (DCC) is used to cool down flue gas to about 40 ℃. Further, CO_2 from flue gas will react chemically with MEA solution. The scrubbed flue gas is emitted to the atmosphere and the rich CO_2 solvent is heated by a lean/rich cross heat exchanger to around 100-110 ℃ before it flows to stripper. The MEA solution is regenerated inside the stripper with vapour flow from the reboiler, while the CO_2 exiting the top of column and is condensed in condenser. Liquid reflux returns to stripper and CO_2 is sent for compression. Regenerated solvent is recycled to the absorber by passing through the cross-heat exchanger where solvent provides its heat to rich solvent. The CO_2 capture process is simulated by Aspen Plus as shown in Figure 5.3 using rate-based mode of RadFrac model which could simulate absorber and stripper with chemical reactions. The model of CO_2 capture unit has been validated in the Abigail González's doctoral thesis [257] where comprehensive flowsheet models of CO_2 absorption have been validated using four data sets of pilot plant [258]. The validation shows that the Aspen rate-based absorber model efficiently simulates the absorber of pilot plant, and it also relies heavily on the MEA-CO_2-water reaction kinetics model and the selected mass transfer correlations. Table 5.3 shows the comparison of simulation results from Abigail's work and Rezazadeh et al [259].

Table 5.3: Comparison of simulation results from Abigail's thesis and Rezazadeh et al.

Comparison	CO_2 capture rate	Rich loading	Absorber fraction to flooding	Reboiler temperature	Reboiler duty
Rezazadeh et al [259]	90%	0.4761	73%	117.2 ℃	3.64 $MW \cdot t^{-1}$ CO_2
Abigail [257]	90%	0.4721	70%	120 ℃	3.56 $MW \cdot t^{-1}$ CO_2

Another section of model includes pumps, heat exchangers, and separators. Blower and pumps are modelled by blocks of expander and pump. Heat exchangers are applied as cooler, lean/rich exchanger, condenser, and reboiler for providing regeneration heat, respectively. Four separators are deployed as DCC, washer, and deaerators, respectively. Their input parameters are summarised in Table 5.4. Details of absorber and stripper are illustrated in subsequent contents.

Table 5.4: Input parameters of MEA-based CO_2 capture model in Aspen plus.

Component	Parameter	Value
Blower	Pressure increase	0.1 bar
	Isentropic efficiency	85%
Pump 1	Discharge pressure	5 bar
Pump 2	Discharge pressure	1.9 bar
Cooler	Outlet temperature	40 ℃
Lean/rich heat exchanger	Hot inlet-cold outlet temperature difference [a]	10 ℃
Reboiler	Cold stream outlet temperature [a]	120 ℃
Condenser	Outlet temperature [b]	40 ℃
DCC	Outlet temperature [a]	45 ℃
Washer	Outlet temperature	45 ℃

[a] Values are taken from reference [260].
[b] Values are taken from reference [257].

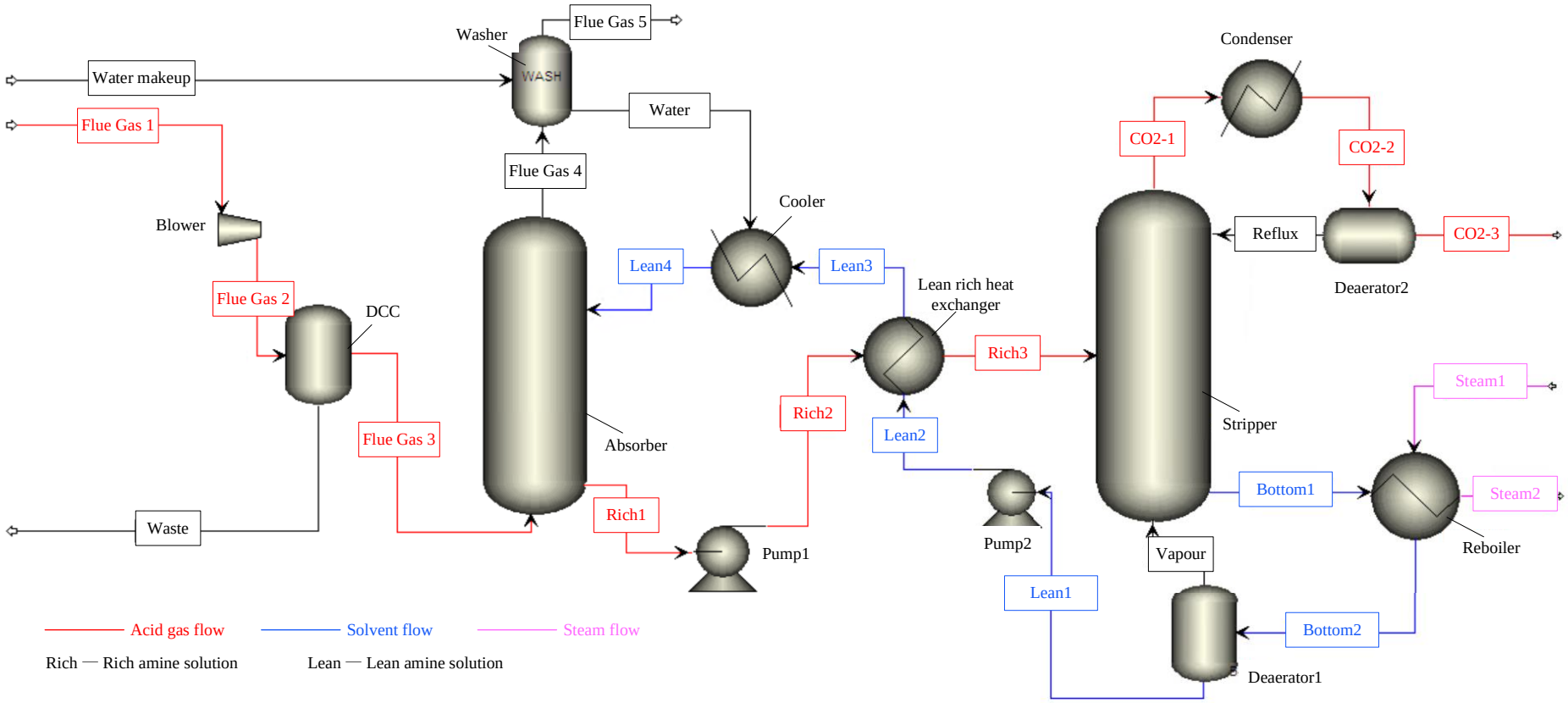

Figure 5.3: Schematic diagram of MEA-based CO_2 capture in Aspen plus.

Sensitivity analysis is a typical way for the design of absorber and stripper. For absorber, the analysis focuses mainly on determining the mass flow of solvent and column size which includes packing height and diameter. Theses parameters are all related to specific CO_2 fraction in the flue gas and CO_2 capture rate. Mass flow rate of solvent could be determined by rich loading which indicates the ratio of moles of CO_2 to moles of MEA in the liquid rich in acid gas exiting absorber bottom. According to equations 5.1 and 5.2, the ideal rich loading should be 0.5 mol CO_2/mol MEA, but it is difficult to dispose 100% CO_2 in the flue gas and lean solvent solution has a small portion of CO_2. Thus rich loading usually covers a certain of range from 0.25 to 0.53 [261]. Rich loading depends on temperature of absorber and partial pressure of CO_2. The latter is calculated as equation 5.4:

$$P_{CO_2} = \varphi_{CO_2,flue} \times P_{tot} \tag{5.4}$$

where P_{CO_2} is partial pressure of CO_2 in the absorber, $\varphi_{CO_2,flue}$ is mole fraction of CO_2 in the flue gas, and P_{tot} is total pressure of the absorber system.

The parameters for designing stripper usually include lean loading, temperature and pressure of stripper. The reactions occurred in the stripper are endothermic. The heat duty is provided by reboiler only for reverse of CO_2 absorption. High temperature and pressure at stripper could accelerate CO_2 mass transfer rate, whereas they also cause problems of solvent degradation and corrosion in the stripper. An appropriate temperature of reboiler needs to be determined for stripper operation. It is verified that 120 ℃ is a recommended temperature which has optimised the experimental results in a pilot plant [262]. Lean loading is defined as moles of CO_2 to moles of MEA in the lean solvent exiting from the bottom of stripper, which is calculated as equation 5.5:

$$Lean = \frac{\dot{n}_{CO_2,lean}}{\dot{n}_{MEA}} \tag{5.5}$$

where n_{CO_2} is mole of CO_2 in the lean solvent, and n_{MEA} is mole of regenerated MEA existing the stripper. With regard to the ratio between mass rate of MEA solution and flue gas, a parameter of *Liq/Gas* ratio is used and is defined as equation 5.6:

$$Liq/Gas = \frac{\dot{m}_{sol}}{\dot{m}_{flue}} \tag{5.6}$$

where m_{sol} and m_{flue} are mass flow rate of solvent and flue gas, respectively.

Absorber and stripper are both packed columns. Packing of two columns increases contact area between gas and liquid phases, and also reduces pressure drop. Generally, the ratios of height to diameter of two columns are larger than 1 [263]. The packed height is a function of theoretical plate

height that is decided by transfer coefficient of gas and liquid phases [264]. When CO_2 has high level concentration, rich loading is the main factor that influences packing height of absorber, while volume of CO_2 is low, packing height is affected by the gas residence time. Column diameter is determined by gas flow rate and gas velocity passing through column, which is expressed as equation 5.7:

$$D = \sqrt{\frac{4Gas}{\pi u_s}} \tag{5.7}$$

where *Gas* is gas volume flow rate, *u* is gas superficial velocity through cross section of column.

Table 5.5 lists basic parameters for absorber and stripper. Details of absorber and stripper design equations are provided in Appendix A. Inlet temperatures of flue gas to absorber and rich solvent to stripper are determined by DCC and lean/rich heat exchanger, respectively. The pressure of stripper is set to guaranteeing temperature of MEA boiling lower than that of MEA degradation [263]. Recommended values for pressure drop of absorber and stripper range from 147-490 pa·m^{-1} packing [259]. The calculation types of absorber and stripper are rate-based approach that considers mass transfer between gas and liquid phases [265]. For both columns, the category of packing is chosen as Sulzer Mellapak 250Y for higher mass transfer efficiency.

Table 5.5: Basic parameters of absorber and stripper.

Parameters	Absorber	Stripper
Inlet temperature (°C)	40	115
Column pressure (bar)	1	1.8[a]
Column pressure drop (bar)	0.03[b]	0.012[b]
Number of stages	20[c]	8[c]
Calculation type	Rate-based[d]	Rate-based[d]
Packing type	Sulzer Mellapak 250Y[b]	Sulzer Mellapak 250Y[b]

[a] Values are taken from reference [263].
[b] Values are taken from reference [259].
[c] Values are taken from reference [257].
[d] Values are taken from reference [265].

The objective of carbon capture system is to capture 90% of the CO_2 in flue gas using 30 wt% MEA solution. Capture rate of 90% is commonly used for design and evaluation of MEA-based capture in open publications [266]. Parametric analysis of absorber is to explore the effect of CO_2 concentration and MEA mass flow rate on the rich loading and height of column and then to decide conditions at constant CO_2 capture rate.

5.2.3 CO_2 compression unit

Recovered CO_2 is further transported to different storage sites which could be underground or deep sea. Pipeline for CO_2 transportation is the one of most common ways. CO_2 needs to be compressed to the pipeline at the pressure ranging from 85-150 bar. It is mainly to ensure a stable phase of CO_2 when it flows along the pipe [255]. Three different phases, i.e., vapour, liquid, and supercritical are viable for CO_2. It is assumed that CO_2 has a long-distance transportation, so the discharge pressure is required to be high to avoid pressure drop and gas volume. In this study, CO_2 is pressurised to the supercritical phase for long distance transportation.

Figure 5.4 shows schematic diagram of CO_2 compression model in Aspen Plus. The validity of the CO_2 compression model has been processed by comparing results from Rezazadeh et al [259] with data available in the public domain [267]. The comparison of CO_2 compression electricity consumption is presented in Table 5.6. The whole CO_2 compression process consists of multi stages to compress CO_2 flow. The number of stages depends on pressure ratio of CO_2, which is defined as final pressure of CO_2 to pressure of CO_2 when it inputs to the compression system. To compress CO_2 from 2 bar to 150 bar, of which pressure ratio is 75, 7 stages are required for compression, conversely, compression system needs more stages. One unit of compression stage include a compressor, an inter-cooler, and a separator. Inter-cooler is used for condensation of water and reducing volume of gas before gas enters next stage. Gas is condensed to 40 ℃ at cooler to stabilise its supercritical status. And reduction of gas volume could save energy for compression. Basic information for compression system in simulation is given in Table 5.7.

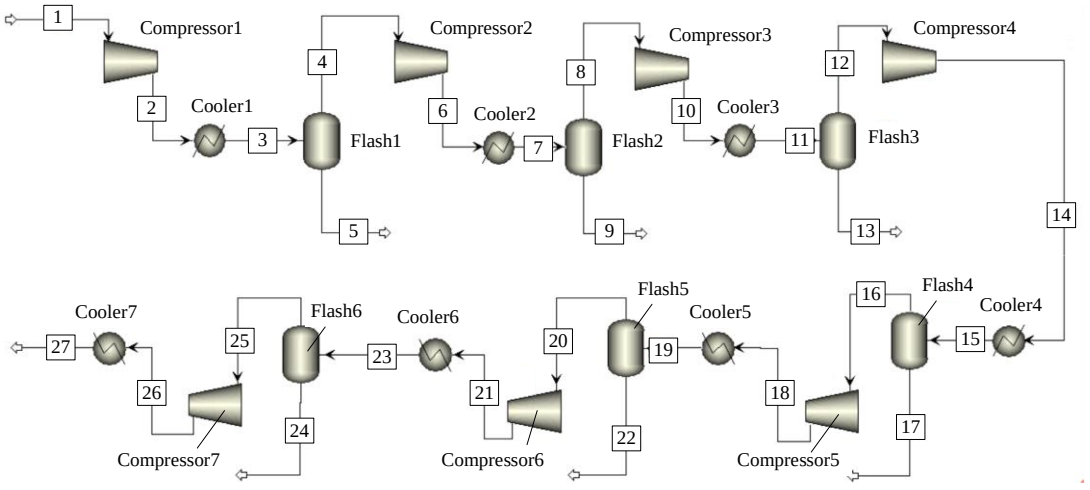

Figure 5.4: Schematic diagram of CO_2 compression in Aspen plus.

Table 5.6: Comparison of CO_2 compression model results.

Parameter	Rezazadeh et al [259]	National Energy Technology Laboratory [267]	Error (%)
CO_2 compression electricity consumption (MWe)	18 MWe	18.977 MWe	5.15

Table 5.7: Input parameters of CO_2 compression model.

Component	Parameter	Value
Compressor 1	Inlet pressure	1.868 bar
	Discharge pressure	4 bar
Compressor 2	Discharge pressure	8 bar
Compressor 3	Discharge pressure	15 bar
Compressor 4	Discharge pressure	30 bar
Compressor 5	Discharge pressure	60 bar
Compressor 6	Discharge pressure	110 bar
Compressor 7	Discharge pressure	150 bar
Cooler 1-7	Condensation temperature	40 ℃
Flash 1-6	Temperature	40 ℃

5.2.4 ORC power generation unit

As indicated in Figure 5.2, the sensible heat of flue gas from hot stoves is recovered as heat source to drive the ORC system. An ORC configuration includes an evaporator, an expander, a condenser and a pump. The system in this study also deploys a preheater, a superheater, and a regenerator to increase inlet and outlet temperature, thus improving thermal efficiency. Organic fluid is directly heated by flue gas from hot stoves via the evaporator and enters the expander as vapour. Then the power generated in the expander is transferred to CO_2 compressor system. Working fluid leaving expander is proceeded to condenser and later is sent to pump for pressurisation. The integration of ORC system could avoid the energy penalty caused by the steam and electricity traditionally generated at CHP plant.

Figure 5.5 presents basic simulation flowsheet of ORC in Aspen Plus. This model has been built and validated in our previous study [268], which is shown in Table 5.8. The relative errors show a good agreement between the reference and previous work. Thus, the ORC model in the previous study is reliable to be used directly in this calculation.

Input parameters for this ORC model are presented in Table 5.9. Assumptions of the ORC model are as follow: (1) ORC cycle operates under steady-state conditions; (2) thermodynamic equilibrium happens at the inlet and outlet of each component; (3) the kinetic energy of heat transfer and working fluid in solar ORC cycles are negligible; (4) heat loss and pressure drops in the system can be

overlooked; and (5) electricity consumption of water valves and refrigerant valves are ignored. Mass flow rate of hot stream is read from hot stove gas of BF model. Mass flow rate of condenser cooling water is set to meet heat demand of MEA regeneration. Inlet temperature of cooling water is read from model of CO_2 capture. Mass flow rate of working fluid is calculated from the energy balance at evaporator. Evaporation and condensing pressures are evaluated based on thermodynamic properties of refrigerant.

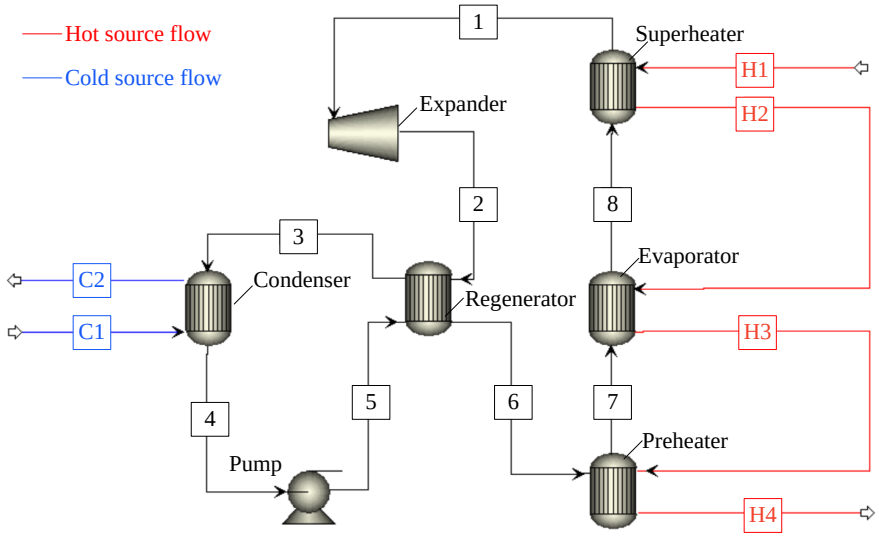

Figure 5.5: Schematic diagram of ORC power generation in Aspen plus.

Table 5.8: Comparison of results between the reference and precious work.

Parameter	T_1 (°C)	m_{wf} ($kg \cdot s^{-1}$)	T_4 (°C)	T_5 (°C)	W_{net} (kW)	Q_h (kW)	η_{ORC} (%)
Kaşka, Ö [194]	92.9	11.06	34.9	35.4	262.2	2479	10.58
Previous study [268]	93.3	11.06	34.87	35.41	244.6	2313	10.57
Error (%)	0.43	0	0.09	0.03	6.71	6.69	0.09

Table 5.9: Input parameters of the ORC model in Aspen Plus [268].

Section	Parameter	Value
Calculation method	Peng-Robinson method	
Fluid pump	Discharge pressure	Evaporation pressure (210 °C)
	Efficiency	0.65
Regenerator	Cold stream outlet temperature	T_6
Preheater	Cold stream outlet vapour fraction	0
Evaporator	Cold stream outlet vapour fraction	1
Superheater	Cold stream outlet temperature	T_1
Expander	Discharge pressure	Condensing pressure
	Isentropic efficiency	0.75
Condenser	Condensation temperature	150 °C

Working fluid	Mass flow rate	51 kg·s^{-1}
Hot stream	Mass flow rate	208.95 kg·s^{-1}
	Inlet temperature	250 °C
Cold stream	Mass flow rate	575 kg·s^{-1}
	Cooling temperature	134 °C

In order to meet the temperature for solvent regeneration ranging of 110 ℃-130 ℃, it is necessary to choose a proper working fluid ensuring the condensing temperature of refrigerant higher than 130℃. In this study, toluene is selected as refrigerant due to its high critical temperature and low environmental impacts, and its basic properties are listed in Table 5.10.

Table 5.10: Basic properties of working fluid [269].

Fluid	Critical Temperature	Critical pressure	Density	Heat of vaporisation
Toluene	318.6 °C	41.26 bar	862.2 kg·m^{-3}	361.3 kJ·kg^{-1}

Figure 5.6 shows the T-s diagram of an ORC system with toluene, which is illustrated as saturated line of working fluid in the temperature versus different entropy. The thermodynamic properties data of toluene is obtained from REFPROP 9 (National Institute of Standards and Technology, Gaithersburg, MD, USA). The blue line in the figure represents ORC cycle with state points, at which fluid goes through a transition between liquid and vapour phases. Densities of toluene from 20 to 800 kg·m^{-3} are also drawn in the figure using dotted lines. At state point 1, toluene enters the expander to deliver work and is expanded to condensing pressure at point 2. Next, toluene passes through regenerator to release part of heat which could preheat toluene after compression at point 5. From 3 to 4, toluene is condensed to a saturated liquid and then it is pressurised in the compressor to evaporation pressure. During the heating process, toluene is first preheated from point 6 to 7, then it is constantly heated at evaporator where it becomes a saturated vapour. After toluene leaves the evaporator and before entering turbine, toluene has a superheated vapour phase. Because toluene is a dry fluid, there is no need for superheating in this cycle.

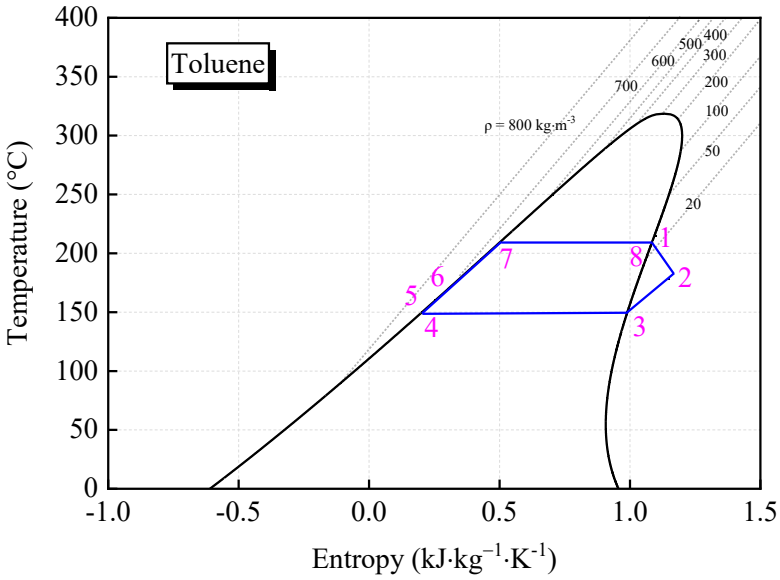

Figure 5.6: T-s diagram of an ORC system using toluene as the working fluid.

The electricity and heat generated by ORC system will be investigated to compare electricity and heat consumption CO_2 capture and compression units. System combined with ORC and CO_2 capture is compared with the reference case using different reducing agents, for the purpose to evaluate benefits for CO_2 capture when waste heat recovery technologies are applied.

5.3 Thermodynamic analysis method of CO_2 capture system with ORC

5.3.1 CO_2 capture and compression system

The effects of design parameters on CO_2 capture system are mainly reflected in the aspects of CO_2 capture rate and energy consumption. Although the final specification of capture system is established based on the constant capture rate, i.e., 90%, adjustments of loading and column characteristics are necessary to control CO_2 capture rate. Generally, the proportion of CO_2 removed from initial flue gas is defined as CO_2 capture rate, which also stands for the amounts of CO_2 captured of per total amounts of CO_2 that input absorber. The capture rate is calculated as equation 5.8:

$$CR_{CO_2} = \frac{\dot{n}_{CO_2,out,str}}{\dot{n}_{CO_2,in,abs}} \tag{5.8}$$

where $\dot{n}_{CO_2,out,str}$ and $\dot{n}_{CO_2,in,abs}$ are mole flow rates of CO_2 exiting stripper and CO_2 entering absorber, respectively.

CO_2 desorption is an endothermic reaction and is driven in the stripper. CO_2 escapes with vaporised water from top of the stripper. Meanwhile, absorbent regenerates in the stripper and requires a large amount of heat which consists of three branches, as shown in equation 5.9 [270]:

$$\dot{Q}_{regen,MEA} = \dot{Q}_{re} + \dot{Q}_{sen} + \dot{Q}_{lat} \tag{5.9}$$

where $\dot{Q}_{regen,MEA}$ is regeneration heat of MEA solvent, it consists of reaction heat $\dot{Q}_{re}$ of CO_2 desorption, sensible heat $\dot{Q}_{sen}$ to heat up rich solution to the regeneration temperature, and latent heat $\dot{Q}_{lat}$ of vaporising water. The regeneration energy varies with different values of lean loading. In our system, regeneration heat of reboiler is provided by condensing steam from ORC system, thus $\dot{Q}_{regen,MEA}$ could also be expressed as equation 5.10:

$$\dot{Q}_{regen,MEA} = \dot{Q}_{cond} = \dot{m}_{\mathrm{c}}(h_{\mathrm{c},2} - h_{\mathrm{c},1}) \tag{5.10}$$

where $\dot{Q}_{cond}$ is heat required for condensation in ORC system, $\dot{m}_{\mathrm{c}}$ is mass flow rate of cooling water, $h_{\mathrm{c},2}$ and $h_{\mathrm{c},1}$ are specific enthalpy of input low pressure steam and outlet cooling flow, respectively. For energy consumed to vaporise water in the stripper to generate steam, $\dot{Q}_{lat}$ is calculated considering energy balance between condenser as shown in Figure 5.3, which is represented in equation 5.11:

$$\dot{Q}_{lat} = \dot{m}_{CO_2,1}h_{CO_2,1} - \dot{m}_{CO_2,3}h_{CO_2,3} - \dot{m}_{reflux}h_{reflux} \tag{5.11}$$

where subscripts of mass flow rate $\dot{m}$ and specific enthalpy h correspond to moist CO_2 exiting from the stripper, dry CO_2, and reflux of water, respectively. As for reaction heat for CO_2 desorption $\dot{Q}_{re}$, an equilibrium is expressed as equation 5.12:

$$\dot{Q}_{re} = \dot{n}_{CO_2,out,str}\Delta h_{re} \tag{5.12}$$

where Δh_{re} is molar reaction enthalpy between CO_2 and MEA. So sensible heat $\dot{Q}_{sen}$ is estimated based on the difference between regeneration heat and sum of latent heat with reaction heat.

Electricity consumed by the compressors 1-7 are expressed as equations 5.13:

$$W_{com,i} = \dot{m}_{CO_2,out,str}(h_{com,i+1} - h_{com,i}) \tag{5.13}$$

where $h_{com,i+1}$ and $h_{com,i}$ are the outlet and input specific enthalpy of the *i*th CO_2 compression stage.

5.3.2 ORC system

The performance analysis of ORC system is based on the thermodynamic model. The general energy balance of the conventional ORC can be expressed as equations 5.14 and 5.15:

$$\sum \dot{m}_{\text{in}} = \sum \dot{m}_{\text{out}} \tag{5.14}$$

$$\dot{Q} + \dot{W} = \sum \dot{m}_{\text{out}} h_{\text{out}} - \sum \dot{m}_{\text{in}} h_{\text{in}} \tag{5.15}$$

where $\dot{Q}$ and $\dot{W}$ are the net heat flow rate and work inputs, h is specific enthalpy of the stream of the system, and $\dot{m}_{\text{in}}$ and $\dot{m}_{\text{out}}$ are inlet and outlet mass flow rates.

Total heat absorbed by working fluid consists of energy transferred from preheater, evaporator, and superheater, and those can be evaluated by equations 5.16-5.19:

$$\dot{Q}_{\text{preheat}} = \dot{m}_{\text{wf}}(h_7 - h_6) = \dot{m}_{\text{w}}(h_{\text{hot},3} - h_{hot,4}) \tag{5.16}$$

$$\dot{Q}_{\text{eva}} = \dot{m}_{\text{wf}}(h_8 - h_7) = \dot{m}_{\text{w}}(h_{\text{hot},2} - h_{\text{hot},3}) \tag{5.17}$$

$$\dot{Q}_{\text{superheat}} = \dot{m}_{\text{wf}}(h_1 - h_8) = \dot{m}_{w}(h_{\text{hot},1} - h_{\text{hot},2}) \tag{5.18}$$

$$\dot{Q}_{\text{h}} = \dot{Q}_{\text{preheat}} + \dot{Q}_{\text{eva}} + \dot{Q}_{\text{superheat}} \tag{5.19}$$

where $\dot{Q}_{\text{preheat}}$, $\dot{Q}_{\text{eva}}$ and $\dot{Q}_{\text{superheat}}$ are thermal energy obtained by working fluids in the preheating, evaporation and superheating process, respectively. The subscripts of specific enthalpy h are based on state points, as shown in Figure 5.6.

The heat balances in the condenser and regenerator can be expressed by equations 5.20 and 5.21:

$$\dot{Q}_{\text{cond}} = \dot{m}_{\text{wf}}(h_3 - h_4) = \dot{m}_{\text{c}}(h_{\text{c},2} - h_{\text{c},1}) \tag{5.20}$$

$$\dot{Q}_{\text{regen}} = \dot{m}_{\text{wf}}(h_2 - h_3) = \dot{m}_{\text{wf}}(h_6 - h_5) \tag{5.21}$$

Energy conservation in the expander and fluid pump is defined by equations 5.22 and 5.23:

$$\dot{W}_{\text{exp}} = \dot{m}_{\text{wf}}(h_1 - h_2) \tag{5.22}$$

$$\dot{W}_{\text{pu}} = \dot{m}_{\text{wf}}(h_5 - h_4) \tag{5.23}$$

The expansion ratio of ORC process R_p is defined as ratio of working fluid inlet pressure to outlet pressure of expander, which is usually described as equation 5.24:

$$R_p = \frac{P_{in,exp}}{P_{out,exp}} \tag{5.24}$$

where $P_{in,exp}$ is expander inlet pressure which is defined by evaporating pressure of working fluid, and $P_{out,exp}$ is expander outlet pressure which equals to condensing pressure of refrigerant.

Net power $\dot{W}_{\text{net}}$ and cycle thermal efficiency of conventional ORC η_{ORC} are presented by equations 5.25 and 5.26:

$$\dot{W}_{\text{net}} = \dot{W}_{\text{exp}} - \dot{W}_{\text{pu}} \tag{5.25}$$

$$\eta_{\text{ORC}} = \frac{\dot{W}_{\text{net}}}{\dot{Q}_{\text{h}}} \tag{5.26}$$

The detailed exergy analysis of the conventional ORC will be illustrated in Chapter 6.

5.4 Performance of integration system

In this section, influence of MEA solution and column parameters, i.e., MEA solution flow rate, rich loading, and the absorber height, are investigated in terms of CO_2 capture rate and reboiler duty. The comparison of energy required for MEA regeneration and CO_2 compression are based on chosen cycle parameters. The benefits of ORC integrating with CO_2 capture are summed up to explore the potential of energy saving and CO_2 reduction.

5.4.1 Effects of MEA solution flow rate on capture rate and reboiler duty

To separate 90% CO_2 from BFG, it is necessary to adjust flow rate of MEA solution to maintain the same capture rate. Flue gases which have different CO_2 concentration would be in relation with various range of MEA flow rate. The effect of the CO_2 concentration and MEA solution flow rate on the capture rate are shown in Figure 5.7. CO_2 concentrations of BFG are 18.2%, 18.3%, 17.7%, 14.8% respectively, which also correspond to the reducing agents used in BF, i.e., only coke, PC with coke, charcoal, and bio-oil. The model also sets initial values of absorber height 24m, and diameter of columns 13m.

It is evident that increasing MEA solution flow rate leads to the rise in capture rate. When BFG has CO_2 concentration of 18.2% and 18.3%, the trends of capture rate with the change of solvent flow rate perform almost the same. CO_2 capture rates of concentration at 18.2% and 18.3% rise from 55.5% to 93.1%, and 55.7% to 93.3%, respectively, with an increase of solvent flow rate from 1000 $kg \cdot s^{-1}$ to 1800 $kg \cdot s^{-1}$. The difference between capture rate of two stream is only 0.2%. MEA solution flow rate that could capture 90% CO_2 from BFG is found at 1715 $kg \cdot s^{-1}$ corresponding to a CO_2 concentration of 18.2%. As CO_2 concentration is increased by 0.1% to 18.3%, 90% capture rate could be achieved by 1708 $kg \cdot s^{-1}$ MEA solution. For flue gas with 17.7% CO_2 concentration, the demand of solvent decreases to 1640 $kg \cdot s^{-1}$. Only 1245 $kg \cdot s^{-1}$ MEA solution is needed to capture 90% CO_2 from BFG that CO_2 concentration is 14.8%. It is worth noting that solvent flow rate cannot infinitely increase at a constant absorber height, otherwise flood of streams would happen in the column. Under the condition of same solvent flow rate, higher CO_2 concentration brings lower CO_2 capture rate. This is because the same amount of MEA reacts with a fixed amount of CO_2 which would account for the great majority of CO_2 in the BFG with low CO_2 concentration.

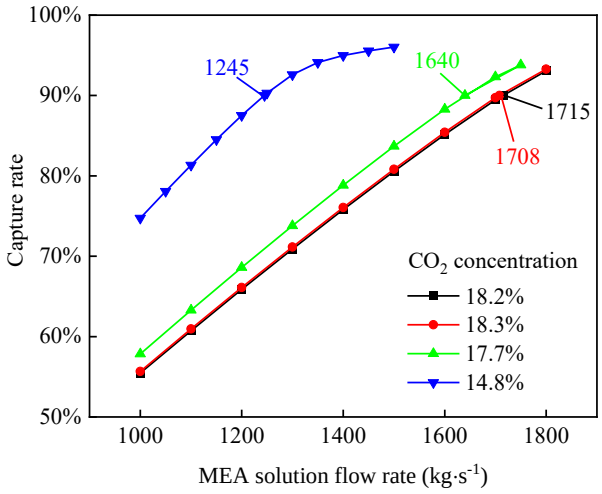

Figure 5.7: CO_2 capture rate at different CO_2 concentration and MEA solution mass flow rate

Figure 5.8 depicts the effects of solvent flue rate on rich loading and rich loading on the CO_2 capture rate. Rich loading indicates MEA loading with CO_2 at outlet of absorber. According to reaction mechanism between MEA and CO_2, rich solution has fractional ions including $MEAH^+$, $MEACOO^-$, HCO_3^-, and CO_3^{2-}, which are associated with MEA and CO_2. After calculating rich loading of four streams of flue gas, it could be found that rich loading presents opposite trends compared to the capture rate. The solvent flow rate ranges from 1000 $kg \cdot s^{-1}$ to 1800 $kg \cdot s^{-1}$, which results in rich loading decreased from 0.4813 to 0.4571. As shown in Figure 5.8(b), the relation of capture rate with rich loading becomes a singer line. Capture rate continuously decreases with the increase of rich loading. Under this condition, higher rich loading usually occurs when lower MEA solution flow rate injects into absorber. Because lower solvent flow rate leads to reduced capture rate, the overall tendency of CO_2 capture rate in relation with rich loading is reasonable. As shown in figure, 90% capture rate presents where rich loading is 0.4687. Capture rate starts to drop sharply after 90%, and this demonstrates that considerable amount of MEA is needed to separate over 90% CO_2 from BFG.

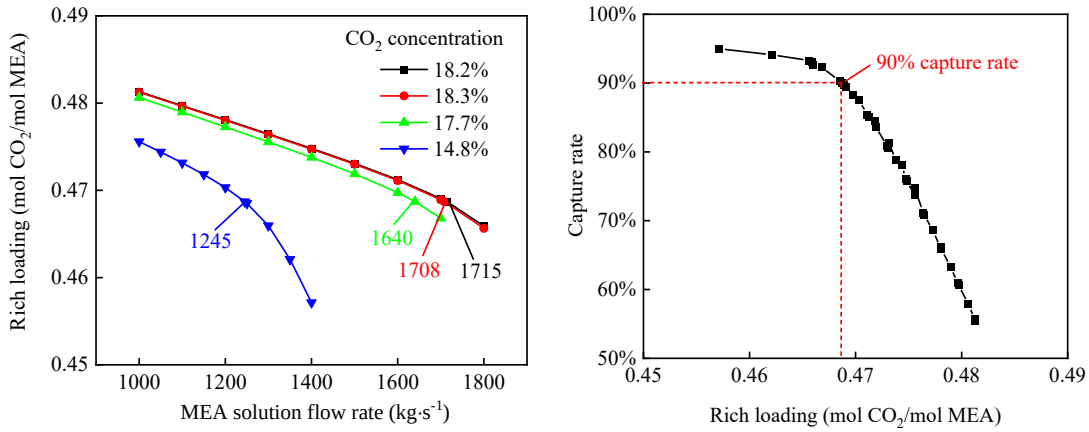

Figure 5.8: (a) Effect of MEA solution flow rate on rich loading; (b) Variation of CO_2 capture rate at different rich loading.

Figure 5.9 shows the trends of reboiler duty which is a crucial point to represent MEA regeneration heat. The MEA solution flow rate increases from 1000 kg·s^{-1} to 1800 kg·s^{-1}. Similar to the results of capture rate, heat required for MEA regeneration increases with more MEA in the stream. The results are comprehensible because the mass of MEA in the lean solution is proportional to the heat duty. Therefore, increased solvent flow leads to higher sensible heat that heats up the MEA. Higher sensible heat corresponds to higher reboiler energy. Since capture rate increases with solvent flow rate, the reboiler duty naturally grows with higher capture rate.

The figure also reflects the effect of CO_2 concentration of flue gas on the reboiler energy. When same amount of lean solvent is regenerated to the cycle, the maximum reboiler energy is found at CO_2 concentration of 14.8%, whereas the minimum reboiler duty occurs at 18.3% concentration. It is indicated that lower CO_2 concentration requires relatively high specific reboiler duty per unit of MEA regenerated. To maintain the CO_2 removal rate at 90%, the lean solvent flow rate increases with the increase of CO_2 concentration, and the demands of heat are 3.452 MJ·kg^{-1} CO_2, 3.450 MJ·kg^{-1} CO_2, 3.451 MJ·kg^{-1} CO_2, 3.456 MJ·kg^{-1} CO_2, respectively for flue gases with CO_2 concentration of 18.2%, 18.3%, 17.7%, and 14.8%. It could be found that the difference among heat duties under conditions of four CO_2 concentration are subtle. Thus the reboiler duty is less sensitive to the CO_2 concentration of flue gas when capture rate is fixed.

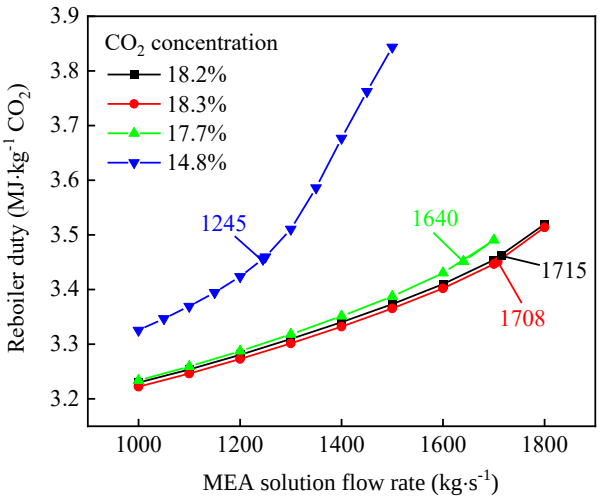

Figure 5.9: Specific reboiler duty vs. various MEA solution flow rates.

5.4.2 Effects of absorber height

This section investigates effects of absorber height on capture rate, rich loading, and reboiler duty at a given flow rate of MEA solution which is related to 90% capture rate. Packing height in the absorber column is a dominate factor that affects contact area and transfer coefficient of gas and liquid streams. It is necessary to set column height properly, otherwise high absorber can slow down the reaction rate and low absorber height would cause flood in the column. Figure 5.10 shows the variation of the capture rate at different height of absorber and CO_2 concentration. It is apparent that four lines under different CO_2 concentration almost gather as one trend. Comparing with Figure 5.7 in which capture rate is jointly affected by solvent flow rate and CO_2 concentration when packing height is constant, capture rate is mostly related with absorber height other than CO_2 concentration when solvent flow rate is fixed. This comparison illustrates that absorber height acts as more prominent role than solution flow rate and CO_2 concentration.

As labelled in figure, to achieve 90% CO_2 separated from flue gas, absorber height needs to be designed as 24 m. Although capture rate presents a rise with higher absorber, the amount of CO_2 removed from flue gas increases swiftly at lower absorber height, i.e., below 20 m. As height of absorber greater than 20 m, the capture rate changes inapparently with the increase of absorber height. It is demonstrated that 100% removal of CO_2 from flue gas needs extremely high column, and this would result in low efficient utilisation of column. This is also the main reason why CO_2 removal rate is usually set as 90% to save cost of building column.

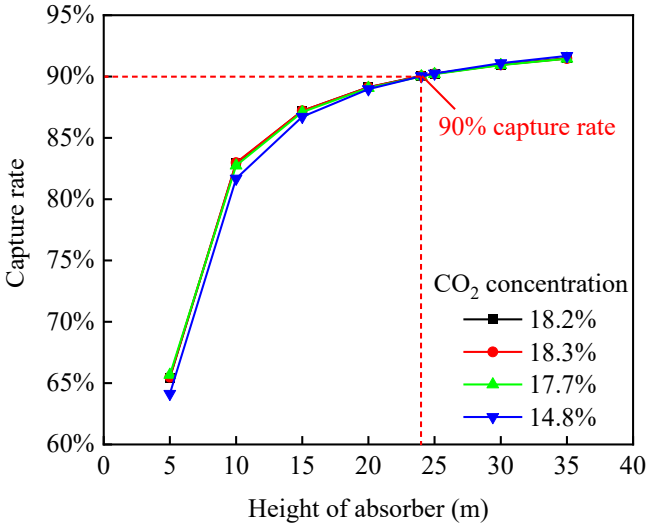

Figure 5.10: CO_2 capture rate at different CO_2 concentration vs. height of absorber (*D*: 13 m).

Effects of CO_2 concentration and absorber height on the rich loading are shown in Figure 5.11. The solvent flow rates at which capture rate is 90% are applied to analyse rich loading. Under this condition, the flow rate of flue gas needs to change accordingly with absorber height, which aims to maintain capture rate as 90%. The relation of flue gas injection rate with height of absorber is shown in Figure 5.12. When absorber height is below 15 m, rich loading and flue gas rate have a dramatic increase and approach to a flat after absorber height greater than 20m. The initial flue gas rates are all around 300 $kg \cdot s^{-1}$. If absorber height is shortened to the lowest length, i.e., 5m, flue gas flow rates are reduced to less than 50 $kg \cdot s^{-1}$ and the rich loading is about 0.3. The reduction rates reach 83% and 37% respectively for flow rate and rich loading. The fact illustrates that a great amount of MEA has not been used at lower absorber height, thus absorber height has to be set higher than 15m. The diagrams also show that CO_2 concentration barely has influence on the rich loading, while flue gas flow rate would decrease with reduction of CO_2 concentration. Rich loading is only affected by CO_2 concentration when absorber height is fixed. As a consequence, absorber height and solvent flow rate are two main factors that control the rich loading.

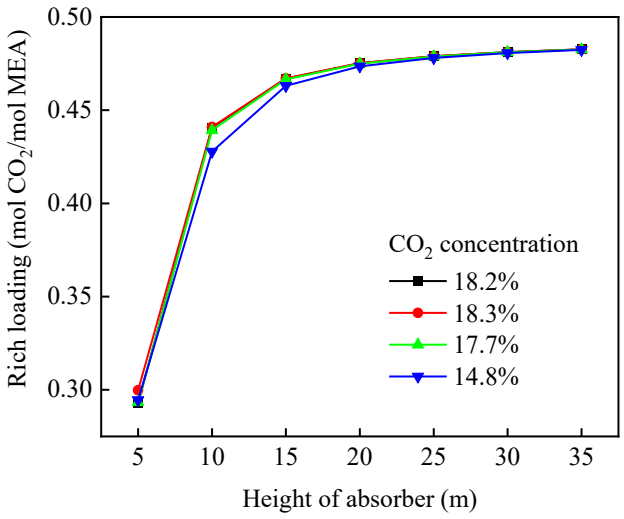

Figure 5.11: Rich loading at different CO_2 concentration vs. height of absorber (*D*: 13 m).

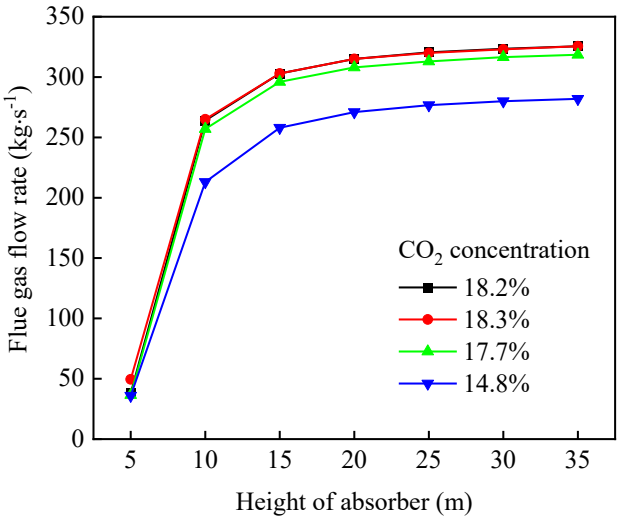

Figure 5.12: Flue gas flow rate at different CO_2 concentration vs. height of absorber (*D*: 13 m).

Effects of absorber height on reboiler duty under the conditions of fixed capture rate and solvent flow rate are shown in Figure 5.13. Overall trend of reboiler duty is opposite to the results of rich loading. It has been observed that the maximum reboiler duty is required at the lowest absorber height, which reaches 13.3 MJ per kilogram CO_2 absorbed for 18.2% CO_2 concentration. Reboiler duties which correspond to CO_2 concentration of 18.3%, 17.7%, and 14.8% at 5 m absorber are 11.1, 12.8, and 12.3 $MJ \cdot kg^{-1}$ CO_2, respectively. Therefore, the reboiler requires relatively high energy to help the generation of the MEA solvent at the lowest absorber height. This happens because, once the

packing height becomes lower, less amount of flue gas can be reacted in the absorber, which results in per unit of CO_2 absorbed needs more regeneration heat.

When the absorber height rises from 5 m to 10 m, heat duty swiftly drops to 4 $MJ \cdot kg^{-1}$ CO_2, then reboiler duty has a slight drop based on different CO_2 concentration. If the column is as high as 35 m, reboiler duty can be decreased to around 3.3 $MJ \cdot kg^{-1}$ CO_2. It is indicated that when packing height is above 10 m, it has a low influence on reboiler duty. This is because the solvent mass rate used here is defined and is sufficient to react with CO_2 in the flue gas. The increment rates of capture rate and flue gas rate with the rise of absorber height after 10 m are close. So the reboiler duty is used only to heat the solvent and reverse the absorption, and is almost irrelevant to the contact area in the column. As it can be seen, except for the first point at 5 m height, the influence of CO_2 concentration on reboiler duty can also be ignored. It is demonstrated that reboiler duty mostly depends on solvent flow rate.

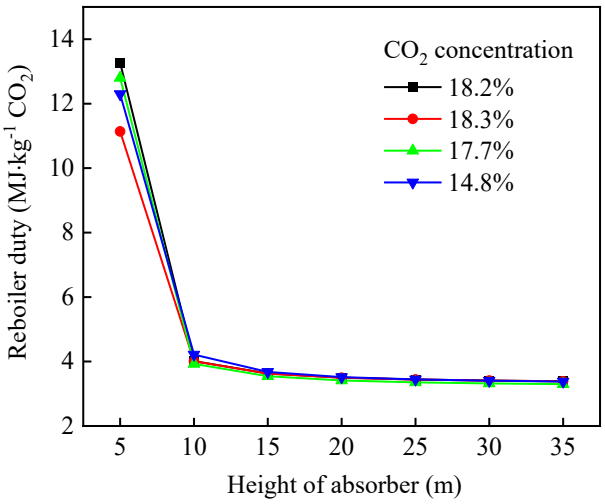

Figure 5.13: Specific reboiler duty at different CO_2 concentration vs. height of absorber (D:13 m).

5.4.3 Energy required for MEA regeneration and CO_2 compression

Energy requirement of MEA-based CO_2 capture system mainly consists of MEA regeneration heat and electricity for CO_2 compression. Figure 5.14 and 5.15 presents results of regeneration heat and compression energy, respectively. Four columns in the figure are associated with four reducing agents applied in the BF and also four CO_2 concentrations. The calculation of energy is based on a system that has 90% capture rate and 24 m absorber height. Regeneration heat that can be calculated

by multiplying reboiler duty and quantity of CO_2 absorbed. Total compression electricity is the sum of specific net work required by seven compressors.

Results show that the heat requirement for solvent regeneration and electricity for compression depend on the CO_2 source. In the Figure 5.14, it is found that the regeneration heats are quite close if CO_2 emissions are from BF processes that only use fossil-based reducing agents. Also the maximum regeneration heat is needed when BF only injects coke as reducing agent. Although reboiler duty of flue gas with 17.7% CO_2 concentration is slightly higher than that of 18.3% CO_2 concentration, the regeneration heat consumption could be improved by 5%. The main reason is that using biomass-based reducing agent in BF reduces CO_2 concentration of flue gas, resulting in decreased amount of CO_2 captured by system. When BF operates with bio-oil, regeneration heat can be greatly reduced by 27.6% to 192.5 MW. Similarly for compression electricity, BF operation with fossil-based reducing agents discharges high CO_2 concentration flue gas, therefore, higher electricity is required for pressurising CO_2. A slight reduction of electricity consumption is found as the result of injection charcoal into BF, which is improved by 4.5% in comparison with BF process that only injects coke. Compression power can also be considerably reduced by using bio-oil in the BF due to the impact of CO_2 concentration of flue gas. Accordingly, bio-oil has the main advantage to improve energy consumption of MEA regeneration and CO_2 compression.

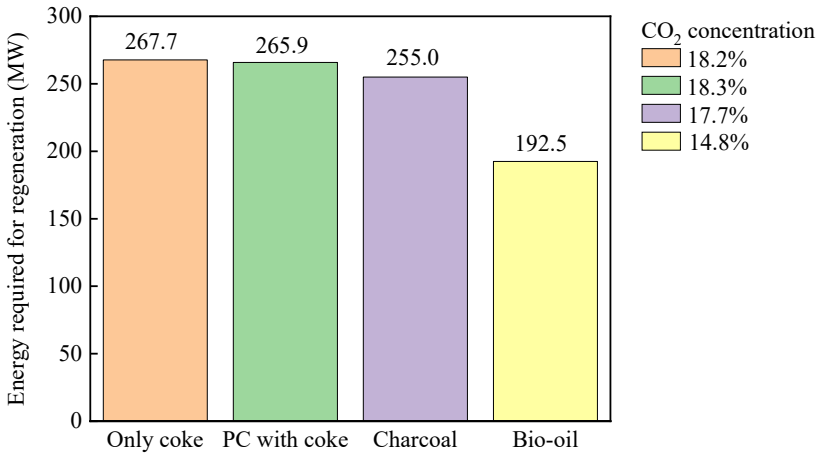

Figure 5.14: Energy required in the reboiler for MEA regeneration at four CO_2 initial concentrations.

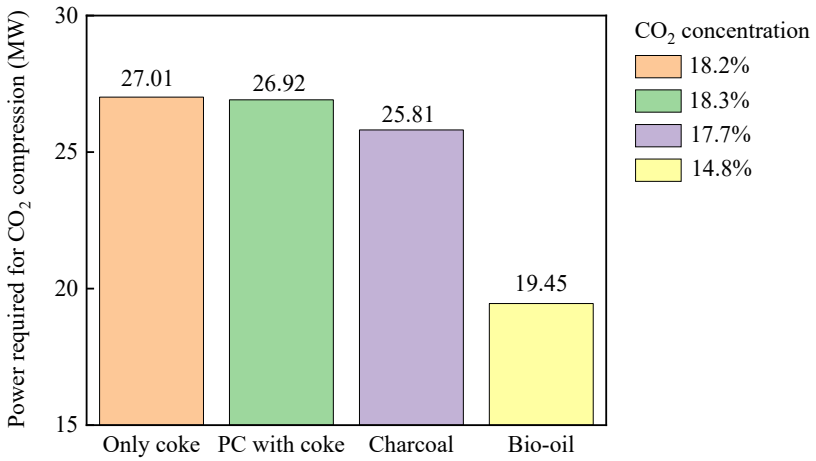

Figure 5.15: Power required for CO_2 compression at four different CO_2 initial concentrations.

5.4.4 Effects of ORC integration with CO_2 capture on energy saving and CO_2 reduction

The proposed ORC system recycles waste heat from hot stove flue gas to generate power for CO_2 compression and provide thermal energy for MEA regeneration. In this section, net work and condensation heat that can be generated by using ORC are analysed. Evaporating temperature predominates the inlet temperature of expander, thereby determining the power output. Compared with evaporating temperature, the temperature of heat source should exceed some range of values. Based on a heat stream at 250 ℃, the highest temperature at which the refrigerant can evaporate is 210 ℃ and a 5 ℃ superheated temperature is assumed. Figure 5.16 shows the changes of net work output and power efficiency with respect to the evaporation temperature of fluid. Black line shows results of net work output corresponding to the left y-axis, and red line represents power efficiency which is labelled on the right y-axis.

It is observed that net work output and power efficiency increase linearly with evaporating temperature. Power output can be increased by 4.5 times from 0.3 MW to 1.72 MW when the evaporating temperature is raised by 50 ℃. The linear mode of power output is because higher expander inlet temperature could drive more power output. Waste heat from exhaust gas provides sufficient quantity of heat for evaporation of working fluid. Power efficiency by using ORC ranges from 0.018 to 0.091, which is improved by up to 4.2 times with 50 ℃ increase of evaporating temperature. Although the power efficiency of ORC is lower than the conventional power generation system, such as the CDQ system which has been applied in the base case with energy efficiency of 26.7%, ORC has high potential to recycle low grade waste heat.

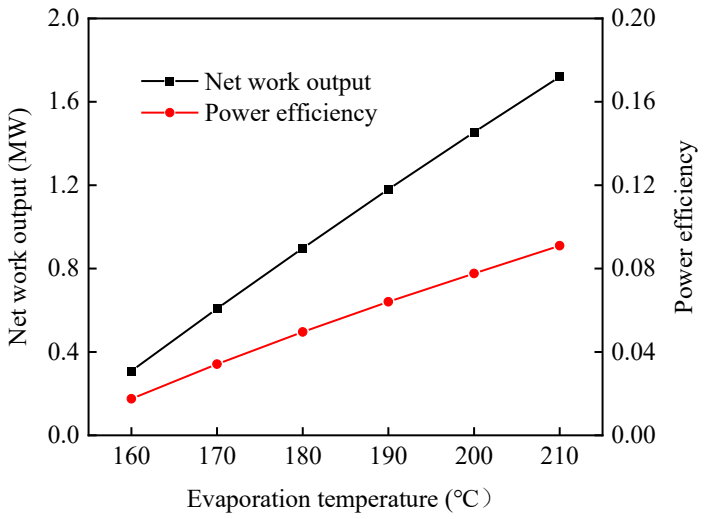

Figure 5.16: Net work output and power efficiency of ORC system vs. different evaporation temperature

The power output at the highest evaporating temperature, i.e., 1.72 MW is utilised to supply a portion of CO_2 compression electricity. Figure 5.17 shows the constitute ratios of electricity utilisation for CO_2 compression and the comparison is still based on four scenarios. As mentioned above, electricity demands of pressurising CO_2 which is originally from four types of flue gas are 27.01 MW, 26.92 MW, 25.81 MW, 19.45 MW, respectively corresponding to only coke, PC with coke, charcoal, bio-oil injections into the BF. This demonstrates that actual consumption of compression electricity is considerably large and far outweighs the power that can be supplied by ORC. It can be seen from figure that the percentage of ORC electricity accounts for up to 9% of the total electricity consumption. And this only happens when bio-oil is injected into BF as auxiliary reducing agent. The rest of electricity expensed by CO_2 compression would be supplied through traditional fossil-based power plants which cause large amount of CO_2 emissions. Since electricity generated by ORC has performance of negative CO_2 emissions, further analysis is to evaluate effects of CO_2 reductions by ORC on total CO_2 emissions of whole site.

The results of CO_2 emissions from power plants using different fossil fuel feedstocks are given in Figure 5.18. Fossil fuels of conventional power plants are chosen as natural gas, coal, and oil, which are similarly applied in Section 3.6.2 for evaluating CO_2 reduction benefits of CDQ and COG cooling. The CO_2 emissions factors of natural gas, coal, and oil when they are generating power are 0.4116,

1.1172, and 1.3409 MT CO_2 eq·TWh^{-1} respectively, and the values are taken from reference [228]. It is assumed that generating capacity of power plant equals to power output from ORC. Therefore, when this quantity of electricity has been replaced by ORC, relevant CO_2 emissions due to fossil fuel power generation would be neutralised. CO_2 reductions are 6.2 kt, 16.8 kt, and 20.2 kt for natural gas, coal, and oil power plants, respectively. Annual CO_2 emissions of iron and steel industry range from 2611 kt to 5622 kt with the change of reducing agents in the BF. In comparison, CO_2 reductions contributed by ORC power generation only account for a small share of total CO_2 emissions, which are less than 1%. It is necessary to further consider thermal energy provided by ORC.

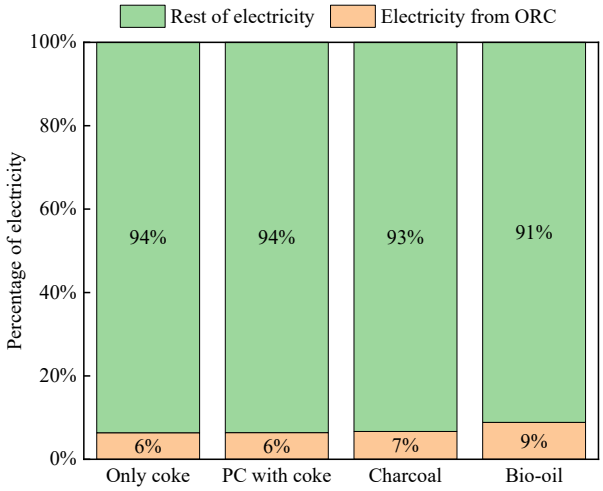

Figure 5.17: Distribution of electricity utilisation for CO_2 compression at four scenarios

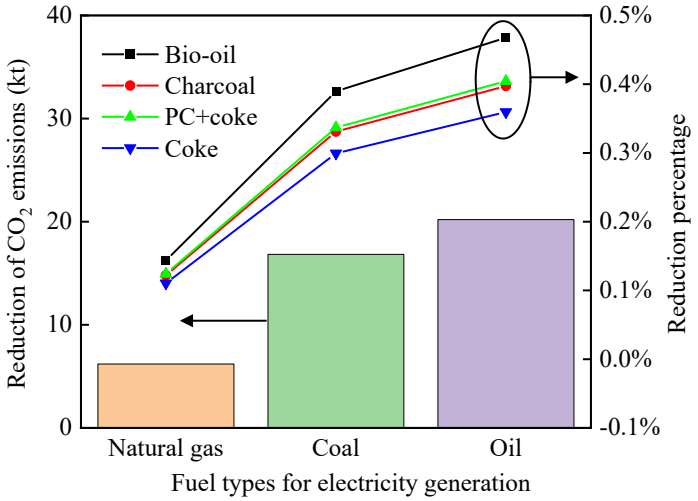

Figure 5.18: CO_2 emissions reduction and reduction percentage when using ORC for providing CO_2 compression electricity

As calculated in Figure 5.14, MEA-based CO_2 capture system encounters a large amount of energy consumption for MEA regeneration. The maximum thermal energy demand could be 267.7 MW when BF completely uses coke as reducing agent. The steam to provide thermal energy is generally extracted from steam turbine cycle combined with fossil-based power plants. As same as power generation, these fuels are coal, natural gas, and oil, and associated CO_2 emissions factors refer to UK government GHG conversion factors report are shown in Table 5.11 [271]. The calculation results of CO_2 emissions from steam generation and related percentages in total CO_2 emissions are shown in Figure 5.19. It is obvious that the steam generation in which coal is combusted contributes to the highest CO_2 emissions, meanwhile the amount of CO_2 emissions accounts for the largest share of total emissions from iron and steel industry when using PC with coke as reducing agents.

Table 5.11: CO_2 emissions factors of steam generation by different fuels [271].

Fuel	Coal	Natural gas	Oil
CO_2 emissions factor (kg $CO_2 \cdot kWh^{-1}$)	0.33	0.18	0.27

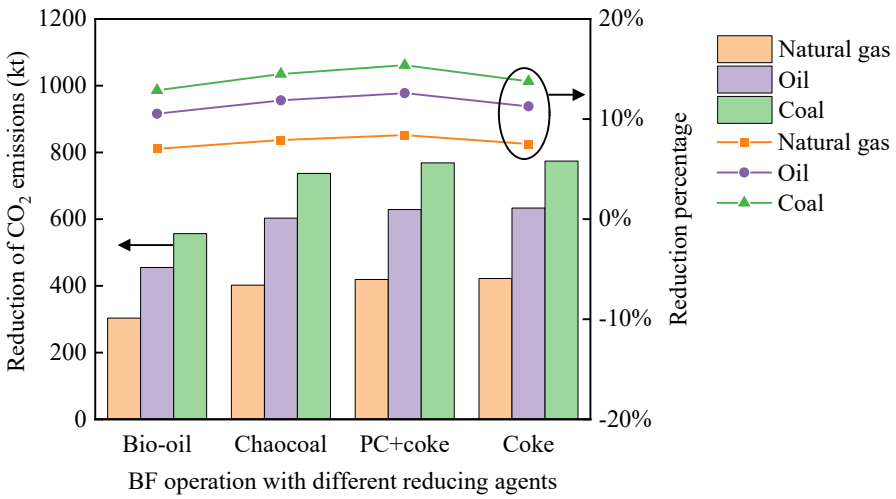

Figure 5.19: CO_2 remissions reduction and reduction percentage when using ORC for providing MEA regeneration heat.

After integrating CO_2 capture with ORC system, MEA regeneration is considered using ORC condensation heat. Temperature of outlet cooling water of condenser is raised to 150 ℃ by saturated working fluid, and the mass flow rate of cooling stream is 575 $kg \cdot s^{-1}$. High temperature and high flow

rate heat source can fully satisfy the energy requirement for MEA regeneration, which means ORC application reduces CO_2 emissions from steam plants where same quantity of steam is generated. The highest CO_2 reduction achieved by ORC is 774 kt and this amount of CO_2 accounts for 13.8% of the total emissions when BF is operated with only coke. It is demonstrated that the effects of ORC used for providing thermal energy are more significant than ORC used for generating power on energy saving and CO_2 emissions.

To summarise effects of CO_2 capture and ORC on energy consumption and CO_2 emissions of integrated iron and steel plant, SEC and CO_2 reduction percentage are given in Table 5.12 and Figure 5.20, respectively. The results of SEC demonstrate that assembling CO_2 capture would increase final energy consumption around 2.0 $GJ \cdot t_{crude\ steel}^{-1}$ due to large amounts of energy demand from MEA regeneration and CO_2 compression. After substituting regeneration heat and partial compression power by using ORC, SEC can be maximumly reduced by 9%. Although final SEC of improved system is slightly higher than that of system without advances, CO_2 emissions of basic system have been dramatically reduced as shown in Figure 5.20. The results show that 69% CO_2 emissions can be reduced when CO_2 capture and ORC are introduced into BF that uses PC and coke as reducing agents. CO_2 capture achieves highly carbon reduction ranging from 44% to 53%. Installation of ORC can further remove total CO_2 emissions from 13% to 16%. It is worth noting that energy consumption still remains a concern for carbon capture, which reveals the importance of renewable and low carbon energy development.

Table 5.12: Specific energy consumption of whole iron and steel sites after combining BF ironmaking with CO_2 capture and ORC.

SEC ($GJ \cdot t_{crude\ steel}^{-1}$)	BF with coke	BF with PC and coke	BF with charcoal	BF with bio-oil
Without CO_2 capture	18.4	17.5	17.8	17.7
With CO_2 capture	20.4	19.5	19.7	19.1
With CO_2 capture and ORC	18.6	17.7	18.0	17.8

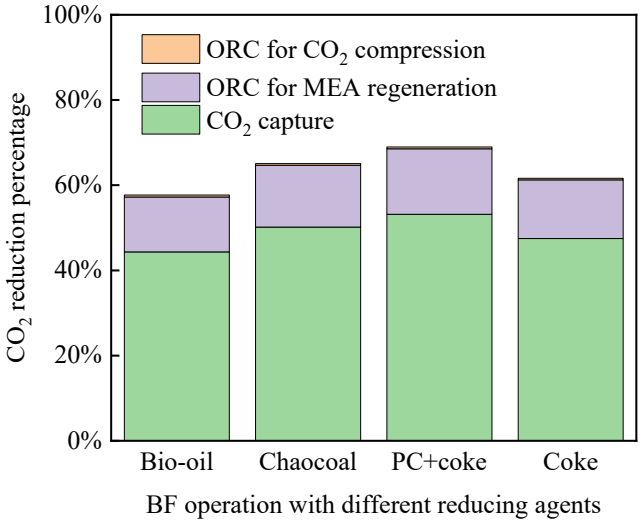

Figure 5.20: CO_2 reduction percentage of total sites when combining ORC with CO_2 capture.

5.4.5 Direct and indirect CO_2 emissions reduction

Energy saving and decarbonised technologies mentioned above are implemented to the basic study system in Chapter 3. The basic case is a plant with integrated iron and steel production lines, of which reducing agent in the BF ironmaking process is PC with coke. Specific CO_2 emissions and total CO_2 emissions of base case are 1.06 $t \cdot t^{-1}_{\text{crude steel}}$ and 4995 kt. The energy saving and decarbonised technologies applied in the plant bring about two types of CO_2 emissions reduction, i.e., direct and indirect reductions. Literally, direct CO_2 reduction is the reduction occurs on-site, and it directly reduces the amount of CO_2 emissions. Indirect CO_2 reduction is a consequence of activities that happen outside the plant boundary, such as electricity generated from fossil-based power plant is substituted by power from CDQ, then CO_2 emissions due to power generation has been indirectly reduced. Table 5.13 lists results of direct and indirect CO_2 emissions reduction of base case after implementing decarbonised technologies.

The improvements that have effects of indirect CO_2 emissions reduction consist of recovering waste heat through CDQ, COG cooling, and ORC. The main functions of these technologies are energy generation, meanwhile output energy can replace electricity or thermal energy from traditional fossil-based power and heat plants. Indirect CO_2 reductions are much less than direct reduction. Injection biomass as auxiliary reducing agent into BF and CO_2 capture are two primary technologies that directly reduce CO_2 emissions. As it can be seen, when bio-syngas is used for Fe_2O_3 reduction, 54% CO_2 emissions can be reduced. After separating 90% CO_2 from flue gas by using MEA-based

CO_2 capture, CO_2 emissions of basic case have been reduced by around 80%. Individual decarbonised technology may not have significant possibility to reduce CO_2 emissions, nevertheless, the combination of various technologies could create great potential of CO_2 mitigation.

Table 5.13: Direct and indirect CO_2 emissions reduction of base case.

Indirect CO_2 reduction	Reduction	Reduction percentage	Reduction	Reduction percentage	Reduction	Reduction percentage
	Oil		Coal		Natural gas	
By using CDQ	280.5 kt	5.6%	233.7 kt	4.7%	86.1 kt	1.7%
By using COG cooling	228.6 kt	4.6%	190.5 kt	3.8%	70.2 kt	1.4%
By using ORC	653.2 kt	13.1%	790.8 kt	15.8%	428.2 kt	8.6%
Direct CO_2 reduction	Charcoal		Bio-oil		Bio-syngas (H_2/CO 1.6)	
	Reduction	Reduction percentage	Reduction	Reduction percentage	Reduction	Reduction percentage
By using biomass	122.2 kt	2.5%	822.5 kt	16.5%	2695.9 kt	54.0%
By using CO_2 capture	2551.7 kt	51.1%	1916.2 kt	38.4%	\	
Final CO_2 emissions	Emissions	Reduction percentage	Emissions	Reduction percentage	Emissions	Reduction percentage
	1021.7 kt	79.5%	956.8 kt	80.8%	999.6 kt	80.0%
Final specific CO_2 emissions	0.22 $t \cdot t_{\text{crude steel}}^{-1}$		0.20 $t \cdot t_{\text{crude steel}}^{-1}$		0.21 $t \cdot t_{\text{crude steel}}^{-1}$	

5.5 Summary

In this chapter, both CO_2 capture and waste heat recovery technologies are adopted to further reduce CO_2 emissions and improve energy consumption of iron and steel plant. MEA-based CO_2 capture and ORC are two technologies that are implemented. The principle and configuration of MEA-based capture are summarised in the chapter. An overall biomass-based BF process combined with CO_2 capture and ORC is proposed. Details of parameters used in each unit are given. Process simulations are accomplished by Aspen Plus.

Simulation results show that capture rate lies in the solvent flow rate, CO_2 concentration, and column height. Absorber height and solvent flow rate are two main factors that control the rich loading. And reboiler duty mostly depends on MEA solution flow rate. In comparison with different reducing agents injected into BF, bio-oil has the most advantage to improve energy consumption of CO_2 capture system. As a result, the lowest energy for MEA regeneration and CO_2 compressions will be consumed for CO_2 capture because bio-oil has significantly lowed the CO_2 concentration of BFG.

An ORC unit with around 1.7 MW is installed for recovering waste heat from hot stove flue gas. Electricity and thermal energy generated by ORC system have ability to indirectly reduce CO_2

emissions. ORC used for providing thermal energy rather than generating power presents more apparent effect on energy saving and CO_2 emissions. Although final SEC of improved system is slightly higher than that of system without advances, CO_2 emissions of basic system can be reduced by up to 69% when CO_2 capture and ORC are introduced into ironmaking process. Finally, direct and indirect CO_2 emissions reductions are summed up. The combination of various decarbonised technologies creates great opportunity to reduce CO_2 emissions.

Chapter 6

Exergy analysis and optimisation of an integrated iron and steel plant

Biomass-based substitution, CO_2 capture, and ORC are implemented to the iron and steel plant and analysed in the above chapters. All these energy conservation and decarbonised technologies are considered in a single objective optimisation of mass or thermal utilisation. It is worth noting that the integrated iron and steel plant is a complicated network of the units that mutually exchange energy and material. Waste heat sources are distributed in different units with various energy grades when considering the real situation of iron and steel industry. From a systematic level point of view, strategies on a single unit would cause linked effects to other processes. A holistic assessment approach is required to evaluate total site, thereby obtaining results of energy saving and CO_2 emissions for an integrated iron and steel plant, as well as the potential for additional energy efficiency improvement. In this chapter, potential for energy saving of iron and steel production is measured by detailed exergy analysis at both unit and plant levels. An optimisation of whole integration system is investigated in order to build an optimal mass-thermal iron and steel network. The general guideline of optimised mass-thermal network in iron and steel industry is finally summarised which may achieve an energy saving target from an overall perspective.

6.1 Mass and thermal network of iron and steel plant

6.1.1 Mass network of iron and steel plant

For a steelwork industry, there are various plants that have a variety of utilities with different chemical and thermal processes where raw materials turn into product. Those processes build up a complex manufacturing system, i.e., interacted mass and thermal energy network. Large amount of parameters and interactions exist within the network, which are the basic units of the entire system [227]. Typical mass network of iron and steel industry is composed of multiple primary energy saving technologies which are applied to each unit. The goal of mass network is to achieve continuous and

compact production to reduce energy consumption and demands [272]. Although these technologies are relatively independent in each process, the implementation of one technology may affect the operation potential of another. For example, the recycling by-product gases implies that there is less flue gas for in-plant use. Substituting coke with biomass-based reducing agent in BF reduces coke production in the coking plant, resulting in fewer coal feedstock. Although higher electricity produced from waste heat expanders could indirectly reduce CO_2 emissions generated from traditional power plants, higher feedings are required for large amount of waste heat, causing more direct CO_2 emissions. Therefore, various process constrains should be included rather than only considering one-way objective in an individual process when establishing the mass network.

Figure 6.1 shows main inputs and outputs structure of potential mass network in iron and steel industry. The possible primary energy optimisation technologies are considered in this network. Black arrows indicate input and output flows of each process, and blue arrows show the connections between different components. Black dotted rectangles inside each production frame represent primary energy saving technologies applied in this system. As summarised in Section 2.2, typical energy saving technologies are listed in the figure for each process, which are installed to improve energy efficiency of system itself. The BF process is the core part that connects upstream and downstream in the iron and steel plant. Improvement of BF operation not only upgrades iron making process, but also has far-reaching effects on the supply chains and product ports. An optimal mass network of iron and steel plant can achieve multi-objective optimisation.

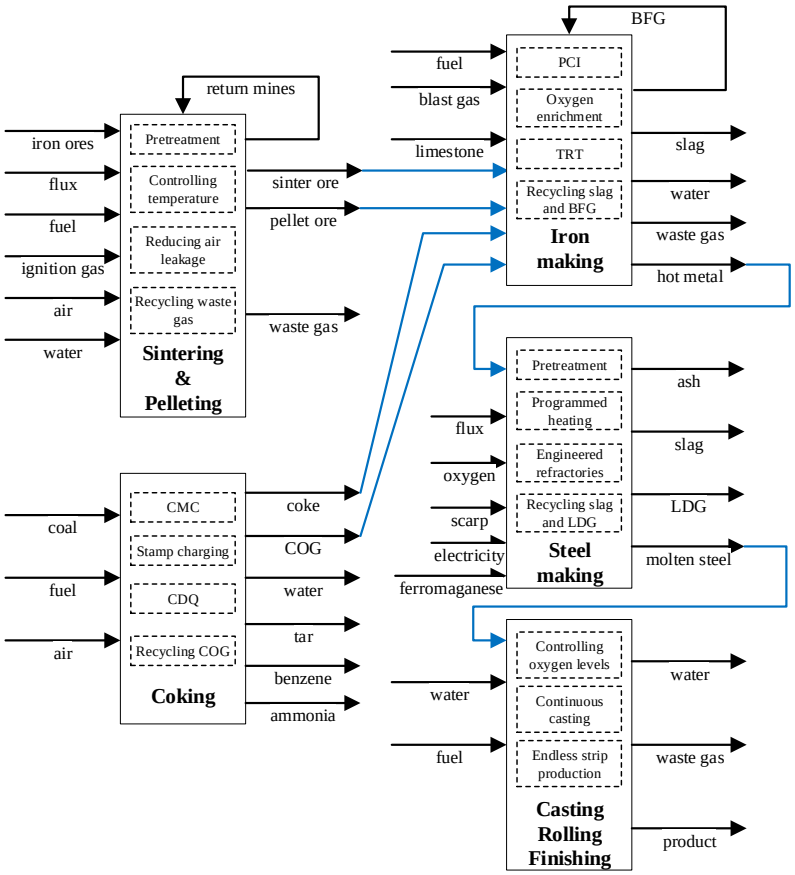

Figure 6.1: Main inputs and outputs in mass network [273].

6.1.2 Thermal network of iron and steel plant

To avoid difficulties for the efficient use with regard to the demands of heating, cooling, power in a specific industrial zone, the secondary energy conversion technologies should be selected in terms of heat sources and heat sinks. Thermal energy storage and energy transportation technologies are indispensable to establish a bridge between sources and ends. The commonly used heat storage technologies for steelwork are sensible heat storage such as stones and steel slags as storage material, and steam accumulator for high temperature heat. The accumulator matches steady steam production from boilers to the short discharge needs of the vacuum processes, which could be used to balance supply and demand of waste heat [274]. For medium and low temperature heat, hot water tank is mainly adopted as an efficient tool [275]. Temperature losses through heat exchangers will be reduced if high quality water is used for circulation. For low temperature waste heat, underground thermal energy storage could be used and supply potentially a high heat capacity at a low cost [276]. Except for these commonly used storage technologies, other heat storage technologies would also be good candidates in the future. Chemical energy storage e.g. CaO can be adopted for high temperature heat

storage while phase change materials (PCM) e.g. inorganic salt can be utilised for middle and low temperature heat, which could be combined with the above conventional sensible energy storage technologies [277, 278]. Energy transportation technologies are generally interdependent on energy storage methods. Conventional technologies aim at moving the heat transfer fluid to the other locations with a good insulation material. But heat loss significantly increases with the increase of transmission distance and time. Compared with these methods, some novel transportation methods are prospective, for example, absorption liquid transportation [279, 280], adsorption solid transportation [281, 282], chemical reactant [283] and mobilised PCM [284, 285].

Schematic diagram of the possible low grade heat thermal network applications is shown in Figure 6.2 [286]. Heat streams are all corresponded to various applications based on their temperature. Except for energy storage and transportation, cascading technologies for power and heat/refrigeration cogeneration/tri-generation are most common ways to improve the heat source utilisation, which have been gradually applied in iron and steel plant and power plant [287]. A basic mass-thermal network could be composed of multiple sets of cascading heat flow lines in iron and steel plant by using heat storage and transportation technologies. The defined network should be further optimised in industrial zones based on reasonable optimisation methods, which will be elaborated in following subsection.

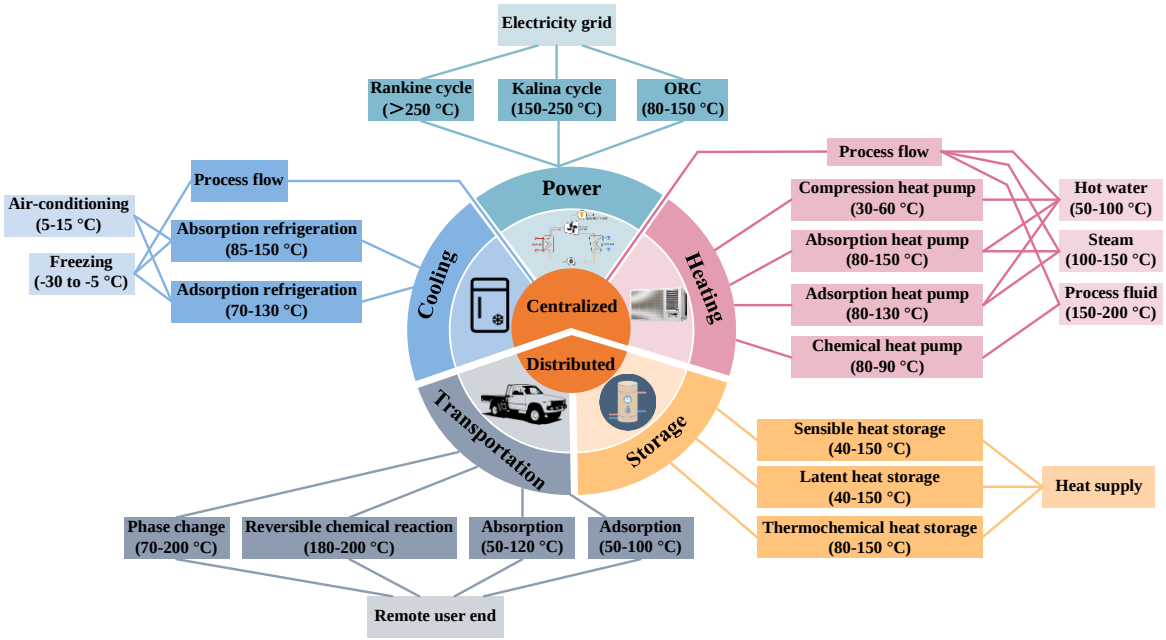

Figure 6.2: Schematic diagram of the possible low grade heat thermal network applications [286].

6.2 Methods used to optimise the mass-thermal network

6.2.1 Summary of common methods

The general system optimisation methods have been performed in iron and steel industry to avoid sub-optimisation and to deliver energy and material efficiency. The conventional optimisation methods include exergy analysis, pinch analysis and mathematical programming. Exergy analysis is a suitable tool for problems that involve different types of materials and transformations [288]. It is useful when comparing two different production routes and potential resource savings for the same output, for example, crude steel produced from BOF and EAF [289]. The exergy efficiency is used to evaluate the industry performance, which can better identify exergy losses along the production chain. Enhanced exergy, exergy economic and exergy environmental analyses are extensions of the conventional exergy analysis [290]. These methods can be used to assess the overall efficiency of whole processes in the network after optimised by the energy saving technologies.

Pinch analysis is a common methodology to minimise energy consumption by optimising heat recovery systems, energy supply methods and process operating conditions [291]. The method allows the calculation of a theoretical maximum level for heat recovery. With more streams available in the consideration of thermal network, more heat can theoretically be recovered in an integrated steel plant [84]. It uses the input data to produce hot and cold composite curves. The maximum potential for heat recovery and a theoretical target for integrated recovery can be revealed from the curves, which will be limited by the complexity of the network of heat exchangers required in practice [84].

Since the network structure is unknown and must be optimally exchanged resources between the plants, this requires the use of mathematical programming methods to formulate a network that includes all the potential mass and energy connections [292]. Through mathematical programming, the optimisation can be defined by a set of equations, the equality/inequality constraints, and an objective function. Various mathematical models for the optimisation of whole process system have been established by analysing different optimisation objectives. For example, an ontology-based approach for Eco-industrial park (EIP) knowledge management is proposed as shown in Figure 6.3 [293]. EIP energy system ontology can be treated as a domain ontology which treats all things in EIP belonging to resource, technology and role. The relationships between each one of them are defined in the domain ontology. A dynamic mixed integer linear programming model for multi-period optimisation of by-product gases is used to optimise distribution of gases in the integrated iron and

steel plant [294]. The proposed model simultaneously optimises the by-product gases distribution, cogeneration system as well as iron and steel making system. The combination of linear programming and nonlinear programming methods and “e-p” analysis is applied to obtain the optimal burdening proportions and operating parameters in BF process [273]. On the basis of industrial metabolism concept, a model is used to analyse the energy flows by using genetic algorithm. The model provides a concise framework, which can be adopted to examine the energy flows, especially focusing on the recovery and utilisation of secondary energy [295]. All of the optimisation models mentioned above could be put forward based on the material and energy flow which focus on saving energy and reducing emissions for iron and steel industry.

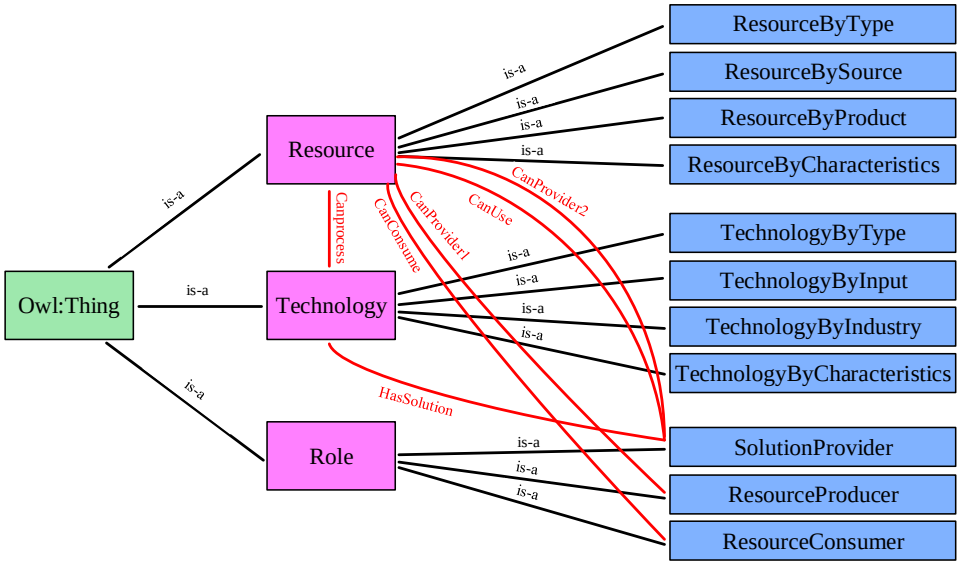

Figure 6.3: Schematic diagrams of domain ontology for EIP energy system [293].

6.2.2 Guideline of optimisation

Among all the related methods, the basic guideline for mass-thermal network optimisation aims to target the maximum energy saving potentials and to develop economically optimal networks connecting recoverable utilities and utility systems, which is generally composed of five steps [296]. The first step is data acquisition. This step is to find out all the plants and processes in the industry, and the number of plant and utility, temperature and pressure of each utility, hot and cold steams, the distance for heat transportation and so on. The second step is to determine all the energy sources and sinks to indicate the energy improvement potentials. Many specialised simulation software tools

(Aspen Plus™ and GateCycle™) will be used at this step, which provides clear operating process and detailed data for plant integration. The third step is to establish a link between the origin and other different utilities which may include new recoverable utilities. Then the fourth step is to determine the maximum potential. The final step is to design optimal energy recovery and reuse networks.

Following the five-step optimisation guideline, it can be seen that the first four steps have been finished in Chapter 3-5. Figure 6.4 shows framework of optimisation where every step has associated with specific chapter. In Chapter 3, general data and information of iron and steel plant are collected. Detailed routes of each utility are also collated, which are prepared for process simulation in Aspen Plus as step 2. The first and the second steps are all performed based on the iron and steel production chain which is shown as blue dotted frame in the figure. Simulation results show that BF ironmaking process has the highest energy consumption and CO_2 emissions, which makes BF process the most recoverable utility that is needed at the step 3. Linkages among BF process and biomass substitution and CO_2 capture are built in Chapter 4 and 5, respectively. Three processes are included in the boundary that is shown as the purple dotted lines for step 3. The maximum energy saving and CO_2 emissions reduction could be obtained by injecting biomass-syngas into BF. Thus the fourth step narrows down the analysis range that only covers BF iron making process. As for integration of CO_2 capture and ORC with different BF cases, the value of variables would have contrasting effects on the objective results. Thus the optimal integration system, i.e., the optimal mass-thermal iron and steel network, is to be analysed at the step 5. Exergy method is chosen as the optimisation method because the integrated system first needs a holistic approach to analyse potentials of energy saving and CO_2 emissions reduction. The fifth step encompasses the range of integration system.

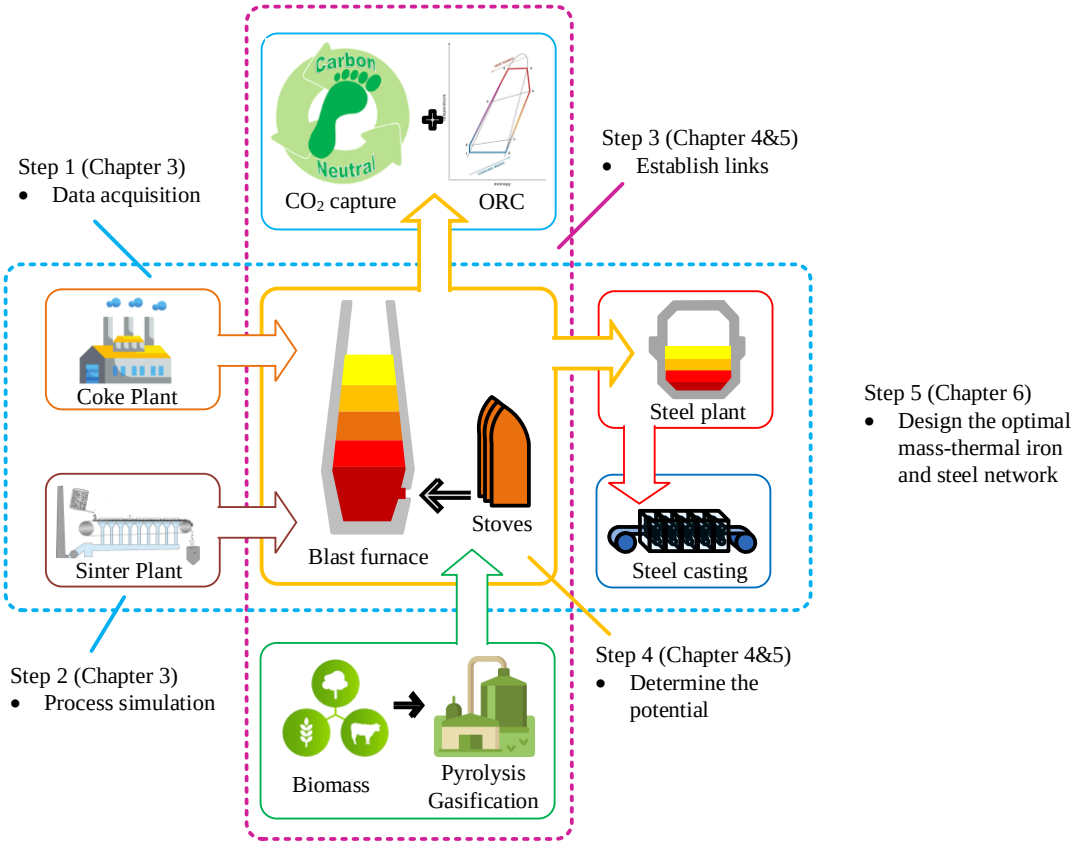

Figure 6.4: Framework of optimising mass-thermal iron and steel network.

6.3 Exergy analysis

6.3.1 Exergy calculation

Exergy is used to define the maximum work that can be extracted from a system or a chemical when it reversibly transforms from a specific condition to the reference environment. The temperature and pressure of reference environment in this study are respectively set as 25 ℃ and 1bar. Unlike the first law of thermodynamics, exergy takes its basis in the second law of thermodynamics, which states that every reaction has an unavoidable destroyed portion. And the loss is described in exergy destruction which is in proportion to the entropy creation of system. The exergy destruction could be shown as equation 6.1:

$$Ex_{destroyed} = T_0 S_{gen} \tag{6.1}$$

The exergy destruction is a value always higher than zero. The specific exergy of a stream is composed of physical and chemical exergy, while the kinetic, potential, nuclear, electrical and magnetic energy are neglected to calculate values of exergy due to their insignificant effects [297]. In other words, capacity of thermal energy and chemical energy to do physical work are described as

physical exergy and chemical exergy, respectively. Physical exergy is calculated using equation 6.2:

$$Ex_{ph} = h - h_0 - T_0(s - s_0) \tag{6.2}$$

where h and s denote specific enthalpy and entropy of component, while h_0 and s_0 are enthalpy and entropy at the reference environment.

For the calculation of the chemical exergy, chemical composition in the reference environment needs to defined. Because iron and steel production processes have complicated materials that are input and output to the process, the standard chemical exergy of these materials under reference environment are used to represent the chemical equilibrium conditions. The chemical exergy is usually calculated as equation 6.3:

$$Ex_{ch} = \sum \varphi_i Ex_{i,0}^{ch} + \Delta G_f \tag{6.3}$$

where φ_i is the mole fraction of the ith element in the reference system, $Ex_{i,0}^{ch}$ is the standard chemical exergy of the ith element, and $\Delta G_{f,i}$ is formation Gibbs energy.

For the chemical exergy of mixture of ideal gases, it turns into equation of 6.4:

$$Ex_{ch} = \sum \varphi_i Ex_{i,0}^{ch} + RT_0 \sum \varphi_i ln x_i \tag{6.4}$$

where R is ideal gas constant. This equation reflects chemical exergy of gases results from their concentration in the atmosphere. Standard chemical exergy of element and reference substances used in the calculation are obtained from reference [298], and detailed values are listed in the Appendix B.

Chemical exergy of fuels is calculated by using a coefficient introduced from Szargut et al [298]. The coefficient f is a factor of exergy converted to LHV of fuel, which is expressed as equation 6.5. For most fuels, the factor is around one and an empirical equation 6.6 is provided for the hydrocarbons in the form of $C_\alpha H_\beta N_\gamma O_\delta$, where α, β, γ, and δ are the number of atoms [299].

$$f = \frac{Ex_{fuel}}{LHV} \tag{6.5}$$

$$f = 1.041 + 0.1728\frac{\beta}{\alpha} + 0.0432\frac{\delta}{\alpha} + 0.2169\frac{\gamma}{\alpha}(1 - 2.062\frac{\beta}{\alpha}) \tag{6.6}$$

As for a system that only transfers thermal energy to do physical work, exergy of heat is defined as equation 6.7:

$$Ex_{heat} = \dot{Q}(1 - \frac{T_0}{T}) \tag{6.7}$$

where Q is the heat flow rate of the stream, and T_0 and T are temperature of reference state and heat

source, respectively.

6.3.2 Exergy balance

As shown in Figure 6.4, the study takes all the iron and steel production processes with energy saving and decarbonised technologies as an integrated system for optimisation. Exergy flow exists among every operation unit and exergy balance of the *i*th process can be expressed as equations 6.8 and 6.9:

$$\sum_1^i \dot{m}_{in} \dot{ex}_{in} = \sum_1^i \dot{m}_{out}\, \dot{ex}_{out} + \dot{I} \tag{6.8}$$

$$\dot{Q}\left(1 - \frac{T_0}{T}\right) + \sum_1^i \dot{m}_{in,i} \dot{ex}_{ch,in} = \dot{W} + \sum_1^i \dot{m}_{out,i} \dot{ex}_{ch,out} + \dot{I} \tag{6.9}$$

where $\dot{I}$ is irreversibility rate of the process and can be calculated as same as exergy destruction, $\dot{ex}_{in}$ and $\dot{ex}_{out}$ are inlet and outlet flow exergies.

The exergy streams among iron and steel production processes not only transfer thermal energy, but also have interaction of chemical substances. Exergy balance of these processes are set up based on the mass network, which can be seen in Figure 6.5. Input exergy of single unit includes chemical exergy of feedstocks and thermal exergy used to drive the chemical reactions. Exergy flows of output contain exergy of product and exergy of waste. Exergy loss inside each unit mainly results from the irreversible transfer of heat.

Two fractionating columns are predominant components in the model of MEA-based CO_2 capture system. The changes of chemical exergy are taken into account for two columns, as well as thermal exergy. Thus exergy balances for absorber and stripper can also be obtained from equation 6.9.

With regard to stream that has no change of chemical components from inlet to outlet, exergy of stream only considers physical exergy. A large amount of heat exchangers, pumps, and expanders in the model of CO_2 capture and waste heat recovery technologies, i.e., CDQ, COG cooling, and ORC have no reaction of chemicals. For pumps that need work input, exergy balance is shown as:

$$\sum_1^i \dot{m}_{in,i} \dot{ex}_{in,i} + \dot{W} = \sum_1^i \dot{m}_{out,i} \dot{ex}_{out,i} + \dot{I} \tag{6.10}$$

Equation 6.11 indicates the exergy balance for expanders which could generate electricity:

$$\sum_1^i \dot{m}_{in,i} \dot{ex}_{in,i} = \sum_1^i \dot{m}_{out,i} \dot{ex}_{out,i} + W + \dot{I} \tag{6.11}$$

And for heat exchangers that only have heat transfers, exergy balance is simply described as:

$$\sum_1^i \dot{m}_{in,i} e\dot{x}_{in,i} = \sum_1^i \dot{m}_{out,i} e\dot{x}_{out,i} + \dot{I} \tag{6.12}$$

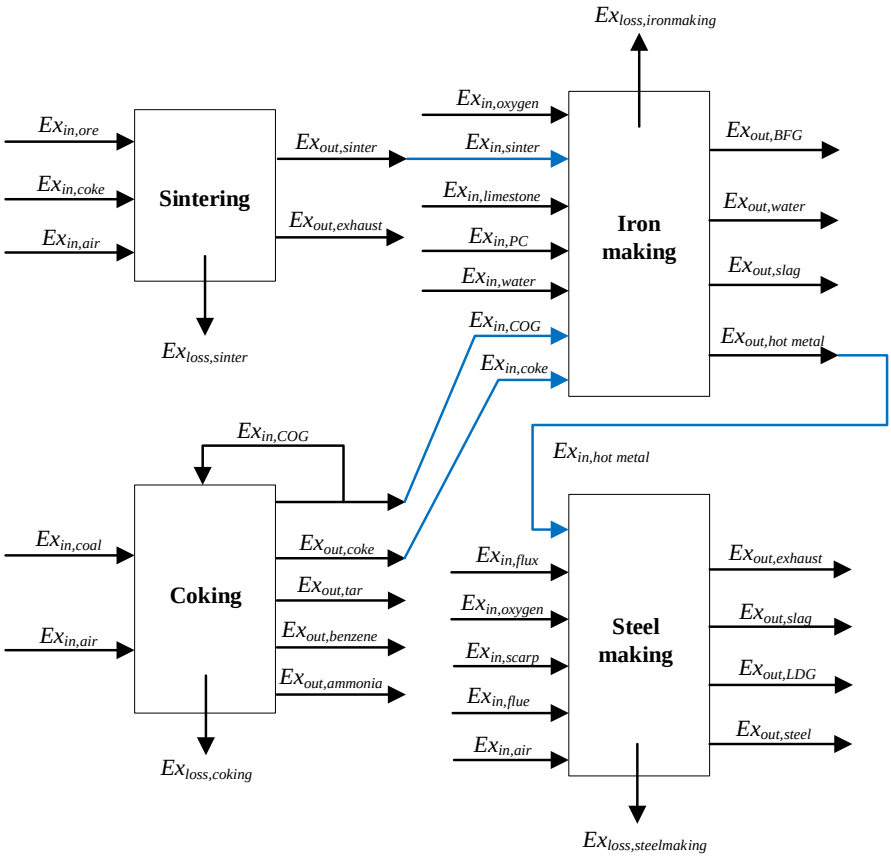

Figure 6.5: Exergy balance for iron and steel production processes.

6.3.3 Exergy efficiency

Exergy analysis is also applied to each process to evaluate efficiency. Exergy efficiency is normally defined as the ratio of the useful exergy output to the input of exergy, as shown in equation 6.12. However, various scenarios would cause different definitions of useful output. For example, in the case of only injecting coke into BF as reducing agent, the exergy of slag and exergy of exhaust are regarded as exergy losses. Comparably, in the case that is combined with CO_2 capture and ORC, CO_2 and waste heat from exhaust gas are recycled for subsequent use, which turns discarded exergy into valuable output. Based on this reason, exergy efficiency is an explicit index to evaluate improvement effects of energy saving and decarbonised measures on the production processes.

$$\eta_{ex} = \frac{Ex_{useful}}{Ex_{in}} = \frac{1 - I}{Ex_{in}} \tag{6.12}$$

Exergy efficiency of the pumps, expanders are obtained from equations 6.13-6.14. For heat exchangers that have no phase changes during heat transfer, the exergy efficiency can be described as equation 6.15. Conversely, for the situation that a phase change occurs when heat flow and cold flow undergo heat exchange, the exergy efficiency is decided by equation 6.16, which is the ratio of thermal exergy from cold side to hot side heat exergy.

$$\eta_{ex,pu} = \frac{\dot{m}_{in}\dot{ex}_{in} - \dot{m}_{out}\dot{ex}_{out}}{\dot{W}_{in,pu}} \tag{6.13}$$

$$\eta_{ex,exp} = \frac{\dot{W}_{out,exp}}{\dot{m}_{in}\dot{ex}_{in} - \dot{m}_{out}\dot{ex}_{out}} \tag{6.14}$$

$$\eta_{ex,hx} = \frac{\dot{m}_c C_{p,c}(T_{c,out} - T_{c,in} - T_o ln\frac{T_{c,out}}{T_{c,in}})}{-\dot{m}_h C_{p,h}(T_{h,out} - T_{h,in} - T_o ln\frac{T_{h,out}}{T_{h,in}})} \tag{6.15}$$

$$\eta_{ex,hx} = \frac{Q(1 - \frac{T_0}{T_c})}{Q(1 - \frac{T_0}{T_h})} \tag{6.16}$$

Exergy efficiency of four production units in iron and steel plant are calculated under five BF scenarios. Also energy efficiency of these systems are compared with results of exergy efficiency. Exergy destruction and exergy efficiency of component of the waste heat recycle and CO_2 capture cycle are obtained from above equations, which are used to evaluate improvement potential of energy saving and decarbonised technologies. All these exergy analyses are conducted based on the results from simulation.

6.4 Results of exergy analysis and discussions

6.4.1 Comparison of energy flow and exergy flow based on different scenarios

Exergy efficiency of four production units in the iron and steel plant are calculated under five BF scenarios, and they are also in comparison with energy efficiency of each unit as shown in Figure 6.6. Five sub-figures represent cases that use coke, PC with coke, charcoal, bio-oil, and bio-syngas in the BF. Two types of columns are respectively energy efficiency in orange, and exergy efficiency in green.

The main difference of two indexes is the definition of useful output. The energy efficiency is the ratio of product energy to the input energy that involves all the feedstock. According to simulation results from Aspen Plus, energy efficiency also can express block efficiency which is designed by

software operating system. Energy efficiencies of sinter and steel making process are 0.64 and 0.71, and remain unchanged with various reducing agents in BF. This is mainly because that change of reducing agent only influences coke rate that is corresponding to coking process rather than sinter and steelmaking. BF ironmaking process has the lowest energy efficiency among four units, and the process only uses coke has the least efficient energy consumption. The highest coke rate in the BF would lead to the most CO_2 discharge, thus increasing invalid energy conversion during the process.

Exergy efficiencies of sinter and steel making process are 0.65 and 0.69, and remain the same of five scenarios. The only variable, i.e., reducing agent has also no effect on exergy efficiencies of sinter and steel making. The most exergy efficient unit takes place in the coking process, which are mainly associated with CDQ and COG cooling. Waste heat recovery technologies turn the underused energy into useful energy, to a large extent, have improved exergy efficiency of coking process. It could be found that when reducing agent in the BF varies from coke to bio-syngas, exergy efficiency of BF can be apparently improved from 0.44 to 0.81. This is due to the injection of bio-syngas into BF reduces CO_2 emissions and increases useful exergy output.

Because reducing agents have no impact on efficiencies of sinter and steelmaking, mass ratio is chosen as variable to investigate influence on thermal performance. Mass ratio is defined as the ratio of input iron ore/pig iron to that of base case. When mass ratio is 1, input iron ore has the same amount as the basic case. Iron ore is the primary feedstock of sinter process where sinter product will be further transported to BF process. Sinter charging determines the production of hot metal. Condensed hot metal becoming pig iron has a great influence on the final crude steel yield. As a result, input quantities of iron ore and pig iron are interdependent. The benchmark of charging rate is iron input of base case, then iron ore and pig iron charging rates would fluctuate 75%. In other words, the charging of iron ore and pig iron are increased or decreased by 0-75%. Input of iron ore ranges from 398.3 $kg \cdot t_{HM}^{-1}$ to 2782.8 $kg \cdot t_{HM}^{-1}$, and pig iron charging increases from 250 $kg \cdot t_{HM}^{-1}$ to 1500 $kg \cdot t_{HM}^{-1}$.

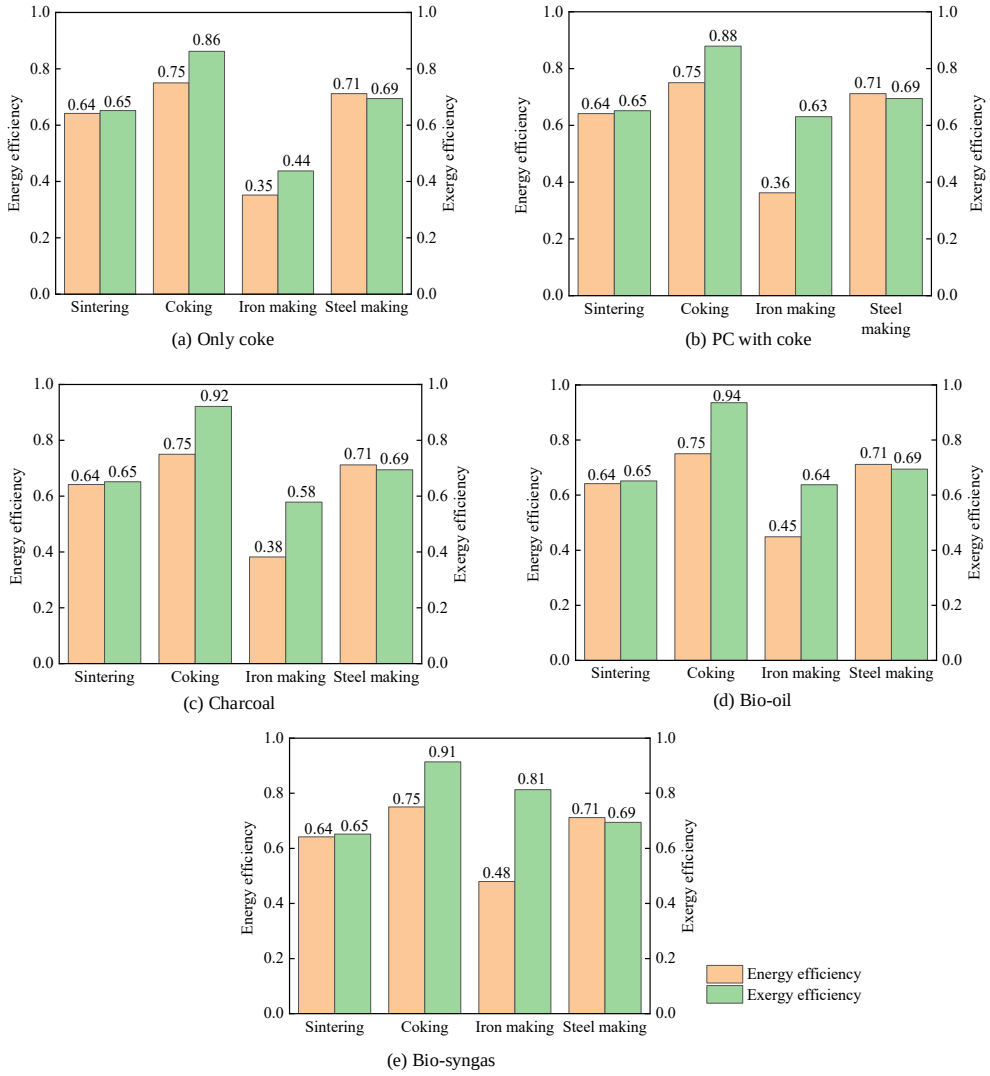

Figure 6.6: Energy and exergy efficiencies of iron and steel plant when BF operates with different reducing agents: (a) only coke, (b) PC with coke, (c) Charcoal, (d) Bio-oil, (e) Bio-syngas.

Figures 6.7 demonstrates energy and exergy efficiencies trends of sinter process with the change of iron ore mass rate. Both energy and exergy efficiencies rise with more iron ore input to the sinter. Energy efficiency of sinter plant increases from 0.35 to 0.73 and has been improved by 113%. In comparison with that, exergy efficiency gently increases from 0.51 to 0.68, and is increased by 33.6%. Especially when the iron ore input is 1.25 times of original iron input, energy efficiency starts to be higher than exergy efficiency. Outlet streams of sinter process consist of exhaust gas and sinter. The calculation of exergy efficiency only considers sinter as useful exergy output. Therefore, with the increment of iron ore input, useful energy output exceeds the useful exergy output, resulting in higher energy efficiency.

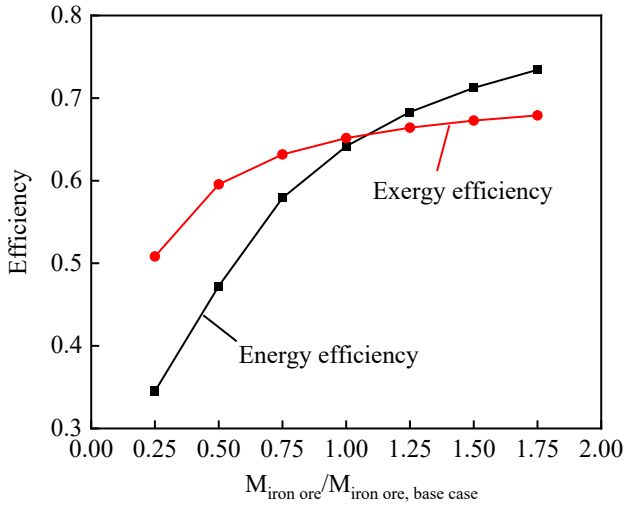

Figure 6.7: Energy and exergy efficiencies of sinter process when iron ore charging ratio of sinter process ranges from 0.25 to 1.75.

Figure 6.8 indicates energy and exergy efficiencies of BOF steelmaking process in terms of different mass ratios. It is evident that energy efficiency increases from 0.39 to 0.71 when the mass ratio increases from 0.25 to 1, and then drops rapidly to 0.62 after mass rate of 1. Because the energy required in the BOF is mostly generated from reaction between pig iron and oxygen, pig iron as the only variable, there is no sufficient oxygen reacted with pig iron when the amount of iron feedstock is higher than that of basic case. Additional iron feedstock has no adequate reaction with oxygen, resulting in decreased energy efficiency of steelmaking process. Different with energy efficiency, exergy efficiency increases continuously when mass ratio varies from 0.25 to 1.5. The exergy efficiency has been improved by 38.5% from 0.55 to 0.76. Despite the increased pig iron would not have reaction in the BOF, it still discharges from furnace as the useful output, as a result, exergy efficiency keeps increasing. It is demonstrated that for sinter and BOF processes, the amount of iron-bearing charging, i.e., iron ore and pig iron acts as a dominant role in energy and exergy efficiencies.

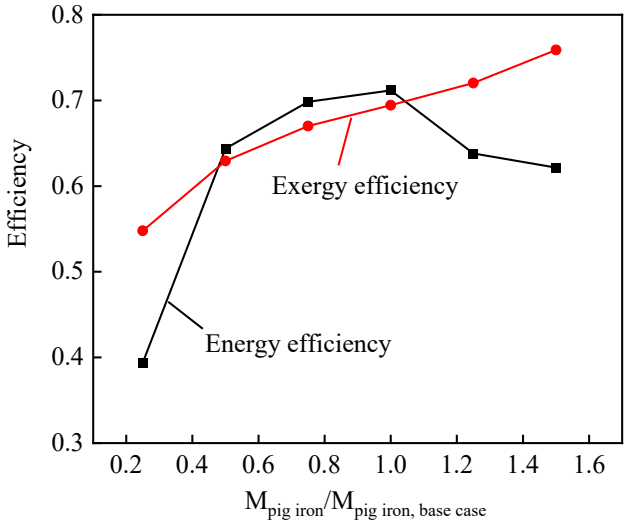

Figure 6.8: Energy and exergy efficiencies of steelmaking process when pig iron charging ratio of steelmaking process ranges from 0.25 to 1.5.

6.4.2 Exergy results of waste heat recovery technologies

Three waste heat recovery technologies i.e., ORC, CDQ and COG cooling have been deployed for BF ironmaking and coking processes. From Table 6.1, we can find results of exergy efficiency before and after integrating these technologies with ironmaking and coking processes. Five situations of reducing agents in BF are analysed. Based on the findings, the exergy efficiency of BF is generally lower than the coking process. After integrating with ORC, exergy efficiencies of BF at all the scenarios are improved due to recycled physical exergy from hot stove exhaust gas. Using bio-syngas with coke as reducing agents has the maximum improvement, and the exergy efficiency is improved by 2% to 83.3%. From the vertical perspective, the injection of bio-syngas has considerably improved exergy efficiency from 43.7% to 81.3% after integration with ORC.

After applying CDQ and COG cooling, exergy efficiencies of coking process are also increased. Coking process would have the maximum exergy efficiency after injecting bio-oil into BF and recycling waste heat from CDQ. Utilising bio-oil in the BF reduces coke rate, correspondingly, input coal in the coking process is decreased. Higher exergy efficiency results from decreased inefficient exergy from coking products. COG cooling also has the ability to improve the exergy efficiency, which averagely increase the efficiency by 2%. The highest exergy efficiency after implementing COG cooling also occurs at case of bio-oil. This is mainly because the effect of bio-oil on reducing coke rate. In comparison, substituting fossil fuel with biomass-based reducing agents in BF has higher

potential to improve exergy efficiency than waste heat recovery technologies.

Table 6.1: Exergy efficiencies before and after deployment of waste heat recovery technologies.

Reducing agents in BF	Exergy efficiency of BF after ORC		Exergy efficiency of coking after CDQ		Exergy efficiency of coking after COG cooling	
	Before	After	Before	After	Before	After
Only coke	43.7%	44.6%	86.2%	92.1%	86.2%	88.2%
PC with coke	63.1%	63.9%	87.9%	93.8%	87.9%	89.9%
Charcoal with coke	57.9%	58.7%	92.1%	98.0%	92.1%	94.1%
Bio-oil with coke	63.8%	64.7%	93.5%	99.2%	93.5%	95.4%
Bio-syngas with coke	81.3%	83.3%	91.4%	97.2%	91.4%	93.3%

To further investigate waste heat recovery technologies, exergy efficiencies of ORC, CDQ and COG are compared with energy efficiencies, and the results are shown in Table 6.2. Based on the equations mentioned before, energy efficiencies of these systems represent the ratio of net work output to the input heat, while exergy efficiencies use input heat exergy. It could be found that all the exergy efficiencies are higher than energy efficiencies. This is due to exergy of heat is determined by the ratio of reference temperature to the heat flow temperature, which the ratio is usually lower than 1. Thus heat exergy of the ORC, CDQ, and COG cooling are smaller than their energy efficiencies. In the horizontal comparison among three technologies, both energy and exergy efficiencies of ORC are smaller than CDQ and COG cooling. It reveals that the efficiency of ORC to transfer thermal into work is lower than traditional steam turbine system, however, ORC has achieved better effect on recycling low grade waste heat.

Table 6.2: Energy and exergy efficiencies of waste heat recovery technologies.

Waste heat recovery technologies	ORC	CDQ	COG cooling
Energy efficiency	9.1%	26.7%	32.8%
Exergy efficiency	19.0%	34.5%	42.3%

Table 6.3 lists exergy efficiency of each utility in the structure of waste heat recovery technologies. Each utility has been examined from the aspects of input exergy, output exergy and exergy efficiency. This calculation aims to find the specific utility that has potential to improve in the whole waste heat recovery system. Pump has the lowest exergy efficiency among all the ORC components. Further measures to reduce exergy destruction of pump are considered as replacing electric pump with thermal driven pump, etc. Condenser of ORC has the highest exergy efficiency,

because outlet temperature of cooling flow needs to be higher than the temperature of MEA regeneration, i.e., 120 ℃. Condenser has higher exergy efficiency with the higher outlet temperature of condenser. Based on this result, it is reasonable that CDQ and COG cooling have the lowest exergy efficiencies of condenser, because the outlet temperature of condenser is close to the reference temperature. A large amount of heat from heat source has been lost rather than heating up the cooling water from condenser, causing the lowest exergy efficiency. Thus following improvement of CDQ and COG cooling focuses on effective utilisation of waste heat from cooling water. Additional, both steam drums of CDQ and COG cooling systems have the highest exergy efficiency. This is demonstrated that water in the evaporators achieves nearly completed evaporation, and only a very small liquids are discharged by the steam drum.

Table 6.3: Exergy analysis of single component in the waste heat recovery systems.

ORC	Ex_{in} (kW)	Ex_{out} (kW)	Exergy efficiency
Preheater	1451.80	1333.24	91.8%
Evaporator	6265.93	5637.34	90.0%
Superheater	209.88	190.57	90.8%
Regenerator	1223.94	1180.80	96.5%
Condenser	5152.49	5084.77	98.7%
Expander	2091.95	1720.15	82.2%
Pump	65.68	49.79	75.8%
CDQ	Ex_{in} (kW)	Ex_{out} (kW)	Exergy efficiency
Coking chamber	151880.65	68386.68	45.0%
Compressor	249.04	202.34	81.2%
Economiser	10277.60	6945.80	67.6%
Evaporator	52552.43	31746.29	60.4%
Superheater 1	6581.41	4929.08	74.9%
Superheater 2	6028.56	4127.79	68.5%
Steam drum	40914.65	40914.65	100.0%
Turbine 1	29105.60	23061.83	79.2%
Turbine 2	7243.12	5526.20	76.3%
Condenser	2995.40	805.16	26.9%
Feed	62.87	29.16	46.4%
Pump 1	6.41	4.90	76.5%
Deaerator	2127.13	1957.70	92.0%
Pump 2	300.02	239.07	79.7%
COG cooling	Ex_{in} (kW)	Ex_{out} (kW)	Exergy efficiency
Evaporator 1	131038.73	41085.42	31.4%
Evaporator 2	45628.94	28097.42	61.6%
Superheater	10637.29	7705.87	72.4%
Steam drum	34168.01	33348.79	97.6%
Turbine 1	23723.45	18797.29	79.2%
Turbine 2	5903.74	4504.30	76.3%
Condenser	2441.49	198.47	8.1%
Feed	51.25	23.77	46.4%
Pump 1	5.22	4.00	76.5%
Pump 2	244.54	194.87	79.7%
Deaerator	2127.13	1957.70	92.0%
Economiser	16529.95	5685.78	34.4%

Figures 6.9-6.11 present exergy destruction contribution of each utility in the three waste heat recovery systems. ORC application with BF operation has total exergy destruction of 1265 kW. Total exergy destruction of CDQ and COG cooling are 121448 kW and 130896 kW, respectively. In the ORC system, even though evaporator has an exergy efficiency of 90%, it still has the highest exergy destruction which accounts to 49.7% of the total exergy destruction. And the largest portions of exergy destruction in the CDQ and COG cooling systems belong to coking chamber and evaporator, respectively. The exergy efficiencies of these two utilities are also not the lowest. Therefore, the magnitude of exergy destruction is related to the amount of exergy, and barely has relationship with exergy efficiency. The portions that contribute exergy destruction lower than 0.1% to the CDQ system are compressor (0.038%), pump 2 (0.05%), feed (0.028%), and pump 1 (0.001%), respectively. Similarly, pump 2, pump 1, and feed in the COG cooling system also have exergy efficiencies lower than 0.1%, which are 0.038%, 0.001%, and 0.021%, respectively. The primary reason is that the utilities have small amount of inlet and outlet exergy,

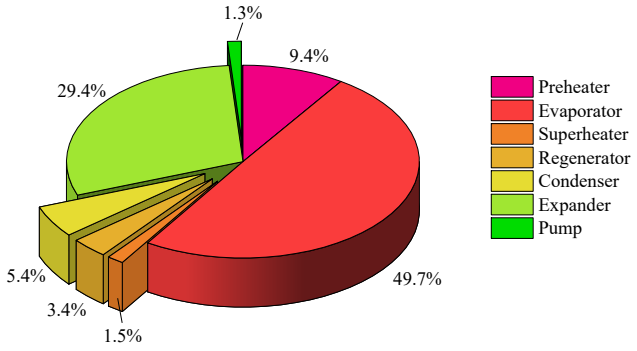

Figure 6.9: Exergy destruction distribution of each facility in the ORC system.

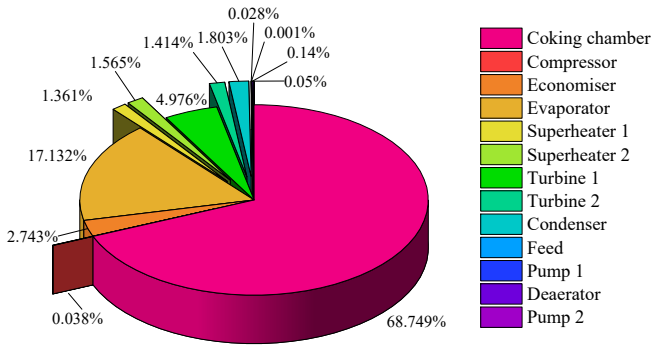

Figure 6.10: Exergy destruction distribution of each facility in the CDQ system.

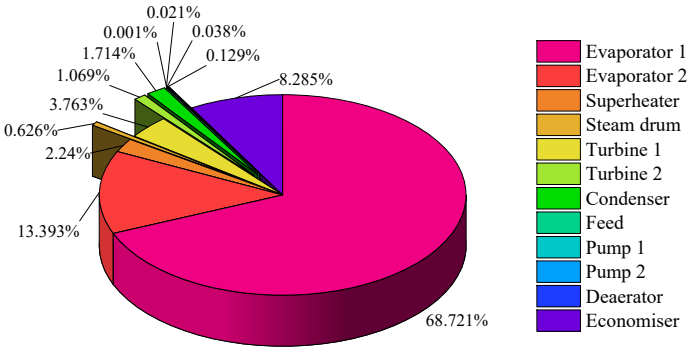

Figure 6.11: Exergy destruction distribution of each facility in the COG cooling system.

6.4.3 Exergy results of MEA-based CO_2 capture

In this section, the exergy analysis is carried out for MEA-based CO_2 capture system which removes CO_2 from BFG. The sources of BFG are BF processes with reducing agents including coke, PC, charcoal, and bio-oil. Based on the definition of exergy efficiency, captured CO_2 could be the useful exergy output from BF process. The exergy efficiency of BF process combined with CO_2 capture is determined by capture rate. Figure 6.12 depicts the change of BF exergy efficiency when capture rate ranges from 50% to 90%. In theory, increased capture rate should lead to the increment of exergy efficiency. As shown in the figure, the exergy efficiency rises of BF operating with coke, PC with coke, and charcoal are inapparent, of which the increase rates are 1.4%, 1%, 1.5%, respectively. In comparison, exergy efficiency is increased by 11.5% when BF is injected bio-oil as auxiliary reducing agent. The variations of exergy efficiency demonstrates that useful exergy output of BF using bio-oil is the highest, whereas exergy of captured CO_2 only accounts for a small share of exergy output as coke, PC, charcoal injected into BF.

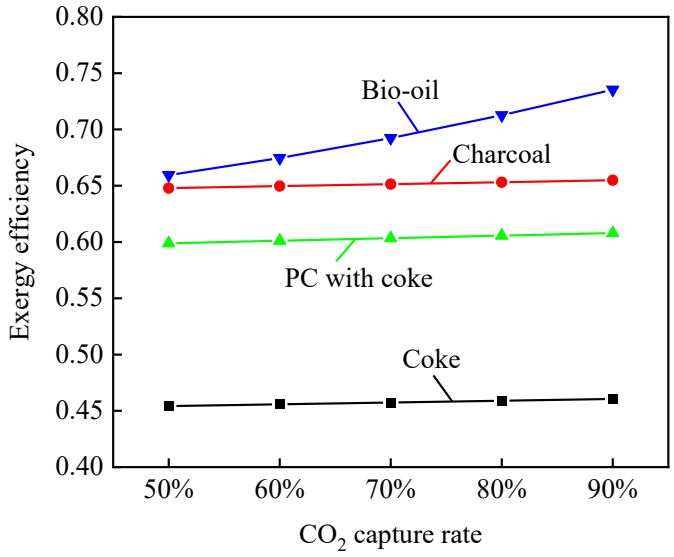

Figure 6.12: Exergy efficiency of BF process at different CO_2 capture rates.

Table 6.4 lists exergy efficiency results of each component in the CO_2 capture system, and has a comparison in BF processes with four different reducing agents. It could be found that the majority of components has no change of exergy efficiency with the variation of reducing agent. Especially the deaerator2 proceeds with zero exergy lost and has exergy efficiency of 100%, followed by pump2, DCC, and lean rich heat exchanger of which the exergy efficiencies are higher than 90%. Washer of the system has the lowest exergy efficiency which is lower than 10%. This is because that no phase change occurs in the washer and temperature of input cooling source, i.e., water is close to the reference temperature. Higher ratio of reference temperature to cooling temperature generates lower cooling stream exergy output, therefore, exergy efficiency of washer is lower than the other components. The result indicates that washer has the most improvement potential that is considered as enhancing recycling of waste heat from lean flue gas. Exergy efficiencies of absorber and stripper are around 38% and 54%, respectively. The values are lower than the general efficiencies of capture system, which demonstrates that two columns also the dominated units of CO_2 capture system need to be further improved by optimising transmission area between gas and liquid. Exergy efficiency of pump1 in the system of BF using bio-oil is lower than other three systems. Pump1 is used to pressurise rich loading. Lowest CO_2 concentration of flue gas from BF using bio-oil reduces effective transfer of pump work, resulting in lower exergy efficiency.

Table 6.4: Exergy analysis of single component in the MEA-based CO_2 capture systems.

Component	Exergy efficiency			
	Only coke	PC with coke	Charcoal	Bio-oil
Blower	87.6%	87.6%	87.6%	87.6%
DCC	97.8%	97.8%	97.8%	97.8%
Absorber	38.1%	38.2%	38.1%	37.8%
Washer	7.9%	7.8%	7.9%	8.6%
Pump1	75.7%	76.4%	72.2%	52.1%
Cooler	43.5%	43.3%	44.7%	52.7%
Lean rich heat exchanger	93.5%	93.5%	93.5%	93.5%
Pump2	99.7%	99.7%	99.7%	99.7%
Stripper	54.4%	54.3%	54.3%	54.6%
Deaerator1	41.8%	41.8%	41.7%	41.1%
Reboiler	52.4%	52.4%	52.4%	52.4%
Condenser	24.2%	24.2%	24.2%	24.2%
Deaerator2	100.0%	100.0%	100.0%	100.0%

Figures 6.13 presents exergy destruction contribution of each component in the MEA-based CO_2 capture system when flue gas is collected from different BF cases. Total exergy destruction of four BF cases are 328272 kW (coke), 326707 kW (PC with coke), 316471 kW (charcoal), 252344 kW (bio-oil). Because deaerator2 has 100% exergy efficiency, it is obvious that no exergy destruction from deaerator2. The largest contribution of exergy destruction belongs to deaerator1 where lean solution and steam are separated. The process is highly irreversible, so it has the maximum amount of exergy destruction. Exergy destruction of reboiler, absorber, and stripper also account for a large portion which is higher than 10%. Similarly to the results that system integrated with waste heat recovery technologies, exergy destruction has no evident relation with exergy efficiency.

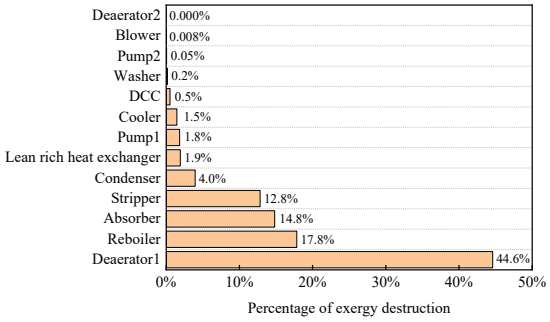

(a) only coke

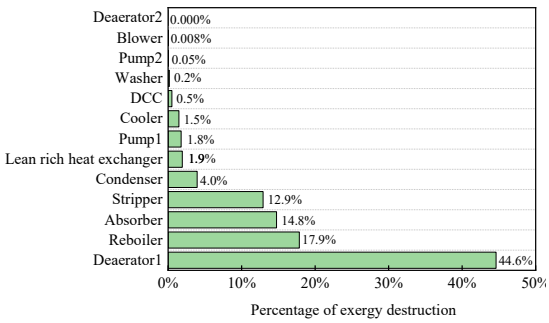

(b) PC with coke

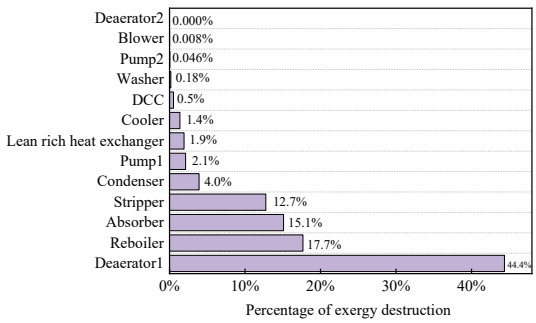

(c) charcoal

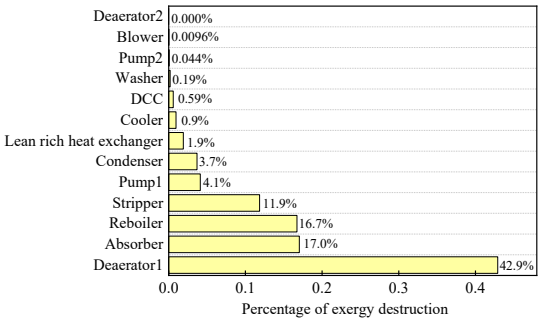

(d) bio-oil

Figure 6.13: Exergy destruction distribution of each component in the MEA-based CO_2 capture system at the cases of: (a) only coke, (b) PC with coke, (c) charcoal, (d) bio-oil as reducing agent.

6.4.4 Further improvement

Based upon the overall exergy analysis of integrated system, further improvement measures are raised, which are described in the following:

(a) Current integration system covers full iron and steel production chain, injection of biomass-based reducing agents, MEA-based CO_2 capture, and ORC system. Exergy analysis has been carried out for the whole system, however, to accomplish high-quality integration, highly efficient use of industrial waste heat by means of energy network utilisation is necessary, which includes heating, power generation, cooling, and storage and transportation technologies. This study has utilised waste heat from coke, COG, BFG, and blast stove exhaust. Temperature of these waste heat are in the range of 180 ℃ to 1100 ℃. As shown in the Table 3.3, there is still large number of waste heat from cooling water and steel slag, which contain low temperature heat and high-grade heat, respectively. Temperature of cooling water is lower than 100 ℃, and it can be recovered by applications presented in Figure 6.2. For high temperature heat contained in the steel slag, waste heat can be recycled for chemical reforming reaction and gasification.

(b) The integrated system is further needed to find out more energy recovery potential by pinch analysis to design a heat exchanger network. In addition, the multi-objective optimisation based on mathematical programming will be considered in the future optimisation process. Multiple objectives application and the extreme values of the operating parameters would be determined to make the optimal target or other optimised parameters such as minimum CO_2 emissions and the lowest cost. A set of mathematical models are necessary to be built for compensating the basic optimisation method in some cases.

6.5 Summary

In this chapter, the concept of mass-thermal network in iron and steel plant is established. Mass network consists of multiple primary energy saving technologies which are applied to each unit of iron and steel industry. Thermal network links heat streams to various applicants based on their temperature. Thus mass-thermal network of iron and steel industry builds up an interacted mass and energy flows where primary and secondary energy saving technologies are implemented to optimise energy use and reduce CO_2 emissions.

The general guideline i.e., 5-step method is summarised to optimise the mass-thermal network. The guideline is built on the wide use of efficient sustainable technologies for iron and steel industry, and it is considered as a method to achieve the objectives of the study. Corresponding contents of each step are described in detail. The fifth step which optimises the whole integrated system is carried out by using exergy analysis.

The results of exergy analysis show that reducing agent is the main factor of BF ironmaking and coking processes. Injection of biomass-based syngas can maximumly increase the exergy efficiency of ironmaking process. Sinter and BOF steelmaking processes are related with mass ratio of hot metal. Usually, higher mass ratio improves exergy and energy efficiencies, whereas for BOF process of which energy efficiency reaches the maximum when mass rate is 1. Eventually, exergy efficiency and exergy destruction are used to investigate improvement potentials at technical level. Bio-syngas and bio-oil have the largest improvement of exergy efficiency of after integration with ORC, and CDQ and COG cooling, respectively. Pump of ORC system and condenser of CDQ and COG cooling need to be further improved. As for MEA-based CO_2 capture system, washer, absorber, and stripper have the most improvement potential. The results also demonstrate that exergy destruction has no evident relation with exergy efficiency.

Chapter 7

Conclusions and future work

This thesis presents a detailed simulation of a 4.7Mt annual steel slab capacity iron and steel plant. Particular primary and secondary energy saving and decarbonised technologies have been applied to iron and steel production process, which finally builds up an integrated iron and steel system, i.e., a mass-thermal iron and steel network. Performance of energy saving and decarbonised technologies have been discussed in the assigned chapter. An exergy analysis is given to the integrated system for evaluating optimisation potential. This chapter will summarise results and contribution of thesis, and also discuss future research.

7.1 Summary of results

In Chapter 2, a comprehensive literature review of primary and secondary energy saving and decarbonised technologies of iron and steel industry are developed. The overarching energy consumption in iron and steel industry is presented. Then primary and secondary energy technologies are clearly reviewed and compared. It could be found that the primary energy technologies aim to reduce the energy demands while the secondary energy technologies consider the conversion of thermal energy. The research gap reveals that fuel substitution technologies and waste heat recovery technologies have wide application prospects in iron and steel industry. Although these technologies have been practiced in many iron and steel cases, the combination of two kinds of measures and an overall optimisation of integrated system have rarely been studied.

Chapter 3 presents a simulation of 4.7 Mt steel capacity iron and steel plant in UK. Detailed metallurgical routes of iron and steel production are described. Further energy saving and decarbonised technologies are applied to this plant based on its fundamental conditions. A comprehensive model of iron and steel production flows is built through the software Aspen Plus. Energy consumption and CO_2 emissions are evaluated for basic iron and steel plant. Total energy consumption and CO_2 emissions of whole production chain are 17.5 GJ and 1.06 $\mathrm{t}\cdot\mathrm{t}_{\mathrm{crude\ steel}}^{-1}$, respectively. The largest energy consumption is 13.04 $\mathrm{GJ}\cdot\mathrm{t}_{\mathrm{crude\ steel}}^{-1}$ at iron making process,

meanwhile BF process emits the largest quantity of CO_2 of 0.5 $t \cdot t^{-1}_{\text{crude steel}}$. Waste heat from hot coke and COG is transferred to form electricity. The renewable electricity could cover 40% of electricity consumed in the plant if coking process has the maximum coke capacity, and it also can indirectly reduce CO_2 emissions from oil, coal, natural gas power plants.

Chapter 4 optimises the energy use of BF first by substituting coke with biomass-based reducing agents. Three possibilities of using charcoal, bio-oil, and bio-syngas are designed to explore the potential of coke replacement and CO_2 emissions reduction. The model of cases is built and simulated by Aspen Plus. The results show that charcoal, bio-oil, and bio-syngas can be utilised in the BF as auxiliary reducers with a certain amount. Coke demand per ton of hot metal can be decreased and CO_2 emissions are reduced when bio-reductants are injected into BF. An optimal coke replacement is operated with 200 $kg \cdot t^{-1}_{HM}$ bio-oil and 222 $kg \cdot t^{-1}_{HM}$ coke. The reaction involving bio-syngas has the most potential to reduce CO_2 emissions, and the favourable H_2/CO ratio ranges from 1.6 to 1.3. However, injection of biomass into BF has rarely influence on sintering and steelmaking.

In Chapter 5, both CO_2 capture and waste heat recovery technologies are adopted to reduce CO_2 emissions and improve energy consumption of iron and steel plant. The principle and configuration of MEA-based capture are summarised in the chapter. Process simulations are accomplished by Aspen Plus. Simulation results determine proper absorber height and solvent flow rate for certain CO_2 capture rate. In comparison with different reducing agents injected into BF, bio-oil has the most advantage to improve energy consumption of CO_2 capture system. An ORC unit with around 1.7 MW is installed for recovering waste heat from hot stove flue gas to provide electricity and thermal energy required by CO_2 capture system. ORC aimed for providing thermal energy rather than generating power presents more significant effect on energy saving and CO_2 emissions. CO_2 emissions from iron and steel plant can be maximumly reduced by 69% when carbon capture and ORC deploy in the ironmaking process. Finally, direct and indirect CO_2 emissions reductions are summed up. The combination of various decarbonised technologies creates great opportunity to reduce CO_2 emissions.

The sixth chapter brings up a concept of mass-thermal network in iron and steel plant based on the applied energy saving and decarbonised technologies mentioned in above chapters. Mass-thermal network of iron and steel industry builds up an interacted mass and energy flows where primary and secondary energy saving technologies are implemented to optimise energy use and reduce CO_2 emissions. A five-step guideline is summarised to optimise the mass-thermal network. The guideline

has been covered and achieved based on the whole contents of thesis. The fifth step which optimises the whole integrated system is carried out by using exergy analysis. The results of exergy analysis show that injection of biomass-based syngas can maximumly increase the exergy efficiency of ironmaking process. Sinter and BOF steelmaking processes are related with mass ratio of hot metal. Bio-syngas has the largest potential to improve exergy efficiency of system after integration with ORC. For CDQ and COG cooling, bio-oil injection presents the considerable improvement potential. Pump of ORC system and condenser of CDQ and COG cooling need to be further improved. Washer, absorber, and stripper of MEA-based CO_2 capture system have the least exergy efficiency.

7.2 Contributions of research

The contributions from research are listed in the following contents:

(a) The simulation of a full iron and steel plant is presented in this research. Sometimes the information given by industry will not cover all the production parameters. The simulation of whole plant can supplement mass and energy flows and corresponding information. It can also provide a basic platform where further energy saving and decarbonised technologies could practice.

(b) A combination of biomass-based reducing agents with BF is designed. The simulation model can contribute fundamental structure of biomass application in the BF ironmaking process. It is feasible to use model to adjust parameter selection for realistic operation.

(c) Specific design of MEA-based CO_2 capture with ORC is presented, which provides the possibility of combination of CO_2 capture and ORC technologies in the iron and steel plant. The utilisation of waste heat recovery technologies can indirectly reduce CO_2 emissions from traditional fossil-based power plant.

(d) A general five-step optimisation guideline is developed for mass-thermal iron and steel network. The guideline can be generally applied in the similar industrial network, thus obtaining the maximum energy saving and economically optimal network that connecting recoverable utilities.

7.3 Future work

There are still several fields that need to be further investigated on the basis of current research results, which are shown as below.

(a) Heat integration and multi-objective optimisation

The integrated system is further needed to find out more energy recovery potential by a heat exchanger network which is designed by pinch analysis. In addition, the multi-objective optimisation based on mathematical programming needs to be considered in the future optimisation process. Multiple objectives application and the extreme values of the operating parameters would be determined to make the optimal target or other optimised parameters. A set of mathematical models are necessary to be built for compensating the basic optimisation method in some cases.

(b) Hydrogen-based iron and steel production

H_2 content in the biomass-based syngas acts as the main function to reduce coke consumption and CO_2 emissions. Thus is it necessary to investigate pure H_2 as reducing agent into BF ironmaking process and evaluate corresponding performance. H_2 can also be used in the iron and steel production in other ways, such as the iron-based chemical looping process. H_2 production, storage and transportation are essential links of all processes. Dynamic model is also needed for further production improvement.

(c) Novel carbon utilisation and conversion technologies

CO_2 captured from iron and steel industry can be further used in some promising biotechnological conversions. One of the emerging ways is to store partial CO_2 in the biomass which can be gasified into methane. Methane can produce H_2 throughout steam methane reforming. Another pathway is to combine biowaste and CO_2 into novel bioplastic or chemical manufacturing, which aims to develop an energy-efficient, environmentally, and economically conversion of CO_2 to high added value chemicals.

(d) Life cycle assessment and techno-economic analysis of carbon capture and utilisation.

Further study also needs to concentrate on environmental impacts and stakeholders' benefits when design a new carbon ustilisation pathway or product. Life cycle assessment and techno-economic analysis are used to evaluate the whole value chain development, and then to identify possible pinch points for sustainable and cost-effective carbon capture and utilisation solutions.

Appendix A

Process design of absorber and stripper

Equations of designing columns refers to the literature [265]. The superficial velocity of the gas is the dominant factor to calculate column diameter, which is related to a parameter called flooding velocity and densities of gas and liquid streams as equation A.1:

$$u_s = u_{flood}\sqrt{\frac{\rho_l - \rho_g}{\rho_g}} \tag{A.1}$$

where ρ_g and ρ_l are densities of gas and liquid streams, u_{flood} is operating flooding velocity of absorber and stripper. The flooding velocity is estimated as equation A.2:

$$u = \frac{CP}{F_p^{0.5}\nu^{0.05}} \tag{A.2}$$

where F_p is the packing factor, ν is the kinematic viscosity of liquid, CP is the capacity factor which is a function of the flow parameter FP that depends on the ratio of the gas flow rate to liquid flow rate, as shown:

$$FP = \frac{Gas_m}{Liq_m}\sqrt{\frac{\rho_g}{\rho_l}} \tag{A.3}$$

where Gas_m and Liq_m are mass flow rates of gas and liquid streams entering packed columns.

The packed height of columns is calculated by summating height of packed stages in the columns, i.e., for a column with N number of stages, the heights for absorber and stripper are shown as:

$$H_{abs} = \sum_{n=1}^{N} HETP_n \tag{A.3}$$

$$H_{str} = \sum_{n=2}^{N-1} HETP_n \tag{A.4}$$

where $HETP_n$ is the height equivalent to a theoretical plate for the *n*th stage in a packed column. The equation used to calculate HETP is given as:

$$HETP_n = \frac{ln\lambda_n}{\lambda_n - 1}(HTU_{g,n} + \lambda_n HTU_{l,n}) \tag{A.5}$$

where HTU and λ_n are height of transfer unit for streams and the stripping factor for the *n*th stage,

respectively. They can be described in detail as below:

$$HTU_{g,n} = \frac{u_{g,s}}{k_{g,n} a_{e,n}} \tag{A.6}$$

$$HTU_{l,n} = \frac{u_{l,s}}{k_{l,n} a_{e,n}} \tag{A.7}$$

$$\lambda_n = \frac{m_n Gas_n}{Liq_n} \tag{A.8}$$

where $u_{g,s}$ and $u_{l,s}$ are superficial velocities for the gas and liquid streams, $k_{g,n}$ and $k_{l,n}$ are mass transfer coefficients for the gas and liquid streams, and $a_{e,n}$ is the effective interfacial area per unit volume of the *n*th packed stage.

Appendix B

Chemical exergies of the elements for reference substances

The values of standard chemical exergy of reference substances are calculated prior to the calculation of standard chemical exergy of other considered elements. Reference substances could appear as gaseous substances, solid species, and ionic and molecular substances. The chemical exergy of reference substances and element are from [298].

Table A.1 Chemical exergies of elements and related reference substances

Element	Chemical element exergy kJ·mol^{-1}	Reference species	Chemical exergy kJ·mol^{-1}
C	410.3	CO_2	19.9
H	236.1 (H_2, g)	H_2O	9.5
N	0.72	N_2	0.72
O	3.97	O_2	3.97
Al	796.1	Al_2SiO_5	3.83
Ca	731.4	$CaCO_3$	18.61
Cl	124.03 (Cl_2, g)	Cl^-	-69.04
Fe	376.99	Fe_2O_3	17.75
S	607.05	SO_4^{2-}	129.21
Mg	629.37	Mg_3Si_4O	21.45
Mn	496.42	MnO_2	35.2
Si	854.1	SiO_2	1.37

The chemical exergies of other substances are calculated by using chemical exergy of elements. Table A.2 lists chemical exergy of these substances.

Table A.2 Chemical exergies of other substances

Components	Chemical exergy kJ·mol^{-1}
Al_2O_3	15.96
CaO	128.94
CH_4 (gas)	831.66
C_2H_4	1358.49
CO (gas)	274.99
Fe_3C	1559.22
FeO	127.34
Fe_3O_4	127.39
HCl	35.75
H_2S	815.31
H_2SO_4	160.53
MgO	61.532

NO	89.02
NO_2	55.83
NH_3	337.85
$(NH_4)_2SO_4$	657.59
SO_2	310.41
SO_3	126.33

References

[1] Administration USEI. International Energy Outlook. 2017.

[2] Stanek W, Czarnowska L, Kalina J. Application of life cycle thermo-ecological cost methodology for evaluation of biomass integrated gasification gas turbine based cogeneration. Applied Thermal Engineering. 2014;70(1):1007-17.

[3] IEA. CO2 emissions from fuel combustion, OECD Publishing, Paris, https://doi.org/10.1787/co2_fuel-2017-en. 2017.

[4] Department of Energy. Waste Heat Recovery: Technology and Opportunities in U.S. 2008.

[5] IEA. Energy Technology Perspectives 2014. Paris. https://www.iea.org/reports/energy-technology-perspectives-2014. 2014.

[6] IEA. Tracking Industrial Energy Efficiency and CO2 Emissions. International Energy Agency. 2007.

[7] Ouyang X, Lin B. An analysis of the driving forces of energy-related carbon dioxide emissions in China's industrial sector. Renewable and Sustainable Energy Reviews. 2015;45:838-49.

[8] Ma G-y, Cai J-j, Zeng W-w, Dong H. Analytical research on waste heat recovery and utilization of China's iron & steel industry. Energy Procedia. 2012;14:1022-8.

[9] IEA Tracking Industry – Iron and steel. https://www.iea.org/reports/tracking-industry-2019/iron-and-steel. 2019.

[10] Gonzalez Hernandez A, Paoli L, Cullen JM. How resource-efficient is the global steel industry? Resources, Conservation and Recycling. 2018;133:132-45.

[11] En T, Shao Y-j, Fan X-g, Ye L-d, Jun W. Application of energy efficiency optimization technology in steel industry. Journal of Iron and Steel Research, International. 2014;21:82-6.

[12] Siitonen S, Tuomaala M, Ahtila P. Variables affecting energy efficiency and CO2 emissions in the steel industry. Energy Policy. 2010;38(5):2477-85.

[13] Johansson MT, Söderström M. Options for the Swedish steel industry – Energy efficiency measures and fuel conversion. Energy. 2011;36(1):191-8.

[14] Zhao X, Bai H, Hao J. A review on the optimal scheduling of byproduct gases in steel making industry. Energy Procedia. 2017;142:2852-7.

[15] Jouhara H, Khordehgah N, Almahmoud S, Delpech B, Chauhan A, Tassou SA. Waste heat

recovery technologies and applications. Thermal Science and Engineering Progress. 2018;6:268-89.

[16] Zhang W. Automotive fuels from biomass via gasification. Fuel Processing Technology. 2010;91(8):866-76.

[17] He K, Wang L. A review of energy use and energy-efficient technologies for the iron and steel industry. Renewable and Sustainable Energy Reviews. 2017;70:1022-39.

[18] Jouhara H, Almahmoud S, Chauhan A, Delpech B, Bianchi G, Tassou SA, et al. Experimental and theoretical investigation of a flat heat pipe heat exchanger for waste heat recovery in the steel industry. Energy. 2017;141:1928-39.

[19] Ma H, Du N, Zhang Z, Lyu F, Deng N, Li C, et al. Assessment of the optimum operation conditions on a heat pipe heat exchanger for waste heat recovery in steel industry. Renewable and Sustainable Energy Reviews. 2017;79:50-60.

[20] Ramirez M, Epelde M, de Arteche MG, Panizza A, Hammerschmid A, Baresi M, et al. Performance evaluation of an ORC unit integrated to a waste heat recovery system in a steel mill. Energy Procedia. 2017;129:535-42.

[21] Wang J, Wang J, Dai Y, Zhao P. Assessment of off-design performance of a Kalina cycle driven by low-grade heat source. Energy. 2017;138:459-72.

[22] Zare V, Palideh V. Employing thermoelectric generator for power generation enhancement in a Kalina cycle driven by low-grade geothermal energy. Applied Thermal Engineering. 2018;130:418-28.

[23] Ullah KR, Saidur R, Ping HW, Akikur RK, Shuvo NH. A review of solar thermal refrigeration and cooling methods. Renewable and Sustainable Energy Reviews. 2013;24:499-513.

[24] Askalany AA, Ernst S-J, Hügenell PPC, Bart H-J, Henninger SK, Alsaman AS. High potential of employing bentonite in adsorption cooling systems driven by low grade heat source temperatures. Energy. 2017;141:782-91.

[25] Pietrzyk K, Ohara B, Watson T, Gee M, Avalos D, Lee H. Thermoelectric module design strategy for solid-state refrigeration. Energy. 2016;114:823-32.

[26] Konstantelos I, Strbac G. Capacity value of energy storage in distribution networks. Journal of Energy Storage. 2018;18:389-401.

[27] Ayele GT, Haurant P, Laumert B, Lacarrière B. An extended energy hub approach for load flow analysis of highly coupled district energy networks: Illustration with electricity and heating. Applied Energy. 2018;212:850-67.

[28] Quader MA, Ahmed S, Ghazilla RAR, Ahmed S, Dahari M. A comprehensive review on energy efficient CO2 breakthrough technologies for sustainable green iron and steel manufacturing. Renewable and Sustainable Energy Reviews. 2015;50:594-614.

[29] Napp TA, Gambhir A, Hills TP, Florin N, Fennell PS. A review of the technologies, economics and policy instruments for decarbonising energy-intensive manufacturing industries. Renewable and Sustainable Energy Reviews. 2014;30:616-40.

[30] González IH, Kamiński J. The iron and steel industry: a global market perspective. Gospodarka Surowcami Mineralnymi. 2011;27:5-28.

[31] Keith Jamison CK, Sabine Brueske, Aaron Fisher. Bandwidth study on energy use an potential energy saving opportunities in u.s. iron and sttel manufacturing. 2015.

[32] Cheng Z, Tan Z, Guo Z, Yang J, Wang Q. Recent progress in sustainable and energy-efficient technologies for sinter production in the iron and steel industry. Renewable and Sustainable Energy Reviews. 2020;131:110034.

[33] Ernst Worrell PB, Maarten Neelis, Eliane Blomen, and Eric Masanet. Energy Efficiency Improvement and Cost Saving Opportunities for the U.S. Iron and Steel Industry. 2010.

[34] Uribe-Soto W, Portha J-F, Commenge J-M, Falk L. A review of thermochemical processes and technologies to use steelworks off-gases. Renewable and Sustainable Energy Reviews. 2017;74:809-23.

[35] Database IET. Rolling mills. http://www.iipinetwork.org/wp-content/Ietd/content/rolling-mills.html.

[36] Worrell E, Price L, Neelis M, Galitsky C, Zhou N. World best practice energy intensity values for selected industrial sectors. 2007.

[37] Energy Information Administration. International Energy Outlook 2016. U.S. 2016.

[38] Hasanbeigi A. Emerging energy-efficiency and carbon dioxide emissions-reduction technologies for the iron and steel industry. 2013.

[39] Price L, Sinton J, Worrell E, Phylipsen D, Xiulian H, Ji L. Energy use and carbon dioxide emissions from steel production in China. Energy. 2002;27(5):429-46.

[40] IEA. Energy Technology Perspectives 2017, IEA, Paris. https://www.iea.org/reports/energy-technology-perspectives-2017. 2017.

[41] Morrow WR, Hasanbeigi A, Sathaye J, Xu T. Assessment of energy efficiency improvement and

CO2 emission reduction potentials in India's cement and iron & steel industries. Journal of Cleaner Production. 2014;65:131-41.

[42] IEA. Energy balance flows. International Energy Agency. https://www.iea.org/sankey/. 2015.

[43] IEA. Energy Technology Perspectives. Pathways to a Clean Energy System. Inernational Energy Agency. . 2012:82.

[44] Yellishetty M, Ranjith PG, Tharumarajah A. Iron ore and steel production trends and material flows in the world: Is this really sustainable? Resources, Conservation and Recycling. 2010;54(12):1084-94.

[45] Wang X, Lin B. Factor and fuel substitution in China's iron & steel industry: Evidence and policy implications. Journal of Cleaner Production. 2017;141:751-9.

[46] Fujii H, Managi S. Which industry is greener? An empirical study of nine industries in OECD countries. Energy Policy. 2013;57:381-8.

[47] Sadoway DR. Electrochemical Pathways Towards Carbon-free Metals Production. Department of Materials Science & Engineering, Massachusetts Institute of Technology, Cambridge, Massachusetts; 2008.

[48] Maizières-lès-Metz JBAGRaD. Global technology roadmap for CCS in industry. Steel sectorial report: contribution to the UNIDO roadmap on CCS. 2010.

[49] New Energy and Industrial Techonology Development Organization. Global Warming Countermeasures : Japanese Technologies for Energy Savings / GHG Emissions Reduction. 2008.

[50] Oda J, Akimoto K, Sano F, Tomoda T. Diffusion of energy efficient technologies and CO2 emission reductions in iron and steel sector. Energy Economics. 2007;29(4):868-88.

[51] Jones DL. Available and emerging technologies for reducing greenhouse gas emissions from the iron and steel industry. US EPA, Office of Air Quality Planning and Standards, Sector Policies and Programs Division. 2012.

[52] Majeski A, Runstedtler A, D'alessio J, Macfadyen N. Injection of Pulverized Coal and Natural Gas into Blast Furnaces for Iron-making: Lance Positioning and Design. ISIJ International. 2015;55(7):1377-83.

[53] European Integrated Pollution Prevention and Control Bureau. Best Available Techniques (BAT) Reference document for iron and steel production emissions directive. 2010.

[54] Chu M, Nogami H, Yagi J-i. Numerical Analysis on Injection of Hydrogen Bearing Materials

into Blast Furnace. ISIJ International. 2004;44(5):801-8.

[55] Chen W-H, Lin M-R, Yu AB, Du S-W, Leu T-S. Hydrogen production from steam reforming of coke oven gas and its utility for indirect reduction of iron oxides in blast furnace. International Journal of Hydrogen Energy. 2012;37(16):11748-58.

[56] Hanrot F, Sert D, Delinchant J, Pietruck R, Bürgler T, Babich A, et al. CO2 mitigation for steelmaking using charcoal and plastics wastes as reducing agents and secondary raw materials. 2009.

[57] Mousa EA, Babich A, Senk D. Iron ore sintering process with biomass utilization. Conference Iron ore sintering process with biomass utilization. p. 1-13.

[58] Mousa E, Wang C, Riesbeck J, Larsson M. Biomass applications in iron and steel industry: An overview of challenges and opportunities. Renewable and Sustainable Energy Reviews. 2016;65:1247-66.

[59] Anyashiki T, Fukada K, Fujimoto H. Development of carbon iron composite process. JFE Tech Rep. 2009;13:1.

[60] Yilmaz C, Wendelstorf J, Turek T. Modeling and simulation of hydrogen injection into a blast furnace to reduce carbon dioxide emissions. Journal of Cleaner Production. 2017;154:488-501.

[61] Ghanbari H, Pettersson F, Saxén H. Sustainable development of primary steelmaking under novel blast furnace operation and injection of different reducing agents. Chemical Engineering Science. 2015;129:208-22.

[62] Nomura S, Callcott TG. Maximum Rates of Pulverized Coal Injection in Ironmaking Blast Furnaces. ISIJ International. 2011;51(7):1033-43.

[63] Halim KSA, Andronov VN, Nasr MI. Blast furnace operation with natural gas injection and minimum theoretical flame temperature. Ironmaking & Steelmaking. 2009;36(1):12-8.

[64] Cores Sánchez A, Ferreira-Barragáns S, Isidro A, Muñiz M. Combustion of waste oils simulating their injection in blast furnace tuyeres. 2009.

[65] Trinkel V, Kieberger N, Bürgler T, Rechberger H, Fellner J. Influence of waste plastic utilisation in blast furnace on heavy metal emissions. Journal of Cleaner Production. 2015;94:312-20.

[66] Slaby S, Andahazy D, Winter F, Feilmayr C, uuml, rgler T. Reducing Ability of CO and H₂ of Gases Formed in the Lower Part of the Blast Furnace by Gas and Oil Injection. ISIJ International. 2006;46(7):1006-13.

[67] Babich A, Senk D, Fernandez M. Charcoal Behaviour by Its Injection into the Modern Blast

Furnace. ISIJ International. 2010;50(1):81-8.

[68] JA NKGLM, Todoschuk T. Direct injection of biofuel in blast furnace ironmaking. Canadian Carbonization Research Association; 2010.

[69] Buergler T, Di Donato A. Biomass gasification for DRI production. Rev Met Paris. 2009;106(10):429-33.

[70] Lu L, Ishiyama O. Recent advances in iron ore sintering. Mineral Processing and Extractive Metallurgy. 2016;125(3):132-9.

[71] Borges W, Melo C, Braga R, Santos E, Maria C, Kojima O, et al. Application of the Hybrid Pelletized Sinter (HPS) process at Monlevade Works. Revue de Métallurgie–International Journal of Metallurgy. 2004;101(3):189-94.

[72] Kuyumcu HZ, Sander S. Stamped and pressed coal cakes for carbonisation in by-product and heat-recovery coke ovens. Fuel. 2014;121:48-56.

[73] Steel Authority of India Limited. Coke Ovens-Sinter-BF-BOF Route. https://sail.co.in/learning-center/coke-ovens-sinter-bf-bof-route. 2008.

[74] Xu Y, Xu J, Sun C, Ma K, Shan C, Wen L, et al. Quantitative comparison of binary particle mass and size segregation between serial and parallel type hoppers of blast furnace bell-less top charging system. Powder Technology. 2018;328:245-55.

[75] Paul Wurth. Blast Furnace Top Charging Technology. http://www.paulwurth.com/Our-Activities/Ironmaking/Blast-Furnace-Top-Charging-Technology. 2012.

[76] Radhakrishnan VR, Maruthy Ram K. Mathematical model for predictive control of the bell-less top charging system of a blast furnace. Journal of Process Control. 2001;11(5):565-86.

[77] Nippon Steel & Sumikin Engineering CO. L. Fluidized Bed type CMC utilizing coke oven exhaust gas CMC (Coal Moisture Control). https://www.eng.nipponsteel.com/business/upload/docs/CMC%20presentation.pdf. 2017.

[78] Fluidized Bed type CMC utilizing coke oven exhaust gas CMC (Coal Moisture Control). Nippon Steel & Sumikin Engineering CO., Ltd. 2017. https://www.eng.nipponsteel.com/business/upload/docs/CMC%20presentation.pdf. 2017.

[79] Machida S, Sato H, Takeda K. Development of the process for producing pre-reduced agglomerates. JFE Technical Report. 2009(13):7-13.

[80] Kitamura S-y. Chapter 1.3 - Hot Metal Pretreatment. In: Seetharaman S, editor. Treatise on

Process Metallurgy. Boston: Elsevier; 2014. p. 177-221.

[81] Hasanbeigi A, Price LK, McKane AT. The State–of-the-Art Clean Technologies (SOACT) for Steelmaking Handbook. Asia Pacific Partnership on Clean Development and Climate: Washington, DC, USA; 2010.

[82] Chitaka TY, von Blottnitz H, Cohen B. The role of decision support frameworks in industrial policy development: A South African iron and steel scrap case study. Sustainable Production and Consumption. 2018;13:113-25.

[83] National Energy Conservation Center. Scrap pretreatment and classification (in Chinese). http://www.chinanecc.cn/website/index.shtml. 2012.

[84] McBrien M, Serrenho AC, Allwood JM. Potential for energy savings by heat recovery in an integrated steel supply chain. Applied Thermal Engineering. 2016;103:592-606.

[85] Madias J, de Córdova M. A review on stamped charging of coals. Conference A review on stamped charging of coals. p. 29-43.

[86] Cui P, Qu K-l, Ling Q, Cheng L-y, Cao Y-p. Effects of coal moisture control and coal briquette technology on structure and reactivity of cokes. Coke and Chemistry. 2015;58(5):162-9.

[87] Feng H, Chen L, Liu X, Xie Z. Constructal design for an iron and steel production process based on the objectives of steel yield and useful energy. International Journal of Heat and Mass Transfer. 2017;111:1192-205.

[88] De Beer J, Worrell E, Blok K. Future technologies for energy-efficient iron and steel making. Annual Review of Energy and the Environment. 1998;23(1):123-205.

[89] An R, Yu B, Li R, Wei Y-M. Potential of energy savings and CO2 emission reduction in China's iron and steel industry. Applied Energy. 2018;226:862-80.

[90] Smil V. Chapter 5 - Modern Ironmaking and Steelmaking: Furnaces, Processes, and Casting. In: Smil V, editor. Still the Iron Age. Boston: Butterworth-Heinemann; 2016. p. 87-114.

[91] Toroghinejad MR, Ashrafizadeh F, Najafizadeh A, Humphreys AO, Liu D, Jonas JJ. Effect of rolling temperature on the deformation and recrystallization textures of warm-rolled steels. Metallurgical and Materials Transactions A. 2003;34(5):1163-74.

[92] Ray RK, Haldar A. TEXTURE DEVELOPMENT IN EXTRA LOW CARBON (ELC) AND INTERSTITIAL FREE (IF) STEELS DURING WARM ROLLING. Materials and Manufacturing Processes. 2002;17(5):715-29.

[93] Vic Cheetham BE. Dry mechanical vacuum pumps for vacuum degassing. Millennium steel. 2005.

[94] Qin S, Chang S. Modeling, thermodynamic and techno-economic analysis of coke production process with waste heat recovery. Energy. 2017;141:435-50.

[95] Bataille C, Luc E, Bigerelle M, Deltombe R, Dubar M. Rolls wear characterization in hot rolling process. Tribology International. 2016;100:328-37.

[96] Geerdes M, Chaigneau R, Kurunov I. Modern blast furnace ironmaking: an introduction (2015): Ios Press, 2015.

[97] Saidur R, Mekhilef S, Ali MB, Safari A, Mohammed HA. Applications of variable speed drive (VSD) in electrical motors energy savings. Renewable and Sustainable Energy Reviews. 2012;16(1):543-50.

[98] de Almeida AT, Fonseca P, Bertoldi P. Energy-efficient motor systems in the industrial and in the services sectors in the European Union: characterisation, potentials, barriers and policies. Energy. 2003;28(7):673-90.

[99] Subhra Dhara MR, A.Mallick, B.N.Pathak, R.K.Nayak, B.C.Roy, A.K.Sahu&S.K.Pan. Maximising sinter machine productivity through identification & checking of air leakage points. R & D Centre for Iron and Steel, SAIL, Ranchi. http://www.meconlimited.co.in/writereaddata/MIST_2016/sesn/tech_2/2.pdf. 2016.

[100] Huber JC, Ruby F, Faral M, Le Coq X. Pilot assessment of the airtight EAF process. Rev Met Paris. 2006;103(4):168-73.

[101] Wang C, Karlsson J, Hooey L, Boden A. Application of oxygen enrichment in hot stoves and its potential influences on the energy system at an integrated steel plant. Conference Application of oxygen enrichment in hot stoves and its potential influences on the energy system at an integrated steel plant. Linköping University Electronic Press, p. 1537-44.

[102] JP Steel Plantech Co. Heat the World, Shape the Future. Product Information. https://steelplantech.com/wp-content/themes/stlp/pdf/products_E.pdf. 2016.

[103] Hasanbeigi A, Arens M, Price L. Alternative emerging ironmaking technologies for energy-efficiency and carbon dioxide emissions reduction: A technical review. Renewable and Sustainable Energy Reviews. 2014;33:645-58.

[104] Nomura S. 12 - The development of cokemaking technology based on the utilization of semisoft

coking coals. In: Suárez-Ruiz I, Diez MA, Rubiera F, editors. New Trends in Coal Conversion: Woodhead Publishing; 2019. p. 335-65.

[105] Qi F, Liu Z, Yao C, Li B. Numerical Study and Structural Optimization of a Top Combustion Hot Blast Stove. Advances in Mechanical Engineering. 2014;7(2):709675.

[106] Japanese Smart Energy Products & Technologies. Top Combustion Hot Blast Stove. https://www.jase-w.eccj.or.jp/technologies/pdf/iron_steel/S-15.pdf. 2019.

[107] Choudhary SK, Ajmani SK. Evaluation of Bottom Stirring System in BOF Steelmaking Vessel Using Cold Model Study and Thermodynamic Analysis. ISIJ International. 2006;46(8):1171-6.

[108] Department of energy. Innovative edge heater produces higher quality steel with fewer defects while reducing energy consumption and greenhouse gas emissions. U.S. https://www.nrel.gov/docs/fy01osti/29373.pdf. 2000.

[109] Narayanan K, Wang W, Blasiak W, Ekman T. Flameless oxyfuel combustion: technology, modeling and benefits in use. Rev Met Paris. 2006;103(5):210-7.

[110] Arvedi G, Mazzolari F, Bianchi A, Holleis G, Siegl J, Angerbauer A. The Arvedi Endless Strip Production line (ESP): from liquid steel to hot-rolled coil in seven minutes. Rev Met Paris. 2008;105(7-8):398-407.

[111] Liu M, Qin Y, Yan H, Han X, Chong D. Energy and water conservation at lignite-fired power plants using drying and water recovery technologies. Energy Conversion and Management. 2015;105:118-26.

[112] Fan X, Chen X, Wang Y. Expert system for sintering process control. Expert Systems: InTech; 2010.

[113] Steel Plantech. Coke Dry Quenching (CDQ). https://steelplantech.com/product/cdq/. 2015.

[114] SMS group G. High productivity with Electric Arc Furnaces. http://www.sms-siemag.com/download/H3_303_EAF_E_Internet.pdf.

[115] Ramesh N. Continuous Casting of Steel and Simulation for Cost Reduction2014.

[116] Sosinsky DJ, Campbell P, Mahapatra R, Blejde W, Fisher F. The CASTRIP® process–recent developments at Nucor Steel's commercial strip casting plant. Metallurgist. 2008;52(11-12):691-9.

[117] National key energy conservation techonologies promotion catalogue 2011 (in Chinese). National Development and Reform Commission. http://iitb.hainan.gov.cn/jnjc/jnjc/jnzcfg/201712/P020180503592785612046.pdf. 2011.

[118] World Steel Association. Steel industry co-products. https://www.worldsteel.org/en/dam/jcr:1b916a6d-06fd-4e84-b35d-c1d911d18df4/Fact_By-products_2018.pdf. 2018.

[119] Oge M, Ozkan D, Celik MB, Sabri Gok M, Cahit Karaoglanli A. An Overview of Utilization of Blast Furnace and Steelmaking Slag in Various Applications. Materials Today: Proceedings. 2019;11:516-25.

[120] Li P. Thermodynamic analysis of waste heat recovery of molten blast furnace slag. International Journal of Hydrogen Energy. 2017;42(15):9688-95.

[121] Japanese Smart Energy Products & Technologies. Dry-process Dust Collector for Blast Furnaces. https://www.jase-w.eccj.or.jp/technologies/pdf/iron_steel/S-13.pdf.

[122] Das B, Prakash S, Reddy PSR, Misra VN. An overview of utilization of slag and sludge from steel industries. Resources, Conservation and Recycling. 2007;50(1):40-57.

[123] Liu J, Yu Q, Zuo Z, Yang F, Han Z, Qin Q. Reactivity and performance of dry granulation blast furnace slag cement. Cement and Concrete Composites. 2019;95:19-24.

[124] Kostura B, Kulveitová H, Leško J. Blast furnace slags as sorbents of phosphate from water solutions. Water Research. 2005;39(9):1795-802.

[125] Singh PK, Katiyar PK, Kumar AL, Chaithnya B, Pramanik S. Effect of Sintering Performance of the Utilization of Blast Furnace Solid Wastes as Pellets. Procedia Materials Science. 2014;5:2468-77.

[126] Omran M, Fabritius T. Utilization of blast furnace sludge for the removal of zinc from steelmaking dusts using microwave heating. Separation and Purification Technology. 2019;210:867-84.

[127] Fisher LV, Barron AR. The recycling and reuse of steelmaking slags — A review. Resources, Conservation and Recycling. 2019;146:244-55.

[128] Annunziata Branca T, Pistocchi C, Colla V, Ragaglini G, Amato A, Tozzini C, et al. Investigation of (BOF) Converter slag use for agriculture in europe. Metall Res Technol. 2014;111(3):155-67.

[129] Yi H, Xu G, Cheng H, Wang J, Wan Y, Chen H. An Overview of Utilization of Steel Slag. Procedia Environmental Sciences. 2012;16:791-801.

[130] Li J, Ma X, Liu H, Zhang X. Life cycle assessment and economic analysis of methanol

production from coke oven gas compared with coal and natural gas routes. Journal of Cleaner Production. 2018;185:299-308.

[131] Chen W-H, Lin M-R, Leu T-S, Du S-W. An evaluation of hydrogen production from the perspective of using blast furnace gas and coke oven gas as feedstocks. International Journal of Hydrogen Energy. 2011;36(18):11727-37.

[132] Wang H, Zhang C, Hu C, Qi Y. Important development trends of coke oven gas utilization in steel plant. Chinese Journal of Iron and Steel. 2008;20:1-12.

[133] Gielen D. CO2 removal in the iron and steel industry. Energy Conversion and Management. 2003;44(7):1027-37.

[134] Ho MT, Allinson GW, Wiley DE. Comparison of MEA capture cost for low CO2 emissions sources in Australia. International Journal of Greenhouse Gas Control. 2011;5(1):49-60.

[135] Razzaq R, Li C, Zhang S. Coke oven gas: Availability, properties, purification, and utilization in China. Fuel. 2013;113:287-99.

[136] Bermúdez JM, Fidalgo B, Arenillas A, Menéndez JA. Dry reforming of coke oven gases over activated carbon to produce syngas for methanol synthesis. Fuel. 2010;89(10):2897-902.

[137] Xie K, Li W, Zhao W. Coal chemical industry and its sustainable development in China. Energy. 2010;35(11):4349-55.

[138] Bermúdez JM, Arenillas A, Luque R, Menéndez JA. An overview of novel technologies to valorise coke oven gas surplus. Fuel Processing Technology. 2013;110:150-9.

[139] Zhao A, Ying W, Zhang H, Ma H, Fang D. Ni–Al2O3 catalysts prepared by solution combustion method for syngas methanation. Catalysis Communications. 2012;17:34-8.

[140] Yang J, Wang X, Li L, Shen K, Lu X, Ding W. Catalytic conversion of tar from hot coke oven gas using 1-methylnaphthalene as a tar model compound. Applied Catalysis B: Environmental. 2010;96(1):232-7.

[141] Yang J, Lee C-H. Adsorption dynamics of a layered bed PSA for H2 recovery from coke oven gas. AIChE Journal. 1998;44(6):1325-34.

[142] Chang K, Li Q, Li Q. Refrigeration cycle for cryogenic separation of hydrogen from coke oven gas. Frontiers of Energy and Power Engineering in China. 2008;2(4):484-8.

[143] Shen J, Wang Z-z, Yang H-w, Yao R-s. A New Technology for Producing Hydrogen and Adjustable Ratio Syngas from Coke Oven Gas. Energy & Fuels. 2007;21(6):3588-92.

[144] Saima WH, Mogi Y, Haraoka T. Development of PSA System for the Recovery of Carbon Dioxide and Carbon Monoxide from Blast Furnace Gas in Steel Works. Energy Procedia. 2013;37:7152-9.

[145] Kasuya F, Tsuji T. High purity CO gas separation by pressure swing adsorption. Gas Separation & Purification. 1991;5(4):242-6.

[146] Ramírez-Santos ÁA, Castel C, Favre E. Utilization of blast furnace flue gas: Opportunities and challenges for polymeric membrane gas separation processes. Journal of Membrane Science. 2017;526:191-204.

[147] Xie H, Yu Q, Zhang Y, Zhang J, Liu J, Qin Q. New process for hydrogen production from raw coke oven gas via sorption-enhanced steam reforming: Thermodynamic analysis. International Journal of Hydrogen Energy. 2017;42(5):2914-23.

[148] Guo J, Hou Z, Gao J, Zheng X. Production of syngas via partial oxidation and CO2 reforming of coke oven gas over a Ni catalyst. Energy & Fuels. 2008;22(3):1444-8.

[149] Maruoka N, Akiyama T. Exergy recovery from steelmaking off-gas by latent heat storage for methanol production. Energy. 2006;31(10):1632-42.

[150] Lundgren J, Ekbom T, Hulteberg C, Larsson M, Grip CE, Nilsson L, et al. Methanol production from steel-work off-gases and biomass based synthesis gas. Applied Energy. 2013;112:431-9.

[151] Guo W, Wang JJ, Gao WG, Wang H. Study on the Preparation of Higher Alcohols Using Blast Furnace Gas and Coke Oven Gas. Advanced Materials Research. 2013;634-638:842-5.

[152] Cheng HW, Lu XG, Hu DH, Ding WZ. Catalytic reforming of model tar compounds from hot coke oven gas for light fuel gases production over bimetallic catalysts. Conference Catalytic reforming of model tar compounds from hot coke oven gas for light fuel gases production over bimetallic catalysts, vol. 152. Trans Tech Publ, p. 860-3.

[153] Kazuhiro HORII NT, Yoshiyuki KITANO, Toshiaki KATO. Processing and Reusing Technologies for Steelmaking Slag. Nippon steel technical report. August 2013;No.104

[154] Zhang H, Wang H, Zhu X, Qiu Y-J, Li K, Chen R, et al. A review of waste heat recovery technologies towards molten slag in steel industry. Applied Energy. 2013;112:956-66.

[155] Mizuochi T, Yagi J, Akiyama T. Granulation of molten slag for heat recovery. Conference Granulation of molten slag for heat recovery. p. 641-6.

[156] Web. Dry Granulation of Blast Furnace Slag for Energy Recovery.

https://www.ispatguru.com/dry-granulation-of-blast-furnace-slag-for-energy-recovery/. 2014.

[157] Barati M, Esfahani S, Utigard TA. Energy recovery from high temperature slags. Energy. 2011;36(9):5440-9.

[158] Meng F, Chen L, Sun F, Yang B. Thermoelectric power generation driven by blast furnace slag flushing water. Energy. 2014;66:965-72.

[159] Luo S, Wang J, Guo X, Liu Z, Sun W. The production of hydrogen-rich gas by wet sludge gasification using waste heat of blast-furnace slag: Mass and energy balance analysis. International Journal of Hydrogen Energy. 2019;44(11):5171-5.

[160] Luo S, Fu J, Zhou Y, Yi C. The production of hydrogen-rich gas by catalytic pyrolysis of biomass using waste heat from blast-furnace slag. Renewable Energy. 2017;101:1030-6.

[161] Yao X, Yu Q, Xu G, Han Z, Xie H, Duan W, et al. The characteristics of syngas production from bio-oil dry reforming utilizing the waste heat of granulated blast furnace slag. International Journal of Hydrogen Energy. 2018;43(49):22108-15.

[162] Sun Y, Chen J, Zhang Z. Biomass gasification using the waste heat from high temperature slags in a mixture of CO2 and H2O. Energy. 2019;167:688-97.

[163] Duan W, Yu Q, Wu T, Yang F, Qin Q. The steam gasification of coal with molten blast furnace slag as heat carrier and catalyst: Kinetic study. International Journal of Hydrogen Energy. 2016;41(42):18995-9004.

[164] Qin YL, Lv XW, Qiu GB, Bai CG. Heat recovery from hot blast furnace slag granulates by pyrolysis of printed circuit boards. Ironmaking & Steelmaking. 2013;40(5):335-41.

[165] Li Y, Dai W-B. Modifying hot slag and converting it into value-added materials: A review. Journal of Cleaner Production. 2018;175:176-89.

[166] Japan Coal Energy Center. Coke Dry Quenching Technology (CDQ). CCT Overview. Iron making and general industry technologies (Iron making technologies). http://www.jcoal.or.jp/eng/cctinjapan/2_3A5.pdf. 2007.

[167] Wu P, Yang C-J. Identification and control of blast furnace gas top pressure recovery turbine unit. ISIJ international. 2012;52(1):96-100.

[168] Modesto M, Nebra SA. Exergoeconomic analysis of the power generation system using blast furnace and coke oven gas in a Brazilian steel mill. Applied Thermal Engineering. 2009;29(11):2127-36.

[169] Hou SS, Chen CH, Chang CY, Wu CW, Ou JJ, Lin TH. Firing blast furnace gas without support fuel in steel mill boilers. Energy Conversion and Management. 2011;52(7):2758-67.

[170] NEFCO. NEFCO supports energy efficiency investment in Ukrainian steel sector. 2010.

[171] Schneider M. Cogeneration for Metal Industry-Utilization of Furnace Off - gases for power generation Africa utility week. 2011;Cape town, South Africa.

[172] García SG, Montequín VR, Fernández RL, Fernández FO. Evaluation of the synergies in cogeneration with steel waste gases based on Life Cycle Assessment: A combined coke oven and steelmaking gas case study. Journal of Cleaner Production. 2019;217:576-83.

[173] Doty S, Turner WC. Energy management handbook: Crc Press, 2004.

[174] Sun K, Tseng C-T, Shan-Hill Wong D, Shieh S-S, Jang S-S, Kang J-L, et al. Model predictive control for improving waste heat recovery in coke dry quenching processes. Energy. 2015;80:275-83.

[175] Abou Elmaaty TM, Kabeel AE, Mahgoub M. Corrugated plate heat exchanger review. Renewable and Sustainable Energy Reviews. 2017;70:852-60.

[176] Zheng B, Sun P, Liu Y, Zhao Q. Heat transfer of calcined petroleum coke and heat exchange tube for calcined petroleum coke waste heat recovery. Energy. 2018;155:56-65.

[177] Zhang J, Zhang H-H, He Y-L, Tao W-Q. A comprehensive review on advances and applications of industrial heat pumps based on the practices in China. Applied Energy. 2016;178:800-25.

[178] Steel Plantech. Sinter Plant-Coller Waste Heat Recovery System (WHRS). https://steelplantech.com/product/whrs/.

[179] Gongduo Z, Shun L, Hui J, Guowei X. Application of Radial Heat Pipe to Heat Recovery of Flue Gas. Conference Application of Radial Heat Pipe to Heat Recovery of Flue Gas. Atlantis Press.

[180] Cuervo-Piñera V, Cifrián-Riesgo D, Nguyen P-D, Battaglia V, Fantuzzi M, Della Rocca A, et al. Blast Furnace Gas Based Combustion Systems in Steel Reheating Furnaces. Energy Procedia. 2017;120:357-64.

[181] Sohani A. Waste heat recovery from SSAb s Steel plant in Oxelösund using a Heat Pump. Conference Waste heat recovery from SSAb s Steel plant in Oxelösund using a Heat Pump.

[182] Wang T, Zhang Y, Peng Z, Shu G. A review of researches on thermal exhaust heat recovery with Rankine cycle. Renewable and Sustainable Energy Reviews. 2011;15(6):2862-71.

[183] Shi L, Shu G, Tian H, Deng S. A review of modified Organic Rankine cycles (ORCs) for internal combustion engine waste heat recovery (ICE-WHR). Renewable and Sustainable Energy

Reviews. 2018;92:95-110.

[184] Zhang X, He M, Zhang Y. A review of research on the Kalina cycle. Renewable and Sustainable Energy Reviews. 2012;16(7):5309-18.

[185] Ando Junior OH, Maran ALO, Henao NC. A review of the development and applications of thermoelectric microgenerators for energy harvesting. Renewable and Sustainable Energy Reviews. 2018;91:376-93.

[186] Utlu Z, Önal BS. Thermodynamic analysis of thermophotovoltaic systems used in waste heat recovery systems: an application. International Journal of Low-Carbon Technologies. 2018;13(1):52-60.

[187] He W, Zhang G, Zhang X, Ji J, Li G, Zhao X. Recent development and application of thermoelectric generator and cooler. Applied Energy. 2015;143:1-25.

[188] IEA. A Power Generating System for Low temperature Heat Recovery. Centre for the Analysis and Dissemination of Demonstrated Energy Technologies (CADDET). 2002.

[189] Global Geothermal Advanced Waste Heat Engineering. Kalina Cycle® Power Plants for waste heat recovery in the iron and steel industry. http://www.globalgeothermal.com/IronSteelIndustry.aspx.

[190] Walsh C, Thornley P. The environmental impact and economic feasibility of introducing an Organic Rankine Cycle to recover low grade heat during the production of metallurgical coke. Journal of Cleaner Production. 2012;34:29-37.

[191] Foresti A, Archetti D, Vescovo R. ORCs in steel and metal making industries: lessons from operating experience and next steps. A Foresti, D Archetti, R Vescovo, Turboden Srl, Via Cernaia 10 Brescia, Italy. 2010;Cernaia 10 Brescia, Italy.

[192] Bause T, Campana F, Filippini L, Foresti A, N M, Pelz T. Cogeneration with ORC at Elebe-Stahlwerke Feralpi EAF Shop. Iron & Steel Technology Magazine. 2015.

[193] Lecompte S, Oyewunmi OA, Markides CN, Lazova M, Kaya A, Broek Mvd, et al. Case study of an organic Rankine cycle (ORC) for waste heat recovery from an electric arc furnace (EAF). Energies. 2017;10(5):649.

[194] Kaşka Ö. Energy and exergy analysis of an organic Rankine for power generation from waste heat recovery in steel industry. Energy Conversion and Management. 2014;77:108-17.

[195] Xu X, Li Y, Yang S, Chen G. A review of fishing vessel refrigeration systems driven by exhaust heat from engines. Applied Energy. 2017;203:657-76.

[196] Xu ZY, Wang RZ. Absorption refrigeration cycles: Categorized based on the cycle construction. International Journal of Refrigeration. 2016;62:114-36.

[197] Jiang L, Wang RZ, Wang LW, Liu JY, Gao P, Zhu FQ, et al. Performance analysis on a novel compact two-stage sorption refrigerator driven by low temperature heat source. Energy. 2017;135:476-85.

[198] Jiang L, Wang LW, Zhou ZS, Zhu FQ, Wang RZ. Investigation on non-equilibrium performance of composite adsorbent for resorption refrigeration. Energy Conversion and Management. 2016;119(Supplement C):67-74.

[199] Saha BB, Akisawa A, Kashiwagi T. Silica gel water advanced adsorption refrigeration cycle. Energy. 1997;22(4):437-47.

[200] Choudhury B, Saha BB, Chatterjee PK, Sarkar JP. An overview of developments in adsorption refrigeration systems towards a sustainable way of cooling. Applied Energy. 2013;104:554-67.

[201] Srikhirin P, Aphornratana S, Chungpaibulpatana S. A review of absorption refrigeration technologies. Renewable and Sustainable Energy Reviews. 2001;5(4):343-72.

[202] Jiang L, Wang LW, Liu CZ, Wang RZ. Experimental study on a resorption system for power and refrigeration cogeneration. Energy. 2016;97:182-90.

[203] Jiang L, Wang L, Wang R, Gao P, Song F. Investigation on cascading cogeneration system of ORC (Organic Rankine Cycle) and CaCl2/BaCl2 two-stage adsorption freezer. Energy. 2014;71:377-87.

[204] Jiang L, Lu H, Wang R, Wang L, Gong L, Lu Y, et al. Investigation on an innovative cascading cycle for power and refrigeration cogeneration. Energy Conversion and Management. 2017;145:20-9.

[205] Zheng D, Chen B, Qi Y, Jin H. Thermodynamic analysis of a novel absorption power/cooling combined-cycle. Applied Energy. 2006;83(4):311-23.

[206] Liu M, Zhang N. Proposal and analysis of a novel ammonia–water cycle for power and refrigeration cogeneration. Energy. 2007;32(6):961-70.

[207] Grosu L, Marin A, Dobrovicescu A, Queiros-Conde D. Exergy analysis of a solar combined cycle: organic Rankine cycle and absorption cooling system. International Journal of Energy and Environmental Engineering. 2016;7(4):449-59.

[208] Masheiti SAA. A thermodynamic and economic simulation modelling study of utilizing low-temperature sources to power absorption and organic rankine cycles. University of Newcastle upon

Tyne. 2011.

[209] Al-Mousawi FN, Al-Dadah R, Mahmoud S. Novel system for cooling and electricity: Four different integrated adsorption-ORC configurations with two expanders. Energy Conversion and Management. 2017;152:72-87.

[210] Cao XC, Chen ZL, Liu YM, Ding ZS, Niu K. A combined cooling heating and power system driven by sinering waste heat system. In: patent C, editor. China2016.

[211] World Steel Association. Sustainable steel at the core of a green economy. https://www.worldsteel.org/en/dam/jcr:5b246502-df29-4d8b-92bb-afb2dc27ed4f/Sustainable-steel-at-the-core-of-a-green-economy.pdf. 2012.

[212] Griffin PW, Hammond GP. Industrial energy use and carbon emissions reduction in the iron and steel sector: A UK perspective. Applied Energy. 2019;249:109-25.

[213] Griffin PW, Hammond GP, Norman JB. Industrial energy use and carbon emissions reduction: a UK perspective. Wiley Interdisciplinary Reviews: Energy and Environment. 2016;5(6):684-714.

[214] Agency IE. Energy Balance Flows. https://www.iea.org/sankey/. 2020.

[215] Cooper SJG, Hammond GP. 'Decarbonising' UK industry: towards a cleaner economy. Proceedings of the Institution of Civil Engineers - Energy. 2018;171(4):147-57.

[216] Association ETES. European Steel in Figures. www. eurofer.eu. 2018.

[217] University N. EPSRC: Thermal Management of Industrial Processes. National sources of low grade heat available from the process industry. Progress Report. 2010.

[218] Williams CL. A Waste Heat Recovery Strategy for an Integrated Steelworks: Cardiff University, 2015.

[219] Li H, Bao W, Li H, Cang D. Energy recovery and abatement potential of CO 2 emissions for an integrated iron and steel making enterprise. Science in China Series E: Technological Sciences. 2010;53(1):129-33.

[220] Sandler SI. Using Aspen Plus in thermodynamics instruction: a step-by-step guide: John Wiley & Sons, 2015.

[221] Schultmann F, Engels B, Rentz O. Flowsheeting-based simulation of recycling concepts in the metal industry. Journal of Cleaner Production. 2004;12(7):737-51.

[222] Garwood TL, Hughes BR, Oates MR, O'Connor D, Hughes R. A review of energy simulation tools for the manufacturing sector. Renewable and Sustainable Energy Reviews. 2018;81:895-911.

[223] Maarten G, Rénard C, Ivan K, Oscar L, John R. Modern Blast Furnace Ironmaking an introduction. 2015.

[224] Futáš P, Pribulová A, Fedorko G, Molnár V. Influence of Steel Scrap in the Charge on the Properties of Gray Cast Iron. ISIJ International. 2017;57(2):374-9.

[225] Association WS. Description of the steel products covered by the worldsteel LCI study.

[226] Suzuki K, Hayashi K, Kuribara K, Nakagaki T, Kasahara S. Quantitative Evaluation of CO2 Emission Reduction of Active Carbon Recycling Energy System for Ironmaking by Modeling with Aspen Plus. Isij International. 2015;55(2):340-7.

[227] Zhang Q, Wei Z, Ma J, Qiu Z, Du T. Optimization of energy use with CO2 emission reducing in an integrated iron and steel plant. Applied Thermal Engineering. 2019;157:113635.

[228] Cossutta M, Foo DCY, Tan RR. Carbon emission pinch analysis (CEPA) for planning the decarbonization of the UK power sector. Sustainable Production and Consumption. 2021;25:259-70.

[229] Tracking Industrial Energy Efficiency and CO2 Emissions. International Energy Agency. https://www.iea.org/publications/freepublications/publication/tracking_emissions.pdf. 2007.

[230] Ho MT, Bustamante A, Wiley DE. Comparison of CO2 capture economics for iron and steel mills. International Journal of Greenhouse Gas Control. 2013;19:145-59.

[231] Suopajärvi H, Pongrácz E, Fabritius T. The potential of using biomass-based reducing agents in the blast furnace: A review of thermochemical conversion technologies and assessments related to sustainability. Renewable and Sustainable Energy Reviews. 2013;25:511-28.

[232] Mathieson JG, Rogers H, Somerville MA, Jahanshahi S. Reducing Net CO₂ Emissions Using Charcoal as a Blast Furnace Tuyere Injectant. ISIJ International. 2012;52(8):1489-96.

[233] Suopajärvi H, Umeki K, Mousa E, Hedayati A, Romar H, Kemppainen A, et al. Use of biomass in integrated steelmaking – Status quo, future needs and comparison to other low-CO2 steel production technologies. Applied Energy. 2018;213:384-407.

[234] Ng WK, Giroux L, MacPhee T, Todoschuk T. Direct injection of biofuel in blast furnace ironmaking. Canadian Carbonization Research Association; 2010.

[235] Xiu S, Shahbazi A. Bio-oil production and upgrading research: A review. Renewable and Sustainable Energy Reviews. 2012;16(7):4406-14.

[236] Guo D, Zhu L, Guo S, Cui B, Luo S, Laghari M, et al. Direct reduction of oxidized iron ore pellets using biomass syngas as the reducer. Fuel Processing Technology. 2016;148:276-81.

[237] Babich A, Gudenau HW, Formoso A, Mavrommatis K, Froehling C, Garcia L. Choice of Technological Regimes of a Blast Furnace Operation with Injection of Hot Reducing Gases. Revista De Metalurgia. 2002;38(4):288-305.

[238] Luo S, Xiao B, Guo X, Hu Z, Liu S, He M. Hydrogen-rich gas from catalytic steam gasification of biomass in a fixed bed reactor: Influence of particle size on gasification performance. International Journal of Hydrogen Energy. 2009;34(3):1260-4.

[239] Tuomi S, Kurkela E, Hannula I, Berg C-G. The impact of biomass drying on the efficiency of a gasification plant co-producing Fischer-Tropsch fuels and heat – A conceptual investigation. Biomass and Bioenergy. 2019;127:105272.

[240] Couto N, Rouboa A, Silva V, Monteiro E, Bouziane K. Influence of the Biomass Gasification Processes on the Final Composition of Syngas. Energy Procedia. 2013;36:596-606.

[241] Almpanis-Lekkas O, Weiss B, Wukovits W. Modelling of an ironmaking melter gasifier unit operation with multicomponent/multiphase equilibrium calculations. Journal of Cleaner Production. 2016;111:161-71.

[242] Zuo H-b, Hu Z-w, Zhang J-l, Li J, Liu Z-j. Direct reduction of iron ore by biomass char. International Journal of Minerals, Metallurgy, and Materials. 2013;20(6):514-21.

[243] Miao X, Wu Q. High yield bio-oil production from fast pyrolysis by metabolic controlling of Chlorella protothecoides. Journal of Biotechnology. 2004;110(1):85-93.

[244] Pohlmann JG, Borrego AG, Osório E, Diez MA, Vilela ACF. Combustion of eucalyptus charcoals and coals of similar volatile yields aiming at blast furnace injection in a CO2 mitigation environment. Journal of Cleaner Production. 2016;129:1-11.

[245] Chung W, Roh K, Lee JH. Design and evaluation of CO2 capture plants for the steelmaking industry by means of amine scrubbing and membrane separation. International Journal of Greenhouse Gas Control. 2018;74:259-70.

[246] Luis P. Use of monoethanolamine (MEA) for CO2 capture in a global scenario: Consequences and alternatives. Desalination. 2016;380:93-9.

[247] Lv B, Guo B, Zhou Z, Jing G. Mechanisms of CO2 Capture into Monoethanolamine Solution with Different CO2 Loading during the Absorption/Desorption Processes. Environmental Science & Technology. 2015;49(17):10728-35.

[248] Ramírez-Santos ÁA, Castel C, Favre E. A review of gas separation technologies within

emission reduction programs in the iron and steel sector: Current application and development perspectives. Separation and Purification Technology. 2018;194:425-42.

[249] Kim H, Lee J, Lee S, Lee I-B, Park J-h, Han J. Economic process design for separation of CO2 from the off-gas in ironmaking and steelmaking plants. Energy. 2015;88:756-64.

[250] Esquivel-Patiño GG, Serna-González M, Nápoles-Rivera F. Thermal integration of natural gas combined cycle power plants with CO2 capture systems and organic Rankine cycles. Energy Conversion and Management. 2017;151:334-42.

[251] Esquivel Patiño GG, Nápoles Rivera F. Global warming potential and net power output analysis of natural gas combined cycle power plants coupled with CO2 capture systems and organic Rankine cycles. Journal of Cleaner Production. 2019;208:11-8.

[252] Pan Z, Zhang L, Zhang Z, Shang L, Chen S. Thermodynamic analysis of KCS/ORC integrated power generation system with LNG cold energy exploitation and CO2 capture. Journal of Natural Gas Science and Engineering. 2017;46:188-98.

[253] Zhao L, Zhao R, Deng S, Tan Y, Liu Y. Integrating solar Organic Rankine Cycle into a coal-fired power plant with amine-based chemical absorption for CO2 capture. International Journal of Greenhouse Gas Control. 2014;31:77-86.

[254] Kurtulus K, Coskun A, Ameen S, Yilmaz C, Bolatturk A. Thermoeconomic analysis of a CO2 compression system using waste heat into the regenerative organic Rankine cycle. Energy Conversion and Management. 2018;168:588-98.

[255] Farajollahi H, Hossainpour S. Application of organic Rankine cycle in integration of thermal power plant with post-combustion CO2 capture and compression. Energy. 2017;118:927-36.

[256] Matino I, Dettori S, Colla V, Weber V, Salame S. Two innovative modelling approaches in order to forecast consumption of blast furnace gas by hot blast stoves. Energy Procedia. 2019;158:4043-8.

[257] González Díaz A. Sequential supplementary firing in natural gas combined cycle plants with carbon capture for enhanced oil recovery. 2016.

[258] Razi N, Svendsen HF, Bolland O. Validation of mass transfer correlations for CO2 absorption with MEA using pilot data. International Journal of Greenhouse Gas Control. 2013;19:478-91.

[259] Rezazadeh F, Gale WF, Hughes KJ, Pourkashanian M. Performance viability of a natural gas fired combined cycle power plant integrated with post-combustion CO2 capture at part-load and temporary non-capture operations. International Journal of Greenhouse Gas Control. 2015;39:397-406.

[260] Sundqvist M, Biermann M, Normann F, Larsson M, Nilsson L. Evaluation of low and high level integration options for carbon capture at an integrated iron and steel mill. International Journal of Greenhouse Gas Control. 2018;77:27-36.

[261] Garcia M, Knuutila HK, Gu S. ASPEN PLUS simulation model for CO2 removal with MEA: Validation of desorption model with experimental data. Journal of Environmental Chemical Engineering. 2017;5(5):4693-701.

[262] Sanchez Fernandez E, Heffernan K, van der Ham LV, Linders MJG, Eggink E, Schrama FNH, et al. Conceptual Design of a Novel CO2 Capture Process Based on Precipitating Amino Acid Solvents. Industrial & Engineering Chemistry Research. 2013;52(34):12223-35.

[263] Madeddu Caahilgvra, Errico Maahilgvra, Baratti Raahilgvra. CO2 Capture by Reactive Absorption-Stripping Modeling, Analysis and Design. 1st ed. 2019. ed2019.

[264] Agbonghae EO, Hughes KJ, Ingham DB, Ma L, Pourkashanian M. Optimal Process Design of Commercial-Scale Amine-Based CO2 Capture Plants. Industrial & Engineering Chemistry Research. 2014;53(38):14815-29.

[265] Nittaya T, Douglas PL, Croiset E, Ricardez-Sandoval LA. Dynamic Modeling and Evaluation of an Industrial-Scale CO2 Capture Plant Using Monoethanolamine Absorption Processes. Industrial & Engineering Chemistry Research. 2014;53(28):11411-26.

[266] Jiang L, Gonzalez-Diaz A, Ling-Chin J, Roskilly AP, Smallbone AJ. Post-combustion CO2 capture from a natural gas combined cycle power plant using activated carbon adsorption. Applied Energy. 2019;245:1-15.

[267] Kuehn NJ, Mukherjee K, Phiambolis P, Pinkerton LL, Varghese E, Woods MC. Current and Future Technologies for Natural Gas Combined Cycle (NGCC) Power Plants. United States2013.

[268] Wang R, Jiang L, Ma Z, Gonzalez-Diaz A, Wang Y, Roskilly AP. Comparative Analysis of Small-Scale Organic Rankine Cycle Systems for Solar Energy Utilisation. Energies. 2019;12(5):829.

[269] Darvish K, Ehyaei MA, Atabi F, Rosen MA. Selection of Optimum Working Fluid for Organic Rankine Cycles by Exergy and Exergy-Economic Analyses. Sustainability. 2015;7(11):15362-83.

[270] Warudkar SS, Cox KR, Wong MS, Hirasaki GJ. Influence of stripper operating parameters on the performance of amine absorption systems for post-combustion carbon capture: Part I. High pressure strippers. International Journal of Greenhouse Gas Control. 2013;16:342-50.

[271] 2019 Government greenhouse gas conversion factors for company reporting. Methodology

paper for emission factors Final report. Department for Business, Energy & Industrial Strategy, UK. 2019.

[272] Lu B, Chen G, Chen D, Yu W. An energy intensity optimization model for production system in iron and steel industry. Applied Thermal Engineering. 2016;100:285-95.

[273] Shen X, Chen L, Xia S, Xie Z, Qin X. Burdening proportion and new energy-saving technologies analysis and optimization for iron and steel production system. Journal of Cleaner Production. 2018;172:2153-66.

[274] González-Roubaud E, Pérez-Osorio D, Prieto C. Review of commercial thermal energy storage in concentrated solar power plants: Steam vs. molten salts. Renewable and Sustainable Energy Reviews. 2017;80:133-48.

[275] Armstrong P, Ager D, Thompson I, McCulloch M. Improving the energy storage capability of hot water tanks through wall material specification. Energy. 2014;78:128-40.

[276] Giordano N, Comina C, Mandrone G. Laboratory scale geophysical measurements aimed at monitoring the thermal affected zone in Underground Thermal Energy Storage (UTES) applications. Geothermics. 2016;61:121-34.

[277] Ortega-Fernández I, Calvet N, Gil A, Rodríguez-Aseguinolaza J, Faik A, D'Aguanno B. Thermophysical characterization of a by-product from the steel industry to be used as a sustainable and low-cost thermal energy storage material. Energy. 2015;89:601-9.

[278] Chen X, Jin X, Liu Z, Ling X, Wang Y. Experimental investigation on the CaO/CaCO3 thermochemical energy storage with SiO2 doping. Energy. 2018;155:128-38.

[279] Lin P, Wang RZ, Xia ZZ, Ma Q. Experimental investigation on heat transportation over long distance by ammonia–water absorption cycle. Energy Conversion and Management. 2009;50(9):2331-9.

[280] Xie X, Jiang Y. Absorption heat exchangers for long-distance heat transportation. Energy. 2017;141:2242-50.

[281] Scapino L, Zondag HA, Van Bael J, Diriken J, Rindt CCM. Energy density and storage capacity cost comparison of conceptual solid and liquid sorption seasonal heat storage systems for low-temperature space heating. Renewable and Sustainable Energy Reviews. 2017;76:1314-31.

[282] Aydin D, Casey SP, Chen X, Riffat S. Novel “open-sorption pipe” reactor for solar thermal energy storage. Energy Conversion and Management. 2016;121:321-34.

[283] Wu S, Zhou C, Doroodchi E, Nellore R, Moghtaderi B. A review on high-temperature thermochemical energy storage based on metal oxides redox cycle. Energy Conversion and Management. 2018;168:421-53.

[284] Guo S, Zhao J, Wang W, Yan J, Jin G, Zhang Z, et al. Numerical study of the improvement of an indirect contact mobilized thermal energy storage container. Applied Energy. 2016;161:476-86.

[285] Li H, Wang W, Yan J, Dahlquist E. Economic assessment of the mobilized thermal energy storage (M-TES) system for distributed heat supply. Applied Energy. 2013;104:178-86.

[286] Wang R. Wise use of low-grade thermal energy. International Symposium of Heat Transfer and Heat Powered Cycle Nottingham, UK2016.

[287] Jiang L, Wang RZ, Wang LW, Gao P, Zhu FQ. Investigation on gradient thermal cycle for power and refrigeration cogeneration. International Journal of Refrigeration. 2017;76:42-51.

[288] Grip C-E, Larsson M, Harvey S, Nilsson L. Process integration. Tests and application of different tools on an integrated steelmaking site. Applied Thermal Engineering. 2013;53(2):366-72.

[289] Carmona LG, Whiting K, Carrasco A, Sousa T. The evolution of resource efficiency in the United Kingdom's steel sector: An exergy approach. Energy Conversion and Management. 2019;196:891-905.

[290] Yılmaz K, Kayfeci M, Keçebaş A. Thermodynamic evaluation of a waste gas-fired steam power plant in an iron and steel facility using enhanced exergy analysis. Energy. 2019;169:684-95.

[291] Ebrahim M, Kawari A. Pinch technology: an efficient tool for chemical-plant energy and capital-cost saving. Applied Energy. 2000;65(1):45-9.

[292] Pan M, Sikorski J, Akroyd J, Mosbach S, Lau R, Kraft M. Design technologies for eco-industrial parks: From unit operations to processes, plants and industrial networks. Applied Energy. 2016;175:305-23.

[293] Zhang C, Romagnoli A, Zhou L, Kraft M. Knowledge management of eco-industrial park for efficient energy utilization through ontology-based approach. Applied Energy. 2017;204:1412-21.

[294] Kong H, Qi E, Li H, Li G, Zhang X. An MILP model for optimization of byproduct gases in the integrated iron and steel plant. Applied Energy. 2010;87(7):2156-63.

[295] Sun Q, Li H, Xu B, Cheng L, Wennersten R. Analysis of secondary energy in China's iron and steel industry – An approach of industrial metabolism. International Journal of Green Energy. 2016;13(8):793-802.

[296] Stijepovic VZ, Linke P, Stijepovic MZ, Kijevčanin ML, Šerbanović S. Targeting and design of industrial zone waste heat reuse for combined heat and power generation. Energy. 2012;47(1):302-13.

[297] Ghorbani B, Salehi G, Ebrahimi A, Taghavi M. Energy, exergy and pinch analyses of a novel energy storage structure using post-combustion CO2 separation unit, dual pressure Linde-Hampson liquefaction system, two-stage organic Rankine cycle and geothermal energy. Energy. 2021;233:121051.

[298] Staneka JSAVW, Valerob A. Towards an International Reference Environment of Chemical Exergy.

[299] Amidpour M, Khoshgoftar Manesh MH. Chapter 5 - Exergy and thermoeconomic evaluation of cogeneration and polygeneration systems. In: Amidpour M, Khoshgoftar Manesh MH, editors. Cogeneration and Polygeneration Systems: Academic Press; 2021. p. 55-74.